Correlated Electronic Structure Theory for Challenging Systems.

Daniel J. Taylor

Submitted for the degree of Doctor of Philosophy (Chemistry)

Heriot-Watt University

School of Engineering and Physical Sciences

February 2015

Abstract

The photochemistry of molecules can be investigated computationally, and this provides great insight into the underlying chemistry and physics. Such computational approaches are challenging and can pose many difficulties compared to ground state methodologies. Care must be taken to accurately describe these systems, as some low-level approximate methods can fail.

The geometrical and electronic structures $(TiO_2)_n$ clusters (n=1-4) have been investigated. These are of enormous technological interest as wide band-gap semiconductors yet the nature of electronic transitions in nano-sized clusters has yet to be fully elucidated. Structures of the neutral closed-shell, radical cationic and radical anionic clusters at each size are described and rationalised in terms of the pseudo-Jahn-Teller effect. We have used high-level response theory to set benchmarks for such systems. The TiO_2 monomer is the simplest of the clusters studied yet proves a stern test for many lower order ab-initio methods. It is shown that high-level methods are required to properly describe this simple molecule.

The Monte Carlo Configuration Interaction method attempts to combine the power of Full CI with a scalability that allows it to be used to study much larger systems. It can be systematically improved and can approach the accuracy of the Full CI method. This method is applied here to investigate potential energy surfaces and multipole moments of a range of small but challenging systems.

This thesis is dedicated to my parents.

Acknowledgements

I would like to begin by thanking everyone who helped me during my studies and the writing of this thesis.

In particular I would like to thank my supervisor Prof. Martin J. Paterson for all of his help, guidance and patience throughout my studies.

Also, I would like to thank Dr Jeremy Coe for his help with the MCCI portion of the thesis.

ACADEMIC REGISTRY

Research Thesis Submission

Name*:*			
School/PGI:			
Version: *(i.e. First, Resubmission, Final)*		Degree Sought (Award **and** Subject area)	

Declaration

In accordance with the appropriate regulations I hereby submit my thesis and I declare that:

1) the thesis embodies the results of my own work and has been composed by myself
2) where appropriate, I have made acknowledgement of the work of others and have made reference to work carried out in collaboration with other persons
3) the thesis is the correct version of the thesis for submission and is the same version as any electronic versions submitted*.
4) my thesis for the award referred to, deposited in the Heriot-Watt University Library, should be made available for loan or photocopying and be available via the Institutional Repository, subject to such conditions as the Librarian may require
5) I understand that as a student of the University I am required to abide by the Regulations of the University and to conform to its discipline.

* *Please note that it is the responsibility of the candidate to ensure that the correct version of the thesis is submitted.*

Signature of Candidate*:*		Date:	

Submission

Submitted By *(name in capitals):*	
Signature of Individual Submitting:	
Date Submitted:	

For Completion in the Student Service Centre (SSC)

Received in the SSC by *(name in capitals):*			
Method of Submission *(Handed in to SSC; posted through internal/external mail):*			
E-thesis Submitted (**mandatory for final theses)**			
Signature:		Date:	

Publications List

[1] Taylor, D. J.; Paterson, M. J., Calculations of the low-lying excited states of the TiO_2 molecule. *The Journal of Chemical Physics* **2010,** 133, 204302.

[2] Taylor, D. J.; Paterson, M. J., Vibronic coupling effects on the structure and spectroscopy of neutral and charged TiO_2 clusters. *Chemical Physics* **2012,** 408, 1-10.

[3] Coe, J. P.; Taylor, D. J.; Paterson, M. J., Calculations of potential energy surfaces using Monte Carlo Configuration Interaction. *The Journal of Chemical Physics* **2012,** 137, 12,19, p. 194111.

[4] Coe, J. P.; Taylor, D. J.; Paterson, M. J., Monte Carlo Configuration Interaction applied to multipole moments, ionization energies, and electron affinities. *Journal of Computational Chemistry* **2013,** 34, 1083-1093.

List of Contents

Chapter 1: Introduction

The development of the field of quantum mechanics early in the last century opened up the possibility for the first time of accurately describing the chemistry of atoms and molecules mathematically. However before the widespread availability of computers, due to the many body nature of these problems, only the simplest of problems could be attempted. As this availability has increased the computational investigation, using accurate models within chemistry, has become progressively commonplace. Computational Chemistry, as this discipline is known, utilizes computers to solve physical models of chemical systems[1, 2]. As computational power has increased over the past decades, so the power to study such chemical systems has also increased and a great number of programs[3-7] have been developed to solve computational problems, allowing the study of larger molecular systems in far greater detail.

One of the first methods developed and perhaps the easiest to conceptually understand was full Configuration Interaction (FCI)[8, 9], which represents the exact solution for a given basis set and in an ideal world it would be applied to all problems. The amount of computer power required for a particular problem increases drastically with the number of atoms (and therefore electrons) in the molecules being studied. Therefore often it is impractical, if not impossible, to use the most powerful and accurate of methods as system sizes increase. Even with the large advances in computer power FCI is intractable for all but the smallest of problems. Consequently, a great deal of research has been devoted to the development of strategies and a hierarchy of computational tools with which to approach larger and larger sized molecular systems[10, 11]. A number of different methods have since been developed which provide an approximate solution using less computer resources. In applying such approximate methods a compromise must be made between the accuracy of the model (or method) used opposed to the time and computer resource devoted to the problem. A balance must be struck to ensure the most accurate result in an acceptable time frame using available computer resources. Care must be taken to ensure the accuracy of any method used or else incorrect conclusion may well be drawn from a poor result. Concurrently with these developments, the ability to follow and predict the processes involved in chemical

reactions, over both ground and excited states[9, 12], computationally has been developing.

The photochemistry of molecules can be investigated computationally, and this provides great insight into the underlying chemistry and physics. Such computational approaches are challenging and can pose many difficulties compared to ground state methodologies. Within the field of photochemistry this can be applied to follow reactions on the excited state surfaces determining possible reaction pathways and possible eventual products[13].

Chapter 2 is intended to provide a background of the theory and computational methods for the material in the subsequent chapters. It begins with an outline of the main ideas and concepts from which quantum chemistry is built upon. Then the various computational methods used in this work are presented along with a discussion of the advantages and disadvantages of each.

In Chapter 3 an investigation of Titanium dioxide clusters with the form $(TiO_2)_n$ (n=1-4) is presented. These structures are the subject of much study due to the potential technological applications for such materials[14, 15]. The TiO_2 monomer is first investigated in some depth. This monomer is the simplest of the clusters studied yet proves a stern test for many lower order ab initio methods. The popular CC2 method has previously been shown to be a robust excited state method for organic chromophores[16, 17]. It was expected to work qualitatively for more strongly correlated systems containing transition metals if the single reference picture was valid, but it is shown that this is not the case. High-level methods are required to properly describe this simple molecule[18]. This is followed by a less in depth study of the n = 2-4 clusters, which also proved problematic for lower order ab initio methods.

In Chapter 4 the investigation of Titanium dioxide clusters continues; structures of the neutral closed-shell, radical cationic and radical anionic clusters at each size are described and rationalised in terms of the pseudo-Jahn-Teller effect (pJT)[19]. It is shown that DFT functionals can demonstrate artificial symmetry breaking for some of these radical clusters. This occurs in a non-systematic way, adding a further difficulty when using such functional methods.

In Chapter 5 the Monte Carlo Configuration Interaction (MCCI) first devised[20] and implemented[21] by J.C. Greer et al is described. This method attempts to combine the power of FCI with a scalability that allows it to be used to study much larger systems. This method is applied here to investigate potential energy surfaces[22] of a range of different challenging systems. It is shown that the MCCI method preforms very well in comparison to the FCI results, while utilising a wave function a fraction the size of that of the FCI.

In Chapter 6 the MCCI method is applied to find the multipole moments[23] of a number of small but challenging systems. With a small fraction of the FCI SD space, MCCI can produce the multipoles very close in value to the FCI result. Then returning to the case of the TiO_2 monomer, MCCI is applied to what was found in chapter 3 to be a surprisingly challenging system. TiO_2 molecule pushes the limits of what the current MCCI program can handle, MCCI results for the system in the final section seem to give satisfactory results. In the Final chapter our conclusions are presented, along with possible work that can be followed to expand on this research.

The results presented in chapters 3 and 4 are of research undertaken by myself, while the work that makes up chapters 5 and 6 of this thesis detail the results of projects additionally involving collaboration with Dr Jeremy Coe, a post-doctoral researcher in the group.

1.1 References

[1] Cramer, C. J., *Essentials of computational chemistry: Theories and models*. 2nd ed.; John Wiley & Sons, Ltd: 2004; p 579.

[2] Jensen, F., *Introduction to computational chemistry*. 2nd ed.; Wiley: 2007.

[3] Dennington, R.; Keith, T.; Millam, J. *Gaussview*, Version 5; *semichem Inc.*: Shawnee Mission, KS, 2009.

[4] H.-J. Werner, P. J. K., G. Knizia, F. R. Manby, M. Schütz, P. Celani, T. Korona, R. Lindh, A. Mitrushenkov, G. Rauhut, K. R. Shamasundar, T. B. Adler, R. D. Amos, A. Bernhardsson, A. Berning, D. L. Cooper, M. J. O. Deegan, A. J. Dobbyn, F. Eckert, E. Goll, C. Hampel, A. Hesselmann, G. Hetzer, T. Hrenar, G. Jansen, C. Köppl, Y. Liu, A. W. Lloyd, R. A. Mata, A. J. May, S. J. McNicholas, W. Meyer, M. E. Mura, A. Nicklass, D. P. O'Neill, P. Palmieri, K. Pflüger, R. Pitzer, M. Reiher, T. Shiozaki, H. Stoll, A. J. Stone, R. Tarroni, T. Thorsteinsson, M. Wang, and A. Wolf, *Molpro, version 2010.1, a package of ab initio programs,* , see http://www.molpro.net.

[5] Frisch, M. J.; Trucks, G. W.; Schlegel, H. B.; Scuseria, G. E.; Robb, M. A.; Cheeseman, J. R.; Scalmani, G.; Barone, V.; Mennucci, B.; Petersson, G. A.; Nakatsuji, H.; Caricato, M.; Li, X.; Hratchian, H. P.; Izmaylov, A. F.; Bloino, J.; Zheng, G.; Sonnenberg, J. L.; Hada, M.; Ehara, M.; Toyota, K.; Fukuda, R.; Hasegawa, J.; Ishida, M.; Nakajima, T.; Honda, Y.; Kitao, O.; Nakai, H.; Vreven, T.; Montgomery Jr., J. A.; Peralta, J. E.; Ogliaro, F. o.; Bearpark, M. J.; Heyd, J.; Brothers, E. N.; Kudin, K. N.; Staroverov, V. N.; Kobayashi, R.; Normand, J.; Raghavachari, K.; Rendell, A. P.; Burant, J. C.; Iyengar, S. S.; Tomasi, J.; Cossi, M.; Rega, N.; Millam, N. J.; Klene, M.; Knox, J. E.; Cross, J. B.; Bakken, V.; Adamo, C.; Jaramillo, J.; Gomperts, R.; Stratmann, R. E.; Yazyev, O.; Austin, A. J.; Cammi, R.; Pomelli, C.; Ochterski, J. W.; Martin, R. L.; Morokuma, K.; Zakrzewski, V. G.; Voth, G. A.; Salvador, P.; Dannenberg, J. J.; Dapprich, S.; Daniels, A. D.; Farkas, ñ. n.; Foresman, J. B.; Ortiz, J. V.; Cioslowski, J.; Fox, D. J. *Gaussian 09*, Gaussian, Inc.: Wallingford, CT, USA, 2009.

[6] Aidas, K.; Angeli, C.; Bak, K. L.; Bakken, V.; Bast, R.; Boman, L.; Christiansen, O.; Cimiraglia, R.; Coriani, S.; Dahle, P.; Dalskov, E. K.; Ekström, U.; Enevoldsen, T.; Eriksen, J. J.; Ettenhuber, P.; Fernández, B.; Ferrighi, L.; Fliegl, H.; Frediani, L.; Hald, K.; Halkier, A.; Hättig, C.; Heiberg, H.; Helgaker, T.; Hennum, A. C.; Hettema, H.; Hjertenæs, E.; Høst, S.; Høyvik, I.-M.; Iozzi, M. F.; Jansík, B.; Jensen, H. J. A.; Jonsson, D.; Jørgensen, P.; Kauczor, J.; Kirpekar, S.; Kjærgaard, T.; Klopper, W.; Knecht, S.; Kobayashi, R.; Koch, H.; Kongsted, J.; Krapp, A.; Kristensen, K.; Ligabue, A.; Lutnæs, O. B.; Melo, J. I.; Mikkelsen, K. V.; Myhre, R. H.; Neiss, C.; Nielsen, C. B.; Norman, P.; Olsen, J.; Olsen, J. M. H.; Osted, A.; Packer, M. J.; Pawlowski, F.; Pedersen, T. B.; Provasi, P. F.; Reine, S.; Rinkevicius, Z.; Ruden, T. A.; Ruud, K.; Rybkin, V. V.; Sałek, P.; Samson, C. C. M.; de Merás, A. S.; Saue, T.; Sauer, S. P. A.; Schimmelpfennig, B.; Sneskov, K.; Steindal, A. H.; Sylvester-Hvid, K. O.; Taylor, P. R.; Teale, A. M.; Tellgren, E. I.; Tew, D. P.; Thorvaldsen, A. J.; Thøgersen, L.; Vahtras, O.; Watson, M. A.; Wilson, D. J. D.; Ziolkowski, M.; Ågren, H., The Dalton quantum chemistry program system. *Wiley Interdisciplinary Reviews: Computational Molecular Science* **2014,** 4, 269-284.

[7] Lischka, H.; Shepard, R.; I. Shavitt; R. M. Pitzer; M. Dallos; Th. Müller; P. G. Szalay; F. B. Brown; R. Ahlrichs; H. J. Böhm; A. Chang; D. C. Comeau; R. Gdanitz; H. Dachsel; C. Ehrhardt; M. Ernzerhof; P. Höchtl; S. Irle; G. Kedziora; T. Kovar; V. Parasuk; M. J. M. Pepper; P. Scharf; H. Schiffer; M. Schindler; M. Schüler; M. Seth; E. A. Stahlberg; J.-G. Zhao; S. Yabushita; Z. Zhang; M. Barbatti; S. Matsika; M. Schuurmann; D. R. Yarkony; S. R. Brozell; E. V. Beck; and J.-P. Blaudeau; M. Ruckenbauer; B. Sellner; F. Plasser; and J. J. Szymczak *Columbus, an ab initio electronic structure program*, release 5.9.2 (2012).

[8] Szabo, A.; Ostlund, N. S., *Modern quantum chemistry : Introduction to advanced electronic structure theory*. 1st ed. rev. ed.; Dover: 1996.

[9] Sherrill, D. C., An introduction to configuration interaction theory. In *School of Chemistry and Biochemistry*, Georgia Institute of Technology: 1995.

[10] Knowles, P.; Schutz, M.; Werner, H.-J., Ab initio methods for electron correlation in molecules. In *winterschool, 21 - 25 February 2000*, Grotendorst, J., Ed. John von Neumann-Institute for Computing: Forschungszentrum Jülich, 2000; Vol. 3, p 638.

[11] Koch, W.; Holthausen, M. C., *A chemist's guide to density functional theory*. 2nd ed.; Wiley-VCH: 2001; p 263.

[12] Cimiraglia, R., Methods of calculation of excited states. In Dipartimento di Chimica, Universita di Ferrara.

[13] Turro, N. J.; Ramamurthy, V.; Scaiano, J. C., *Principles of molecular photochemistry an introduction*. 1st edition ed.; University Science Books: 2009.
[14] Glassford, K. M.; Chelikowsky, J. R., *Physical Review B* **1993,** 47, 12550-12553.
[15] Hashimoto, K.; Irie, H.; Fujishima, A., TiO_2 photocatalysis: A historical overview and future prospects. *Japanese Journal of Applied Physics* **2005,** 44.
[16] Sauer, S. P. A.; Schreiber, M.; Silva-Junior, M. R.; Thiel, W., Benchmarks for electronically excited states: A comparison of noniterative and iterative triples corrections in linear response coupled cluster methods: CCSDR(3) versus CC3. *Journal of Chemical Theory and Computation* **2009,** 5, 555-564.
[17] Schreiber, M.; Silva-Junior, M. R.; Sauer, S. P. A.; Thiel, W., Benchmarks for electronically excited states: CASPT2, CC2, CCSD, and CC3. *The Journal of Chemical Physics* **2008,** 128, 134110.
[18] Taylor, D. J.; Paterson, M. J., Calculations of the low-lying excited states of the TiO_2 molecule. *The Journal of Chemical Physics* **2010,** 133, 204302.
[19] Taylor, D. J.; Paterson, M. J., Vibronic coupling effects on the structure and spectroscopy of neutral and charged TiO_2 clusters. *Chemical Physics* **2012,** 408, 1-10.
[20] Greer, J. C., Estimating full configuration-interaction limits from a monte-carlo selection of the expansion space. *Journal of Chemical Physics* **1995,** 103, 1821-1828.
[21] Tong, L. Y.; Nolan, M.; Cheng, T. W.; Greer, J. C., A monte carlo configuration generation computer program for the calculation of electronic states of atoms, molecules, and quantum dots. *Computer Physics Communications* **2000,** 131, 142-163.
[22] Coe, J. P.; Taylor, D. J.; Paterson, M. J., Calculations of potential energy surfaces using monte carlo configuration interaction. *The Journal of Chemical Physics* **2012,** 137, 12, 19 p.194111
[23] Coe, J. P.; Taylor, D. J.; Paterson, M. J., Monte carlo configuration interaction applied to multipole moments, ionization energies, and electron affinities. *Journal of Computational Chemistry* **2013,** 34, 1083-1093.

Chapter 2: Theory

In this chapter some important theories and methods of computational chemistry are introduced with the aim of providing a background for the work presented within this thesis. A good introduction to computational and theoretical chemistry can be found in Refs. [1-6].

2.1 Born-Oppenheimer Approximation

The Born-Oppenheimer approximation (BOA) is one of the most important concepts in chemistry. Through this approximation the motion of the electrons is decoupled from the motion of the nuclei. This approximation informs the very vocabulary with which molecules and their chemistry are thought about and described. Without the electronic potential energy surface (PES), defined by this theory, the definition of most concepts of molecular structure (such as equilibrium configuration, bond-lengths, bond-angles, dihedral angles, etc.) cannot be made[7].

There is a very significant difference in the mass of an electron in comparison to the mass of a nucleus. The mass of a single proton (the lightest possible nucleus) is over 1800 times heavier than the mass of an electron. As a consequence of this fact the nuclei move far slower than the surrounding electrons and in the relative time scale of the electron movement the nuclei of the molecule would be seen to have hardly moved. The motion of the nuclei can therefore be considered as separate from the motion of the electrons. This is the basis of the BOA where the positions of the nuclei are treated as fixed parameters around which the electrons move. The nuclei in turn experience a time-averaged electronic "force-field" which gives rise to molecular vibrations. The motions of the two different types of particle are therefore decoupled and the solution to the molecular quantum mechanical problems becomes a two-stage process: 1. Solve the electronic problem for the electrons in the field of the nuclei, 2. Solve the nuclear motion problem using the solution to the electronic problem as the potential in the nuclear problem.

The BOA works well for most cases and has a central role in chemistry and physics. Without it the concept of the potential energy surface would be lost and with it a large number of conceptual ideas would also be lost. However when there is a strong coupling between the electronic and nuclear motion the BOA breaks down. Even then the BOA, particularly the concept of the PES, remains and is used as a starting point in more advanced treatments of the coupled electronic and nuclear motion.

Intuitively one can see that moving the nuclei such that the electronic state (and chemical bonding) of a molecule abruptly changes must involve a strong coupling between the electrons and the nuclei. An example of strong coupling between the electronic and nuclear motion is the case of a conical intersection where two energy states cross. At these crossing points where there is an exact degeneracy between electronic states the approximation breaks down completely. Indeed the modern derivation of the BOA also includes a dependence on the energy difference between electronic states. Thus it is now apparent that two factors control whether the BOA is valid, the electron-nuclear mass difference (usually always valid) and crucially also the energy difference between adjacent electronic states. The closer in energy a pair of states get then the more the BOA breaks down, until at the point of degeneracy it becomes undefined, technically there is a singularity in derivative coupling (a term neglected in the BOA)[8-13]. Conical intersections are described in more detail later in this chapter, but note here that it is this feature of having multiple electronic states involved that presents the main difficulties for accurate computational treatment of photochemical problems.

2.2 Potential Energy Surfaces (PES)

The PES of a molecule is a 3N-6 dimensional surface, where N is the number of nuclei. So even for a small molecule with few atoms it can be very complex. From this PES the minimum and transition state geometries for these nuclei can be recovered as critical points of the surface; examples of these features are demonstrated in Figure 2-1.

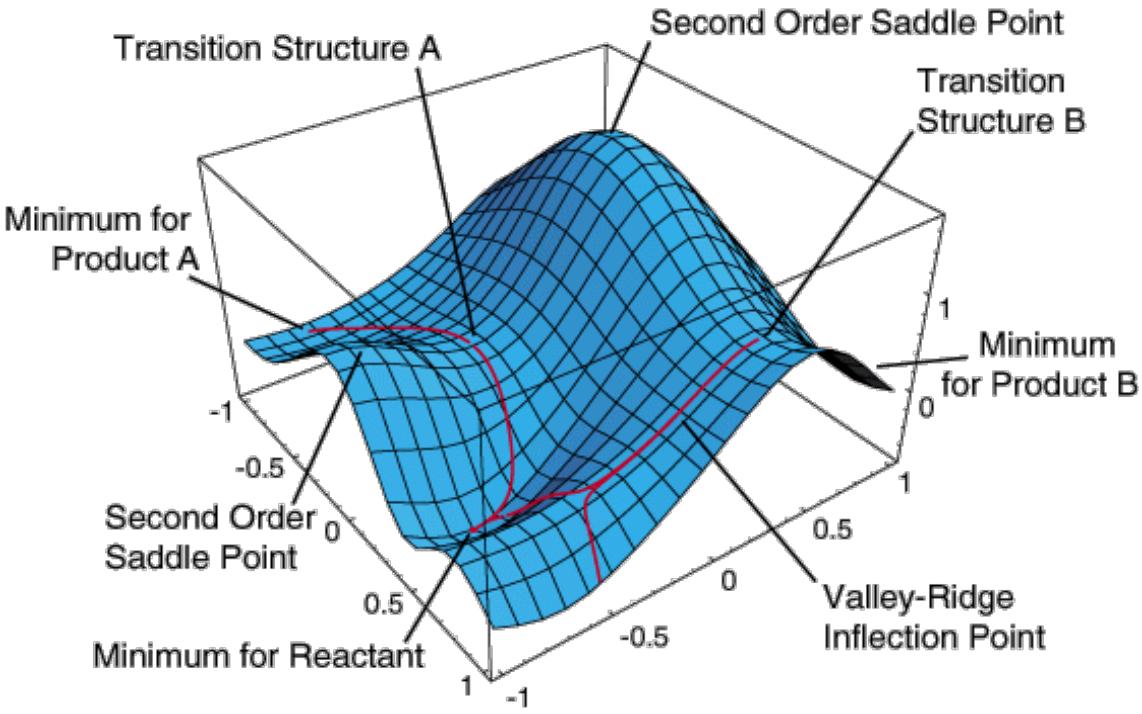

Figure 2-1: Example potential energy surface in 3 Dimensions, where the vertical axis is the energy and the horizontal axes are the molecular coordinates. Local minima, transition states and the paths between them on the PES are shown. From Ref. [14].

Due to this complexity searching for important features of the surface (minima, transition states, conical intersections, etc.) can be challenging.

2.2.1 Excited States

When a molecule absorbs one or more photons it is promoted into an excited electronic state. In these excited states the electrons have become distributed into a higher energy configuration. Each excited state can have a different chemistry to the ground state because of its different electron arrangements and the extra energy they have from the absorbed photon(s). There are several ways that the molecule can lose this excess energy and in doing so it is possible that the molecule can undergo a chemical change.

2.2.2 Reaction Pathways

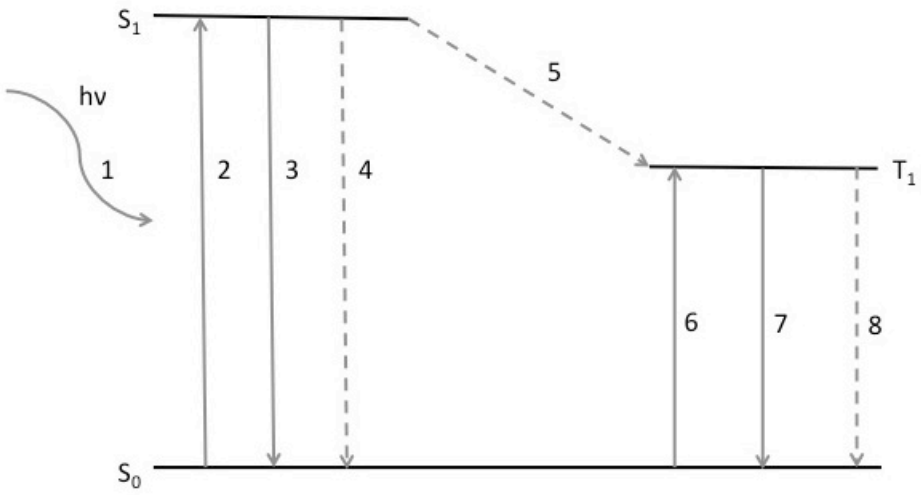

Figure 2-2: Jablonski diagram showing the various ways the state of a given molecule can change. The vertical dimension here is the energy. The transitions between the ground (S_0), first excited state (S_1) and first triplet state (T_1) are shown, but the routes are applicable for transitions between any two appropriate states.

Figure 2-2 is an example of an energy state diagram, often called a Jablonski diagram. It is a reproduction of a similar diagram published in [6]. The black lines of the figure represent the electronic energy levels of a molecule and show the relative energy separations. The levels have been separated out in such a way as to make the figure easier to understand. The various elements of the figure are numbered as:

1 Electromagnetic radiation incident on the molecule, with energy hν, where ν is the frequency.

2 An excitation of the molecule by the absorbed photon(s) to a higher state, in the case of the figure to the first excited singlet electronic state (S_1).

3 Fluorescence, the emissions of photons to lower the molecule back to the ground state, i.e., a radiative process not changing the electronic spin-state.

4 Internal conversion, non-adiabatic radiationless transition between states of the same spin, i.e., a non-radiative process.

5 An Intersystem crossing, non-adiabatic radiationless transition between states of different spin. In this case from S_1 to T_1.

6 Spin-forbidden absorption of a photon exciting the molecule to a state of different spin (here S_0 to T_1).

7 Phosphorescence, the emission of photons to lower the molecule from the T_1 state to the ground state, i.e., a radiative process involving a change in spin state.

8 Intersystem crossing from the excited triplet state (T_1) to return to the singlet ground state non-radiatively.

These are the routes through which the state of a molecule can change. They fall into two categories; those that involve the absorption or emission of photons, and those where the molecule non-adiabatically decays to a lower energy state, with the excess energy in the system being retained in the molecule in the form of kinetic energy. The table below (Table 2-1) shows the relative time scales for photoreactions. It is worth mentioning that the main difference between fluorescence and phosphorescence is the time scale over which each occurs. Phosphorescence is a much slower process than fluorescence. Although not included in the table it is clear that, as intersystem crossing is a competitive process to fluorescence, for intersystem crossing to be effective it must occur on a shorter timescale than fluorescence.

Photoreaction type	*Rate (s^{-1})*	*Time scale (s)*
Fluorescence	10^{6}-10^{12}	ps-μs
Phosphorescence	10^{-1}-10^{6}	μs-s
Passing through a conical intersection	10^{13}-10^{11}	~100 fs-10 ps
Electron excitations	~10^{15}	fs

Table 2-1: Relative time scales for photoreactions

Figure 2-3 shows an example of a schematic PES for the ground state and first excited state of a molecule. This figure from Ref. [15] shows a 2-D slice along the reaction coordinates of a model PES, which demonstrates transitions between S_0 and S_1 as introduced in Figure 2-2.

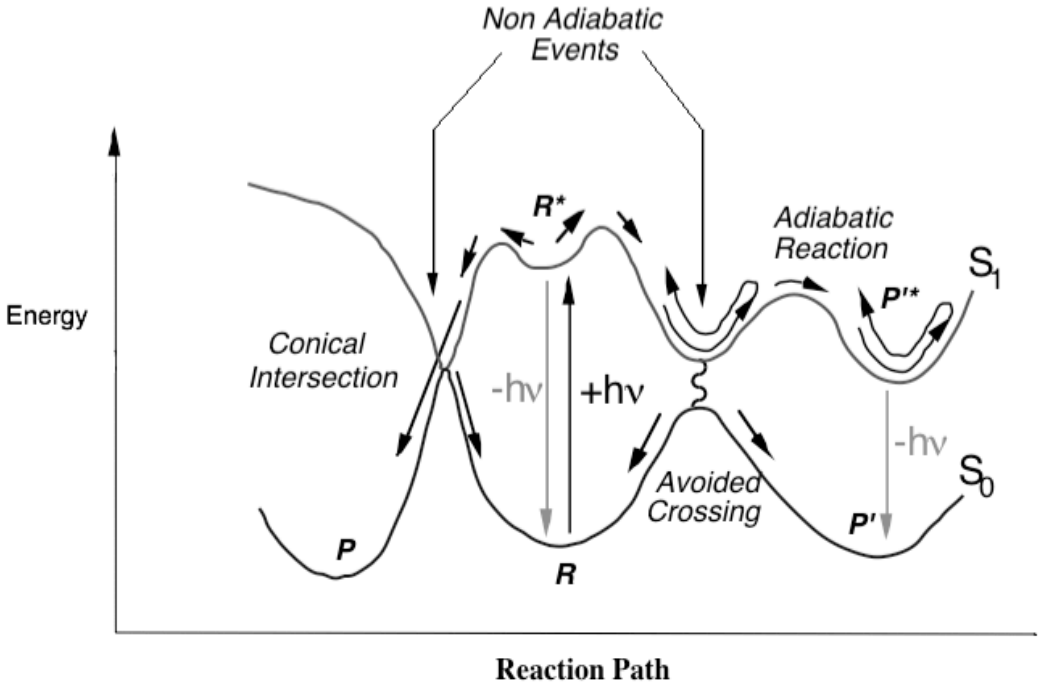

Figure 2-3: Schematic diagram of the PES of the ground and first excited singlet states (S_0 and S_1) featuring a conical intersection and an avoided crossing. Demonstrating the possible reaction pathways of a reactant R on the PES. From Ref. [15].

Considering the S_0 surface first it can be seen that it has three minima corresponding to a reactant, R, and two possible products, P and P′. Note that by "product" a stable configuration of the nuclei that differs from the initial configuration is meant. Between the reactant and the products there are energy barriers, consistent with transition states, that would have to be overcome on the ground state in order for the reactant to change to either product. However, if the reactant R is excited to the first exited state S_1 becoming R* a number of other possible reaction paths become available.

From its position on the S_1 PES, R* will begin to move adiabatically about the surface and of course can return to the ground state by emitting a photon. If the transition state barriers on the S_1 surface aren't too high the molecule can move to the other points marked on the S_1 PES changing its structure accordingly as it evolves. Note that in an excited electronic state the molecule will usually have excess kinetic energy available after a vertical transition. There are three such points marked on the figure and each represents a possible reaction path to the products on the ground state. At the point marked P′* the molecule has reached a point where it corresponds to the excited state of a product P′ marked on the ground state. If a photon were emitted at this point the molecule would radiatively return to the ground state as the product P′. Note here that the emitted radiation will generally be of longer wavelength than the originally

absorbed radiation since some of the original photon energy has been converted to kinetic energy of the nuclei. The reaction of turning R into P′ has occurred, R has changed into P′ not by a reaction on the ground state PES, but by an adiabatic reaction on the S_1 PES where R* becomes P′*. This example of a photochemical reaction is completely analogous to standard ground state chemistry, the difference being that transition barriers may be more easily overcome along the reaction coordinate in an excited electronic state.

There are two other examples of non-adiabatic internal conversions shown in Figure 2-3. Firstly, there is an avoided crossing where a minima on the S_1 is close in energy to a maximum on the ground state, at this point a radiationless decay via Landau-Zener effect can occur[16]. Once back on the ground state surface, depending on the geometry of the molecule, it can then proceed down the slope to either return to R or end up as the product P′. The second point is a conical intersection; at a conical intersection there is a point of degeneracy between the two surfaces as they actually cross. That is, at a conical intersection different electronic states have the same energy. It is a route through which the molecule can travel directly from the excited to the ground state, either returning to R or becoming the product P. The principle difference between internal conversion via an avoided-crossing or via a conical intersection is the timescales involved. Internal conversion via an avoided crossing is quite slow compared to radiationless decay via a conical intersection. It is also worth noting that in the case of polyatomic molecules it is believed there will generally be a conical intersection on the PES close to an avoided crossing.

2.2.3 Conical Intersections

As discussed earlier the BOA is an important tool that allows for chemical processes to be accurately conceptualised. However, when the motion of the nuclei and electron in a molecular system become strongly coupled, it is no longer possible to persist with an approximation that separates them. The Born Oppenheimer approximation breaks down. One such feature of the PES that exhibits such coupling is known as a conical intersection[10]. Conical intersections provide a channel through which radiationless, ultra-fast state transitions in a molecular system can occur. They have been the subject

of a great deal of work over the past 20 years[8-13, 16, 17]. These phenomena have proven difficult to investigate experimentally and provide an example of where theory and computation have helped advance the understanding of chemical processes. At the point where two or more energy states cross, where the energy levels are degenerate, the motions of the electron and nuclei become strongly coupled. When the two energy levels have different spin states this results in a surface-crossing seam that exists in M-1 dimensions. Between surfaces of the same spin however, such crossings produce a conical intersection that is actually a connected subspace of dimension M-2, called a seam (M = 3N-6, where N is number of nuclei in the system).

By travelling through the conical intersection the molecule can change from one state to another in a radiationless transition. The time scale for this is on the order of tens to hundreds of femtoseconds (the time-periods for vibrational motion of the nuclei). It is for this reason the conical intersections are also commonly called photochemical funnels. Most commonly these intersections occur between the ground state and a low-lying excited state, but do occur between higher excited states. It has been found that in polyatomic organic molecules, which typically have a high density of electronic states, that there is a high likelihood of a molecule in an excited state on the PES encountering a conical intersection before it can decay to a lower state by another path[16]. A graphical representation of a conical intersection is presented in Figure 2-4.

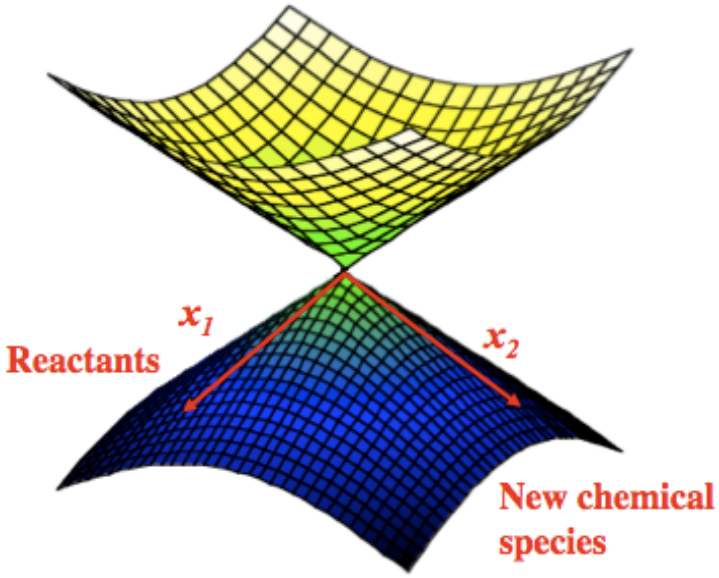

Figure 2-4: Diagram of a model Conical intersection between two states. The vertical direction is the energy and the horizontal dimensions are the gradient difference (x_1) and the interstate coupling (x_2). A reactant molecule vertically excited to the upper excited state can move on that surface through the conical intersection, returning to the original Reactants or becoming a new chemical species.

A conical intersection is characterised on the 3N-6 dimensional PES as a point at which motion in only two of the 3N-6 vibrational degrees of freedom break the degeneracy. The conical intersection is not in fact a single point, but is rather a seam made up of an infinite number of conical intersections connected by the intersection space coordinates, i.e., the remaining 3N-8 vibrational degrees of freedom[17].

The two vectors for which the degeneracy is lifted are known as the gradient difference (x_1) and the interstate coupling (x_2)[17] and have the form:

$$x_1 = \frac{\partial(\mathrm{E}_2 - \mathrm{E}_1)}{\partial \xi} \tag{2.1a}$$

$$x_2 = \left\langle C_2^t \middle| \frac{\partial \mathbf{H}_{elec}}{\partial \xi} \middle| C_1 \right\rangle \tag{2.1b}$$

Where the C_i are the configuration interaction eigenvectors (i.e., the excited and ground state adiabatic wave functions), $\mathbf{H}_{elec}$ is the Hamiltonian and ξ is a vector of Cartesian displacements. The two vectors x_1 and x_2 form a plane that governs the vibrational motion of the nuclei travelling through a conical intersection. The conical intersection can in effect serve as a photochemical pathway to several different minima. This could be the original reactant or one of several possible products. Thus reaction pathways become possible that differ to ground state chemistry. The outcome of a transition through a conical intersection depends both on its shape determined by the surfaces that form it and on the local topography of those surfaces[18, 19].

2.2.4 The Jahn-Teller Effect

The Jahn-Teller effect involves a (non-adiabatic) vibronic coupling between the components of a degenerate electronic state, as obtained from the clamped-nucleus Born-Oppenheimer Hamiltonian, for a molecule with non-abelian point group symmetry[20]. Thus, the Jahn-Teller geometry is a conical intersection between the potential energy surfaces of the component states at the high-symmetry geometry[17]. The non-adiabatic couplings can be expanded in a Taylor series leading to the concept

of linear, quadratic, etc. Jahn-Teller couplings[20]. The famous Jahn-Teller theorem[21] showed that such linear terms are non-zero for all orbitally degenerate molecules belonging to non-abelian point groups. The symmetries of vibrational modes giving rise to non-zero linear or quadratic Jahn-Teller couplings are easily derived from group theory. It should also be noted that general (non-symmetry imposed) conical intersections also have linear vibronic couplings between the (accidentally) degenerate electronic states via the von-Neumann-Wigner theorem[17]. In linear molecules, however, symmetry dictates that the linear vibronic couplings between components of a degenerate state are zero[22]. This is the well known Renner-Teller effect, and degenerate linear molecules may thus have both surfaces displaying positive curvatures, both displaying negative curvatures, or one positive and one negative curvature at the point of degeneracy (types-I, -II, and –III in terminology of Ref. [17]). The intersection here is therefore of a glancing nature.

2.2.4.1 Pseudo-Jahn-Teller Effect

The pseudo-Jahn-Teller (pJT) effect involves the coupling of non-degenerate states at second-order in vibrational displacements and is in many ways similar to the Renner-Teller effect (type-II) but with a finite energy gap between adiabatic potential energy surfaces rather than a degeneracy.

It should be noted that there is a varying terminology in the literature regarding certain aspects of the Jahn-Teller and pJT effects. The pJT effect is sometimes confusingly called the second-order Jahn-Teller effect but this term is best used to describe true (quadratic) Jahn-Teller coupling. Another practice is to use the term pJT to describe the coupling of a true Jahn-Teller system to a non-degenerate electronic state[20]. In the work of this thesis pJT is defined to mean the coupling of a non-degenerate electronic state (in the work of this thesis this is the ground state) to an excited electronic state via a non-totally symmetric vibration (or independent sets of vibrations).

The pJT effect is a very useful tool for the explanation of the local curvature of adiabatic potential surfaces of different states of a molecule[22-24]. It has been successfully applied in many areas of organic and inorganic chemistry[17, 25-29]. Its importance in structural chemistry is that it provides a mechanism by which non-degenerate states can mix via molecular vibrations. For example it provides details of

the vibronic couplings between non-degenerate electronic ground states, at high-symmetry geometries, with excited electronic states. Historically it has been used to explain why a particular system distorts from, an expected, higher symmetry geometry to a lower symmetry one[22-24, 30, 31].

The pJT effect results in potential surfaces where the lower sheet displays a quadratic instability due to coupling with an excited electronic state. The coupling causes the states to mix under a non-totally symmetric vibration. The mixing stabilizes the lower state while destabilizing the upper state. Indeed Bersuker and co-workers have proved that the pJT effect is the only source of instability in non-degenerate polyatomic molecules[32] (and References therein). They have also detailed many examples of this in action, and in recent years have shown that the excited states do not necessarily need to be too low-lying[23].

In Figure 2-5 an example of the pJT effect between the ground electronic (S_0) and first excited state (S_1) of $Mo_2(DXylF)_2$- $(O_2CCH_3)_2(\mu_2\text{-}O)_2$ complex is shown[29]. The ideal D_{2h} symmetry structure is distorted along the rhomboidal distortion normal coordinate, leading to equivalent minima of C_{2h} symmetry, by the pJT coupling between ground electronic (S_0) and first excited state (S_1). The pJT effect is discussed in more detail in Chapter 4, where it is applied to rationalise the structures of neutral and charged clusters of $(TiO_2)_n$ (n=1-4).

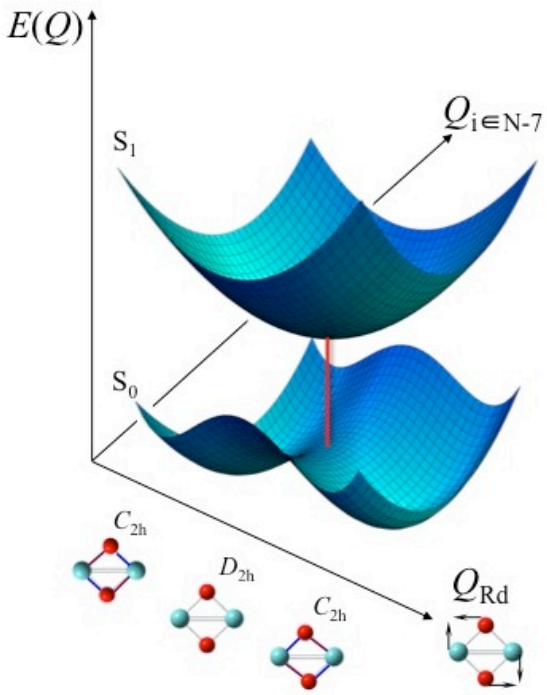

Figure 2-5: Schematic PES of the ground electronic (S_0) and first excited state (S_1) $Mo_2(DXylF)_2$-$(O_2CCH_3)_2(\mu_2\text{-}O)_2$ complex. Pseudo-Jahn-Teller coupling between the two electronic states gives the lower potential energy surface negative curvature along the rhomboidal distortion normal coordinate, leading to equivalent minima of C_{2h} symmetry. Adapted from [29].

2.3 Molecular Orbitals

The molecular orbital describes the distribution of a single electron in the electric field generated by the nuclei of the molecule and the average field of its other electrons. Molecular orbitals are described as a "fundamental quantity" in quantum chemistry[33].

The wave function that describes a single electron is called an orbital. A spatial orbital $\psi_i(\mathbf{r})$, is a function that describes the spatial distribution of an electron for any given value of **r** (where **r** is the position of the electron). However, in order to completely describe an electron, the spin of the electron must be taken into account. The electron can either have α (spin up) or β spin (spin down). So for each spatial orbital, two spin orbitals, $\chi(x)$, can be formed. The x used here denotes that the orbital is now dependant upon a spin co-ordinate (ω) as well as the original position coordinate. Where:

$$\chi_{2i-1}(x) = \psi_i(\boldsymbol{r})\alpha(\omega) \quad or \quad \chi_{2i}(x) = \psi_i(\boldsymbol{r})\beta(\omega) \tag{2.2}$$

In practice the spatial orbitals used are molecular orbitals (MO) constructed using a linear combination of the atomic orbitals (AO). Where in practice these AO are represented by a set of known basis set functions. Expanding such an unknown function in a set of known functions is not an approximation only if the basis set of known functions is complete. However, in order for the basis set to be complete it must include an infinite number of functions, which is impossible in actual calculations. It is of course desirable to represent the MO of a molecule as accurately as possible. The two factors that influence this are: the size of the basis set and how accurately the individual basis functions represent the MO. The more closely an individual basis function represents an unknown MO, the fewer basis functions are needed to represent it to the required level of accuracy. Inversely the less closely an individual basis function represents the MO, the more basis functions are required for an accurate representation and therefore for greater accuracy the larger the basis set used the better.

2.3.1 Basis Sets

The MO can be represented by a set of known basis set functions as,

$$\psi_i(\boldsymbol{r}) = \sum_{\mu=1}^{K} C_{\mu i}\phi_\mu(\boldsymbol{r}) \tag{2.3}$$

Here $\phi_\mu(\mathbf{r})$ is the known basis set function and $C_{\mu i}$ is a variable that describes the weight of each of those basis set functions in the molecular orbital $\psi_i(\mathbf{r})$. The most common form of basis sets used are made up of exponential basis functions, which have the general form:

$$\phi_\mu(\boldsymbol{r}) = f(x,y,z)e^{-\zeta r^n} \tag{2.4}$$

Where n=1 corresponds to the Slater type orbitals (STO) and n=2 corresponds to Gaussian type orbitals (GTO). ζ controls how quickly the function drops off as the distance from the nucleus increases, essentially defining the orbital size.

Originally basis functions were made up of STO that mirror the distribution of an electron around a nucleus. But the multi-centre integrals involved in polyatomic molecular calculations were difficult to solve and hampered early development. The introduction of Gaussian type orbitals (GTO) greatly simplified such calculations. Individually the GTO poorly describe the atomic orbital, lacking the "cusp" at the nucleus and dropping off too quickly far from the nucleus. This is overcome by using a number of GTO to model each AO. Thus, a greater number of GTO are required to describe each AO than would be required if STO were used. Even though GTO are inferior to STO as a basis set for representing MO, requiring more functions, this is more than compensated for by the relative decrease in the difficulty of the calculations required[2].

A basis set that contains the fewest possible functions to describe a system is known as a minimum basis set. As the size of the basis set is increased the result approaches the basis set limit, which is the limit that would be reached if an infinite basis were used. At the basis set limit there is no longer an approximation in the basis set and any difference from the experimental result is due to other approximations.

The first method used to improve on this minimum basis set is to increase the number of functions. The first step in such improvements is the doubling of all basis functions, known as 'Double Zeta' (DZ). Then triple zeta (TZ) where the number of functions are tripled and so on. However, the core orbitals of an atom are essentially independent from other atoms within a molecule, meaning that multiplying the number of these core orbitals does not really benefit the basis. This leads to the so-called 'split valence basis' where only the valence orbitals of the basis set are increased.

A further improvement that can be used to improve a given basis set is the addition of polarisation functions. These functions, of higher angular momentum functions than those included in the minimum basis functions, are important as they both assist in accurately describing the MO and as they aid in recovering electron correlation (vide infra) by providing space for the electrons to 'avoid' one another.

A large amount of the total energy of a given system is accounted for by the 1s-electrons. Hence, minimising the energy of a molecule will emphasize the optimisation of the core orbitals over the outer valence orbitals. Many properties that depend on the

wave function far from the molecule can therefore be poorly described. More generally the chemistry of a molecule is mainly dependent on the valence orbitals of the wave function and it is obviously a disadvantage if these orbitals are poorly described. These problems are overcome by augmenting the energy-optimised basis set with diffuse functions.

2.3.1.1 Contracted Basis Sets

Adding in all of these functions to the minimal basis set increases the accuracy, but this comes at greater computational cost. Equivalently, reductions in the basis set size come with a loss in accuracy and so a balance must be struck between accuracy and computational cost. Combining the full set of basis functions (primitive GTOs, PGTOs) in fixed linear combinations results in functions called contracted GTOs (CGTOs), which reduces the size of the basis set. Using these CGTO provides an increase in computational efficiency, but at the cost of lowering the accuracy and flexibility of the basis set.

There is very little change in the inner core orbitals as they are largely independent of their environment. Also, the inner core orbitals require a larger number of GTOs to describe them, because as previously stated GTO do not naturally describe the wave function cusp at the nucleus. These orbitals are therefore ideal for basis set contraction, as the downsides of the contraction are minimised.

2.3.1.2 Pople Basis Sets

An example of a classic minimum basis set is the STO-3G basis set developed by Pople and co-workers, which uses three gaussian functions contracted to form an approximate single STO representation of each atomic orbital. Very popular forms of split valence basis set are those of Pople, which have the form:

$$\text{k-nlmG} \tag{2.5}$$

The G at the end of the basis name indicates that the basis uses GTO, the k at the front indicates how many PGTOs are used for the core orbitals. After the dash (-) the nlm indicate how many PGTOs are used in each contraction of the split valence. 2 values

(nl) would indicate split valence, while here nlm indicates a triple split valence. For example 6-31G is a split valence basis, where the core orbitals are a contraction of 6 PGTOs, the inner valence orbitals are a contraction of 3 PGTO and the outer valence is a single PGTO with no contraction.

If polarisation functions are added to the basis this is indicated by terms that appear after the G. A common alternate notation is the use of * to indicate each level of polarisation functions that have been added. For instance, 6-31G* is equivalent to 6-31G(d) that has added d-type polarisation functions to heavier atoms and 6-31G** is 6-31G(d,p), which also has p-type polarisation added to hydrogen atoms. The addition of diffuse functions is indicated by the addition of + or ++ before the G. The + means diffuse s and p functions are added to heavier atoms and ++ mean that additionally diffuse s functions are added to hydrogen. These basis sets have been defined mainly for the first row elements, though some second row elements have been derived for some of the basis sets[2].

The disadvantage of segmented contraction type basis sets, such as the Pople basis sets, is that it is difficult to estimate what the basis set limit for a calculation would be. Also it is not clear that a property of interest is converged with respect to basis set size from a series of calculations. This is partly due to the fact that different PGTOs are used to produce each of the segmented basis sets. More modern accurate basis sets use a general contraction scheme that generate a sequence of basis sets that converge toward the basis set limit.

2.3.1.3 Atomic Natural Orbital Basis Sets (ANO)

The Atomic natural orbital (ANO) basis set is a contraction of a large set of PGTO made up of natural orbitals generated using a correlation calculation on the free atom[34]. The natural orbitals are those that diagonalise the density matrix and the ANO contraction selects important combinations of the PGTO from the magnitude of the orbital occupation numbers from the correlation calculation. By gradually altering the selection threshold of the occupation number an even-tempered sequence of contracted basis sets can be generated. This sequence of basis sets systematically converges toward the basis set limit.

2.3.1.4 Correlation Consistent Basis Sets

The main disadvantage of ANO is that a very large number of PGTO are required when converging toward the basis set limit. Dunning and co-workers proposed correlation consistent basis sets as a way to produce comparable results to the ANO basis sets, while using a smaller set of PGTOs. Correlation consistent basis sets are designed for recovering the correlation of the valence electrons and are built such that functions that contribute similar amounts of correlation energy are all added at the same stage.

A sequence of cc basis sets that increase in quality are defined in terms of the final number of contracted functions. These are known by the acronyms: cc-pVDZ, cc-pVTZ, cc-pVQZ, cc-pV5Z and cc-pV6Z (correlation consistent polarised Valence Double/ Triple/ Quadruple/ Quintuple/ Sextuple Zeta). The prefix aug- indicates that diffuse functions have been added to the energy-optimised cc basis set. Tight functions can also be added to the basis set in order to recover correlation contributions involving the core orbitals. These basis sets have the acronyms cc-pCVXZ (X=D, T, Q, 5).

The number of correlation consistent basis sets have been expanded extensively by Peterson et al to greatly increase the scope of systems that the cc basis sets can be applied [35]. These include all-electron correlation consistent basis sets for the first row transition metals[36]. Relativistic effects become more prominent in heavier elements as the electrons of the core attain relativistic speeds. Pseudo-potentials that represent the core orbital of the atom can account for these relativistic effects and such basis sets have been produced[35]. In the work of this thesis relativistic effects are neglected, as only first and second row elements are considered and the focus is on electron correlation effects only.

2.4 The Schrödinger Equation

$$\mathbf{H}|\Psi\rangle = \mathrm{E}|\Psi\rangle \tag{2.6}$$

This is the simplest form of the Schrödinger equation. The wave function, Ψ, is a probability wave that exists for any chemical system and which describes where the

particles of that system are most likely to be found. The wave function itself is not an observable quantity. Ψ is defined such that $|\Psi(r,t)|^2$ is the probability density of a particle being found at a point *r* at a given time *t*. Also, the integral of this probability density over all space must be normalised, intuitively to be understood that the particle must be somewhere in space. By the application of known operators to these wave function properties of the system can be determined. These mathematical expressions are in the form of eigenvalue equations, whereby an operator acts on the wave function to give the original wave function multiplied by a scalar value, called an eigenvalue. This eigenvalue is the observable of interest. The main aim of modern quantum chemistry is to obtain an accurate approximation to the wave function of a given system, from which the properties of that system may be determined. The most common way of achieving this is by finding a solution to the Schrödinger Equation.

H is the Hamiltonian operator, which is applied to the wave function and E are the eigenvalues that correspond to the energy of the system. The Hamiltonian operator for a given system of nuclei and electrons is as follows

$$\mathbf{H} = -\sum_{i=1}^{\mathrm{N}} \frac{1}{2}\nabla_i^2 - \sum_{\mathrm{A}=1}^{\mathrm{M}} \frac{1}{2M_A}\nabla_{\mathrm{A}}^2 - \sum_{i=1}^{\mathrm{N}}\sum_{\mathrm{A}=1}^{\mathrm{M}} \frac{\mathrm{Z_A}}{|\mathbf{R}_A - \mathbf{r}_i|} + \sum_{i=1}^{\mathrm{N}}\sum_{j>i}^{\mathrm{N}} \frac{1}{|\mathbf{r}_i - \mathbf{r}_j|} + \sum_{\mathrm{A}=1}^{\mathrm{M}}\sum_{\mathrm{B}>\mathrm{A}}^{\mathrm{M}} \frac{\mathrm{Z_A Z_B}}{|\mathbf{R}_\mathrm{A} - \mathbf{R}_B|} \quad (2.7)$$

Which can be written symbolically as

$$\mathbf{H} = \mathbf{T}_e + \mathbf{T}_\mathrm{n} + \mathbf{V}_{e\mathrm{n}} + \mathbf{V}_{\mathrm{ee}} + \mathbf{V}_{nn} \quad (2.8)$$

The Hamiltonian determines the total energy of the molecule. It sums up the separate energy contributions made by the interactions between the individual elements in the molecular system, i.e. the mutual attractions and repulsions of the positively charged nuclei and negatively charged electrons. Where each part is an operator that sum together to find the total energy, **T** being the kinetic energy of the electrons and nuclei respectively and **V** being the coulomb attractions and repulsions between them.

When the system is perturbed by the introduction of external potential acting on the molecule, this can be accounted for by extending the Hamiltonian with extra terms. Looking at this Hamiltonian it can be seen that it will be far from a simple task to

analytically obtain a wave function for a general molecular system. The system is in a constant state of flux, each element in the system is moving in a potential created by the other particles, which are themselves also moving, constantly changing the potential imposed on these same other particles. Thus quantum chemistry is a true many-body problem and the subject has been developed by making systematic levels of approximation to solve the complex many-body problem.

It is at this stage that the Born-Oppenheimer approximation is introduced. Through this approximation the motion of the electrons decoupled from the motion of the nuclei, greatly simplifying the molecular Schrödinger equation.

Clearly now, as the nuclei are fixed, $\mathbf{T}_n=0$ and $\mathbf{V}_{nn}$ can be replaced by a constant (V_{nn}). The electronic Schrödinger equation now has the form:

$$\mathbf{H}_{elec}\Phi_{\text{elec}} = \mathrm{E}_{elec}\Phi_{elec} \tag{2.9}$$

Where,

$$\mathbf{H}_{elec} = \mathbf{T}_e + \mathbf{V}_{e\text{n}} + \mathbf{V}_{ee} + \mathrm{V}_{nn} \tag{2.10}$$

and

$$\Phi_{elec} = \Phi_{elec}(\{\mathbf{r}_i\};\{\mathbf{R}_{\text{A}}\}) \tag{2.11}$$

Notice also that the form of the wave function has also changed becoming the electronic wave function; a semi-colon rather than a comma separates the part in brackets. This indicates that the while the function still depends explicitly on the positions of the electrons, **r**, it now depends parametrically on the positions of the nuclei, **R**. The operators can now be collected according to the number of electron indices,

$$\begin{aligned} \mathbf{h}_{\text{i}} &= -\frac{1}{2}\nabla_i^2 - \sum_{A=1}^{M}\frac{Z_A}{|\mathbf{R}_A - \mathbf{r}_i|} \\ \mathbf{g}_{ij} &= \frac{1}{|\mathbf{r}_i - \mathbf{r}_j|} \\ \mathbf{H}_e &= \sum_{i}^{N}\mathbf{h}_i + \sum_{j>i}^{N}\mathbf{g}_{ij} + \mathrm{V}_{nn} \end{aligned} \tag{2.12}$$

Where $\mathbf{h}_i$ is the one-electron operator and $\mathbf{g}_{ij}$ is the two-electron operator.

In the following sections the main computational chemistry methods used in this thesis will be introduced. Such electronic structure methods fall into three categories: ab initio (Latin for "from the beginning"), semi-empirical methods, and density functional theory. One of the most important ab initio methods is the Hartree-Fock method, as it provides the starting point upon which later ab initio methods build on.

2.5 Hartree-Fock Approximation

The Hartree-Fock approximation, which is equivalent to the molecular orbital approximation, is that each electron can be thought of as occupying a single distinct orbital. From this approximation, Hartree-Fock (HF) equation is derived, which is one of the most important ab initio methods developed to provide approximate solutions to the electronic Schrödinger equation. It has been successfully used to describe many systems, though it does have its limitations. HF usually constitutes the starting point from which more accurate methods have been developed.

The wave function for an N electron system can be constructed using a set of one-electron spin orbitals. The simplest wave function that can be constructed for an N electron system is that of a single Slater determinant (SD); the requirement that the many electron wave function be anti-symmetric with respect to electron interchange, as a consequence of the Pauli exclusion principle, being adhered to in a determinantal wave function. The form of this is shown below

$$\Psi(x_1, x_2, \cdots, x_{\mathrm{N}}) = (N!)^{-1/2} \begin{vmatrix} \chi_i(x_1) & \chi_j(x_1) & \cdots & \chi_k(x_1) \\ \chi_i(x_2) & \chi_j(x_2) & \cdots & \chi_k(x_2) \\ \vdots & \vdots & \ddots & \vdots \\ \chi_i(x_{\mathrm{N}}) & \chi_j(x_{\mathrm{N}}) & \cdots & \chi_k(x_{\mathrm{N}}) \end{vmatrix} \tag{2.13}$$

The $(N!)^{-1/2}$ term is the normalisation constant where as above N is the total number of electrons. Substituting this wave function into the electronic Schrödinger equation yields:

$$E = \langle \Psi_0 | \mathbf{H}_{elec} | \Psi_0 \rangle \tag{2.14}$$

Where $\mathbf{H}_{elec}$ is the full electronic Hamiltonian and E is the energy found using the set of spin orbitals in the SD. The variational principle states that the best possible wave function is the one that gives the lowest energy ($E=E_0$). Minimising E with respect to the choice of spin orbitals yields the HF equation, which determines the optimal spin orbitals. The HF equation is an eigenvalue equation of the form:

$$\boldsymbol{f}(i)\chi(x_i) = \varepsilon\chi(x_i) \tag{2.15}$$

$\mathbf{f}(i)$ is the Fock operator and has the form

$$\boldsymbol{f}(i) = \mathbf{h}_i + v^{\mathrm{HF}}(i) \tag{2.16}$$

In the HF equation (2.15) the many electron wave function seen in the electronic Schrödinger equation (2.9) has been replaced by the spin orbital of a single electron, *i*. The first term of the Fock operator is the one-electron operator (*vide supra*). While, the second term $v^{\mathrm{HF}}(i)$ is something new; it is the HF potential. It represents the average potential acting on the electron *i* by all of the other electrons. This is represented using the coulomb operator (**J**) and the exchange operator (**K**) as:

$$v^{HF}(i) = \sum_{j}^{N} \left(\mathbf{J}_j - \mathbf{K}_j\right) \tag{2.17}$$

where

$$\begin{aligned} J_{ij} &= \langle \chi_i(i)\chi_j(j) | \mathbf{g}_{12} | \chi_i(i)\chi_j(j) \rangle \\ K_{ij} &= \langle \chi_i(i)\chi_j(j) | \mathbf{g}_{12} | \chi_j(i)\chi_i(j) \rangle \end{aligned} \tag{2.18}$$

Using the self-consistent field method, the HF eigenvalue problem (2.15) can be solved iteratively to obtain the best set $\{\chi_k\}$ of orthogonal HF spin orbitals with orbital energies $\{\varepsilon_k\}$. The N electrons of the system occupy the N lowest energy spin orbitals. The SD formed from these occupied orbitals is the HF ground state wave function and is the best variational approximation to the ground state of the system. However the sum of the ε_k of the occupied χ_k does not equate to HF energy (E_{HF}), due to double

counting of the electron-electron interactions. The E_{HF} of the system can be computed as:

$$E_{HF} = \sum_{i=1}^{N} \varepsilon_i - \frac{1}{2}\sum_{ij}^{N}\left(J_{ij} - K_{ij}\right) + V_{nn} \tag{2. 19}$$

During these calculations, one- and two-electron integrals are required. One-electron integrals, also known as core integrals, are used with the one-electron operator. The two-electron integrals are required for the $\nu^{HF}(i)$ part. In conventional HF methods, the two-electron integrals are calculated and saved before the SCF procedure begins[2].

2.6 Electron Correlation

It is in this use of an average field, in the form of the HF potential, that the HF approximation loses accuracy. The use of such a field neglects the correlation effects of the electrons. The energy calculated by the HF method, E_{HF}, is always larger than or equal to the exact non-relativistic BO energy E_0. Therefore the correlation energy can be defined as:

$$\mathrm{E}_{corr} = \mathrm{E}_0 - \mathrm{E}_{\mathrm{HF}} \tag{2.20}$$

This correlation energy, missing from the HF method, results because of the HF potentials failure to properly account for instantaneous repulsions between the electrons in the system. The correlation energy proves important, as many of the features of a given molecule PES cannot be described accurately without the inclusion of this energy.

The correlation energy can further be divided into two forms, dynamic and static correlation. Dynamic correlation arises from this neglect of instantaneous electron repulsion (usually a large number of small collective effects), while static correlation is a result of a single determinant being qualitatively incapable of describing the system. Thus dynamic correlation is always missing but there is not always any static correlation, for example at a stable minima the correlation energy is almost exclusively dynamic in origin. When static correlation is weak, HF provides a good approximation

of the wave function, allowing the use of single reference methods that build upon HF to be used to recover the dynamic correlation. However, at stretched geometries near dissociation, for excited electronic states and near electronic degeneracies static correlation becomes much more important. These wave functions are no longer dominated by a single electronic configuration and the HF wave function stops being a good fit. Multi-configurational and multireference methods must be used in such cases to accurately describe the wave function[37]. This delineation of the two types of correlation is not completely rigorous and only the total combined correlation should be considered as a well-defined quantity. A problem being that methods (such as CASSCF discussed later) designed to recover static correlation invariably also recover (a somewhat uncontrolled) amount of dynamic correlation. Further dynamic correlation can be recovered using perturbative methods (for example CASPT2) at the expense of even more computer time.

The main aim of the methods that have built on the HF method is to attempt to recover the correlation energy and resolve an energy value for a system closer to the exact energy. The three main methods that have been developed to achieve this are Configuration Interaction (CI), Many-Body Perturbation Theory (MBPT) and Coupled Cluster theory (CC). All three go beyond a single electronic configuration description of the molecular system and of the three perhaps the easiest to understand is Configuration Interaction[37-39].

2.7 Configuration Interaction

The HF method uses a single Slater determinant to define the wave function of a molecular system. This Slater determinant represents a single configuration that the electrons adopt in the spin orbitals defined. The configuration is of the ground state where the N electrons of the system occupy the N lowest energy spin orbitals. The basic idea of CI is that by adding other Slater determinants to the wave function, which represent other electron configurations, higher energy orbitals in the wave function can become partially filled. This has the effect of increasing the average distance between the electrons, recovering part of the electron correlation energy. If this is extended so

that every possible electron configuration is included in the wave function it is called full Configuration Interaction (FCI). The FCI wave function can be written as:

$$|\Phi\rangle = c_0|\Psi_0\rangle + \sum_{ra} c_a^r|\Psi_a^r\rangle + \sum_{\substack{a<b \\ r<s}} c_{ab}^{rs}|\Psi_{ab}^{rs}\rangle + \sum_{\substack{a<b<c \\ r<s<t}} c_{abc}^{rst}|\Psi_{abc}^{rst}\rangle + \cdots \tag{2.21}$$

The first term ($c_0|\Psi_0\rangle$) represents the ground state configuration. The second term ($\sum_{ra} c_a^r|\Psi_a^r\rangle$) represents all of the configurations where a single electron has been excited to a higher orbital. The third term includes all of the doubly excited determinants and so it goes on until all possible determinants are included. The expansion coefficients preceding the determinants in each of the terms give the weight of that determinant in the final wave function. By optimising these coefficients the occupancy of each spin orbital can be determined, it is this that allows the orbitals to become partially filled. If FCI is expanded in an infinite basis set the wave function constructed would be the exact wave function and all of the correlation energy would be recovered. However, as it is obviously not possible to use an infinite basis, the wave function constructed in a given basis using FCI represents the best approximation of the exact wave function possible for that basis. As larger and larger basis sets are used so the wave function defined converges towards the exact wave function. FCI is in practice the exact solution to the Schrödinger equation for a given basis set, but the complications associated with performing such calculations have restricted the application of FCI to only the smallest of systems.

Given a basis set of 2K one-electron spin orbitals and an N electron molecular system, the number of N electron Slater determinants required for FCI is

$$\binom{2\mathrm{K}}{\mathrm{N}} = \frac{(2\mathrm{K})!}{\mathrm{N}!\,(2\mathrm{K}-\mathrm{N})!} \tag{2.22}$$

For all but the smallest system the number of determinants required for a FCI makes the calculations totally impractical. Using symmetry considerations and/or configuration state functionals (CSF) the size of system studied can be increased slightly by reducing the number of terms involved in the FCI calculation. A CSF is a symmetry-adapted linear combination of SDs constructed to have the same quantum numbers as the wave function of the system being studied. Fewer CSFs are required to express the wave

function in comparison to SDs, which reduces the size of the FCI calculation. Though this comes at the price of having to first generate the CSFs and the increase in system size that can be studied is marginal. FCI remains important still as it provides a basis from which new approximate methods can be built and also in providing a benchmark for such methods developed[37].

The two factors that restrict the size of system that can be investigated using a FCI calculation are (i) the generation of, and possible need to store, the H_{ij} matrix and (ii) the diagonalisation of the matrix H_{ij} becoming extremely large as the size of the system increases. These problems are addressed directly by in someway restricting the size of the H_{AB} matrix that is generated. This is possible because of the many configurations generated very few contribute significantly to the energy solution for the system. The problem though is that it hasn't proved possible to predict in advance which of the configurations generated in a FCI calculation are the important ones.

Determining which of the possible configurations to include in a CI calculation, and which can be left out, is therefore a main concern for all CI methods. It becomes necessary to develop truncated versions of the FCI method that recover as much of the correlation energy as possible, while lowering the computational cost to a more practical level. Two approaches used to achieve this are to literally truncate the FCI wave function (2.21) and through the use of Multi-Configuration Self-Consistent Field methods (MCSCF).

2.7.1 Truncated CI

The most common way to truncate the FCI calculation is by restricting what levels of excited determinant are included in the wave function. So for example CISD is configuration interaction with singles and doubles, only the terms that represent single and double electron excitations are included. For a small molecule at equilibrium geometry the CISD method will recover around 95% of the correlation energy[39]. The physical basis for this truncation is that the Hamiltonian operator (2.8) contains only two-body Coulomb terms and thus the most important extra determinants will be those differing by up to two spin-orbitals. Such truncated methods can still require a large number of determinants, though fewer than FCI, and care must be used to insure that the

truncated method used still accurately models the system. A relatively new method for truncating FCI is Monte Carlo Configuration Interaction (MCCI) that uses a randomly selected set of configurations in the wave function[40-46]. The MCCI method is the focus of work in chapters 5 and 6 and the method is described in more depth there.

A method that doesn't calculate energy values that scale linearly with the size of molecular systems is said to not be size consistent. All truncated CI methods are not size consistent. This is a problem, as the energies of different systems can't be easily compared, as there is no linear relationship between them.

2.7.2 MCSCF

The MCSCF method involves generating a number of configurations determined by a given set of rules. This involves classifying the one-electron spin orbitals into various sections, each defining how the electrons are treated in the multi-configurations generated. The basic equation for the MCSCF wave function is:

$$|\Psi_{MCSCF}\rangle = \sum_{I} c_I |\Psi_I\rangle \tag{2.23}$$

The wave function is generated by simultaneously optimising both the expansion coefficients (c_I) and the molecular orbitals using self-consistent field method. A prominent example of MCSCF is the Complete Active Space Self-Consistent Field (CASSCF) method that uses a FCI calculation on a subset of the molecular orbitals.

2.7.2.1 Complete Active Space Self-Consistent Field (CASSCF)

A description of the CASSCF method is included in some of the references at the start of this chapter, however it is a specialised method and is described in more detail in more advanced texts[7, 33, 47]. Within the CASSCF method the one-electron spin orbitals are divided into three classes: core, valence and virtual. Figure 2-6 below shows a comparison between the molecular orbital partitions used in HF and those in CASSCF[1].

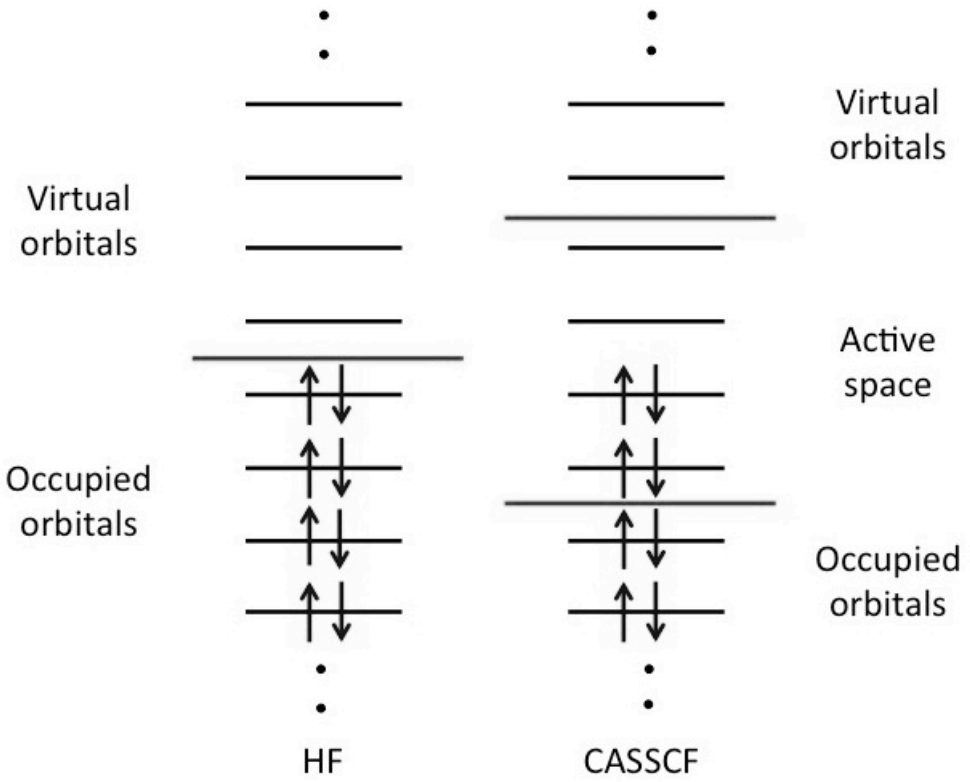

Figure 2-6: Comparison of HF and CASSCF MO

The core orbitals are a set of spin orbitals that are considered doubly occupied for every configuration in the CASSCF wave function, while the virtual spin orbitals are always empty. Between these two is the valence orbitals, which is a set of partially occupied orbitals within which a FCI expansion happens. These rules determine the possible configurations that can be included in the wave function. A set of Slater determinants (or spin-adapted configuration state functions) is generated for every possible excitation of these valence electrons within the valence orbitals, for which the core orbitals are always doubly occupied and the virtual orbitals are always empty. The configurations generated allow for the spin orbitals in the valence orbitals to become partially filled recovering part of the correlation energy in the same way as the standard CI method. This separation of orbitals is possible because it is assumed that the lower energy orbitals of the molecule are effectively constant for the chemical process under consideration. The main objective of CASSCF is not to recover dynamic correlation through large CI expansions but rather to obtain a qualitatively correct wave function when static correlation is important, i.e. when several electronic configurations are equally important. The power of CASSCF is the dual optimization of both orbitals and CI expansion coefficients. Thus, the orbitals obtained represent the best orbitals possible for the given CI expansion. Note that in standard CI methods the orbitals are

fixed (usually HF ones), and the CI expansion is very slowly convergent in these fixed orbitals.

CASSCF is considered to be a non black box method. The user is required to define which orbitals are included in each section, which requires an understanding of the molecular system and the problem to be investigated. Unlike the other methods previously described, where the user merely had to define the method and basis set. Thus in CASSCF the art of running calculations is to define the orbital subspaces appropriately for the system under investigation. It is entirely probable that two aspects of the same chemical system would require differently defined active spaces.

2.8 Perturbation Methods

Given a reference solution that is close to the exact solution, perturbation theory can be used to improve the reference solution in relation to the exact solution. All types of correction (S, D, T, Q, etc.) are added to the reference wave function up to a given order (2, 3, 4, etc.). Perturbation methods are used in quantum mechanics to recover dynamic correlation where static correlation has been adequately treated in the reference configuration(s). In effect the Hamiltonian can be defined as consisting of two parts $\mathbf{H}_0$ the reference and a perturbation $\mathbf{H}'$,

$$\mathbf{H} = \mathbf{H}_0 + \lambda \mathbf{H}' \tag{2.24}$$

where λ is variable that determines the strength of the perturbation and the perturbed Schrödinger equation is given as:

$$\mathbf{H}\Psi = W\Psi \tag{2.25}$$

Here if λ=0, $\mathbf{H}=\mathbf{H}_0$, $\Psi=\Phi_0$ and $W=E_0$. As the perturbation is increased from zero to a finite value, W and Ψ must also change. They can be written as a Taylor expansion in the powers of λ.

$$W = \lambda^0 W_0 + \lambda^1 W_1 + \lambda^2 W_2 + \lambda^3 W_3 + \cdots + \lambda^n W_n \tag{2.26}$$

$$\Psi = \lambda^0\Psi_0 + \lambda^1\Psi_1 + \lambda^2\Psi_2 + \lambda^3\Psi_3 + \cdots + \lambda^n\Psi_n \tag{2.27}$$

The Ψ_1, Ψ_2,… and W_1,W_2,… are the first-order, second-order, etc., corrections. Setting the λ parameter to 1, the nth-order energy or wave function becomes a sum of the terms up to order n. This creates a hierarchy of perturbation corrections converging on the exact solution. For example the Moller-Plesset (MP) perturbation theory, which uses the Fock operators as its basis (MP2, MP3, etc.).

Using the CASSCF method the static correlation is recovered returning a qualitatively correct wave function. Further to this a perturbative calculation can be included to recover additional dynamic correlation, this is the so-called CASPT2 calculation that includes a second-order perturbative correction[33].

2.9 Coupled Cluster Theory (CC)

The coupled cluster method differs from CI theory in that its wave function is constructed in the exponential ansatz[7, 48].

$$|\Psi\rangle = e^{\mathbf{T}}|\Psi_0\rangle \tag{2.28}$$

Where $|\Psi_0\rangle$ is the Hartree-Fock reference wavefunction and **T** is the cluster operator, which has the form:

$$\mathbf{T} = \mathbf{T}_1 + \mathbf{T}_2 + \mathbf{T}_3 + \cdots + \mathbf{T}_n \tag{2.29}$$

$\mathbf{T}_1$ is the operator for all single excitations; $\mathbf{T}_2$ is the operator for all double excitations and so on until all possible excitations are included. Expanding $e^{\mathbf{T}}$ as a Taylor series:

$$e^{\mathbf{T}} = 1 + \mathbf{T} + \frac{1}{2!}\mathbf{T}^2 + \frac{1}{3!}\mathbf{T}^3 + \cdots = \sum_{k=0}^{\infty}\frac{1}{k!}\boldsymbol{T}^k \tag{2.30}$$

Combining this with (2.29) gives:

$$e^{\boldsymbol{T}} = \mathbf{1} + \boldsymbol{T}_1 + \left(\boldsymbol{T}_2 + \frac{1}{2}\boldsymbol{T}_1^2\right) + \left(\boldsymbol{T}_3 + \boldsymbol{T}_2\boldsymbol{T}_1 + \frac{1}{6}\boldsymbol{T}_1^3\right) + \cdots \quad (2.31)$$

Where the first term (**1**) will include the reference wave function, $\mathbf{T}_1$ includes all the single excitations, the first bracket all the doubles and so on. When the equation is expanded to include all possible terms it is equivalent to the FCI equation, with all of the same problems. The strength of CC is that when the wave function is truncated at a certain excitation level, the exponential form of the wave function allows that higher excitations are included in the solution as products of the lower excitation levels. For instance at the CCSD level the so-called "connected" triplet excitations ($\mathbf{T}_3$) are left out but disconnected triplet excitations remain ($\boldsymbol{T}_2\boldsymbol{T}_1 + \frac{1}{6}\boldsymbol{T}_1^3$). A hierarchy of approximate CC methods is produced by this truncation (Table 2-2), which has very good improvements in accuracy at each step.

CC method	**T**	$e^{\mathbf{T}}$
CCS	$\mathbf{T}_1$	$\mathbf{1} + \boldsymbol{T}_1 + \frac{1}{2}\boldsymbol{T}_1^2 + \frac{1}{6}\boldsymbol{T}_1^3 + \cdots$
CCSD	$\mathbf{T}_1 + \mathbf{T}_2$	$\mathbf{1} + \boldsymbol{T}_1 + \boldsymbol{T}_2 + \frac{1}{2}\boldsymbol{T}_1^2 + \boldsymbol{T}_2\boldsymbol{T}_1 + \frac{1}{6}\boldsymbol{T}_1^3 + \cdots$
CCSDT	$\mathbf{T}_1 + \mathbf{T}_2 + \mathbf{T}_3$	$\mathbf{1} + \boldsymbol{T}_1 + \boldsymbol{T}_2 + \frac{1}{2}\boldsymbol{T}_1^2 + \boldsymbol{T}_3 + \boldsymbol{T}_2\boldsymbol{T}_1 + \frac{1}{6}\boldsymbol{T}_1^3 + \cdots$

Table 2-2: First three truncated CC methods with their cluster operator and the exponential of the cluster operator up to

In practice, the cost of the methods increases dramatically with each step in the hierarchy. CCSDT is a very computationally expensive method and could only be applied to the smallest of systems. However, methods in between CCS and CCSD and between CCSD and CCSDT can be constructed using additional approximations[48].

One-way to achieve this is to add in approximations of missing connected excitations using perturbation theory. A perturbative non-iterative correction is added to the truncated CC method to approximate methods higher in the hierarchy. The most popular example of this is the CCSD(T) method where the CCSD result is corrected by adding estimations of the connected triples from MP4 to approximate CCSDT.

A major drawback of these intermediate methods, which utilise perturbative corrections, is that their non-iterative nature means they cannot be used to calculate excitation

energies and frequency-dependent molecular properties[48]. This has given rise to two new intermediate CCn methods (CC2 and CC3) designed to be able to calculate these molecular properties.

In the CC2 method the singles are treated in the same way as CCSD, where possible perturbations in an orbital un-relaxed fashion are accounted for, but the doubles are approximated to the lowest non-vanishing order of a fluctuation operator. The same philosophy is applied in higher order to produce CC3 as an approximated CCSDT model. The treatment of singles and doubles in CC3 is identical to that of CCSDT, while the triples are approximated to the lowest non-vanishing order[48]. In terms of the quality of the results the excited state results of CC2 are comparable to the MP2 results for the ground state. While those of CC3 are comparable to CCSD(T), which is considered the 'gold standard' of ground state quantum chemistry.

CC2 has been successfully combined with the resolution of identity approximation to allow wave function based calculations of excited states in large organic molecules[49]. This method is currently one of the most frequently used methods for excited electric states outside of TD-DFT, e.g., in the program Turbomole[50], and is believed to be a robust excited state method for organic chromophores having generally performed well in benchmarks[51, 52]. Later in this thesis CC2, and other lower cost CC methods, are applied to inorganic systems. For that discussion it is important to note that in order to achieve consistency between the electron correlation and orbital relaxation the CC operators are similarity transformed via the singles operators and amplitudes. This is a very dramatic effect on the utility of the CCn methods when the singles amplitudes are large, i.e., when the HF orbitals are very poor in strongly correlated systems.

In Figure 2-7 the hierarchy CC methods is plotted against a basis set that systematically improves in quality. By simultaneously improving both the FCI limit can be approached.

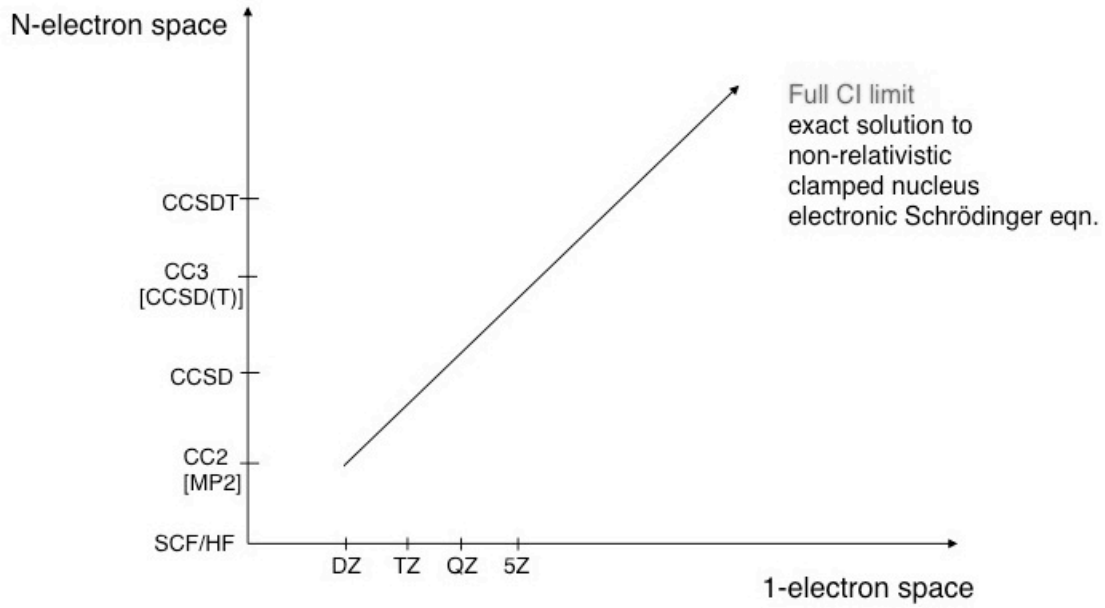

Figure 2-7: Coupled cluster N-electron space against the basis set 1-electron space. Both axes provide a systematic route to improve on the calculated results, approaching the FCI limit.

2.10 Density Functional Theory (DFT)

Density functional theory (DFT) differs from the methods discussed earlier in that, rather than a wave function basis, it is based on electron density. Hohenberg and Kohn proved that the ground state electronic energy is completely described by the electron density, ρ, of the system. A functional for the total energy can be defined in the same way as the Hamiltonian for wave function methods, but using the electron density as a variable.

$$\mathrm{F}[\rho(\boldsymbol{r})] = \mathbf{T}_e[\rho(\boldsymbol{r})] + \boldsymbol{V}[\rho(\boldsymbol{r})] + \mathrm{E}_{ncl}[\rho(\boldsymbol{r})] \tag{2.32}$$

$\mathbf{T}_e$ is the electron kinetic energy, $\boldsymbol{V}$ is the coulomb interactions and E_{ncl} is the non-classical portion due to self-interaction correction, exchange (i.e., anti-symmetry) and electron correlation effects. Of these only the coulomb interactions can be explicitly defined. Early attempts to design DFT models weren't successful as there is a difficulty in computing the electron kinetic energies from such models. However, in 1965 Kohn and Sham introduced the ideas that the electron density should be represented by a set of non-interacting orbitals. Therefore, considering the non-interacting kinetic energy rather than the true kinetic energy, which alleviated this problem. Crucially, these non-

interacting orbitals should be taken to have the same density as those of the system where the electrons do interact. However, the non-interacting kinetic energy is not equal to the true kinetic energy ($\mathbf{T}_{ks} \neq \mathbf{T}$). To account for the difference the functional is separated to include the so-called exchange-correlation energy.

$$\mathrm{F}[\rho(\boldsymbol{r})] = \mathbf{T}_{ks}[\rho(\boldsymbol{r})] + \boldsymbol{V}[\rho(\boldsymbol{r})] + \mathrm{E}_{\mathrm{XC}}[\rho(\boldsymbol{r})] \tag{2.33}$$

Where:

$$\mathrm{E}_{\mathrm{XC}}[\rho(\boldsymbol{r})] = \mathbf{T}_{c}[\rho(\boldsymbol{r})] + \mathrm{E}_{ncl}[\rho(\boldsymbol{r})] \tag{2.34}$$

$\mathbf{T}_c$ is the correction to the kinetic energy. In essence the exchange-correlation energy contains all of the unknowns and this is the major problem for DFT, that the exact form of the exchange-correlation functional is unknown. The effort to approximate this unknown has spawned a host of different density functional methods. A hierarchy of DFT functionals has been formed, however often a better result is found with a simpler functional (B3LYP) than for more powerful, higher ranked functionals. With the further problems that while a good result is found for one system the functional won't automatically work well for another containing different atoms and that it is impossible to systematically improve the results.

The most popular of the DFT methods is B3LYP[53]. It is made up of the Becke's exchange 3 parameter functional (B3), which incorporates a percentage of the exact exchange from the Hartree-Fock method, with the LYP functional of Lee, Yang and Parr[54]. B3LYP can be further combined with a long-range correction using the coulomb-attenuating method (CAM), in the form of CAM-B3LYP[55].

2.11 Response Theory

The linear response theory assumes that there is a weak perturbation to the Hamiltonian, meaning that the solution can be written in terms of the eigenstates of the unperturbed system.

$$\boldsymbol{H}(t) = \boldsymbol{H}_0 + \boldsymbol{V}(t) \tag{2.35}$$

The perturbation can be usually an oscillating electric field, which has the form:

$$\boldsymbol{V}(t) = \sum_k e^{-i\omega_k t}\,\mathbf{Q}\boldsymbol{F}_k \tag{2.36}$$

Where ω_k is the frequency of the field, $\mathbf{F}_k$ is the field strength and **Q** is the perturbation operator. The expectation value of a given operator **P** can be expanded in terms of the perturbations Q, R, …etc. [2].

$$\begin{aligned}\langle \boldsymbol{P}\rangle(t) = \langle \boldsymbol{P}\rangle(0) &+ \sum_k e^{-i\omega_k t}\,\langle\langle \mathbf{P};\mathbf{Q}\rangle\rangle_{\omega_k}\mathbf{F}_k \\ &+ \frac{1}{2}\sum_{k,l} e^{-i(\omega_k-\omega_l)t}\,\langle\langle \mathbf{P};\mathbf{Q},\mathbf{R}\rangle\rangle_{\omega_k,\omega_l}\mathbf{F}_k\mathbf{F}_l + \cdots\end{aligned} \tag{2.37}$$

The first term ($\langle \boldsymbol{P}\rangle(0)$) is the static expectation value, the second term is the linear response, the third term is the quadratic response, and so on. In the case of an excitation of the molecule by light the perturbation **Q** is the dipole operator ($\boldsymbol{\mu}$) and $\mathbf{F}_k$ is a vector containing the x,y,z components of the field. When **P**=**Q**=**R**=$\boldsymbol{\mu}$, equation (2.37) is the linear response term $\langle\langle \mu;\mu\rangle\rangle_{\omega_k}$, which gives information on the excited state transitions. In the energy representation the linear response equation has the form:

$$\langle\langle \boldsymbol{\mu_a},\boldsymbol{\mu_b}\rangle\rangle_{\omega_k} == -\boldsymbol{\Pi}^{ab}\sum_{j\neq 0}\frac{\langle\psi_0|\boldsymbol{\mu_a}|\psi_j\rangle\langle\psi_j|\boldsymbol{\mu_b}|\psi_0\rangle}{(\omega_k-\omega_j)} \tag{2.38}$$

Poles occur where $\omega_k = \omega_j$. They correspond to excitation energies and the residues give the oscillator strengths between the ground state (ψ_0) and the excited state of interest (ψ_j).

In this representation all excitations are considered e.g. all single excitations and de-excitations, all double excitations and de-excitations, etc. At this level everything is exact, analogous to the FCI approach, but is very computationally expensive. Therefore, truncating the method, restricting the excitation level, generates an approximate version. The simplest approximate version corresponds to using the

Hartree-Fock reference and including only single excitations and de-excitations, which is known as the Random phase approximation (RPA). This is identical to the time-dependent Hartree-Fock (TD-HF) method[56] and corresponds to the time-dependent density functional method (TD-DFT) of DFT[56, 57]. When used with the coupled cluster wave function this approach is known as the Equation of Motion method (EOM-CC), the most common version of which is EOM-CCSD[58]. If the expansion is extended to the second order and a MP reference wave function is used, this is the second order polarisation propagator approximation (SOPPA) method[59]. The hybrid SOPPA(CCSD) method[60] corresponds to the SOPPA method with the first- and second- order perturbation coefficients replaced with the CCSD amplitudes.

CC and DFT methods are ostensibly ground state methods and aren't therefore directly applicable to excited states. Response theory provides a means by which such ground state methods can be applied to excited states. Excitation energies and transition moments are obtained from poles and residues of response functions using otherwise ground state methods in conjunction with response theory.

When combined with hierarchy of CC methods, response theory can produce a hierarchy of results for these excitation energies and transition moments. The response theory results are systematically improved as higher order CC methods are applied (CCS, CC2, CCSD, CC3, ... etc.).

2.12 References

[1] Cramer, C. J., *Essentials of computational chemistry: Theories and models*. 2nd ed.; John Wiley & Sons, Ltd: 2004; p 579.

[2] Jensen, F., *Introduction to computational chemistry*. 2nd ed.; Wiley: 2007.

[3] Szabo, A.; Ostlund, N. S., *Modern quantum chemistry : Introduction to advanced electronic structure theory*. 1st ed. rev. ed.; Dover: 1996.

[4] Atkins, P.; de Paula, J., *Atkins' physical chemistry*. Seventh Edition ed.; Oxford University Press: 2002.

[5] Atkins, P.; Friedman, R., *Molecular quantum mechanics*. Fourth Edition ed.; Oxford University Press: 2005.

[6] Turro, N. J.; Ramamurthy, V.; Scaiano, J. C., *Principles of molecular photochemistry an introduction*. 1st edition ed.; University Science Books: 2009.

[7] Cimiraglia, R., Methods of calculation of excited states. In Dipartimento di Chimica, Universita di Ferrara.

[8] Atchity, G. J.; Xantheas, S. S.; Ruedenberg, K., Potential-energy surfaces near intersections. *Journal of Chemical Physics* **1991,** 95, 1862-1876.

[9] Levine, B. G.; Martinez, T. J., Isomerization through conical intersections. *Annual Review of Physical Chemistry* **2007,** 58, 613-634.

[10] Worth, G. A.; Cederbaum, L. S., Beyond born-oppenheimer: Molecular dynamics through a conical intersection. *Annual Review of Physical Chemistry* **2004,** 55, 127-158.

[11] Yarkony, D. R., Diabolical conical intersections. *Reviews of Modern Physics* **1996,** 68, 985-1013.

[12] Yarkony, D. R., Conical intersections: Diabolical and often misunderstood. *Accounts of Chemical Research* **1998,** 31, 511-518.

[13] Yarkony, D. R., Nuclear dynamics near conical intersections in the adiabatic representation: I. The effects of local topography on interstate transitions. *Journal of Chemical Physics* **2001,** 114, 2601-2613.

[14] Simons, J., *An introduction to theoretical chemistry*. Cambridge University Press: 2003.

[15] Robb, M. A.; Garavelli, M.; Olivucci, M.; Bernardi, F., A computational strategy for organic photochemistry. *REVIEWS IN COMPUTATIONAL CHEMISTRY, VOL 15* **2000,** 15, 87-146.

[16] Bernardi, F.; Olivucci, M.; Robb, M. A., Potential energy surface crossings in organic photochemistry. *Chemical Society Reviews* **1996,** 25, 297-369.

[17] Paterson, M. J.; Bearpark, M. J.; Robb, M. A.; Blancafort, L.; Worth, G. A., Conical intersections: A perspective on the computation of spectroscopic Jahn-Teller parameters and the degenerate 'intersection space'. *Physical Chemistry Chemical Physics* **2005,** 7, 2100-2115.

[18] Paterson, M. J.; Bearpark, M. J.; Robb, M. A.; Blancafort, L., The curvature of the conical intersection seam: An approximate second-order analysis. *Journal of Chemical Physics* **2004,** 121, 11562-11571.

[19] Paterson, M. J.; Robb, M. A.; Blancafort, L.; DeBellis, A. D., Mechanism of an exceptional class of photostabilizers: A seam of conical intersection parallel to excited state intramolecular proton transfer (esipt) in o-hydroxyphenyl-(1,3,5)-triazine. *Journal of Physical Chemistry A* **2005,** 109, 7527-7537.

[20] Worth, G. A.; Cederbaum, L. S., Beyond born-oppenheimer: Molecular dynamics through a conical intersection. *Annual Review of Physical Chemistry* **2004,** 55, 127-158.

[21] Jahn, H. A.; Teller, E., Stability of polyatomic molecules in degenerate electronic states. I. Orbital degeneracy. *Proceedings of the Royal Society of London. Series A, Mathematical and Physical Sciences* **1937,** 161, 220-235.

[22] Bersuker, I. B., Modern aspects of the Jahn-Teller effect theory and applications to molecular problems. *Chemical Reviews* **2001,** 101, 1067-1114.

[23] Bersuker, I. B., The Jahn-Teller effect as a general tool for solving molecular and solid state problems: Novel findings. *J. Mol. Struct.* **2007,** 838, 44-52.

[24] Bersuker, I. B.; Balabanov, N. B.; Pekker, D.; Boggs, J. E., Pseudo-Jahn-Teller origin of instability of molecular high-symmetry configurations: Novel numerical method and results. *Journal of Chemical Physics* **2002,** 117, 10478-10486.

[25] Bearpark, M. J.; Blancafort, L.; Robb, M. A., The pseudo-Jahn-Teller effect: A CASSCF diagnostic. *Molecular Physics* **2002,** 100, 1735-1739.

[26] Blancafort, L.; Bearpark, M. J.; Robb, M. A., Ring puckering of cyclooctatetraene and cyclohexane is induced by pseudo-Jahn-Teller coupling. *Molecular Physics* **2006,** 104, 2007-2010.

[27] McKinlay, R. G.; Paterson, M. J., The Jahn–Teller effect in binary transition metal carbonyl complexes, *The Jahn-Teller Effect*. In Köppel, H.; Yarkony, D. R.; Barentzen, H., Eds. Springer Berlin Heidelberg: 2009; Vol. 97, pp 311-344.

[28] McKinlay, R. G.; Zurek, J. M.; Paterson, M. J., Vibronic coupling in inorganic systems: Photochemistry, conical intersections, and the Jahn-Teller and pseudo-Jahn-Teller effects. In *Advances in inorganic chemistry*, Rudi van Eldik; Harvey, J., Eds. Elsevier Inc.: 2010; Vol. 62, p 351.

[29] Zurek, J. M.; Paterson, M. J., Theoretical study of the pseudo-Jahn-Teller effect in the edge-sharing bioctahedral complex $mo_2(dxyif)_2(o_2cch_3)_2(\mu_2\text{-}o)_2$. *Inorg. Chem.* **2009,** 48, 10652-10657.

[30] Paterson, M. J.; Chatterton, N. P.; McGrady, G. S., View from the bridge: A pseudo-Jahn-Teller approach to transition metal hydrosilane complexes. *New J. Chem.* **2004,** 28, 1434-1436.

[31] Pearson, R. G., Concerning Jahn-Teller effects. *Proceedings of the National Academy of Sciences of the United States of America* **1975,** 72, 2104-2106.

[32] Bersuker, I. B., *The Jahn-Teller Effect*. Cambridge University Press: Cambridge, UK ; New York, 2006; p xvi, 616 p.

[33] Roos, B. O., Multiconfigurational quantum chemistry. In *Theory and applications of computational chemistry: The first forty years*, Dykstra, C., Ed. Elsevier B. V.: 2005; pp 725-764.

[34] Pou-Amérigo, R.; Merchán, M.; Nebot-Gil, I.; Widmark, P.-O.; Roos, B., Density matrix averaged atomic natural orbital (ANO) basis sets for correlated molecular wave functions. *Theoret. Chim. Acta* **1995,** 92, 149-181.

[35] Peterson, K. A. Peterson research group: Correlation consistent basis sets. http://tyr0.chem.wsu.edu/~kipeters/basis.html

[36] Balabanov, N. B.; Peterson, K. A., Systematically convergent basis sets for transition metals. I. All-electron correlation consistent basis sets for the 3d elements Sc--Zn. *The Journal of Chemical Physics* **2005,** 123, 064107-15.

[37] Knowles, P.; Schutz, M.; Werner, H.-J., Ab initio methods for electron correlation in molecules. In *winterschool, 21 - 25 February 2000*, Grotendorst, J., Ed. John von Neumann-Institute for Computing: Forschungszentrum Jülich, 2000; Vol. 3, p 638.

[38] Shavitt, I., The history and evolution of configuration interaction. *Molecular Physics* **1998,** 94, 3-17.

[39] Sherrill, D. C., An introduction to configuration interaction theory. In School of Chemistry and Biochemistry, Georgia Institute of Technology: 1995.

[40] Coe, J. P.; Taylor, D. J.; Paterson, M. J., Calculations of potential energy surfaces using Monte Carlo configuration interaction. *The Journal of Chemical Physics* **2012,** 137, -.

[41] Coe, J. P.; Taylor, D. J.; Paterson, M. J., Monte Carlo configuration interaction applied to multipole moments, ionization energies, and electron affinities. *Journal of Computational Chemistry* **2013,** 34, 1083-1093.

[42] Greer, J. C., Estimating full configuration-interaction limits from a monte-carlo selection of the expansion space. *Journal of Chemical Physics* **1995,** 103, 1821-1828.

[43] Greer, J. C., Consistent treatment of correlation-effects in molecular dissociation studies using randomly chosen configurations. *Journal of Chemical Physics* **1995,** 103, 7996-8003.

[44] Greer, J. C., Monte carlo configuration interaction. *Journal of Computational Physics* **1998,** 146, 181-202.

[45] Grein, F., Density functional theory and multireference configuration interaction studies on low-lying excited states of TiO_2. *Journal of Chemical Physics* **2007,** 126, 034313.

[46] Győrffy, W.; Bartlett, R. J.; Greer, J. C., Monte carlo configuration interaction predictions for the electronic spectra of Ne, CH_2, C_2, N_2, and H_2O compared to full configuration interaction calculations. *Journal of Chemical Physics* **2008,** 129, 064103.

[47] Robb, M. A.; Bernardi, F., Ab initio modelling of chemical reactivity using mc-scf and vb methods. *Theoretical and Computational Models for Organic Chemistry* **1991,** 339.

[48] Christiansen, O., Coupled cluster theory with emphasis on selected new developments. *Theor Chem Account* **2006,** 116, 106-123.

[49] Hättig, C.; Weigend, F., CC2 excitation energy calculations on large molecules using the resolution of the identity approximation. *The Journal of Chemical Physics* **2000,** 113, 5154-5161.

[50] *Turbomole v6.2 2010*, a development of University of Karlsruhe and Forschungszentrum Karlsruhe GmbH, 1989-2007, TURBOMOLE GmbH, since 2007; available from http://www.turbomole.com.

[51] Sauer, S. P. A.; Schreiber, M.; Silva-Junior, M. R.; Thiel, W., Benchmarks for electronically excited states: A comparison of noniterative and iterative triples corrections in linear response coupled cluster methods: CCSDR(3) versus CC3. *Journal of Chemical Theory and Computation* **2009,** 5, 555-564.

[52] Schreiber, M.; Silva-Junior, M. R.; Sauer, S. P. A.; Thiel, W., Benchmarks for electronically excited states: CASPT2, CC2, CCSD, and CC3. *The Journal of Chemical Physics* **2008,** 128, 134110.

[53] Becke, A. D., Density-functional thermochemistry. Iii. The role of exact exchange. *The Journal of Chemical Physics* **1993,** 98, 5648-5652.

[54] Lee, C.; Yang, W.; Parr, R. G., Development of the colle-salvetti correlation-energy formula into a functional of the electron density. *Physical Review B* **1988,** 37, 785-789.

[55] Yanai, T.; Tew, D. P.; Handy, N. C., A new hybrid exchange‚äìcorrelation functional using the coulomb-attenuating method (CAM-B3LYP). *Chem. Phys. Lett.* **2004,** 393, 51-57.

[56] Dreuw, A.; Head-Gordon, M., Single-reference ab initio methods for the calculation of excited states of large molecules. *Chemical Reviews* **2005,** 105, 4009-4037.

[57] Stratmann, R. E.; Scuseria, G. E.; Frisch, M. J., An efficient implementation of time-dependent density-functional theory for the calculation of excitation energies of large molecules. *The Journal of Chemical Physics* **1998,** 109, 8218-8224.

[58] Stanton, J. F.; Bartlett, R. J., The equation of motion coupled-cluster method. A systematic biorthogonal approach to molecular excitation energies, transition probabilities, and excited state properties. *The Journal of Chemical Physics* **1993,** 98, 7029-7039.

[59] Packer, M. J.; Dalskov, E. K.; Enevoldsen, T.; Jensen, H. J. r. A.; Oddershede, J., A new implementation of the second-order polarization propagator approximation (SOPPA): The excitation spectra of benzene and naphthalene. *The Journal of Chemical Physics* **1996,** 105, 5886-5900.

[60] Sauer, S. P. A., Second-order polarization propagator approximation with coupled-cluster singles and doubles amplitudes - SOPPA(CCSD): The polarizability and hyperpolarizability of li^-. *Journal of Physics B: Atomic, Molecular and Optical Physics* **1997,** 30, 3773.

Chapter 3: Excited States of TiO_2 Clusters - Challenges for Computational Chemistry.

Titanium dioxide (TiO_2) has been the focus of much attention in recent years, both experimentally[1-11] and computationally[12-24], mainly due to the potential applications for which it would appear to be suitable[25, 26]. Also as TiO_2 is often seen as the simplest transition metal oxide, due to its relatively simple ground state electronic structure, and therefore an ideal candidate for studies of such systems.

The low cost and relative abundance of TiO_2 has meant that it has always had a broad range of, perhaps menial, applications from paint, to sunscreen and toothpaste. However, since the 1972 discovery of the photocatalytic splitting of water on the surface of TiO_2 under UV light[27] the number of potential applications has been greatly expanded. These new applications seem promising for tackling important problems in energy and environmental sciences[28]. Therefore, a good understanding of the electronic structure of bulk and nanoclusters of TiO_2 is of paramount importance in these endeavours. Especially as TiO_2 nanoclusters display some fascinating quantum size effects, whereby unique (non-bulk) cluster properties may be observed[15]. In the development of such applications an effort has been made to enhance the natural properties of the material. One example is the ambition to make TiO_2 active at certain visible wavelengths and a number of possible solutions for this are being tested, including electron and hole doping, and photosensitisation[6, 28-30]. In order to better develop this material for future applications a detailed understanding of the interplay between electronic and geometrical structure is desirable.

In recent years experimental and theoretical studies on $(TiO_2)_n$ nanoclusters have been on-going to understand the basic nature of the bonding, electronic transitions, electron attachment, quantum size effects, and how the electronic structure of the clusters evolves to that of the bulk materials (e.g., the rutile and anatase phases). It should be noted that TiO_2 clusters are inherently difficult to work with experimentally for a number of reasons. These include the fact that for larger cluster sizes there are a greater number of possible isomers, there is often a very high density of electronic, vibrational and rotational states, and the clusters can be easily fragmented in ionisation

processes[5]. Regardless of these problems neutral[5], positive[4, 7, 10], and negative[9, 11] TiO_2 clusters have been produced in the gas-phase and are the recent focus of experimental efforts at better understanding the electronic structure of TiO_2.

Computational studies of TiO_2 typically have two driving factors; firstly to find cluster models that can be used as accurate substitutes for the bulk material itself, and secondly to discover any unique properties of the clusters themselves. For example work has been undertaken to consider how changing the size and shape of TiO_2 clusters affect their attributes, such as excitation energies, in comparison to the bulk band-gap[24]. TiO_2 clusters have been investigated using many of the methods of quantum chemistry[20]. Such clusters have the advantage that, as they involve relatively fewer atoms than for example bulk slab models, they are more accessible to higher accuracy computational methods.

In the two chapters that follow a computational study of the small $(TiO_2)_n$ clusters n=1-4, including the neutral closed-shell, radical cation, and radical anion species, is presented. Firstly the $(TiO_2)_n$ n=1-4 neutral structures, which were used as a starting point for the subsequent investigations, are described. Then in the rest of chapter 3 an investigation of the low-lying singlet excited states of $(TiO_2)_n$ clusters n=1-4 using a range of methods is presented. Starting with a more in-depth look at the TiO_2 monomer, followed by a less in-depth look at the low-lying excited states of the $(TiO_2)_n$ clusters n=2-4 clusters.

In Chapter 4 the geometry of some of the neutral clusters is rationalised in terms of the pseudo-Jahn-Teller effect (pJT). The pJT effect in charged radical clusters is then considered and it is seen that vibronic coupling will often cause the radical clusters to adopt a different geometry to that of the neutral.

3.1 Neutral $(TiO_2)_n$ n=1-4 Structures.

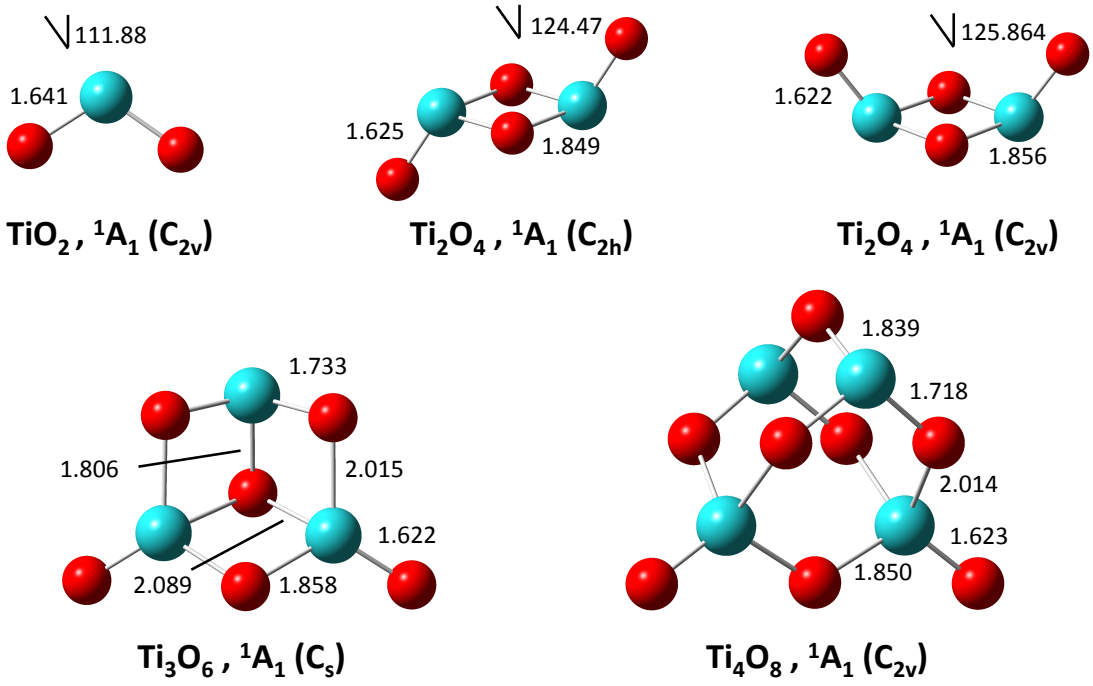

Figure 3-1: Neutral $(TiO_2)_n$ (n=1-4) structures symmetries and electronic states optimised at B3LYP/cc-pVTZ level.

In Figure 3-1 the structures of five neutral clusters of $(TiO_2)_n$ for n=1-4, including two energetically relevant isomers for the n=2 system are presented. The geometries of the n=1 and 2 clusters are discussed in more detail in the next chapter, where they are rationalised in terms of the pseudo-Jahn-Teller effect. As the value of n is increased so the number of possible stable isomers of each cluster size also increases and this study has been limited to consider only those clusters up to n=4. In part this is due to the use of correlated methods such as CASSCF and EOM-CCSD for calibration purposes but it is hoped that the paradigm will be equally relevant to larger clusters as well. Indeed in chapter 4 it is shown that the pJT effect can be used to rationalise the various isomeric forms of $(TiO_2)_2$ and also the ways of interconverting between them.

The structures presented in Figure 3-1 are optimised at the B3LYP level. The n=1 monomer has a C_{2v} symmetry with a bond-length of 1.64 Å and an angle of about 111.88°. This compares well with computational results of *Dixon et al*[20] who reported a bond-length of 1.666 Å and angle of 112.4° at the CCSD(T) level. There are two n=2 structures shown; both consist of a central square formed by the two titanium and two oxygen; the difference being the relative positions of the terminal oxygen. The C_{2v} structure square has side of length 1.86 Å (1.870 Å), Ti-terminal oxygen bond

length 1.62 Å (1.645 Å) and angle 125.86°. The C_{2h} structure has a square side length of 1.85 Å (1.863 Å), Ti-terminal oxygen bond length 1.63 Å (1.648 Å) and angle 124.47°. The values which appear in brackets are those also reported in [20] at the CCSD(T) level and it can be seen that there is good agreement with them. This is also true for the bond-lengths in both the (C_s) n=3 structure and the (C_{2v}) n=4 structure. The structures found here optimised using B3LYP agree well with those of the higher-level CCSD(T) calculations (which can be set as benchmark results for the neutral species).

3.2 Calculations of the Low-Lying Excited States of the TiO_2 Molecule

3.2.1 Background

Highly correlated methods such as CCSD(T) have been used on neutral and anion clusters up to n=4 and these provide the most accurate benchmark results available for ground state structures[20]. The isolated TiO_2 molecule has been the subject of several studies aimed at elucidating its geometry and electronic spectroscopy[2, 8, 9, 18, 20, 21, 31-34]. However, the first applications of correlated response theory to the problem of the excited states of this molecule are presented here.

The development of computational methods to treat electronically excited states has gathered pace in the last decade or so. In addition to complex multireference techniques applied to small and medium sized molecules (e.g., MRCI and CASPT2), nowadays a correlated treatment of electronic excitations is possible via the coupled cluster response hierarchy (CCS, CC2, CCSD, CC3). Here a systematic improvement in molecular properties (e.g., excitation energies and transition moments) is obtained at each subsequent level of the hierarchy[35, 36]. The calculation of excitation energies in larger molecular systems is possible using both wave function and density functional techniques. For example the second-order CC2 response method has emerged as a reliable and relatively low cost way to study a range of states in a balanced manner. Hättig has presented a review of second-order excited state methods[37], while Sauer et al. have analysed the performance of such methods in organic molecules[38]. The CC2 method in particular has become invaluable to account for multi-configurational

character in excited states (e.g., state-mixing), and in the study of charge transfer excitations. Time-dependent linear response density functional theory also now has a prominent position as used to study excited states of large molecular systems.

3.2.2 Results and Discussion

The geometry of TiO_2 was optimized using B3LYP in conjunction with the cc-pVTZ basis (*vide infra*). The ground electronic state is a closed-shell singlet with a C_{2v} geometry. The optimized geometrical parameters are, TiO bond-length: 1.644 Å, and OTiO bond-angle: 111.9°. These compare well with the detailed MRCI study by Grein which gave the minimum ground state geometry as TiO bond-length: 1.640 Å, and OTiO bond-angle: 112.0°[18]. Other theoretical work at the CCSD(T)/aug-cc-pVTZ level gave optimized geometrical parameters of TiO bond-length: 1.663 Å, and OTiO bond-angle: 112.4°[20].

The one electron basis sets used for the coupled-cluster calculations discussed in detail below were atomic natural orbitals (ANOs). For oxygen the ANO-1 set[39] was contracted (6s5p3d2f)/[4s3p2d1f], while for titanium the ANO-3 set[40] was contracted (8s7p6d5f4g)/[7s6p4d2f1g]. For the density functional linear response calculations the cc-pVTZ basis was used (standard cc-pVTZ for oxygen ([4s3p2d1f] contracted basis functions), and Petersen's cc-pVTZ for titanium[41] ([7s6p4d2f1g] contracted basis functions)).

As the coupled cluster response calculations are benchmark results all electrons were correlated. The effect of tight core correlation functions was determined by comparing linear response CCSD excitation energies for the 1 $^1B_2$ and 1 $^1A_2$ states using the cc-pwCVTZ basis (Petersen's [9s8p6d3f2g] contraction for titanium[41], and the standard cc-pCVTZ for oxygen of [6s5p3d1f] contracted functions). The core correlation functions changed the excitation energy by less than 0.05 eV, while the frozen core approximation (oxygen 1s, titanium 1s2s2p) gave rise to a difference of around 0.1 eV. However, freezing the titanium semi-core (3s3p) gave extremely poor results, out by more than 5 eV for the 1 $^1B_2$ state. The effect of extra diffuse functions was determined by comparing the 1 $^1B_2$ and 1 $^1A_2$ excitation energies using the cc-pVDZ and cc-pVTZ

basis sets with their augmented counterparts, aug-cc-pVDZ (standard augmented functions for oxygen giving [4s3p2d], while Petersen's diffuse set[41] was added for titanium to give [7s6p4d2f]), and aug-cc-pVTZ (standard augmented functions for oxygen giving [5s4p3d2f], while Petersen's diffuse set[41] was added for titanium to give [8s7p5d3f2g]). In going from cc-pVDZ to aug-cc-pVDZ both excitation energies increase by around 0.1 eV, while the difference between cc-pVTZ and aug-cc-pVTZ is less than 0.05 eV. The difference between aug-cc-pVDZ and cc-pVTZ is also less than 0.05 eV. Continuing further in this vein the affect of adding Rydberg-type orbitals[42] to the basis on the 1 $^1B_2$ state excitation energy was also checked. Thus the ANO basis discussed above was augmented with centre-of-mass s, p, d, and f functions with half-integer quantum number ranging from 4.5 to 8.5. At the CCSD level the Rydberg basis gave an excitation energy of 2.381 eV, compared to 2.386 eV without these additional functions. Therefore this state has almost no Rydberg character and is a pure valence excited state.

	CIS/CCS	*CIS(D)*	*SOPPA*	*SOPPA(CCSD)*	*CC2*	*CCSD*	*CCSDR(3)*	*CC3*
1 $^1B_2$	4.433	0.000	-0.914	-1.018	0.219	2.386	2.247	2.370
1 $^1A_2$	5.112	2.285	-0.891	-0.987	0.704	3.045	2.730	2.376
1 $^3B_2$	4.263		-0.873	-0.979	0.284	2.333		2.489
1 $^3A_2$	4.671		-0.844	-0.942	0.748	3.016		2.498
2 $^1B_2$	5.260	0.000	-0.232	-0.368	1.161	3.213	3.053	3.291
1 $^3A_1$	4.267		0.509	0.372	2.764	3.083		3.522
2 $^1A_1$	4.833	0.000	0.624	0.466	2.745	3.315	3.478	3.599
3 $^1A_1$	5.456	0.000	1.059	0.906	3.363	4.027	4.250	3.677
1 $^3B_1$	4.518		0.542	0.414	2.999	3.375		3.804
1 $^1B_1$	4.984	0.000	0.623	0.499	3.061	3.599	3.766	3.890
2 $^1A_2$	5.321	-0.439	1.621	1.462	3.665	3.969	4.175	3.998
2 $^1B_1$	5.230	0.000	0.949	0.833	3.217	3.711	3.889	4.002

Table 3-1: TiO_2 vertical excitation energies (in eV) from 1 $^1A_1$ ground state to lowest singlet and triplet states, obtained with a variety of wave function methods using an ANO basis.

Table 3-1 presents the results of wave function methods including CCS/CIS, which for single-excitation dominated states give excitation energies correct to first-order; a range of second-order methods: CIS(D)[43], CC2[44], the second-order polarization propagator approximation (SOPPA)[45], SOPPA with CCSD amplitudes replacing MP2 ones (SOPPA-CCSD)[46], and those obtained from the full CCSD linear response function (equivalent to equation-of-motion-CCSD (EOM-CCSD) for excitation energies); and CC3[47], and CCSDR(3)[48], in which the excitation energies are correct

to 3rd-order due to the inclusion of connected triples. CCSDR(3) is a non-iterative approximation to the benchmark CC3 method. The *Dalton 2.0* program[49] was used for all wave function based excited state calculations. The spectrum for TiO_2 obtained from CCSDR(3) excitation energies and CCSD oscillator strengths is plotted in Figure 3-2.

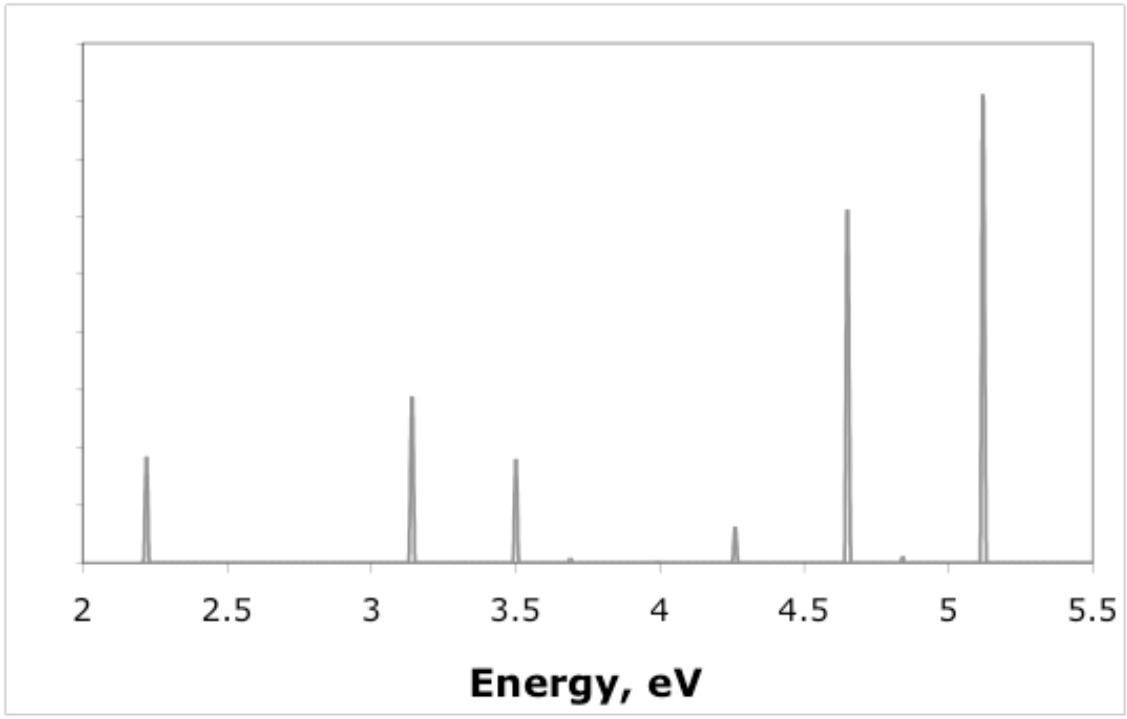

Figure 3-2: Spectra for TiO_2 obtained from CCSDR(3) excitation energies and CCSD oscillator strengths

In Figure 3-3 the excitation energies for the first singlet excited $^1B_2$ state as calculated using a range of CC methods are presented. The accuracy of the methods used increases going from left to right. Each of the lines of the plot represent the results calculated using a different basis set. In general for such plots oscillatory behaviour in the result is expected, as the accuracy of the CC method used increases and the result closes in on the correct result for the given basis set. The results will oscillate about the correct result for the given basis set and gradually converge to this value. This would seem to be true of the blue and green lines, but not the red. Comparing the results of the smaller (blue line) and Larger (red line) basis sets in Figure 3-3 there is reasonably good agreement between the results up to CCSD, but that the CC3 results are very different. In general the CC2 results are poor, being almost as far from the results of the more accurate methods as the SCF.

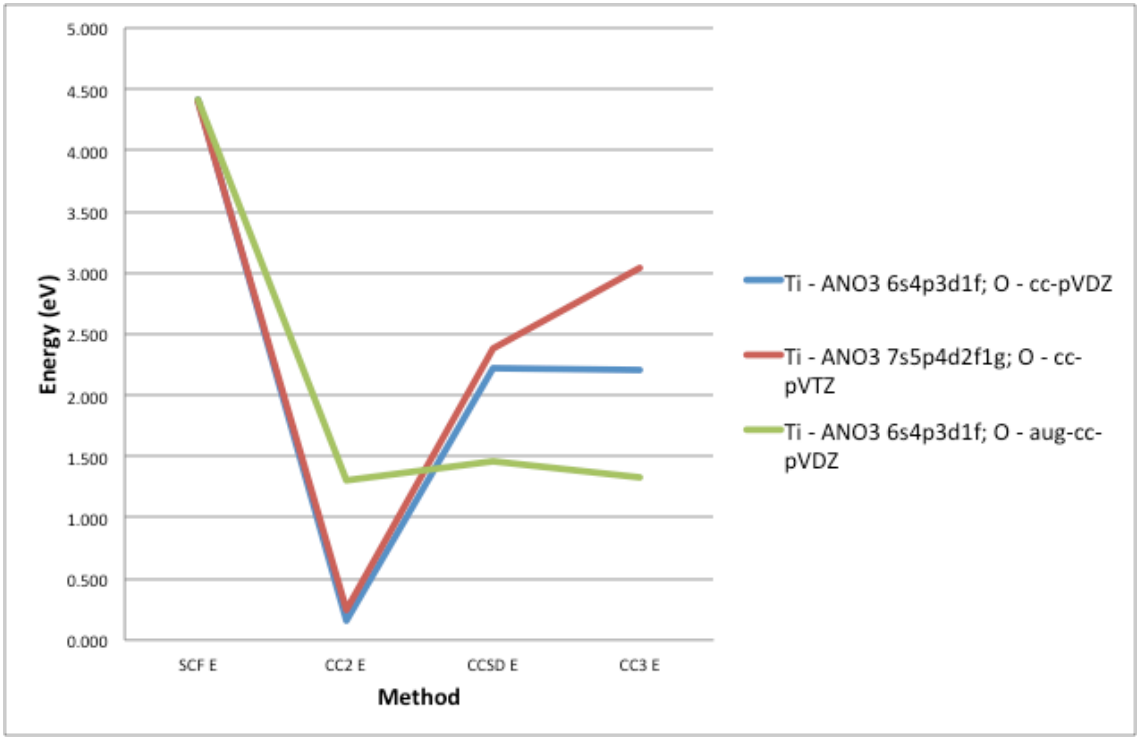

Figure 3-3: Excitation energy against computational method for the first excited state ($^1B_2$) of TiO_2. The results using 3 different basis sets is shown for comparison. The accuracy of the methods used increases moving left to right.

The green line demonstrates the results where the basis set for Ti is consistent with that used for the blue line, but with diffuse functions added to the oxygen basis set. This does show the oscillatory behaviour, but converges to a result about half of the expected result.

In Figure 3-4 the Oscillator strength against computational method for the first excited state ($^1B_2$) of TiO_2 are shown. These results pair with those of Figure 3-3. These curves should have the same oscillatory nature as those of the excited energy and this appears to be true of all of the curves. Due to computational constraints the CC3 oscillator strengths for the larger basis sets were not calculated. Therefore it is unclear if the difference between the red and blue curves at the CC3 level shown in Figure 3-3 is repeated here. Again the green curve where diffuse functions are added to oxygen converges to an oscillator strength which is different from the two other curves.

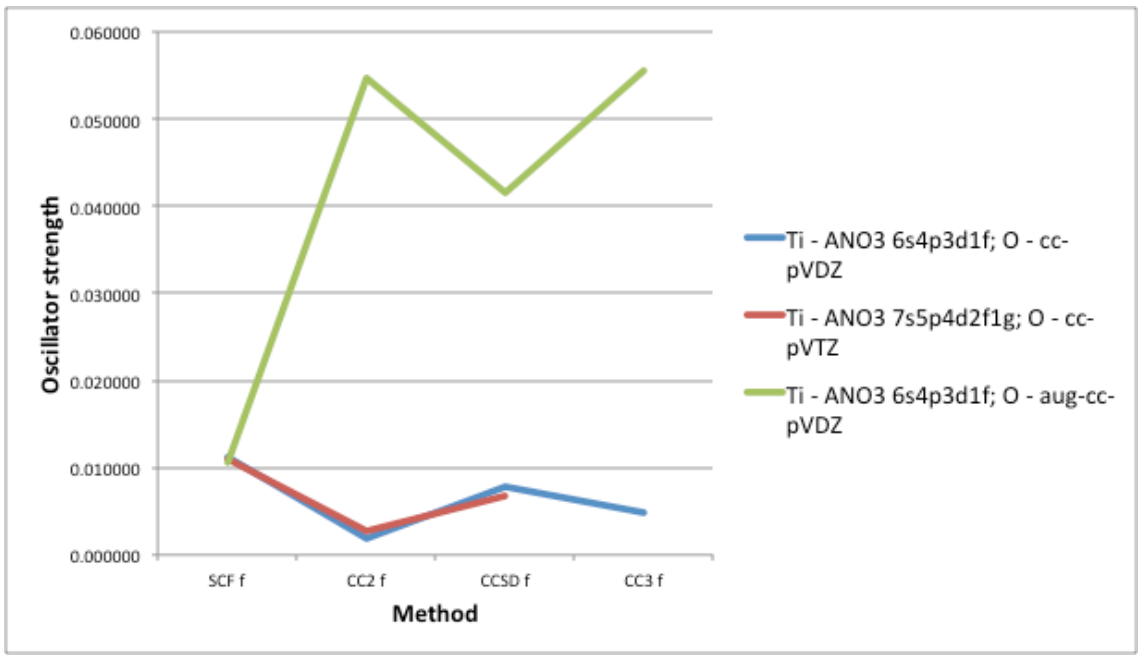

Figure 3-4: Oscillator strength against computational method for the first excited state ($^1B_2$) of TiO_2. The results using 3 different basis sets is shown for comparison. The accuracy of the methods used increases moving left to right.

Excitation energy against computational method for the second singlet excited state ($^1A_2$) of TiO_2 are plotted in Figure 3-5.

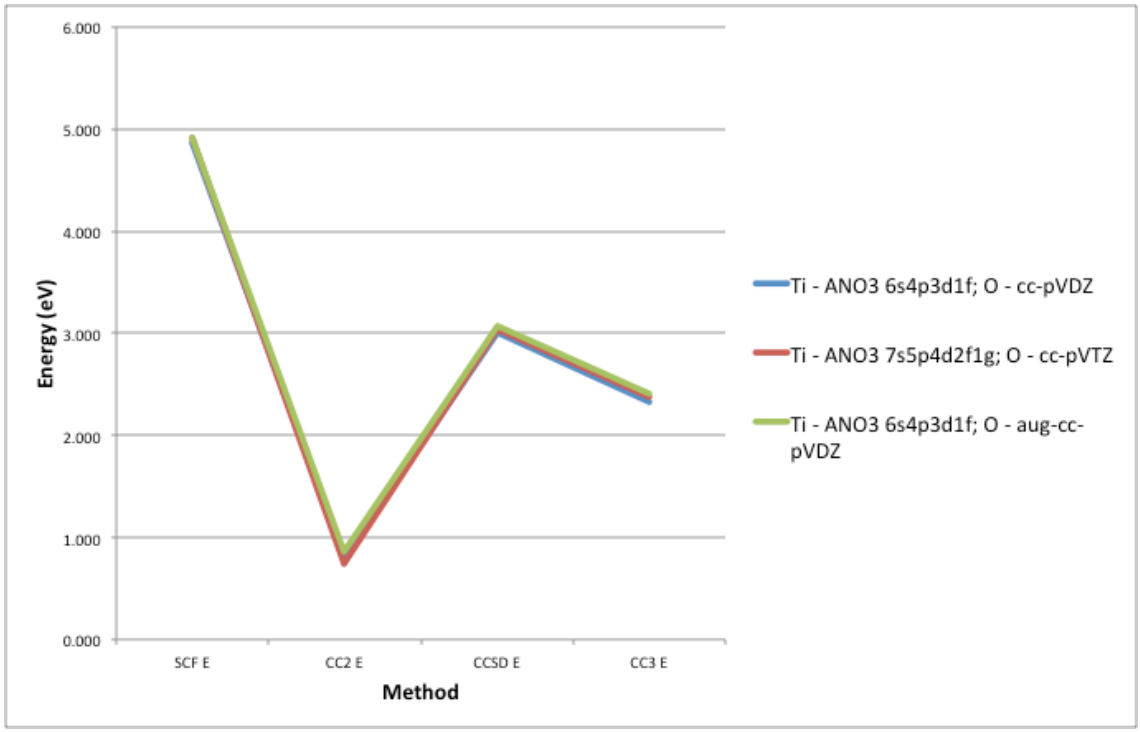

Figure 3-5: Excitation energy against computational method for the second singlet excited state ($^1A_2$) of TiO_2. The results using 3 different basis sets is shown for comparison. The accuracy of the methods used increases moving left to right.

As $^1A_2$ is a dark state all calculated oscillator strengths were zero. Unlike those of the first excited state the excitation energy results of the $^1A_2$ state are well behaved. There is little difference in the results using the different sized basis sets and the oscillatory behaviour is clearly evident. In section 3.3 the low-lying singlet excited states of $(TiO_2)_n$ molecules n=2-4 are investigated and similar plots of the first excited state are presented. Where possible the results have been calculated using the same small (blue) and large (red) basis sets, though for the larger cluster sizes only the small basis set is considered. In each case there is oscillatory behaviour in the curves and very little difference in the results using the different sized basis sets (where available). The inconsistency in the results for the first excited state of TiO_2 demonstrates the difficulty inherent with describing this state.

In Table 3-2 the results of time-dependent linear response Hartree-Fock (TD-HF) and density functional theory (TD-DFT) are presented. For TD-DFT the functionals chosen are the popular B3LYP functional, the Coulomb attenuated extension of this (CAM-B3LYP[50]) designed to correctly describe charge transfer excitations, and the M06L functional[51] from the Truhlar family (expected to give best performance of this family for transition metal containing systems). The *Gaussian 09* program[52] was used for these calculations.

	TD-HF	*TD-B3LYP*	*TD-CAM-B3LYP*	*TD-M06L*
$1\ ^3B_2$	3.420	2.519	2.744	3.110
$1\ ^1B_2$	4.397	2.633	2.868	3.172
$1\ ^3A_2$	3.965	3.119	3.297	3.271
$1\ ^3A_1$	2.641	3.208	3.254	3.751
$1\ ^1A_2$	4.906	3.241	3.429	3.367
$2\ ^1B_2$	4.992	3.353	3.580	3.704
$2\ ^1A_1$	4.767	3.487	3.696	4.187
$1\ ^3B_1$	3.969	3.535	3.653	3.989
$1\ ^1B_1$	4.861	3.788	4.017	4.290
$2\ ^1B_1$	4.934	4.021	4.143	4.406
$2\ ^1A_2$	4.946	4.098	4.287	4.716
$3\ ^1A_1$	5.131	4.209	4.370	4.568

Table 3-2: TiO_2 vertical excitation energies (in eV) from $1\ ^1A_1$ ground state to lowest singlet and triplet states, obtained with time-dependent (TD) Hartree-Fock and density functional methods using the cc-pVTZ basis.

It is clear that there is significant variation with these methods for the electronic states considered: the lowest two singlet states, and the lowest triplet state of each symmetry type. The experimental excitation energy for the S_1 state is 2.3 eV, as originally obtained by McIntyre et al[53]. This refers to the adiabatic (0-0) transition however, so the vertical excitation energy will be a little higher. One of the most recent spectroscopic experiments measured the absorption of TiO_2 after preparation of TiO_2^- trapped in a Neon matrix at 6 K, followed by electron detachment of the trapped species[2]. The spectrum thus obtained shows (adiabatic) band onsets around 2.37 eV and 3.37 eV. These bands were assigned to the 1 $^1B_2$ and 1 $^1B_1$ excited states.

For the 1 $^1B_2$ state CCSD, CCSDR(3), and CC3 are all within 0.1 eV of the experimental value of Ref. [53]. Probably any of the third order values is the most accurate, but it should be noted that since vibrational effects (not considered here) can be between 0.01 and 0.1 eV it is difficult to say which. This state is dominated by single-excitations and is thus appropriate for both coupled-cluster and density functional response theory (all response methods having some problems for doubly-excited states). The CC2 method breaks down completely here with an excitation energy of only 0.21 eV, while the non-iterative CIS(D) also breaks down with an excitation energy of almost zero. At the CIS level the first two states of B_2 symmetry are almost 1 eV apart and thus one might not except any problems related to quasi-degeneracy. However comparing the absolute excitation energies in Table 3-1 it is clear that correlation effects are so strong here that such zeroth order states are not appropriate for the perturbative CIS(D) method and also cause serious problems for CC2 and the SOPPA based methods, which generate negative excitation energies. The TD-DFT results for this state are better, especially B3LYP and CAM-B3LYP, although M06L is in error by around 0.6 eV.

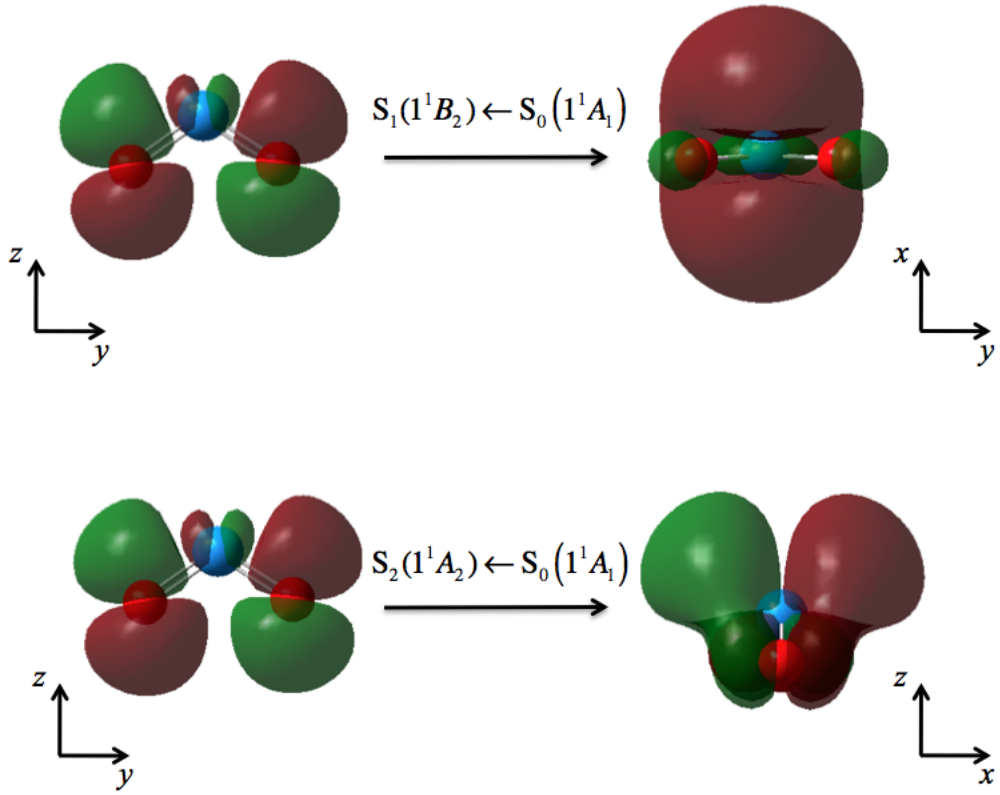

Figure 3-6: Natural transition orbitals obtained from TD-CAM-B3LYP/cc-pVTZ for the first two singlet excitations. The S_1 state is represented as a transition from oxygen p_π-orbitals to a titanium $3d_{x2-y2}/4s$ orbital, while the S_2 state is represented as a transition from oxygen p_π-orbitals to a titanium $3d_{xz}/4p_x$ orbital.

In Figure 3-6 the natural transition orbitals[54] for the TD-CAM-B3LYP excitations to the 1 $^1B_2$ and 1 $^1A_2$ states are shown. All methods except TD-HF and CCS/CIS correctly predict that the 1 $^1B_2$ and 1 $^3B_2$ states are very close in energy. The results for the vertical ground state singlet (1 $^1A_1$) to the first excited triplet (1 $^3B_2$) can be compared with previous high-level calculations obtained by explicitly optimizing each state separately[20]. The CCSD(T)/aug-cc-pVDZ adiabatic triplet excitation result of 2.24 eV by Dixon et al[20] is in line with the CC3 result of 2.489 eV when the excited geometry relaxation is taken into account (*vide infra*). It is also noted that the experimental estimate for the HOMO-LUMO band-gap from photoelectron spectroscopy is 2.22 eV[11]. For the 1 $^1B_2$ state the calculated oscillator strengths are: 0.0025 (CC2), 0.0068 (CCSD), 0.0120 (TD-HF), 0.0067 (TD-B3LYP), 0.0060 (TD-CAM-B3LYP), 0.0034 (TD-M06L). The 1 $^1A_2$ state is electric dipole forbidden.

CASSCF calculations (using *Gaussian 09*), with 12 electrons in 12 active orbitals generating 427350 singlet configurations, in conjunction with the cc-pVTZ basis discussed above have also been performed. Using state-specific CASSCF there is considerable orbital relaxation in the 1 $^1B_2$ state. The S_1 vertical excitation energy is

2.80 eV. The one-electron density matrix elements for the S_1 state show two singly occupied orbitals, which are almost identical to the TD-CAM-B3LYP natural transition orbitals shown in Figure 3-6. The CAS(12,12) T_1 vertical excitation energy is 2.83 eV. Previous calculations indicate that the ground state is quite well described by a single configuration wave function[20, 31, 32]. The CASSCF results also indicate that this is the case, although it should be noted that the CCSD $\hat{T}_1$ diagnostic is relatively high (0.04). Previously, Li et al[20] have also noted this point. The MRCI values of Grein are 2.43 eV for the 1 $^1B_2$ state, 3.09 eV for the 1 $^1A_2$ state, 2.40 eV 1 $^3B_2$ state, and 3.07 eV 1 $^3A_2$ state[18]. For all the states considered the error in CCSD is on average around 0.3 eV compared to CC3, while for CCS/CIS the error is several eV. CC2 fails badly for the 1 $^{1,3}B_2$ and 1 $^{1,3}A_2$ states but performs better for the states above these. CIS(D) fails for all states with the strange exception of the 1 $^1A_2$ state in which CIS(D) is fortuitously within 0.09 eV of the CC3 result. CC3 gives much closer excitation energies for the 1 $^1B_2$ and 1 $^1A_2$, and 1 $^3B_2$ and 1 $^3A_2$ pairs of states. This is not seen in CCSD or CCSDR(3) where the $^1A_2$ dark state excitation energy is over 0.5 eV above that of the 1 $^1B_2$ state.

The adiabatic excitation energy of the lowest excited S_1 (1 $^1B_2$) state have also investigated, as detailed in Table 3-3.

Method [a]	*Vertical* [b]	*Adiabatic* [c]
CIS/CCS	4.433	4.082
CIS(D)	0.000	-1.239
CC2	0.219	-0.573
CCSD	2.386	2.062
CCSDR(3)	2.247	1.864
CC3	2.370	2.083
TD-B3LYP	2.633	2.345
TD-CAM-B3LYP	2.868	2.593
TD-M06L	3.172	2.883

Table 3-3: Comparison of TiO_2 1 $^1B_2 \leftarrow$ 1 $^1A_1$ vertical and adiabatic excitation energies (in eV).
[a] ANO basis for CC response (all electrons correlated), and cc-pVTZ basis for TD-DFT.
[b] Calculated at ground state B3LYP/cc-pVTZ optimized geometry.
[c] Calculated at 1 $^1B_2$ state EOM-CCSD/cc-pVTZ optimized geometry.

The excited state geometry was optimized at the equation-of-motion CCSD (EOM-CCSD) level (using *Gaussian 09*), using the cc-pVTZ basis discussed above. The geometry for this state is not linear, as predicted by earlier studies[31], but rather has a

OTiO angle of 101.0°, while the TiO bond-length is 1.672 Å. TD-DFT geometry optimization for this state gives very similar results: OTiO angle of 100.4° and TiO bond-length of 1.672 Å for TD-B3LYP, and OTiO angle of 104.8° and TiO bond-length of 1.659 Å for TD-CAM-B3LYP. This is in good agreement with the most recent spectroscopic characterization of TiO_2 which shows vibrational progressions associated with the $^1B_2$ transition consistent with the OTiO angle reducing, and the TiO bonds lengthening while maintaining C_{2v} symmetry[2, 8, 34]. The adiabatic excitation energies in Table 3-3 are around 0.3 – 0.4 eV lower than the corresponding vertical excitation energy, and the poor performance of CIS(D) and CC2 is again apparent.

Finally, the most recent spectroscopic characterization of the molecule used Stark effect spectroscopy to determine the permanent electric dipole moments of the ground $1\ ^1A_1$ state and $1\ ^1B_2$ excited state[8, 34]. These properties have been computed at the optimized geometries for each state (Table 3-4).

Method[a]	*$1\ ^1A_1$*[b]	*$1\ ^1B_2$*[c]
CCS	8.07 D	4.12 D
CC2	3.60 D	-
CCSD	6.74 D	3.70 D
CCSD(T)	7.00 D	-
MRCI[d]	6.73 D	5.07 D
Expt.[e]	6.33 ± 0.07 D	2.55 ± 0.08 D

Table 3-4: Comparison of permanent electric dipole moments of $1\ ^1A_1$ and $1\ ^1B_2$ states.
[a] ANO basis (all electrons correlated).
[b] Coupled cluster results, using orbital unrelaxed response, calculated at ground state B3LYP/cc-pVTZ optimized geometry.
[c] Coupled cluster results, using orbital unrelaxed response, calculated at $1\ ^1B_2$ state EOM-CCSD/cc-pVTZ optimized geometry.
[d] Reference [18].
[e] Reference [8].

For the ground state the CCSD and CCSD(T) methods perform well, although CCSD(T) is slightly further from the experimental value than CCSD or the MRCI results in Ref. [18]. It has been found that due to the charge transfer in the $1\ ^1B_2$ excited state, from O to Ti (Table 3-1), that the dipole moment of this state is greatly reduced (to around 2.55 D). The CCSD result for this state is in reasonable agreement with Ref. [8] at 3.70 D. The only other theoretical estimate of this property came from the MRCI studies in Ref. [18], which gave a value of 5.07 D. Clearly this is a challenging electronic state and future computation of the geometry and dipole moment (also

including vibrational averaging) at third-order or higher in a large basis set is desirable to fully reconcile with experiment.

3.3 Calculations of the Low-Lying Singlet Excited States of $(TiO_2)_n$ n=2-4.

3.3.1 Results and Discussion

A hierarchy of coupled-cluster response methods (LR-CC) were used, in addition to equation of motion CCSD (EOM-CCSD) and TD-DFT methods, to study the low-lying singlet excited states of the $(TiO_2)_n$ neutral clusters (n=2-4 shown in Figure 3-1). It is worth noting that the LR-CCSD and EOM-CCSD methods are completely equivalent for excitation energies, though not necessarily for transition moments. The two excitation energies computed should be the same, all things being equivalent. The differences in the results are purely due to the different basis sets used for each method. The one electron basis sets used for the LR-CC methods were the cc-pVDZ basis set for oxygen and the ANO-3 [6s4p3d1f] set for titanium. While the cc-pVDZ basis sets were used for both titanium and oxygen for all EOM-CCSD and TD-DFT calculations. Of the basis sets used the ANO basis is expected to be slightly better than the cc-pVDZ basis and so in this case the LR-CCSD calculations expected to be slightly better than the EOM-CCSD. The TD-DFT functionals chosen are the B3LYP functional and the Coulomb attenuated extension of this, CAM-B3LYP. All calculations were performed using the GAUSSIAN03 program[55] with the exception of the coupled-cluster response calculations, which were performed using the Dalton program[49].

In Figure 3-7 the first 20 CCSDR(3) excitation energies are plotted as a function of cluster size (n). The excited states can be seen to compress together as n increases. This may be representative of the band structure of the TiO_2 bulk forming as the cluster size increases.

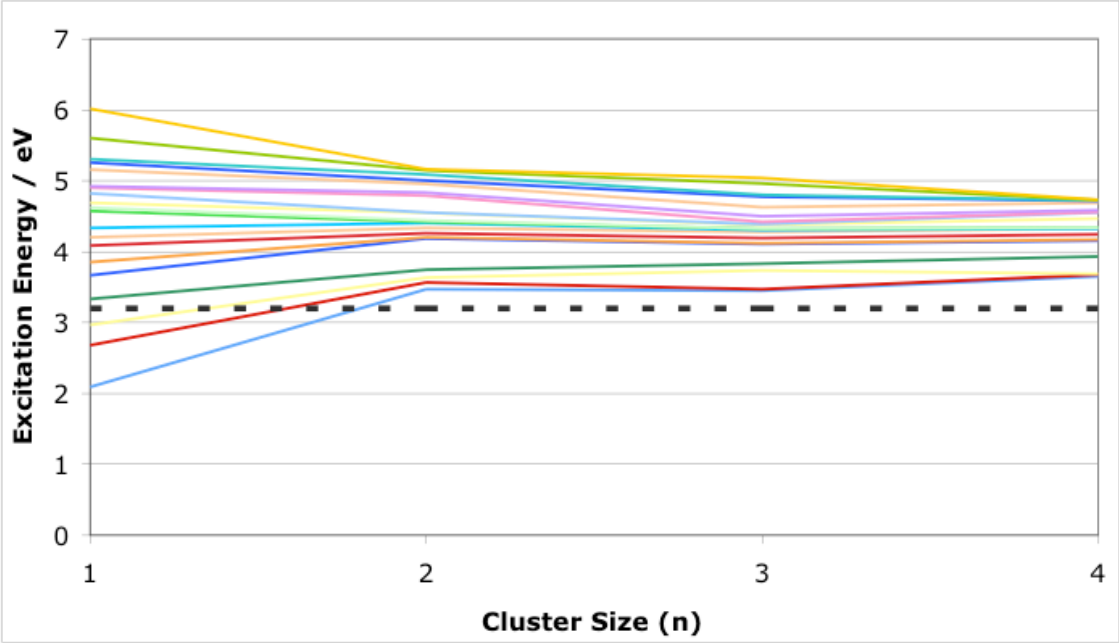

Figure 3-7: First 20 CCSDR(3) excitation energies as a function of cluster size (n)

In the next section the vertical excitation energies (in eV) from ground state to low-lying singlet states, obtained with a variety of methods are presented. The coupled-cluster response methods results represent the first five singlet excited states for each excitation symmetry. While the EOM-CCSD and TD-DFT methods results are of the first ten excited states independent of the symmetry. The exception being the case of n=4 where only the first 5 EOM-CCSD results are presented. The results are ordered according the order of the CCSD results, as the CCSD results for the monomer are believed to be qualitatively correct.

3.3.1.1 $(TiO_2)_2 - C_{2h}$

Table 3-5 shows the vertical excitation energies from the ^1A_g ground state to several of the lowest excited singlet states for the TiO_2 dimer with C_{2h} symmetry.

	CIS/CCS	*CC2*	*CCSD*	*CCSDR(3)*	*CC3*	*EOM-CCSD*	*TD-B3LYP*	*TD-CAM-B3LYP*
$1\ ^1B_g$	5.624	1.855	3.671	3.469	3.233	3.7204	3.729	4.0135
$1\ ^1A_u$	5.651	2.019	3.729	3.565	3.343	3.7831	3.874	4.0997
$1\ ^1B_u$	5.284	2.159	3.836	3.630	3.369	3.9115	3.894	4.1878
$1\ ^1A_g$	5.302	2.284	3.919	3.746	3.479	4.0053	4.082	4.3133
$2\ ^1B_u$	5.677	2.854	4.155	4.184	4.057	4.2036	4.326	4.5259
$2\ ^1A_g$	5.704	3.024	4.165	4.198	4.138	4.2177	4.325	4.5405

2 ^1B_g	5.895	3.095	4.546	4.331	4.088	4.5369	4.325	4.7008
3 ^1B_u	6.077	3.070	4.550	4.256	4.134	-	4.539	4.7746
3 ^1B_g	6.064	3.313	4.614	4.400	4.235	4.6769	4.481	4.8096
2 ^1A_u	5.921	3.292	4.624	4.415	4.209	4.6817	4.268	4.8083
3 ^1A_g	6.086	3.068	4.719	4.439	4.207	-		
3 ^1A_u	6.084	3.352	4.754	4.552	4.385	4.7583		
4 ^1B_g	6.506	3.350	4.807	4.545	4.455			
5 ^1B_g	6.852	3.984	4.980	4.953	4.920			
4 ^1A_u	6.563	3.755	4.983	5.003	4.605			
4 ^1B_u	6.461	3.643	5.010	4.787	4.609			
5 ^1A_u	6.869	4.083	5.050	4.833	4.952			
4 ^1A_g	6.496	3.895	5.252	5.086	4.541			
5 ^1A_g	6.890	4.259	5.455	5.142	4.929			
5 ^1B_u	6.759	4.150	5.471	5.158	4.746			

Table 3-5: $(TiO2)_2$ C_{2h} symmetry vertical excitation energies (in eV) from 1 $^1A_{1g}$ ground state to lowest singlet states, obtained with a variety of methods

As stated the results are ordered according the order of the CCSD results, however none of the methods order the states consistently with the CCSD results, each having a different order. All of the methods apart from CIS/CCS correctly find the 1 ^1B_g excited state as the first excited state. If only the first five excitations are considered, the results do correlate with the order of the CCSD results with exception of those of the CIS/CCS and B3LYP methods. The CIS/CCS results are completely different, while those of B3LYP differ in the order of the 5th and 6th excitation where they are found to be extremely close in energy (a difference of 0.001 eV).

In Figure 3-8 the excitation energy against computational method for the first singlet excited state (^1B_g) of $(TiO_2)_2$ with C_{2h} symmetry are plotted. The results of two different basis sets are shown, the blue line corresponding to the smaller of the two. The oscillatory nature of the curve is present for both curves and there is very little difference in the results of the different basis sets.

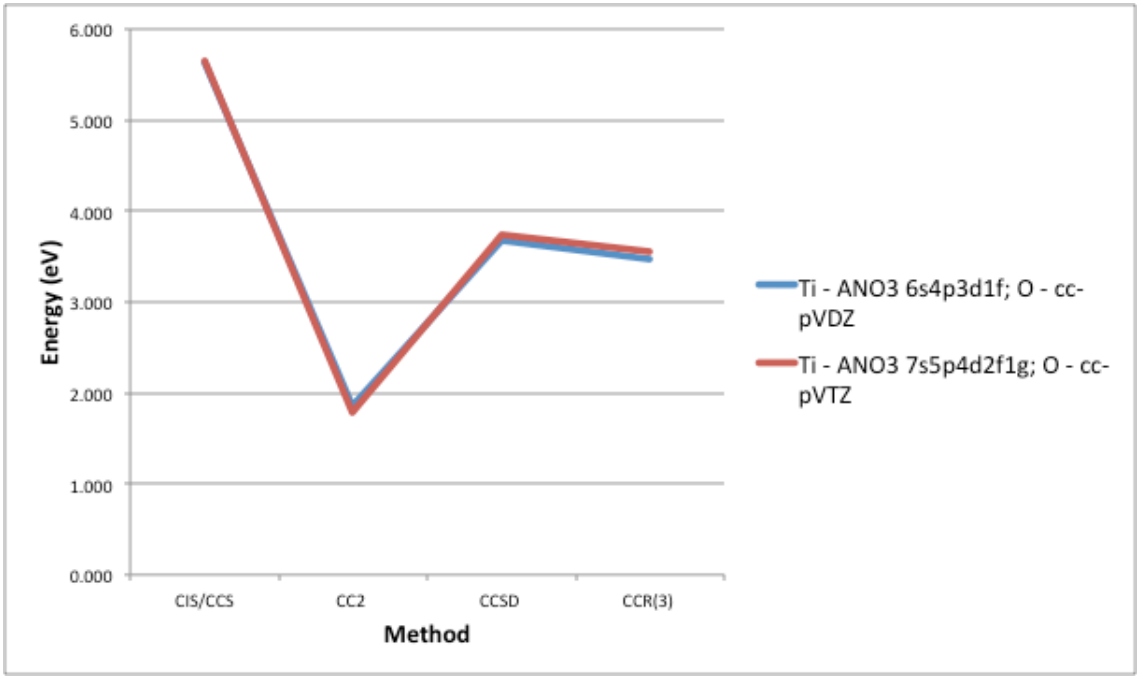

Figure 3-8: Excitation energy against computational method for the first singlet excited state (^1B_g) of $(TiO_2)_2$ with C_{2h} symmetry. The results using 2 different basis sets is shown for comparison. The accuracy of the methods used increases moving left to right.

The 1 ^1B_g state of $(TiO_2)_2$ with C_{2h} symmetry is a dark state and so the oscillator strengths of the excitation were zero for all methods.

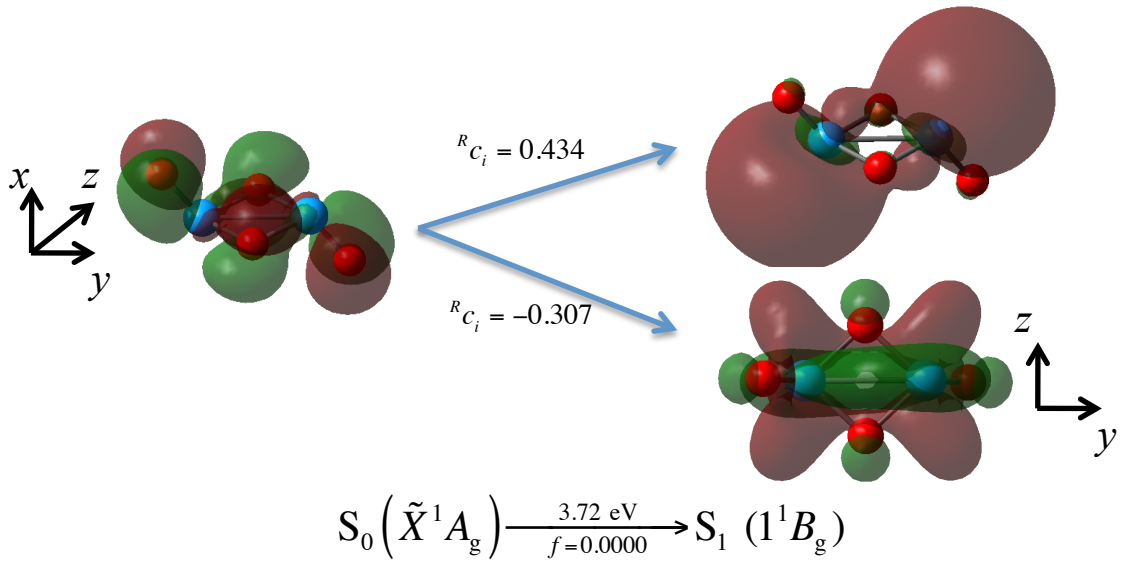

Figure 3-9: transition orbitals for the first singlet excitations for $(TiO_2)_2$ C_{2h} obtained from EOM-CCSD/cc-pVDZ.

In Figure 3-9 the transition orbitals for the EOM-CCSD excitations to the 1 ^1B_g state are shown. This excitation is represented by a transition from p-type oxygen orbitals to a combination of different d-type orbitals of titanium. The spectrum for $(TiO_2)_2$ with C_{2h}

symmetry obtained from CCSDR(3) excitation energies and CCSD oscillator strengths is plotted in Figure 3-10.

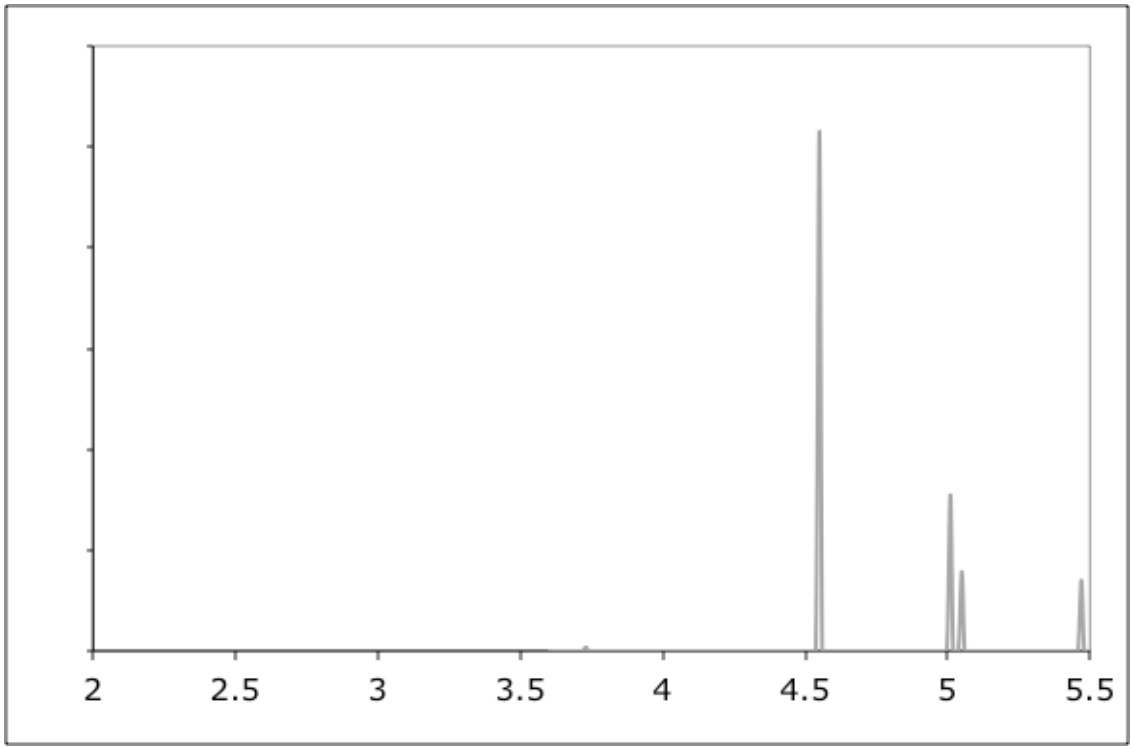

Figure 3-10: Spectra for $(TiO_2)_2$ C_{2h} obtained from CC(3) excitation energies and CCSD oscillator strengths.

3.3.1.2 $(TiO_2)_2 - C_{2v}$

In Table 3-6 the results of the C_{2v} symmetry dimer are presented and again they are ordered with respect to the CCSD results, although again over the states calculated none of the other methods match this order.

	CIS/CCS	*CC2*	*CCSD*	*CCSDR(3)*	*CC3*	*EOM-CCSD*	*TD-B3LYP*	*TD-CAM-B3LYP*
1 $^1B_1$	5.347	1.486	3.262	3.104	2.951	3.2833	3.2576	3.5995
1 $^1A_2$	5.505	1.695	3.525	3.379	3.154	3.5497	3.6111	3.8771
1 $^1A_1$	5.072	1.961	3.578	3.441	3.210	3.6306	3.5289	3.8891
1 $^1B_2$	5.090	1.973	3.743	3.620	3.377	3.7672	3.7129	4.007
2 $^1B_2$	5.498	2.135	3.895	3.652	3.481	3.8787	3.8813	4.156
2 $^1A_1$	5.445	2.899	4.043	4.150	4.087	4.0511	4.1709	4.3728
3 $^1B_2$	5.878	3.065	4.059	4.101	4.085	4.0708	4.2043	4.4072
2 $^1A_2$	5.788	2.507	4.138	3.917	3.769	4.0957	3.9178	4.2668
2 $^1B_1$	5.804	2.833	4.449	4.173	3.995	4.4229	4.3048	4.605
3 $^1A_1$	5.885	3.060	4.636	4.422	4.128	-	-	
3 $^1B_1$	5.929	3.328	4.681	4.614	4.306	-	-	
4 $^1B_1$	6.443	3.570	4.731	4.617	4.433	-	-	
3 $^1A_2$	5.914	3.315	4.744	4.770	4.256	4.6481	4.2786	
5 $^1B_1$	6.629	3.792	4.797	4.740	4.560			

4 $^1A_1$	6.436	3.401	4.876	4.641	4.371
4 $^1A_2$	6.356	3.573	4.976	4.683	4.643
5 $^1A_2$	7.193	3.749	5.085	4.916	4.754
4 $^1B_2$	6.245	3.885	5.236	5.196	4.537
5 $^1B_2$	6.745	4.211	5.377	5.210	4.940
5 $^1A_1$	6.584	4.170	5.492	5.382	4.807

Table 3-6: $(TiO_2)_2$ C_{2v} symmetry vertical excitation energies (in eV) from 1 $^1A_1$ ground state to lowest singlet states, obtained with a variety of methods.

All of the methods, with the exception of CIS/CCS, correctly find the first excited state as the 1 $^1B_1$ excited state. Considering only the first five excitations, here both the CIS/CCS and B3LYP methods fail to predict the correct order of the singlet excitations. However, the other results do correlate with the ordering of the CCSD results over these first five states.

In Figure 3-11 the excitation energy against computational method for the first singlet excited state ($^1B_1$) of C_{2v} geometry of the $(TiO_2)_2$ cluster are plotted. The results of two different basis sets are shown, the blue line corresponding to the smaller of the two. The oscillatory nature of the curve is present for both curves and there is very little difference in the results of the different basis sets.

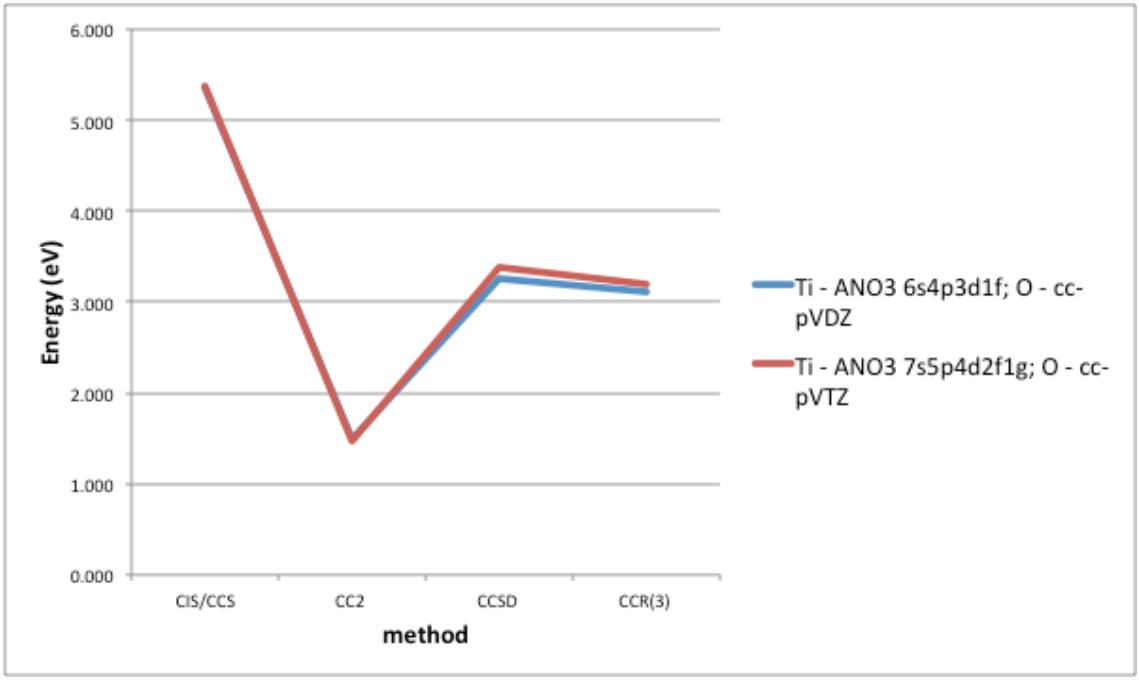

Figure 3-11: Excitation energy against computational method for the first singlet excited state ($^1B_1$) of $(TiO_2)_2$ with C_{2v} symmetry. The results using 2 different basis sets is shown for comparison. The accuracy of the methods used increases moving left to right.

Oscillator strength against computational method for the first singlet excited state ($^1B_1$) of $(TiO_2)_2$ with C_{2v} symmetry are plotted in Figure 3-12. The oscillator strengths for the

methods larger than CCSD were not calculated due to computational constraints. There are fewer points so it is difficult to say the curve is still oscillatory. There is a difference in the results at the SCF level, but this disappears at the CC2 level. At the CC2 level the oscillator strength is found to be almost zero (0.000047 for the smaller basis and 0.000052 with the larger) for both basis set sizes. At the CCSD level there is a very slight difference in the oscillator strengths at the different basis set size (8×10^{-5}).

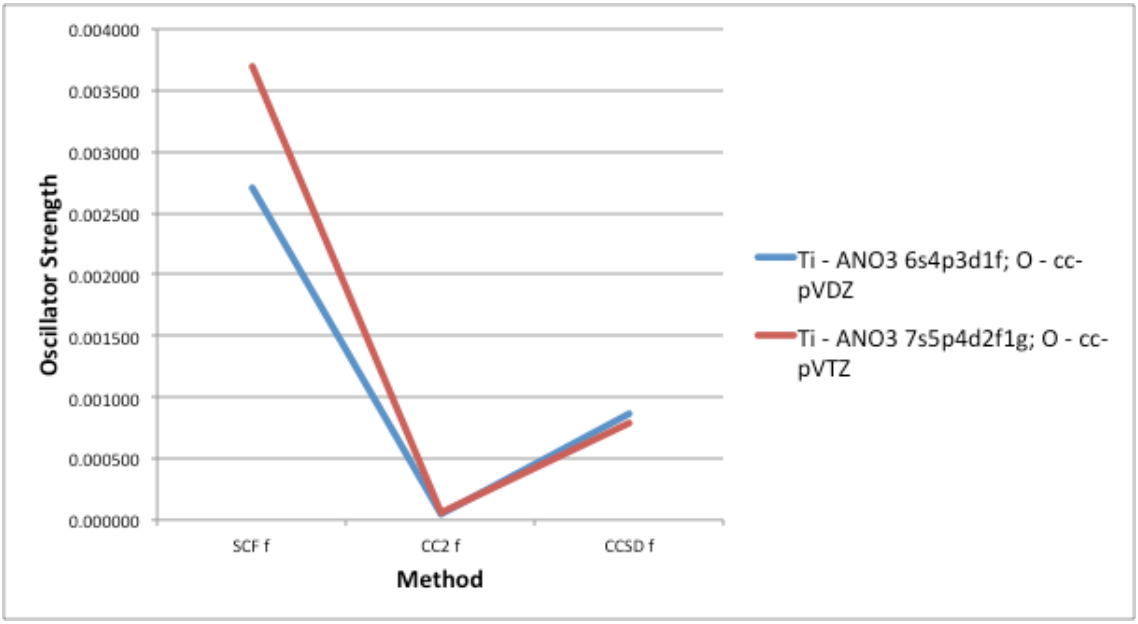

Figure 3-12: Oscillator strength against computational method for the first singlet excited state ($^1B_1$) of $(TiO_2)_2$ with C_{2v} symmetry. The results using 2 different basis sets is shown for comparison. The accuracy of the methods used increases moving left to right.

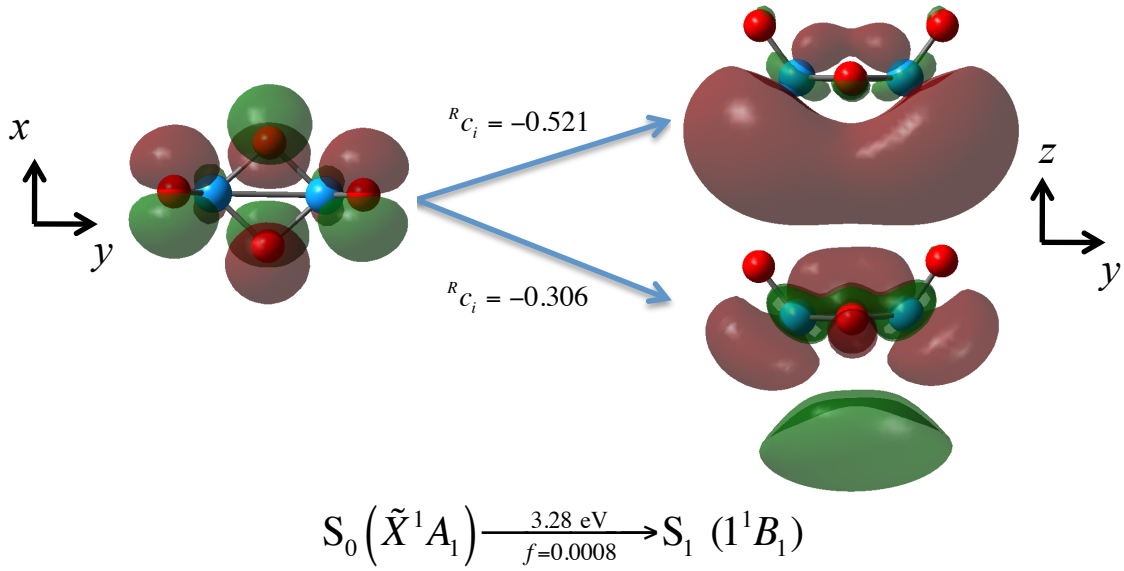

Figure 3-13: First singlet excitations for $(TiO_2)_2$ C_{2v} obtained from EOM-CCSD/cc-pVDZ.

In Figure 3-13 the transition orbitals for the EOM-CCSD excitations to the 1 $^1B_1$ state are shown. The transition is from the p-type orbitals of oxygen to the d_z^2-type orbitals

of titanium. The spectrum for $(TiO_2)_2$ with C_{2v} symmetry obtained from CCSDR(3) excitation energies and CCSD oscillator strengths is plotted in Figure 3-14.

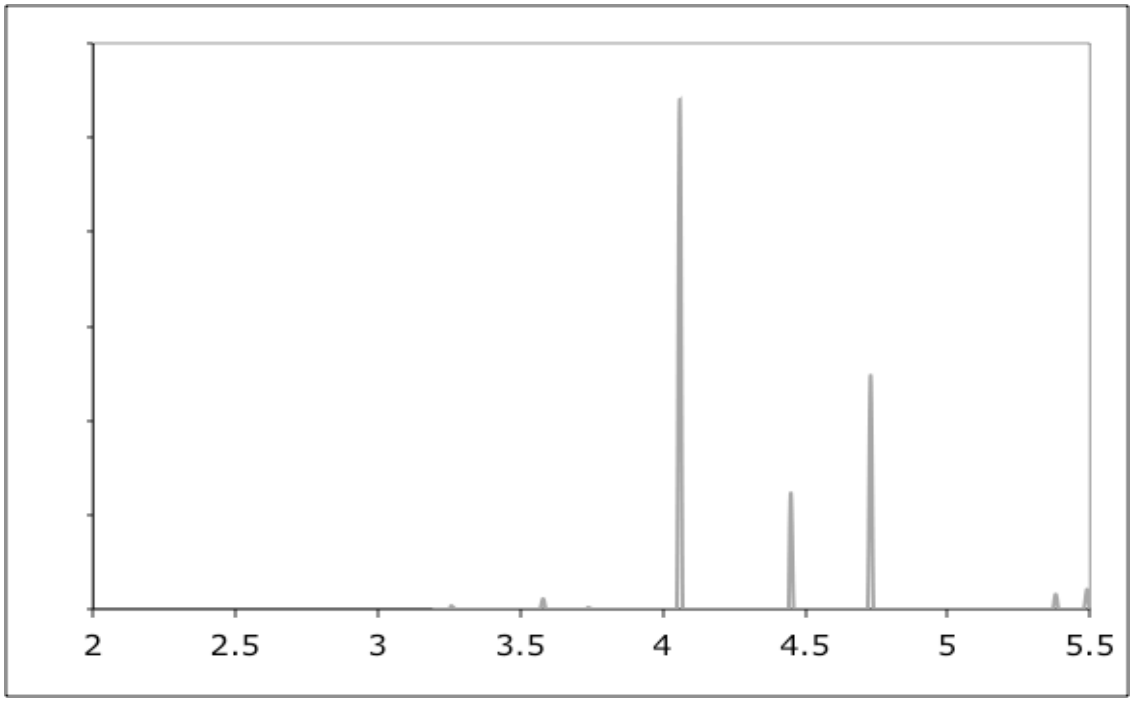

Figure 3-14: Spectra for $(TiO_2)_2$ C_{2v} obtained from CC(3) excitation energies and CCSD oscillator strengths.

3.3.1.3 $(TiO_2)_3$

In Table 3-7 the results of the C_s symmetry $(TiO_2)_3$ molecule are presented. Over the states considered with each method, none of the methods agree with each other as to the ordering of the states. In this case CC2 and the two DFT methods incorrectly find the first excited state to be 1 $^1A'$, rather than the correct 1 $^1A''$ state.

	CIS/CCS	*CC2*	*CCSD*	*CCSDR(3)*	*EOM-CCSD*	*TD-B3LYP*	*TD-CAM-B3LYP*
1 $^1A''$	5.520	1.782	3.809	3.448	3.866900	3.651	4.1662
1 $^1A'$	5.521	1.649	3.987	3.470	3.993300	2.9927	4.0621
2 $^1A''$	6.007	1.975	4.165	3.830	4.178300	3.8237	4.3343
2 $^1A'$	6.008	2.006	4.223	3.735	4.312800	3.6976	4.4604
3 $^1A'$	6.036	2.691	4.337	4.106	4.380100	3.7254	4.5715
3 $^1A''$	6.062	2.437	4.388	4.113	4.388900	3.9276	4.5315
4 $^1A'$	6.103	2.724	4.435	4.277	4.465200	3.7996	4.668
4 $^1A''$	6.111	2.667	4.436	4.190	4.433400	4.0481	4.6037
5 $^1A'$	6.317	2.850	4.542	4.303	4.540800	3.866	4.7004
6 $^1A'$	6.347	2.893	4.560	4.377	-	-	4.7910
5 $^1A''$	6.138	2.741	4.561	4.321	4.554000	4.1103	
6 $^1A''$	6.349	2.929	4.574	4.324			
7 $^1A''$	6.402	2.978	4.708	4.419			
7 $^1A'$	6.498	2.930	4.724	4.383			

8 $^1A'$	6.522	3.015	4.878	4.498
8 $^1A''$	6.590	3.250	4.912	4.799
9 $^1A'$	6.861	3.179	4.915	4.623
10 $^1A'$	6.871	3.357	4.985	4.771
9 $^1A''$	6.849	3.483	5.052	4.956
10 $^1A''$	6.868	3.579	5.270	5.038

Table 3-7: $(TiO_2)_3$ C_s symmetry vertical excitation energies (in eV) from 1 $^1A_1$ ground state to lowest singlet states, obtained with a variety of methods.

Again considering the first 5 states, there is a poor general agreement as to the ordering of the states. CIS/CCS, CCSD and EOM-CCSD all agree with each other as to the ordering of the states. But none of the results of the other methods are consistent with this ordering, or with each other.

In Figure 3-15 Excitation energy against computational method for the first singlet excited state ($^1A''$) of $(TiO_2)_3$ are plotted. Due to computational constraints only the small basis set is considered. The oscillatory nature of the curve is present.

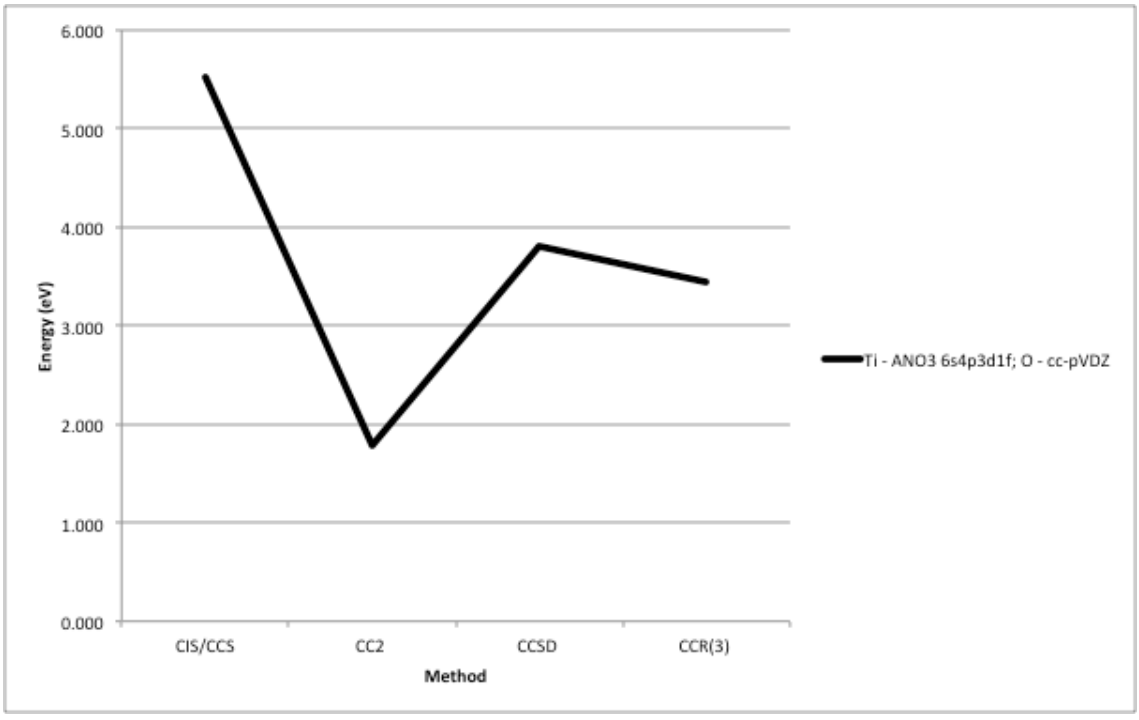

Figure 3-15: Excitation energy against computational method for the first singlet excited state ($^1A''$) of $(TiO_2)_3$. The accuracy of the methods used increases moving left to right.

In Figure 3-16 the oscillator strength against computational method for the first singlet excited state ($^1A''$) of $(TiO_2)_3$ is presented. Again the small number of points make it difficult to define the curve as oscillatory.

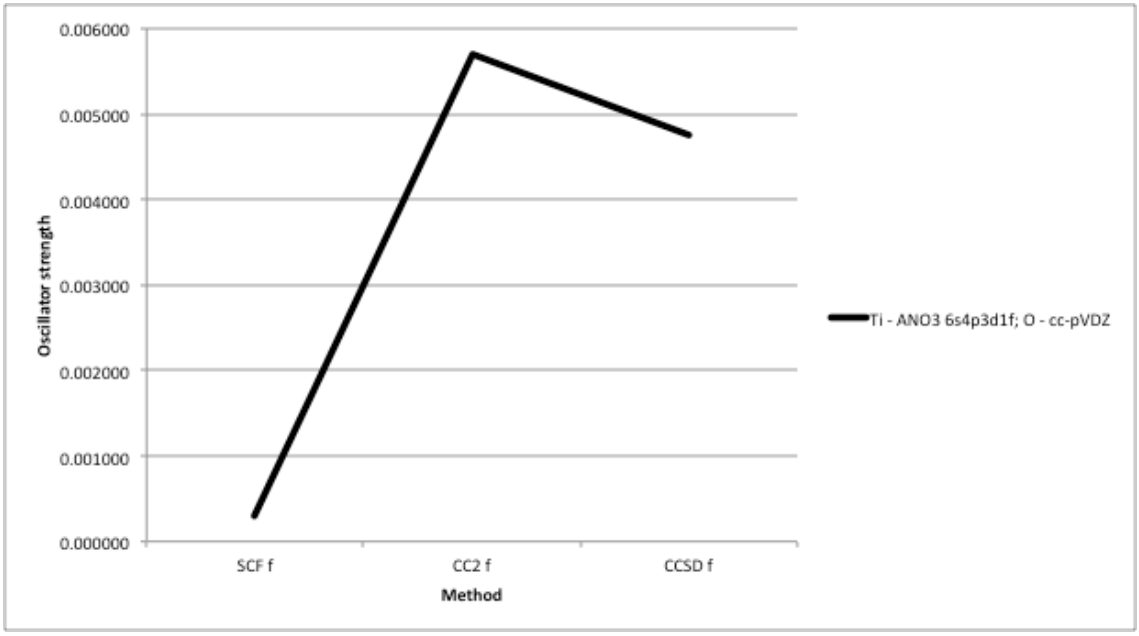

Figure 3-16: Oscillator strength against computational method for the first singlet excited state ($^1A''$) of $(TiO_2)_3$. The accuracy of the methods used increases moving left to right.

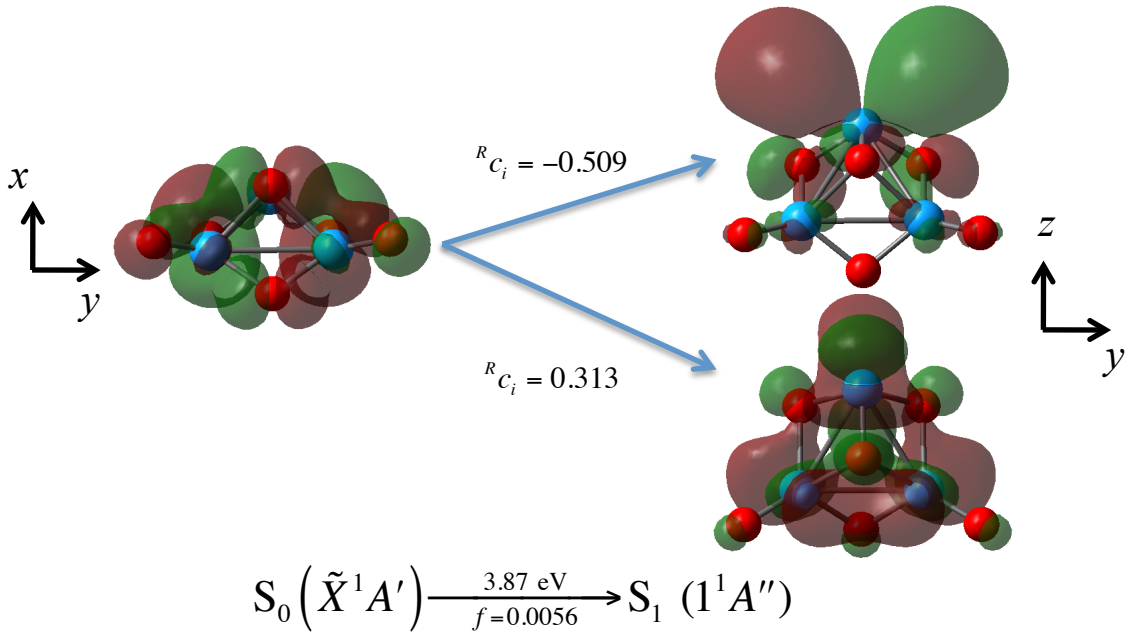

Figure 3-17: First singlet excitations for $(TiO_2)_3$ obtained from TD-CAM-B3LYP/cc-pVTZ.

In Figure 3-17 the transition orbitals for the TD-B3LYP excitations to the 1 $^1A''$ state are shown. This transition is represented by an excitation from the orbitals of oxygen to the d-type orbitals of titanium. The spectrum for $(TiO_2)_3$ obtained from CCSDR(3) excitation energies and CCSD oscillator strengths is plotted in Figure 3-18.

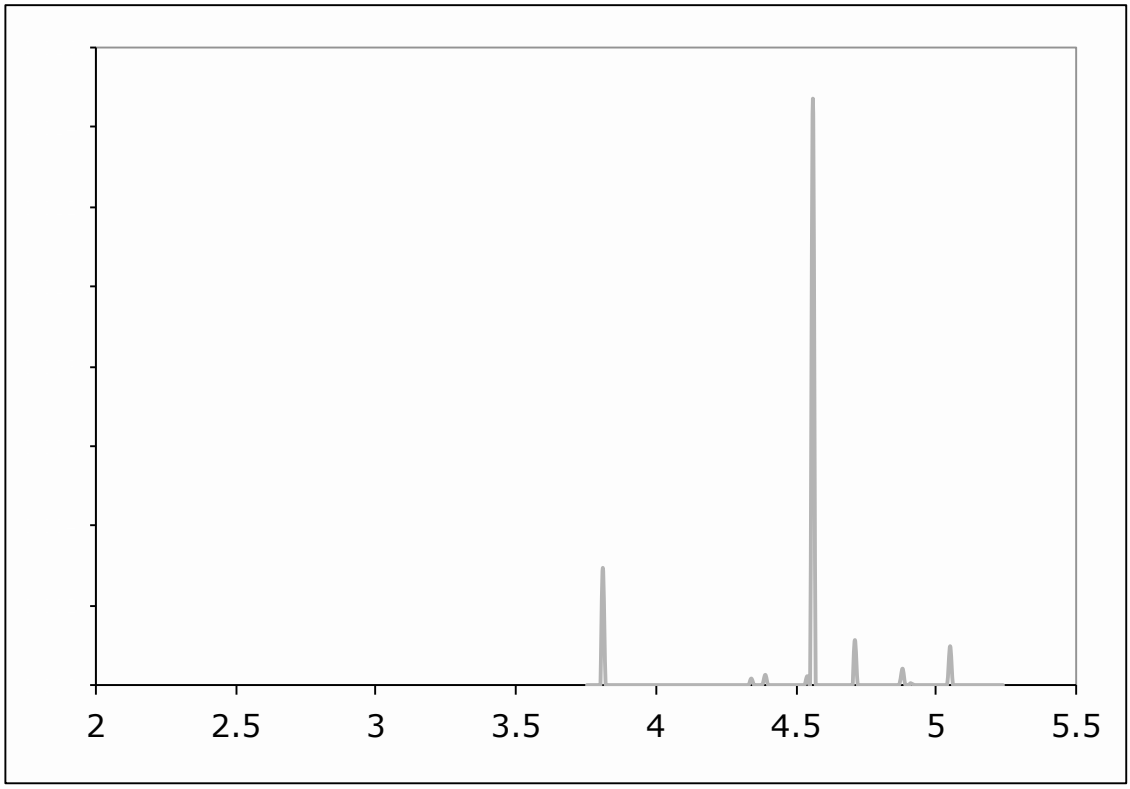

Figure 3-18: Spectra for $(TiO_2)_3$ obtained from CC(3) excitation energies and CCSD oscillator strengths.

3.3.1.4 $(TiO_2)_4$

In Table 3-8 the results of the C_{2v} symmetry $(TiO_2)_4$ molecule are presented. Again there is no consistency in the ordering of the states over the states considered by each method. But this time, even if a small subset of the first 5 excitations is considered there is no correlation between the ordering of the excitations. Even when just the first excited is considered there is little agreement. CIS/CCS predicts it to be $1\ ^1A_2$. CCSD predicts it to be $1\ ^1B_1$, while EOM-CCSD predicts $1\ ^1B_2$. There is however general agreement between the rest of the methods, which all predict $1\ ^1A_1$, but given these methods have been found to be less reliable with these $(TiO_2)_n$ systems it is difficult to say they are correct.

	CIS/CCS	*CC2*	*CCSD*	*CCSDR(3)*	*EOM-CCSD*	*TD-B3LYP*	*TD-CAM-B3LYP*
$1\ ^1B_1$	6.084	1.625	3.649	3.265	4.001300	2.7722	4.108
$1\ ^1A_1$	6.104	1.520	3.677	3.063	3.753100	2.4444	3.777
$1\ ^1A_2$	5.931	1.633	3.684	3.290	3.740500	3.2482	4.004
$1\ ^1B_2$	5.942	1.661	3.927	3.403	3.703000	3.2377	3.953
$2\ ^1A_1$	6.168	1.887	4.151	3.652	-	3.3889	4.202
$2\ ^1B_2$	6.148	2.335	4.168	3.729	-	3.5275	4.464
$2\ ^1A_2$	6.101	2.001	4.244	3.768	4.230200	3.5175	4.263
$2\ ^1B_1$	6.113	2.540	4.320	4.026		3.163	4.315
$3\ ^1A_1$	6.453	2.499	4.323	3.997		3.5358	-

3 $^1B_2$	6.352	2.474	4.336	3.835	-	-
3 $^1A_2$	6.196	2.552	4.338	4.092	-	-
4 $^1A_1$	6.484	2.908	4.466	4.014	-	-
4 $^1A_2$	6.351	2.775	4.550	4.206	-	-
3 $^1B_1$	6.244	2.560	4.557	4.196	3.1956	4.443
4 $^1B_2$	6.396	2.852	4.580	3.916		-
4 $^1B_1$	6.531	2.742	4.686	4.332		4.476
5 $^1B_2$	6.551	2.875	4.714	4.463		
5 $^1B_1$	6.688	3.075	4.719	4.545		
5 $^1A_1$	6.687	3.196	4.727	4.577		
5 $^1A_2$	6.482	3.102	4.733	4.524		

Table 3-8: $(TiO_2)_4$ Symmetry vertical excitation energies (in eV) from 1 $^1A_1$ ground state to lowest singlet states, obtained with a variety of methods

Plots for the first singlet excited state ($^1B_2$) of $(TiO_2)_4$ were not made, as it is unclear from the results which state is the first excited state. The spectrum for $(TiO_2)_4$ obtained from CCSDR(3) excitation energies and CCSD oscillator strengths is plotted in Figure 3-19.

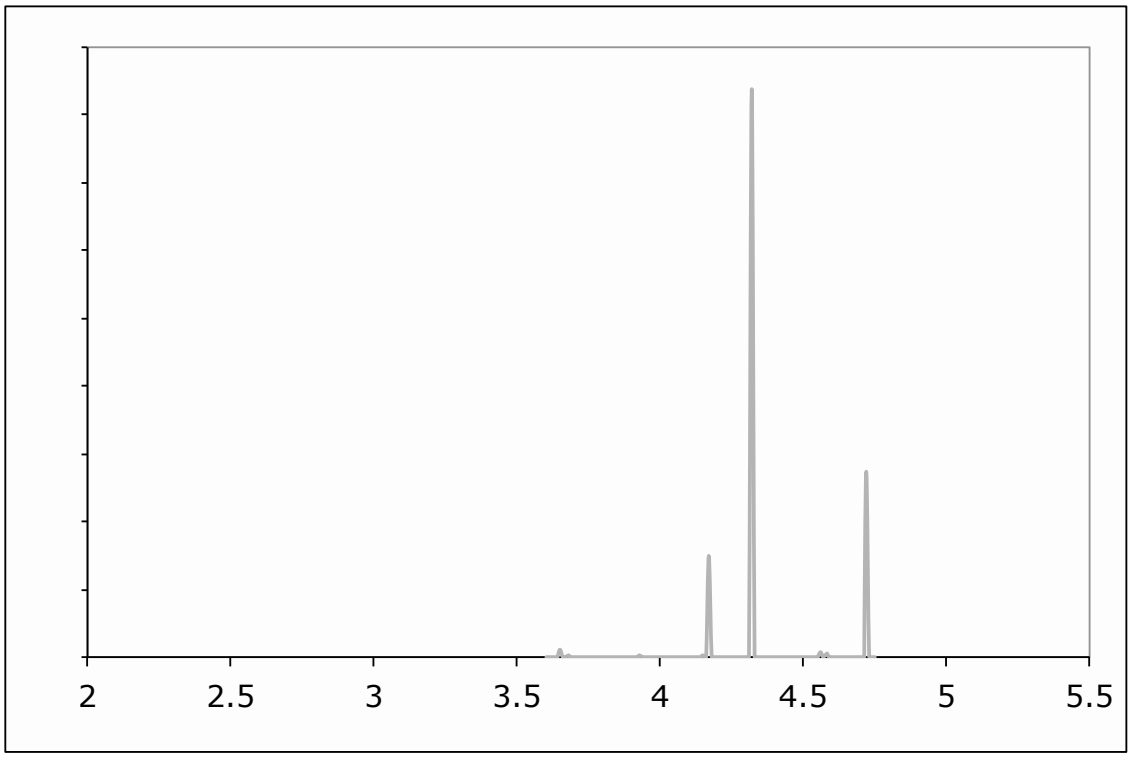

Figure 3-19: Spectra for $(TiO_2)_4$ obtained from CC(3) excitation energies and CCSD oscillator strengths.

3.4 Conclusions

On the basis of the TiO_2 monomer results it is concluded that caution should be exercised when applying lower cost excited state response methods to some transition

metal oxide systems, even though *a priori* it would be expected that there should be few problems regarding the nature of the system and the states involved. Strong but differing electron correlation effects present in the ground and valence excited electronic states may present problems in such systems. These effects are not so strong as to invalidate single-reference approaches completely, and CCSD works very well, and DFT can also do so. However the approximate second-order approaches discussed above may breakdown when applied to such systems.

The results for the n=2-4 clusters have also been presented, but difficulty in gaining any consistency in the ordering of states between results was found. This may be due to the differences in the basis sets used. The LR-CC methods used cc-pVDZ basis set for oxygen and the ANO-3 [6s4p3d1f] set for titanium. While the EOM-CCSD and TD-DFT calculations used the cc-pVDZ basis sets for both titanium and oxygen. Of the basis sets used the ANO basis is thought to be slightly better than the cc-pVDZ basis and so in this case the LR-CCSD result to be slightly better than the EOM-CCSD. Though if only the LR-CC are considered in isolation there is still a disparity in the results and that this disparity worsens as the cluster size increases. If only the first five excited states are considered at the n=2 cluster size the higher order CCSD, CCSDR(3) and CC3 methods all find the same ordering of the states, this is not true of the larger clusters. At n=3 these 3 methods find a different ordering from each other, though the CCSD is consistent with the EOM-CCSD. While at n=4 none of the methods agree as to the ordering of the excited states, even when restricted to considering only the first five. In fact at n=4 it is unclear which state is the first excited state.

Since the work in this thesis was completed, further work was undertaken that extended upon its findings[56-59].

3.5 References

[1] Albaret, T.; Finocchi, F.; Noguera, C., Density functional study of stoichiometric and O-rich titanium oxygen clusters. *Journal of Chemical Physics* **2000,** 113, 2238-2249.

[2] Garkusha, I.; Nagy, A.; Guennoun, Z.; Maier, J. P., Electronic absorption spectrum of titanium dioxide in neon matrices. *Chemical Physics* **2008,** 353, 115-118.

[3] Hwu, Y.; Yao, Y. D.; Cheng, N. F.; Tung, C. Y.; Lin, H. M., X-ray absorption of nanocrystal TiO2. *Nanostructured Materials* **1997,** 9, 355-358.

[4] Jadraque, M.; Sierra, B.; Sfounis, A.; Velegrakis, M., Photofragmentation of mass-selected titanium oxide cluster cations. *Applied Physics B-Lasers and Optics* **2010,** 100, 587-590.

[5] Matsuda, Y.; Bernstein, E. R., On the titanium oxide neutral cluster distribution in the gas phase: Detection through 118 nm single-photon and 193 mn multiphoton ionization. *Journal of Physical Chemistry A* **2005,** 109, 314-319.

[6] Rehman, S.; Ullah, R.; Butt, A. M.; Gohar, N. D., Strategies of making TiO_2 and ZnO visible light active. *Journal of Hazardous Materials* **2009,** 170, 560-569.

[7] Velegrakis, M.; Sfounis, A., Formation and photodecomposition of cationic titanium oxide clusters. *Applied Physics a-Materials Science & Processing* **2009,** 97, 765-770.

[8] Wang, H. L.; Steimle, T. C.; Apetrei, C.; Maier, J. P., Characterization of the x $^1A_1$, and a $^1B_2$ electronic states of titanium dioxide, TiO_2. *Physical Chemistry Chemical Physics* **2009,** 11, 2649-2656.

[9] Wu, H. B.; Wang, L. S., Electronic structure of titanium oxide clusters: TiO_y (y=1-3) and $(TiO_2)_n$ (n=1-4). *Journal of Chemical Physics* **1997,** 107, 8221-8228.

[10] Yu, W.; Freas, R. B., Formation and fragmentation of gas-phase titanium oxygen cluster positive-ions. *Journal of the American Chemical Society* **1990,** 112, 7126-7133.

[11] Zhai, H.-J.; Wang, L.-S., Probing the electronic structure and band gap evolution of titanium oxide clusters $(TiO_2)_n$ - (n = 1-10) using photoelectron spectroscopy. *Journal of the American Chemical Society* **2007,** 129, 3022-3026.

[12] Albaret, T.; Finocchi, F.; Noguera, C., Ab initio simulation of titanium dioxide clusters. *Applied Surface Science* **1999,** 144-145, 672-676.

[13] Albaret, T.; Finocchi, F.; Noguera, C., First principles simulations of titanium oxide clusters and surfaces. *Faraday Discussions* **1999**, 285-304.

[14] Calatayud, M.; Maldonado, L.; Minot, C., Reactivity of $(TiO_2)_n$ clusters (n=1-10): Probing gas-phase acidity and basicity properties. *Journal of Physical Chemistry C* **2008,** 112, 16087-16095.

[15] Calatayud, M.; Minot, C., Is there a nanosize for the activity of TiO_2 compounds? *Journal of Physical Chemistry C* **2009,** 113, 12186-12194.

[16] Daude, N.; Gout, C.; Jouanin, C., Electronic band-structure of titanium-dioxide. *Physical Review B* **1977,** 15, 3229-3235.

[17] Glassford, K. M.; Chelikowsky, J. R., Structural and electronic-properties of titanium-dioxide. *Physical Review B* **1992,** 46, 1284-1298.

[18] Grein, F., Density functional theory and multireference configuration interaction studies on low-lying excited states of TiO_2. *Journal of Chemical Physics* **2007,** 126, 034313.

[19] Hamad, S.; Catlow, C. R. A.; Woodley, S. M.; Lago, S.; Mejias, J. A., Structure and stability of small TiO_2 nanoparticles. *Journal of Physical Chemistry B* **2005,** 109, 15741-15748.

[20] Li, S. G.; Dixon, D. A., Molecular structures and energetics of the $(TiO_2)_n$ (n=1-4) clusters and their anions. *Journal of Physical Chemistry A* **2008,** 112, 6646-6666.

[21] Liu, Y. Z.; Yuan, Y. B.; Wang, Z. B.; Deng, K. M.; Xiao, C. Y.; Li, Q. X., Assignment of photoelectron spectra of $(TiO_2)_n$ with n=1-3. *Journal of Chemical Physics* **2009,** 130.

[22] Qu, Z. W.; Kroes, G. J., Theoretical study of the electronic structure and stability of titanium dioxide clusters $(TiO_2)_n$ with n=1-9. *Journal of Physical Chemistry B* **2006,** 110, 8998-9007.

[23] Qu, Z. W.; Kroes, G. J., Theoretical study of stable, defect-free $(TiO_2)_n$ nanoparticles with n = 10-16. *The Journal of Physical Chemistry C* **2007,** 111, 16808-16817.

[24] Qu, Z. W.; Zhu, H., Do anionic titanium dioxide nano-clusters reach bulk band gap? A density functional theory study. *Journal of Computational Chemistry* **2010,** 31, 2038-2045.

[25] Chen, X.; Mao, S. S., Titanium dioxide nanomaterials: Synthesis, properties, modifications, and applications. *Chemical Reviews* **2007,** 107, 2891-2959.

[26] Chen, X. B., Titanium dioxide nanomaterials and their energy applications. *Chinese Journal of Catalysis* **2009,** 30, 839-851.

[27] Fujishima, A.; Honda, K., Electrochemical photolysis of water at a semiconductor electrode. *Nature* **1972,** 238, 37.

[28] Di Valentin, C.; Finazzi, E.; Pacchioni, G.; Selloni, A.; Livraghi, S.; Paganini, M. C.; Giamello, E., N-doped tio$_2$: Theory and experiment. *Chemical Physics* **2007,** 339, 44-56.

[29] Ariga, H.; Taniike, T.; Morikawa, H.; Tada, M.; Min, B. K.; Watanabe, K.; Matsumoto, Y.; Ikeda, S.; Saiki, K.; Iwasawa, Y., Surface-mediated visible-light photo-oxidation on pure TiO_2(001). *Journal of the American Chemical Society* **2009**.

[30] Mowbray, D. J.; Martinez, J. I.; Lastra, J. M. G.; Thygesen, K. S.; Jacobsen, K. W., Stability and electronic properties of TiO_2 nanostructures with and without B and N doping. *Journal of Physical Chemistry C* **2009,** 113, 12301-12308.

[31] Ramana, M. V.; Phillips, D. H., A computational study of the TiO_2 molecule. *Journal of Chemical Physics* **1988,** 88, 2637-2640.

[32] Walsh, M. B.; King, R. A.; Schaefer, H. F., The structures, electron affinities, and energetic stabilities of TiO_n and TiO_n- (n=1- 3). *The Journal of Chemical Physics* **1999,** 110, 5224-5230.

[33] Matsuda, Y.; Bernstein, E. R., On the titanium oxide neutral cluster distribution in the gas phase: Detection through 118 nm single-photon and 193 nm multiphoton ionization. *The Journal of Physical Chemistry A* **2004,** 109, 314-319.

[34] Zhuang, X.; Le, A.; Steimle, T. C.; Nagarajan, R.; Gupta, V.; Maier, J. P., Visible spectrum of titanium dioxide. *Physical Chemistry Chemical Physics* **2010,** 12, 15018-15028.

[35] Koch, H.; Christiansen, O.; Jørgensen, P.; Olsen, J., Excitation energies of BH, CH_2 and Ne in full configuration interaction and the hierarchy CCS, CC2, CCSD and CC3 of coupled cluster models. *Chem. Phys. Lett.* **1995,** 244, 75-82.

[36] Christiansen, O.; Koch, H.; Jørgensen, P.; Olsen, J., Excitation energies of H_2O, N_2 and C_2 in full configuration interaction and coupled cluster theory. *Chem. Phys. Lett.* **1996,** 256, 185-194.

[37] Hättig, C., Structure optimizations for excited states with correlated second-order methods: CC2 and ADC(2). In *Advances in quantum chemistry*, Jensen, H. J. Ö., Ed. Academic Press: 2005; Vol. Volume 50, pp 37-60.

[38] Sauer, S. P. A.; Schreiber, M.; Silva-Junior, M. R.; Thiel, W., Benchmarks for electronically excited states: A comparison of noniterative and iterative triples corrections in linear response coupled cluster methods: CCSDR(3) versus CC3. *Journal of Chemical Theory and Computation* **2009,** 5, 555-564.

[39] Widmark, P.-O.; Malmqvist, P.-Ö.; Roos, B. r., Density matrix averaged atomic natural orbital (ANO) basis sets for correlated molecular wave functions. *Theoret. Chim. Acta* **1990,** 77, 291-306.

[40] Pou-Amérigo, R.; Merchán, M.; Nebot-Gil, I.; Widmark, P.-O.; Roos, B., Density matrix averaged atomic natural orbital (ANO) basis sets for correlated molecular wave functions. *Theoret. Chim. Acta* **1995,** 92, 149-181.

[41] Balabanov, N. B.; Peterson, K. A., Systematically convergent basis sets for transition metals. I. All-electron correlation consistent basis sets for the 3d elements Sc--Zn. *The Journal of Chemical Physics* **2005,** 123, 064107-15.

[42] Kaufmann, K.; Baumeister, W.; Jungen, M., Universal gaussian basis sets for an optimum representation of rydberg and continuum wavefunctions. *Journal of Physics B: Atomic, Molecular and Optical Physics* **1989,** 22, 2223.

[43] Head-Gordon, M.; Rico, R. J.; Oumi, M.; Lee, T. J., A doubles correction to electronic excited states from configuration interaction in the space of single substitutions. *Chem. Phys. Lett.* **1994,** 219, 21-29.

[44] Christiansen, O.; Koch, H.; Jørgensen, P., The second-order approximate coupled cluster singles and doubles model CC2. *Chem. Phys. Lett.* **1995,** 243, 409-418.

[45] Packer, M. J.; Dalskov, E. K.; Enevoldsen, T.; Jensen, H. J. r. A.; Oddershede, J., A new implementation of the second-order polarization propagator approximation (SOPPA): The excitation spectra of benzene and naphthalene. *The Journal of Chemical Physics* **1996,** 105, 5886-5900.

[46] Sauer, S. P. A., Second-order polarization propagator approximation with coupled-cluster singles and doubles amplitudes - SOPPA(CCSD): The polarizability and hyperpolarizability of li^-. *Journal of Physics B: Atomic, Molecular and Optical Physics* **1997,** 30, 3773.

[47] Christiansen, O.; Koch, H.; Jørgensen, P., Response functions in the CC3 iterative triple excitation model. *The Journal of Chemical Physics* **1995,** 103, 7429-7441.

[48] Christiansen, O.; Koch, H.; Jørgensen, P., Perturbative triple excitation corrections to coupled cluster singles and doubles excitation energies. *The Journal of Chemical Physics* **1996,** 105, 1451-1459.

[49] Aidas, K.; Angeli, C.; Bak, K. L.; Bakken, V.; Bast, R.; Boman, L.; Christiansen, O.; Cimiraglia, R.; Coriani, S.; Dahle, P.; Dalskov, E. K.; Ekström, U.; Enevoldsen, T.; Eriksen, J. J.; Ettenhuber, P.; Fernández, B.; Ferrighi, L.; Fliegl, H.; Frediani, L.; Hald, K.; Halkier, A.; Hättig, C.; Heiberg, H.; Helgaker, T.; Hennum, A. C.; Hettema, H.; Hjertenæs, E.; Høst, S.; Høyvik, I.-M.; Iozzi, M. F.; Jansík, B.; Jensen, H. J. A.; Jonsson, D.; Jørgensen, P.; Kauczor, J.; Kirpekar,

S.; Kjærgaard, T.; Klopper, W.; Knecht, S.; Kobayashi, R.; Koch, H.; Kongsted, J.; Krapp, A.; Kristensen, K.; Ligabue, A.; Lutnæs, O. B.; Melo, J. I.; Mikkelsen, K. V.; Myhre, R. H.; Neiss, C.; Nielsen, C. B.; Norman, P.; Olsen, J.; Olsen, J. M. H.; Osted, A.; Packer, M. J.; Pawlowski, F.; Pedersen, T. B.; Provasi, P. F.; Reine, S.; Rinkevicius, Z.; Ruden, T. A.; Ruud, K.; Rybkin, V. V.; Sałek, P.; Samson, C. C. M.; de Merás, A. S.; Saue, T.; Sauer, S. P. A.; Schimmelpfennig, B.; Sneskov, K.; Steindal, A. H.; Sylvester-Hvid, K. O.; Taylor, P. R.; Teale, A. M.; Tellgren, E. I.; Tew, D. P.; Thorvaldsen, A. J.; Thøgersen, L.; Vahtras, O.; Watson, M. A.; Wilson, D. J. D.; Ziolkowski, M.; Ågren, H., The Dalton quantum chemistry program system. *Wiley Interdisciplinary Reviews: Computational Molecular Science* **2014,** 4, 269-284.

[50] Yanai, T.; Tew, D. P.; Handy, N. C., A new hybrid exchange, correlation functional using the coulomb-attenuating method (CAM-B3LYP). *Chem. Phys. Lett.* **2004,** 393, 51-57.

[51] Zhao, Y.; Truhlar, D., The M06 suite of density functionals for main group thermochemistry, thermochemical kinetics, noncovalent interactions, excited states, and transition elements: Two new functionals and systematic testing of four M06-class functionals and 12 other functionals. *Theor Chem Account* **2008,** 120, 215-241.

[52] M. J. Frisch, G. W. T., H. B. Schlegel, G. E. Scuseria, ; M. A. Robb, J. R. C., G. Scalmani, V. Barone, B. Mennucci, ; G. A. Petersson, H. N., M. Caricato, X. Li, H. P. Hratchian, ; A. F. Izmaylov, J. B., G. Zheng, J. L. Sonnenberg, M. Hada, ; M. Ehara, K. T., R. Fukuda, J. Hasegawa, M. Ishida, T. Nakajima, ; Y. Honda, O. K., H. Nakai, T. Vreven, J. A. Montgomery, Jr., ; J. E. Peralta, F. O., M. Bearpark, J. J. Heyd, E. Brothers, ; K. N. Kudin, V. N. S., R. Kobayashi, J. Normand, ; K. Raghavachari, A. R., J. C. Burant, S. S. Iyengar, J. Tomasi, ; M. Cossi, N. R., J. M. Millam, M. Klene, J. E. Knox, J. B. Cross, ; V. Bakken, C. A., J. Jaramillo, R. Gomperts, R. E. Stratmann, ; O. Yazyev, A. J. A., R. Cammi, C. Pomelli, J. W. Ochterski, ; R. L. Martin, K. M., V. G. Zakrzewski, G. A. Voth, ; P. Salvador, J. J. D., S. Dapprich, A. D. Daniels, ; O. Farkas, J. B. F., J. V. Ortiz, J. Cioslowski, ; Fox, D. J. *Gaussian 09, revision a.02*, Gaussian, Inc., Wallingford CT: 2009.

[53] McIntyre, N. S.; Thompson, K. R.; Weltner, W., Spectroscopy of titanium oxide and titanium dioxide molecules in inert matrices at 4°K. *The Journal of Physical Chemistry* **1971,** 75, 3243-3249.

[54] Martin, R. L., Natural transition orbitals. *The Journal of Chemical Physics* **2003,** 118, 4775-4777.

[55] M. J. Frisch, G. W. T., H. B. Schlegel, G. E. Scuseria,; M. A. Robb, J. R. C., J. A. Montgomery, Jr., T. Vreven,; K. N. Kudin, J. C. B., J. M. Millam, S. S. Iyengar, J. Tomasi,; V. Barone, B. M., M. Cossi, G. Scalmani, N. Rega,; G. A. Petersson, H. N., M. Hada, M. Ehara, K. Toyota,; R. Fukuda, J. H., M. Ishida, T. Nakajima, Y. Honda, O. Kitao,; H. Nakai, M. K., X. Li, J. E. Knox, H. P. Hratchian, J. B. Cross,; V. Bakken, C. A., J. Jaramillo, R. Gomperts, R. E. Stratmann,; O. Yazyev, A. J. A., R. Cammi, C. Pomelli, J. W. Ochterski,; P. Y. Ayala, K. M., G. A. Voth, P. Salvador, J. J. Dannenberg,; V. G. Zakrzewski, S. D., A. D. Daniels, M. C. Strain,; O. Farkas, D. K. M., A. D. Rabuck, K. Raghavachari,; J. B. Foresman, J. V. O., Q. Cui, A. G. Baboul, S. Clifford,; J. Cioslowski, B. B. S., G. Liu, A. Liashenko, P. Piskorz,; I. Komaromi, R. L. M., D. J. Fox, T. Keith, M. A. Al-Laham,; C. Y. Peng, A. N., M. Challacombe, P. M. W. Gill,; B. Johnson, W. C., M. W. Wong, C. Gonzalez, and J. A. Pople *Gaussian 03, revision d.01*, Gaussian, Inc., Wallingford CT: 2004.

[56] Almeida, N. M. S.; McKinlay, R. G.; Paterson, M. J., Excited electronic states of MnO_4^-: Challenges for wavefunction and density functional response theories. *Chemical Physics* **2015,** 446, 86-91.

[57] Berardo, E.; Hu, H.-S.; Kowalski, K.; Zwijnenburg, M. A., Coupled cluster calculations on TiO_2 nanoclusters. *The Journal of Chemical Physics* **2013,** 139, 064313.

[58] Berardo, E.; Hu, H.-S.; Shevlin, S. A.; Woodley, S. M.; Kowalski, K.; Zwijnenburg, M. A., Modeling excited states in TiO_2 nanoparticles: On the accuracy of a TD-DFT based description. *Journal of Chemical Theory and Computation* **2014,** 10, 1189-1199.

[59] Berardo, E.; Hu, H.-S.; van Dam, H. J. J.; Shevlin, S. A.; Woodley, S. M.; Kowalski, K.; Zwijnenburg, M. A., Describing excited state relaxation and localization in TiO_2 nanoparticles using TD-DFT. *Journal of Chemical Theory and Computation* **2014,** 10, 5538-5548.

Chapter 4: Vibronic Coupling Effects on the Structure and Spectroscopy of Neutral and Charged TiO_2 Clusters.

4.1 Theoretical Background

Bulk TiO_2 (e.g., the rutile phase) is a wide band gap semiconductor[1]. Therefore doping in a variety of forms is an important factor. Clusters with an extra electron (radical anions), or an excess hole (radical cations), are useful models to study how the doping can affect the electronic and geometrical structure. Indeed as detailed below comparison of the charged clusters with the neutrals show many differences in structure.

As discussed below the geometry of some of the neutral clusters is best rationalised in terms of the pseudo Jahn-Teller effect (pJT), whereby vibronic coupling between the ground and excited states causes the clusters to adopt preferred shapes. This is then extended to look at the pJT effect in the charged radical clusters, where the constraints placed on the electronic structure theory are even more severe, but again it can be seen that vibronic coupling will often cause the radical cluster to adopt a different geometry to that of the neutral; this results in charge localisation on the cluster, which can be different between the radical cations and anions.

An expansion that describes the pJT effect was used first in bonding problems by Bader[2] and over the years there have been many rigorous (non-perturbative) descriptions of the pJT effect. Perhaps the simplest to illustrate the concept is the second-order perturbative expansion of the lower (non-degenerate) potential surface (E) originally due to Pearson[3], this is shown in equation (4.1)

$$E(Q_i) = E_0 + Q_i \left\langle \Psi_0 \left| \frac{\partial \boldsymbol{V}}{\partial Q} \right| \Psi_0 \right\rangle + \frac{Q_i^2}{2} \left\langle \Psi_0 \left| \frac{\partial^2 \boldsymbol{V}}{\partial Q_i^2} \right| \Psi_0 \right\rangle + Q_i^2 \sum_j \frac{\left[\left\langle \Psi_0 \left| \frac{\partial \boldsymbol{V}}{\partial Q_i} \right| \Psi_j \right\rangle \right]^2}{(E_0 - E_j)} \qquad (4.1)$$

E_0 is the energy at the expansion point, and **V** is the nuclear-nuclear and nuclear-electronic terms in the Hamiltonian, while the second term of this expression is, by

definition, zero for the optimised structure of a non-degenerate state (Ψ_0) (i.e., zero gradient). The third has been proved to always be positive by Bersuker et al[4] (and references therein). The final term is always negative as the energy (E_j) of the excited state (Ψ_j) is always greater than that of Ψ_0. There is one such expansion along each of the 3N-6 normal vibrational coordinates ($Q_i \in 3N\text{-}6$) of the molecule at the (high-symmetry) expansion geometry. It is the relative magnitude of the two quadratic terms that determine the stability of the molecule at this geometry. If for a given vibrational coordinate Q_i the sum of these two terms is negative then the geometry is unstable and there will be a pJT distortion along this vibrational coordinate. Symmetry can be used to determine if the final term is non-zero or not as the vibronic matrix element must transform as the totally symmetric (TS) irreducible representation (irrep) of the point group, i.e.,

$$\left\langle \Psi_0 \left| \frac{\partial V}{\partial Q_i} \right| \Psi_j \right\rangle \neq 0 \text{ iff } \Gamma_{\Psi_0} \otimes \Gamma_{Q_i} \otimes \Gamma_{\Psi_j} \supset \Gamma_{TS} \tag{4.2}$$

Many computational methods have been used in studying in the pJT effect down the years. An interesting one developed in recent years is based upon symmetry restrictions to a CASSCF Hessian matrix calculation first proposed by Bearpark *et al*[5]. This is based upon the notion that while CASSCF energies and gradients (of non-degenerate states) only require a many-electron basis (Slater determinants or spin adapted configuration state functions CSFs) that spans the irrep of the state in question, the Hessian contains terms that couple configurations of different symmetries. The analytical CASSCF Hessian obtained by solving the coupled perturbed multi-configuration self-consistent-field (CP-MCSCF) equations contains terms accounting for both orbital vibronic coupling and also non-adiabatic (state) vibronic couplings[5]. Thus the second-order terms in (equation (4.1)) are evaluated in obtaining the CASSCF Hessian matrix. The key to applying this to the pJT effect is to evaluate two comparative Hessians built from configurations spanning all irreps, and that of only the state under investigation. The pJT effect is manifest by noting a change in curvature (i.e., a change from real to imaginary frequency) along a mode of a given symmetry. This indicates that a pJT coupling has been "switched on" by including the configurations of appropriate symmetry in the wave function. This will be illustrated in the results below. The CASSCF pJT method can be regarded as a benchmark approach as it explicitly calculates the wave functions and couplings, and not only shows if such a

vibronic coupling is present, but also can detail the nature of the states involved via the configurations in the excited wave functions. However this comes at a price as the CP-MCSCF equations are very computationally expensive, and such approaches are at present limited to around 2000 many-electron basis functions. Nonetheless the method has been used with considerable success in both organic and inorganic chemistry[5-11].

Density functional theory (DFT) has emerged as an accurate and cost-effective way of studying the electronic and geometrical structure of a range of systems from small to large molecules and solids[12]. Time-dependent density functional theory (TD-DFT) has further extended the scope of the method and is nowadays the most used method to study electronically excited states in medium and large molecules[13]. While there may be problems with multireference electronic states DFT may sometimes be used to qualitatively understand the pJT effect via inspection of vibrational normal modes and excited orbitals from TD-DFT calculations[10]. Thus the CASSCF method has been used to calibrate the DFT (and TD-DFT) on the TiO_2 systems (*vide infra*), and then DFT (and TD-DFT) were applied to the larger clusters for which CASSCF is not feasible. Equation of motion coupled cluster singles and doubles (EOM-CCSD) is also used to calibrate some of the TD-DFT excited state computations. In the previous chapter (chapter 3) it was shown that TD-DFT is often competitive with much more expensive many-body response methods applied to TiO_2. Regarding the computations on the radical systems there is one other aspect that must be considered when applying single-reference methodologies such as DFT: namely spurious symmetry breaking[15]. This occurs when a lower symmetry wave function can be found which is lower in energy than a wave function displaying the correct point group symmetry. While multi-configurational self-consistent field methods, such as CASSCF, don't have this problem as they allow for the correct mixing of competing configurations[16, 17], such problems often occur in unrestricted Hartree-Fock treatments of radicals. In unrestricted density functional investigations on high-spin radicals it has generally been found that such problems do not plague DFT to the same degree[15]. The problem of spurious, or artificial, symmetry breaking is highlighted by Dixon *et al*[18] in their discussion of the equilibrium geometries of $(TiO_2)_n$ anionic clusters. A check for spurious symmetry breaking was made by comparing the energetics of the high-symmetry species in the absence of any symmetry constraints on the wave function via infinitesimal non-totally symmetric structural changes. Spurious symmetry breaking is observed as correspondingly large energetic changes that display a derivative discontinuity. It is

shown below using a combination of CASSCF, Brueckner doubles and B3LYP calculations with broken symmetry that, at least in the case of the monomers, the symmetry breaking appears to be real. Even if both spurious symmetry breaking and the related issue of multi-configurational states aren't present some functionals may still fail to properly describe the system being studied. Such problems mean that DFT cannot be expected to perform "across the board" when applied to such radical systems and note in the results where TD-DFT with B3LYP does not properly describe such electronic states.

4.2 Computational Details

All DFT, TD-DFT, and EOM-CCSD calculations where carried out with the Gaussian 09 program[19], while CASSCF calculations were run using the Gaussian 03 program[20]. As discussed above DFT is sometimes more stable with regard to spurious (wave function) symmetry breaking than unrestricted Hartree-Fock. However this may be dependent on the functional chosen and basis set used. A range of calibration tests were run using a variety of functionals and basis sets, and compared with large scale CASSCF for neutral, and radical species of the two smallest clusters. It was found that all hybrid functionals show a similar behaviour and for the radical species are stable, in contrast to Hartree-Fock calculations on some of the same systems. It is also noted that with hybrid functionals spin-contamination was relatively low for the radicals considered. Again for excited states it was found that hybrid functionals give the best results in comparison to both CASSCF and EOM-CCSD. Therefore the B3LYP functional was used for all of the DFT calculations discussed below. Several basis sets were investigated and it was found that the cc-pVTZ basis gave the best balance between accuracy and computational cost. For oxygen this was the standard cc-pVTZ basis set of Dunning *et al*[21], while the set optimised for 3d transition metals of Peterson *et al*[22] was used for Titanium. The exception being any DFT calculations involving the anion where diffuse functions where added to the basis sets of both oxygen and titanium. For the anion diffuse functions were added, taken from the aug-cc-pVTZ basis (diffuse s and p for O, and diffuse s, p, and d for Ti). Due to the expense of the pJT CASSCF calculations requiring analytical Hessian evaluation the cc-pVDZ

basis was used for these, and calibrated by checking that geometries and excitation energies were close to the cc-pVTZ values.

In the next section a couple of the neutral structures (n=1 and 2) are rationalised in terms of the pJT effect. Then the radical cation and anion structures are considered and it is shown how they differ from the neutral and each other. Again this is rationalized in terms of appropriate vibronic couplings with electronically excited states in the pJT effect.

4.3 Neutral Clusters

4.3.1 TiO_2

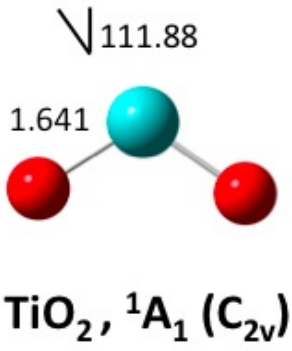

Figure 4-1: TiO_2 ground state minimum has a bent geometry with C_{2v} symmetry

As discussed in chapter 3 TiO_2 has a bent geometry with C_{2v} symmetry. With B3LYP the linear geometry is a second-order saddle-point with a doubly degenerate imaginary frequency for the pair of vibrational (bending) modes with Π_u symmetry. This can be rationalised in terms of the pJT effect in the form of an excited electronic state ($^1\Delta_u$ at 0.76 eV) mixing with the ground electronic state as the molecule bends. The CASSCF pJT diagnostic (*vide supra*) was performed on a geometry also optimised using CASSCF. Using CAS(8,8), built from appropriate orbitals to describe the states, and evaluating the Hessian using all CSFs (total = 1764) gives a doubly-degenerate imaginary frequency for the bending mode, while using the only CSFs of A_g symmetry (total=256, derived from the ground $^1\Sigma_g^+$ electronic state in the D_{2h} subgroup used by the program) gives this pair of modes as having a real frequency. The $^1\Delta_u$ state corresponds to a transfer of electron density from the oxygens to the titanium and this

partial charge transfer when mixed with the ground electronic state favours the bent form. Further the excited state has slightly less anti-bonding character along the TiO bonds and slightly greater bonding with respect to the angle bend, and these factors favour the minimum with shorter TiO bonds and angle 111.88° shown in Figure 4-1.

4.3.2 $(TiO_2)_2$

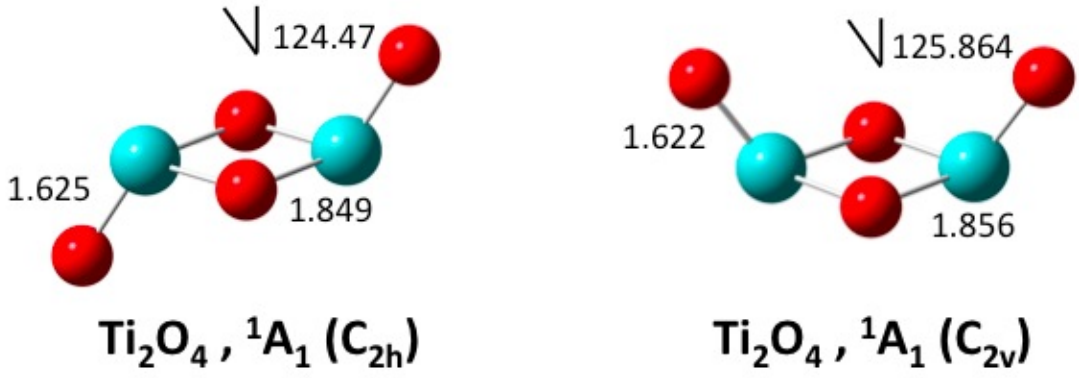

Figure 4-2: B3LYP optimised ground state minimum geometries of two low-lying isomers of $(TiO_2)_2$

The optimised B3LYP geometries of two lying isomers of $(TiO_2)_2$ are shown in Figure 4-2, while the ground state adiabatic potential energy surface for $(TiO_2)_2$ in the space of the two terminal oxygen atoms bending is shown in Figure 4-3.

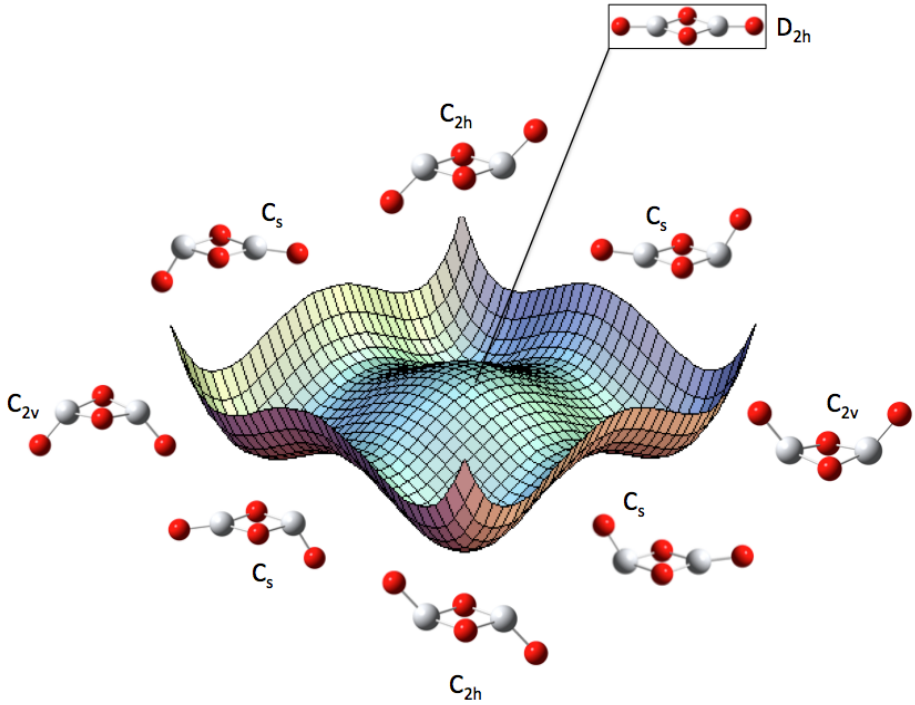

Figure 4-3: $(TiO_2)_2$ ground state adiabatic potential energy surface showing double pseudo-Jahn-Teller effect relating D_{2h} second-order saddle-point with C_{2h} and C_{2v} minima.

The planar D_{2h} structure in the centre of the figure is a second-order saddle point. Bending one of the oxygens up and the other down leads to a C_{2h} structure (maintaining the inversion centre), while bending both in the same direction leads to a C_{2v} structure. The vibrations are shown schematically in Figure 4-4(a) and (b) below. Clearly one can take linear combination of these vibrations such that only one terminal oxygen moves out of plane and this results in a C_s structure, which is a saddle-point on the surface with the transition vector corresponding to the in-plane terminal oxygen moving in the same direction as the other (C_{2h} minimum), or opposite (C_{2v} minimum). The barrier heights are 1.031 eV for C_{2h}-D_{2h}, 0.769 eV for C_{2v}-D_{2h}, and 0.190 eV for C_s-D_{2h}. The primary orbitals corresponding to the excited states involved are also given in Figure 4-4.

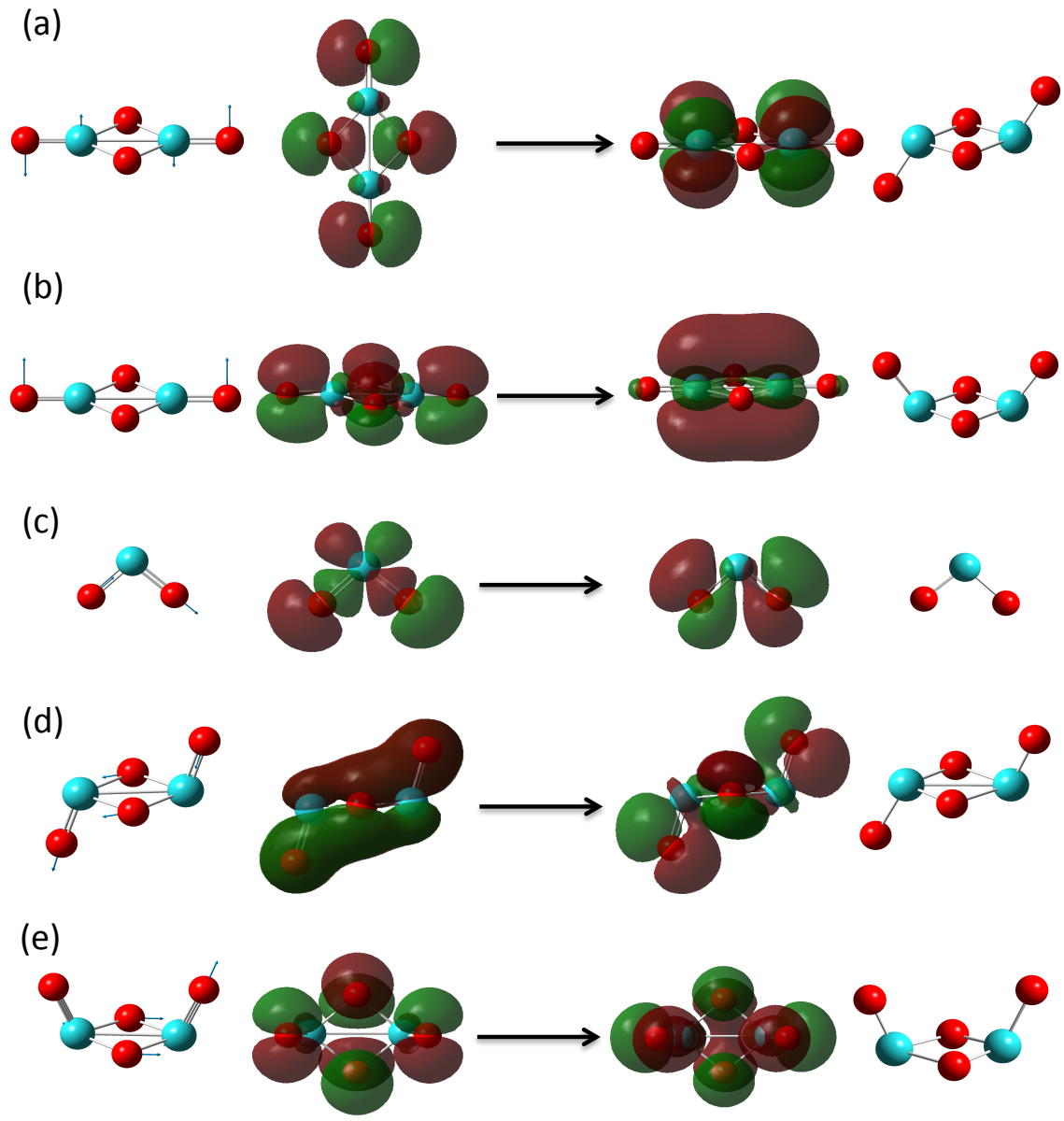

Figure 4-4: Orbitals and vibrations involved in pJT coupling in selected TiO_2 clusters. (a) Neutral $(TiO_2)_2$ $D_{2h} \rightarrow C_{2h}$; (b) Neutral $(TiO_2)_2$ $D_{2h} \rightarrow C_{2v}$; (c) Cation TiO_2^{+} $C_{2v} \rightarrow C_s$; (d) Cation $(TiO_2)_2^{+}$ $C_{2h} \rightarrow C_s$, (e) Cation $(TiO_2)_2^{+}$ $C_{2v} \rightarrow C_s$.

For the $D_{2h} \rightarrow C_{2h}$ distortion (B_{2g} symmetry) the excited state responsible for the coupling is of B_{2g} symmetry since the ground state is totally symmetric (^1A_g). For the $D_{2h} \rightarrow C_{2v}$ distortion (B_{3u} symmetry) the excited state responsible for the coupling is therefore of B_{3u} symmetry. Similar to the linear TiO_2 discussed above these states involve a partial transfer of charge from the terminal oxygens to the titaniums. Again the nature of the states that mix stabilise the respective structure on the ground state surface. This system is therefore an example of double-pJT system. The EOM-CCSD and TD-B3LYP results for the low-lying valence states in the system are generally within 0.2 eV of each other.

4.4 Radical Cations

In the following sections the results of calculations for the radical cations and anions are presented. It is noted that there is a similarity in these results to those presented previously by Qu and Kroes[23], here they are rationalised in terms of the pseudo-Jahn-Teller effect. A summary of the relevant excitation energies for the radical cations is presented below in Table 4-1.

Cation	*Ground state symmetry*	*Excited state symmetry*	*ΔE (eV)*
TiO_2^+	$^2B_2$	$^2A_1$	2.56
$(TiO_2)_2^+$ - C_{2h}	^2B_u	^2A_g	2.18
	^4A_u	^4B_g	1.28
$(TiO_2)_2^+$ - C_{2v}	$^2A_1$	$^2B_2$	1.13
	$^4B_1$	$^4A_2$	1.28
$(TiO_2)_3^+$	$^2A'$	$^2A''$	0.75
$(TiO_2)_4^+$	$^2A_1$	$^2B_2$	0.83
	$^4B_2$	$^4B_1$	1.02

Table 4-1: Symmetry of vibronically coupled states and vertical energy differences for radical $(TiO_2)_n$ cations discussed in text. ΔE (eV) calculated using TD-B3LYP.

4.4.1 TiO_2^+

The minimum structure of the TiO_2 doublet cation has a C_s symmetry minimum, rather than the C_{2v} symmetry common to the neutral discussed above, anion discussed below and the cationic quartet minimum shown in Figure 4-5.

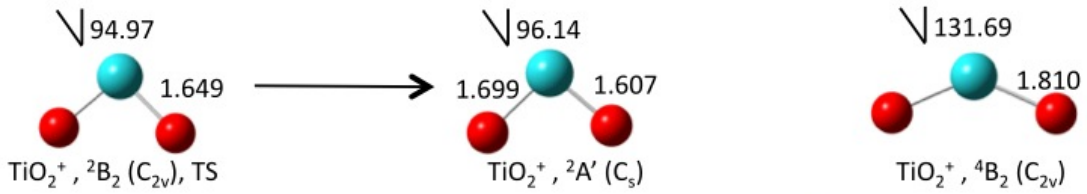

Figure 4-5: Cation TiO_2 structures, symmetries and electronic states optimised at the B3LYP/cc-p-VTZ level.

The C_{2v} symmetry structure in this case appears to be a transition state with a single imaginary frequency along the asymmetric stretch vibrational coordinate. The C_s geometry, shown in Figure 4-5, has bond-lengths of 1.70 and 1.61 Å and a bond angle of 96.14°. This is a large distortion from the neutral minimum geometry with a bond-length change of about 0.05 Å concurrent with a reduction of bond angle of about 15°. The C_{2v} transition state has bond-lengths of 1.65 Å, a bond angle of 94.96° and has a $^2B_2$ ground state. The symmetry of the imaginary vibrational coordinate is also B_2 suggesting that the ground state is coupled with an excited state of A_1 symmetry. Using TD-B3LYP at the transition structure the lowest excited state of A_1 symmetry was found to at 2.56 eV.

As well as the B3LYP functional, a number of different functionals were tried during the investigation of this structure. In the work of Dixon *et al*[18] LSDA calculations (BP86 and PW91) are used that show imaginary frequencies found for Anionic $(TiO_2)_n$ clusters were the result of artificial symmetry breaking. The BP86 and PW91 functionals also calculated the C_{2v} TiO_2^+ structure to have no imaginary frequency. However, a test of the B3LYP functional which forces lower symmetry in the calculation shows no effect of artificial symmetry breaking and the recent M06 functional set of Truhlar *et al*[24], all bar M06-L functional, agree with the B3LYP result. This result was also confirmed with a Brueckner doubles calculation where again the C_{2v} structure was a transition state and the C_s structure was found to be the minimum. The C_{2v} transition state was re-optimised using the CASSCF with a (7,7)

active space of appropriate valence orbitals. The CASSCF optimised geometry differed very slightly from that of B3LYP. Using a further CAS(7,7) calculation that included all configuration state functions an imaginary frequency was calculated for the CASSCF optimised geometry. Since the CASSCF method is not affected by artificial symmetry breaking this confirms the validity of the B3LYP calculation. It would seem here that extreme care must be taken when choosing a DFT functional for such systems.

For the pJT test, the CASSCF frequency calculation was repeated using only those configuration state functions of the ground state symmetry (B_2) no imaginary frequencies were found. A schematic of this effect is shown in Figure 4-6.

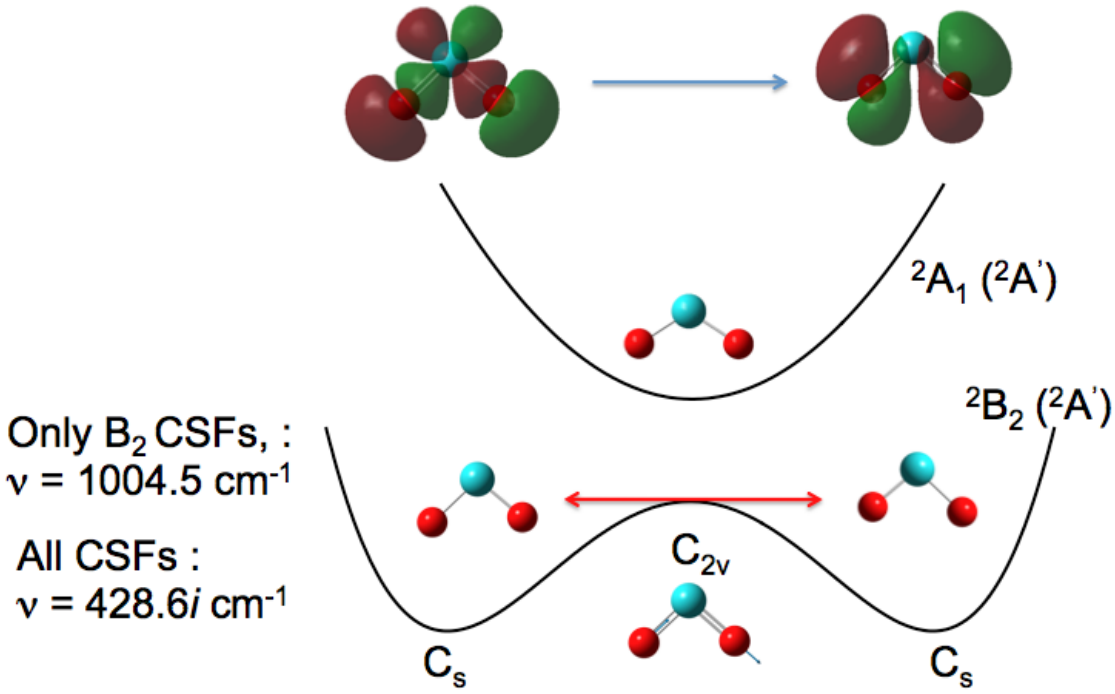

Figure 4-6: TiO_2^{+} lowest adiabatic and excited potential energy curves with respect to anti-symmetric (b_2) bending vibration. Pseudo-Jahn-Teller effect involves coupling of ground state ($^2B_2$) with excited ($^2A_1$) state at C_{2v} geometry, and is manifest as differing curvatures obtained from CAS(7,7)/cc-pVDZ (Ti)-cc-pVTZ (O) with many-electron basis configurations of only B_2 symmetry versus those of all symmetries.

Also shown are the primary orbitals involved in the transition. Again it is noted that the B3LYP generally agrees well with the CASSCF results, although the B3LYP surface is flatter than the CASSCF one (the B3LYP imaginary frequency is 209.7i cm^{-1} while the CASSCF is 428.6i cm^{-1}). This feature was previously observed in using this method to look at the pJT effect in a bioctahedral molybendum complex. It is believed that this is due to the features of multi-configuration character that the DFT cannot model; although in both cases the curvature is qualitatively correct[11].

4.4.2 $(TiO_2)_2^+$

The structures presented for the $(TiO_2)_2^+$ are those optimised from the C_{2h} and C_{2v} neutral minima using B3LYP. These calculations were repeated using two M06 functionals (M06 and M06-L), which were found to be in good agreement with B3LYP. However, PW91 and BP86 calculate one imaginary frequency for C_{2h} and none for C_{2v}, and, using the forced symmetry test both B3LYP and M06 do appear to show some artificial symmetry breaking.

4.4.2.1 $(TiO_2)_2^+ - C_{2h}$

In the n=2 cation cluster a transition state of C_{2h} symmetry similar in structure to the C_{2h} neutral minima is found. The structure of the transition state differs from that of the neutral in that Ti-terminal oxygen bond-lengths are slightly longer, the sides of the Ti-O-Ti-O square are slightly shorter and that the Ti-Ti-Terminal oxygen bonds angles are smaller at 109.22° (Figure 4-7).

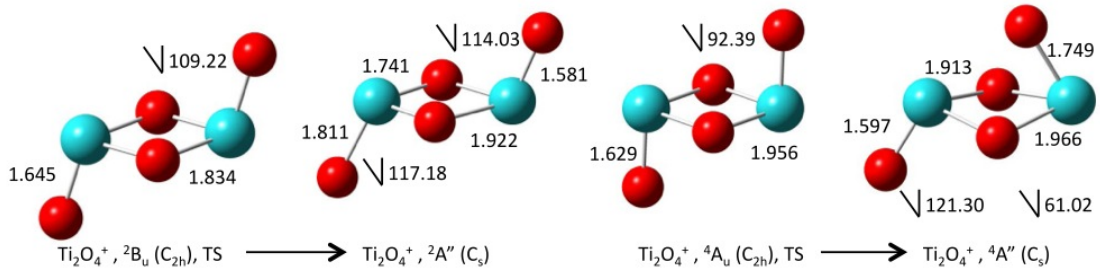

Figure 4-7: Cation $(TiO_2)_2$ C_{2h} structures, symmetries and electronic states optimised at B3LYP/cc-pVTZ level.

Following the single imaginary frequency the C_s minima shown in Figure 4-7 was optimised. The symmetries of the molecule, and that of the vibration, dictate that there must be an equivalent minimum where the vibration is followed in the opposite direction. This pJT distortion occurs due to coupling between the ground state (^2B_u) and excited state of A_g symmetry. Using TD-B3LYP at the transition state geometry the lowest excited state of A_g symmetry was found at 2.18 eV. The bond-lengths of the C_s minima follow a bonding pattern where by a shortened bond-length is neighboured by a lengthened bond-length, with respect to the transition structure, and vice-versa.

There is also a breaking of symmetry at the Ti-Ti-terminal O bonds angles where they are no longer equal, one being 117.18° and the other 114.03°. The vibration and primary orbitals involved are shown in Figure 4-4 (d).

The quartet state similarly has a pair of C_s symmetry minima divided by a C_{2h} transition state. This quartet transition state differs from the neutral minima in that the Ti-Ti-terminal oxygen bonds angle is smaller at 92.39° and that the central Ti-O-Ti-O square sides are longer at 1.96 Å (Figure 4-7). This geometry is distorted due to vibronic coupling between the ^4A_u ground state and a ^4B_g excited state, found to be 1.28 eV from the ground state using TD-B3LYP. In the C_s minima the central square is slightly pinched; the oxygens are distorted slightly out of the plane formed by the square, there is an asymmetry in the bond angles of the terminal oxygen (61.02° and 121.30°), and there is the same pattern of alternating lengthening and shortening of bond-lengths with respect to the transition state, as seen for the doublet. This distortion of the central square out of the planar geometry is due to the proximity of the terminal oxygen with a bond angle of 61.02°.

4.4.2.2 $(TiO_2)_2^+ - C_{2v}$

On the doublet potential energy surface of the n=2 cluster there is also a transition state of C_{2v} symmetry (Figure 4-8).

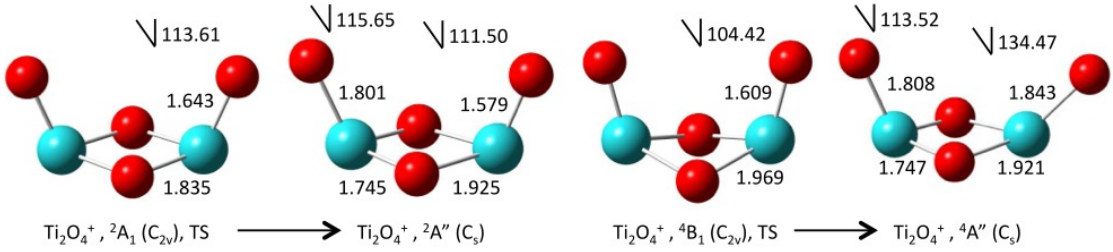

Figure 4-8: Cation $(TiO_2)_2$ C_{2v} structures, symmetries and electronic states optimised at B3LYP/cc-pVTZ level.

This structure differs from the neutral C_{2v} structure in that the bond angle is smaller (113.61°), the bonds of the square are slightly shorter and the bonds to the terminal oxygen are slightly longer. This transition state separates two identical minima found along the imaginary vibration of the transition state. These minima have C_s symmetry and have common features with the C_s minima associated with the C_{2h} transition state. While not being the same structure they both exhibit the alternating bond-lengths and

the differing terminal oxygen bond angles. The pJT effect seen in this example results from a coupling of the $^2B_2$ excited state 1.13 eV from the $^2A_1$ ground state (vibration and orbitals shown Figure 4-4 (e)).

For the quartet state there is also a transition state of C_{2v} symmetry and a $^4B_1$ ground state. Here the terminal oxygen forms smaller angles with the titanium atoms (104.42°) than seen with the neutral structure. The proximity of these oxygen atoms seems to have an effect on the oxygen in the central square distorting them out of the plane. The C_s minimum structure shown in the Figure 4-8 shows that the bond angles of the Ti-Ti-terminal oxygen have increased, relieving the pressures on the central oxygen and that they have relaxed back to the planar arrangement of the central square. This structure also shows alternating bond-lengths. TD-B3LYP shows the coupling state in this case to be $^4A_2$ and the energy difference is 1.28 eV.

4.4.3 $(TiO_2)_3^+$

The minimum structure for the n=3 doublet cluster was found by optimising from the neutral C_s structure is one of C_1 symmetry (Figure 4-9).

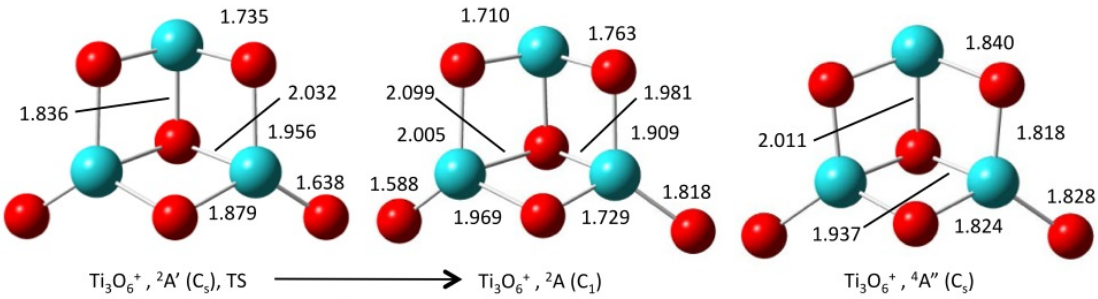

Figure 4-9: Cation $(TiO_2)^3$ structures, symmetries and electronic states optimised at B3LYP/cc-pVTZ level.

In the same way as previously described the alternate long and short bonds break the molecular symmetry and result in charge localisation. TD-B3LYP shows the pJT coupling state in this case to be ^2A" and the energy difference to be 0.75 eV. The quartet state for this species has a C_s minimum and shows no pJT effect relative to the C_s neutral structure although some bond-lengths differ (Figure 4-9).

4.4.4 $(TiO_2)_4^+$

Optimisation of the geometries from the C_{2v} neutral minimum structure, on both the doublet and quartet potential energy surfaces, converges on a corresponding C_{2v} transition state for each (Figure 4-10).

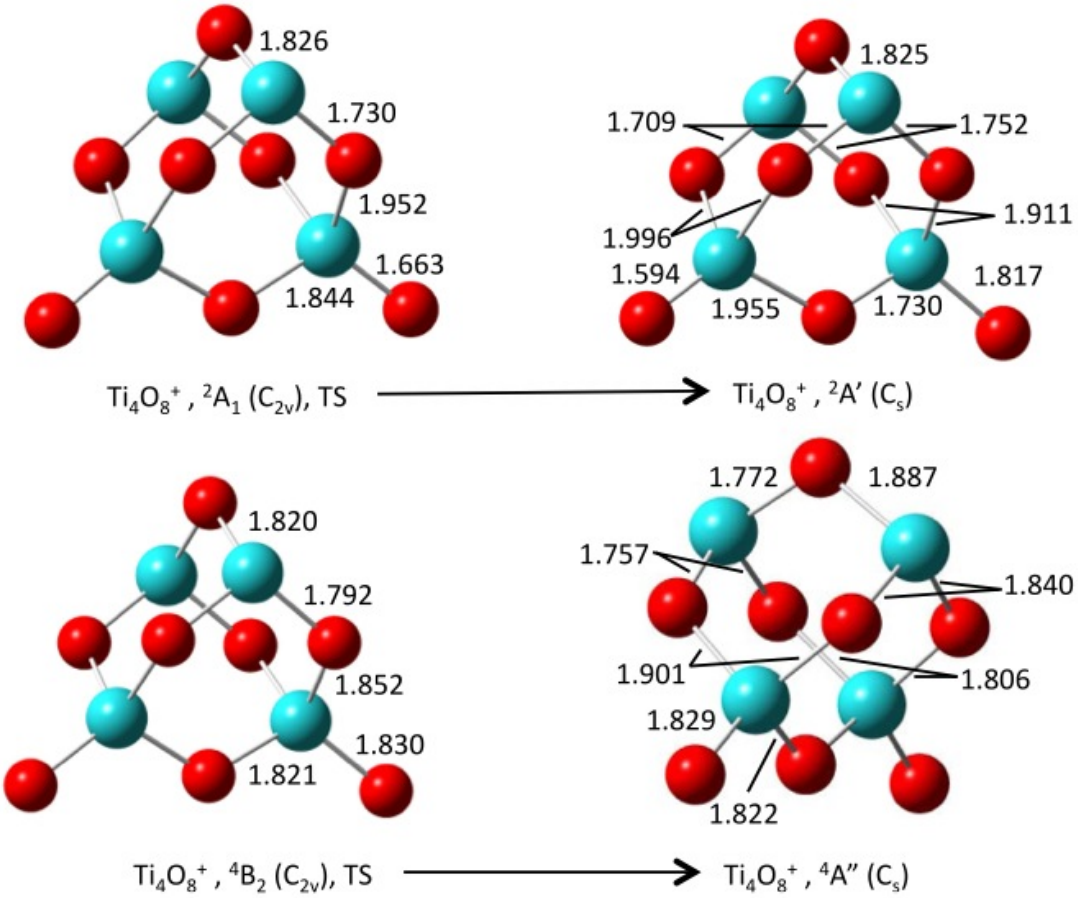

Figure 4-10: Cation $(TiO_2)_4$ structures, symmetries and electronic states optimised at B3LYP/cc-pVTZ level.

These transition states differ structurally from each other, and the neutral minimum, only in terms of the relative bond-lengths. Both the doublet and quartet minimise from these C_{2v} transition states to minima of C_s symmetry. The major difference between these minima is that the relative orientations of their σ_h symmetry planes are perpendicular to each other. Where one of the σ_h symmetry planes can be thought of as containing the top most oxygen and the titanium atom to which it is directly bonded forming a plane from the top to bottom of the molecule, the second σ_h symmetry plane is perpendicular to the first containing the top most oxygen and the two titanium atoms to which it is not directly bonded. The two C_s minima also differ in their relative bond-

lengths. TD-B3LYP shows the coupling state in the case of the doublet to be $^2B_2$ with the $^2A_1$ ground at an energy difference of 0.83 eV, and for the quartet to be a coupling between the $^4B_2$ ground and a $^4B_1$ state with an energy difference of 1.02 eV.

4.5 Radical Anions

A summary of the relevant excitation energies for the radical anions is presented below in Table 4-2.

Anion	*Ground state symmetry*	*Excited state symmetry*	*ΔE (eV)*
TiO_2^-	$^4A_2$	$^4B_1$	0.18
$(TiO_2)_2^-$ - C_{2h}	^2A_g	^2B_u	0.65
	^4A_g	^4B_u	-0.84
$(TiO_2)_2^-$ - C_{2v}	$^4B_2$	$^4A_1$	1.46
$(TiO_2)_3^-$	$^4A'$	$^4A''$	-0.17
$(TiO_2)_4^-$	$^4B_1$	$^4A_2$	0.49

Table 4-2: Symmetry of vibronically coupled states and vertical energy differences for radical $(TiO_2)_n$ anions discussed in text. ΔE (eV) calculated using TD-B3LYP.

4.5.1 TiO_2^-

The minimum structure of the TiO_2 anion monomer is a doublet with C_{2v} symmetry (Figure 4-11)

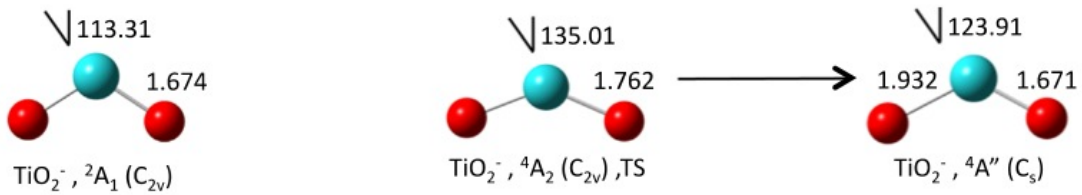

Figure 4-11 Anion TiO_2 structures, symmetries and electronic states optimised at the B3LYP/cc-p-VTZ level.

In comparison to the neutral minima there is only a slight increase in the bond-length from 1.64 to 1.67 Å and a small difference in the bond angle 113.31° from 111.88°. It is when considering the quartet state of this anion that a more dramatic difference is

observed. In the quartet state the C_{2v} geometry is a transition state with a single negative frequency in the asymmetric stretching vibration. This transition state has a bond-length of 1.76 Å and a bond angle of 135.01° (Figure 4-11). In this case there again seems to be some artificial symmetry breaking with B3LYP, but the C_{2v} structure optimised using CAS(7,7) was also found to be a transition state, which re-optimised to a C_s minima. The same flattening of the B3LYP surface is apparent (the B3LYP imaginary frequency is 447.9i cm^{-1} while the CASSCF is 1645.0i cm^{-1}). By distorting the molecule along this asymmetric stretching coordinate the C_{2v} symmetry of the molecule is broken and an optimisation from this point proceeds to the minimum geometry. This occurs due to vibronic coupling of the $^4A_2$ ground state with an excited state of $^4B_1$ symmetry, which is only 0.18 eV above. The resulting C_s minimum has bond-lengths of 1.94 and 1.67 Å and a bond angle of 123.89°.

4.5.2 $(TiO_2)_2^- - C_{2h}$

Taking as a starting point the C_{2h} structure of the neutral n = 2 cluster an optimisation of the anionic doublet is made to a structure of C_{2h} symmetry, which is found to be a transition state (Figure 4-12).

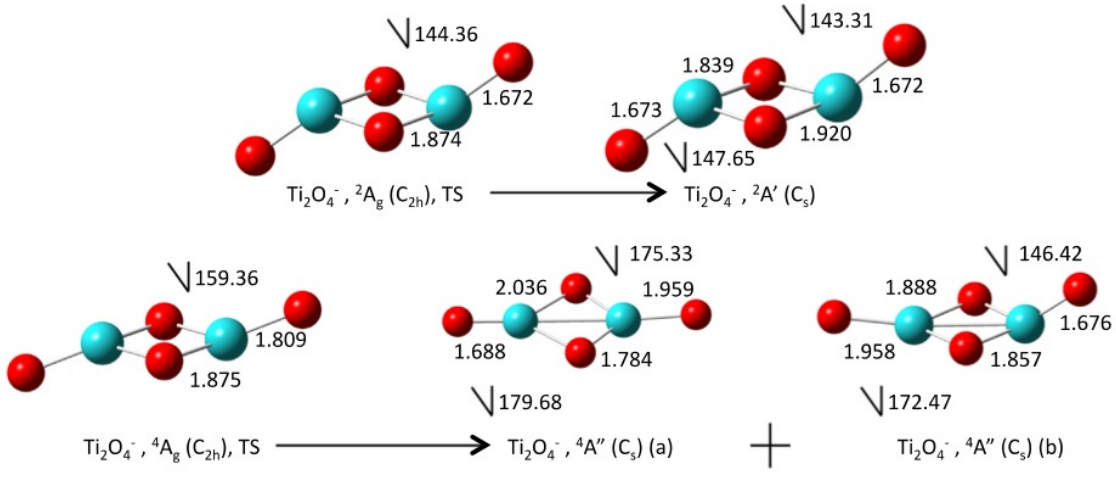

Figure 4-12: Anion $(TiO_2)_2$ C_{2h} structures, symmetries and electronic states optimised at B3LYP/cc-pVTZ level.

This transition state differs from the neutral geometry due to both a flattening of the structure, where the angles made by the terminal oxygen with the titanium are increased toward a planar geometry, and a general lengthening of the bonds. As reported by

Dixon *et al*[18] BP86 and PW91 calculate no imaginary frequency for the C_{2h} structure. The M06 functional also finds the C_{2h} structure to be a minimum, but using the forced symmetry test B3LYP does not appear to show artificial symmetry breaking. This result is at odds with that of [18], but given B3LYP's apparent agreement with CASSCF calculations it is believed to be a true symmetry breaking. Again though, this highlights the care that must be taken with these very tricky radical systems. A displacement of the structure breaking the C_{2h} symmetry optimises the B3LYP calculation to a pair of minima of C_s symmetry. The pJT coupling of the ground state (^2A_g) in this case is with one of ^2B_u symmetry and the energy difference is around 0.65 eV.

The ^4A_g quartet state of C_{2h} symmetry is found to be a second-order saddle point with 2 imaginary frequencies (2646.66i cm^{-1} and 92.670i cm^{-1}) and optimising from this structure along each of the negative vibration optimises to the two ^4A" C_s minima (a from 2646.66i cm^{-1} and b from 92.670i cm^{-1}) shown in Figure 4-12. The smaller imaginary frequency persists even when using an ultrafine numerical integration grid in the DFT. The B3LYP method is found to show artificial symmetry breaking here. Using BP86 and PW91 functionals a single imaginary frequency is calculated corresponding to the larger imaginary frequency of the B3LYP calculation. The ^4A_g quartet ground state is found to couple with a ^4B_u excited state. The TD-B3LYP excitation energy is negative, another indication of the failure of B3LYP to describe this system and related to the spurious symmetry breaking one obtains from a C_{2h} B3LYP Kohn-Sham solution.

4.5.3 $(TiO_2)_2^- - C_{2v}$

The lowest doublet ($^2A_1$) minimum structure is one of C_{2v} symmetry. Here there is no distortion of the molecule due to any vibronic coupling. The structure differs from that of the neutral by a general increase in bond-lengths and by an increase in the Ti-Ti-terminal oxygen angle flattening the molecule (Figure 4-13).

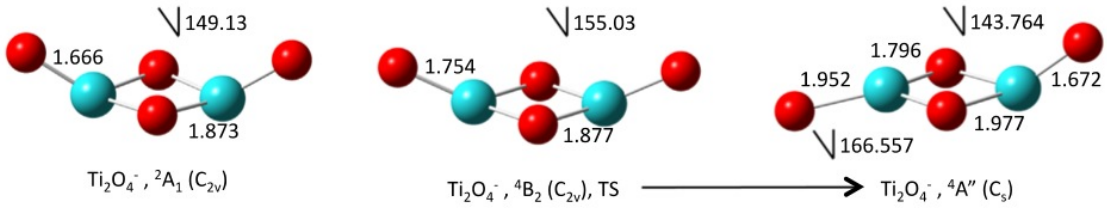

Figure 4-13: Anion $(TiO_2)_2$ C_{2v} structures, symmetries and electronic states optimised at B3LYP/cc-pVTZ level.

For the quartet state ($^4B_2$) the C_{2v} structure is detected to be a transition state with a single imaginary frequency, but again there would seem to be some artificial symmetry breaking present. Optimisation along the vibration coordinate associated with this imaginary frequency results in a minimum with the structure ^4A" C_s shown in Figure 4-13. The pJT coupling state in this case is $^4A_1$ and the energy difference to be around 1.46 eV.

4.5.4 $(TiO_2)_3^-$

Here the results for the n=3 anion structures are the opposite of those for the cation (Figure 4-14).

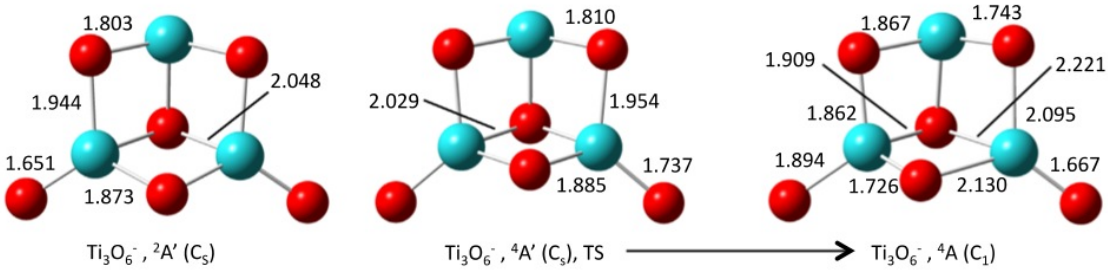

Figure 4-14: Anion $(TiO_2)^3$ structures, symmetries and electronic states optimised at B3LYP/cc-pVTZ level.

The doublet minimum (^2A') has a C_{2v} structure, similar to the neutral and cation quartet minima. The anion quartet (^4A') results mirror those of the cation doublet with a C_s transition state distorting to C_1 minima, where alternating long and short bond-lengths, and localising of the charge have distorted the C_s symmetry. These similarities extend only to the general structures but differ as to the relative bond-lengths (Figure 4-14). For the quartet the pJT coupling is from the ^4A' ground state to a ^4A" excited state. Using TD-DFT, B3LYP hasn't properly described the excited state as the calculated energy difference is -0.17.

4.5.5 $(TiO_2)_4^-$

The doublet ($^2A_1$) minimum optimised from the C_{2v} symmetry also is found to have C_{2v} symmetry (again opposite to the cation) (Figure 4-15).

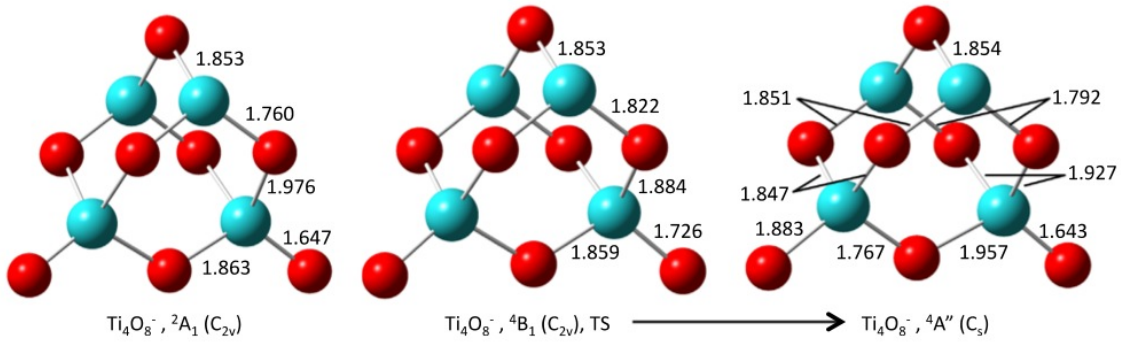

Figure 4-15: Anion $(TiO_2)_4$ structures, symmetries and electronic states optimised at B3LYP/cc-pVTZ level.

The quartet C_{2v} structure is found to be a transition state separating ($^4B_1$) minima of C_s symmetry where the σ_h symmetry plane bisects the molecule through the top most oxygen and the two titanium atoms to which it is not directly bonded (Figure 4-15). The pJT coupling state is $^4A_2$ at 0.49 eV from the ground state.

4.6 Conclusions

How the pseudo-Jahn-Teller effect is manifest in certain neutral, cation, and anion clusters of TiO_2 has been shown using a variety of computational techniques. These vibronic interactions can be understood in terms of a CASSCF diagnostic. It has also been shown that generally the B3LYP density functional gives reasonably accurate results on this challenging class of systems, although like all current functionals does display pathological artificial symmetry breaking in some systems. Furthermore time-dependent density functional theory is able to aid in a qualitative understanding of the vibronic couplings when there is no artificial symmetry breaking. The interaction of electronic states coupled via nuclear vibrations gives rise to distinct geometrical features in all the clusters and is responsible for the degree of charge localisation in the radical clusters. It was found that the positive and negative radical clusters often undergo

different vibronic interactions and consequently adopt differing geometries. It is hoped these results will contribute to on-going experimental and theoretical efforts aimed at understanding the nature of quantum size effects in size-selected TiO_2 nanoclusters.

4.7 References

[1] Zhai, H.-J.; Wang, L.-S., Probing the electronic structure and band gap evolution of titanium oxide clusters $(TiO_2)_n$ - (n = 1-10) using photoelectron spectroscopy. *Journal of the American Chemical Society* **2007,** 129, 3022-3026.

[2] Bader, R. F. W., Vibrationally induced perturbations in molecular electron distributions. *Can J Chemistry* **1962,** 40, 1164-1175.

[3] Pearson, R. G., Concerning Jahn-Teller effects. *Proceedings of the National Academy of Sciences of the United States of America* **1975,** 72, 2104-2106.

[4] Bersuker, I. B., *The jahn-teller effect*. Cambridge University Press: Cambridge, UK ; New York, 2006; p xvi, 616 p.

[5] Bearpark, M. J.; Blancafort, L.; Robb, M. A., The pseudo-Jahn-Teller effect: A CASSCF diagnostic. *Molecular Physics* **2002,** 100, 1735-1739.

[6] Blancafort, L.; Bearpark, M. J.; Robb, M. A., Ring puckering of cyclooctatetraene and cyclohexane is induced by pseudo-Jahn-Teller coupling. *Molecular Physics* **2006,** 104, 2007-2010.

[7] McKinlay, R. G.; Paterson, M. J., The Jahn–Teller effect in binary transition metal carbonyl complexes, *The Jahn-Teller Effect*. In Köppel, H.; Yarkony, D. R.; Barentzen, H., Eds. Springer Berlin Heidelberg: 2009; Vol. 97, pp 311-344.

[8] McKinlay, R. G.; Zurek, J. M.; Paterson, M. J., Vibronic coupling in inorganic systems: Photochemistry, conical intersections, and the Jahn-Teller and pseudo-Jahn-Teller effects. In *Advances in inorganic chemistry*, Rudi van Eldik; Harvey, J., Eds. Elsevier Inc.: 2010; Vol. 62, p 351.

[9] Paterson, M. J.; Bearpark, M. J.; Robb, M. A.; Blancafort, L.; Worth, G. A., Conical intersections: A perspective on the computation of spectroscopic Jahn-Teller parameters and the degenerate 'intersection space'. *Physical Chemistry Chemical Physics* **2005,** 7, 2100-2115.

[10] Paterson, M. J.; Chatterton, N. P.; McGrady, G. S., View from the bridge: A pseudo-Jahn-Teller approach to transition metal hydrosilane complexes. *New J. Chem.* **2004,** 28, 1434-1436.

[11] Zurek, J. M.; Paterson, M. J., Theoretical study of the pseudo-Jahn-Teller effect in the edge-sharing bioctahedral complex $MO_2(dxyif)_2(O_2CCH_3)_2(\mu_2\text{-}O)_2$. *Inorg. Chem.* **2009,** 48, 10652-10657.

[12] Riley, K. E.; Op't Holt, B. T.; Merz, K. M., Critical assessment of the performance of density functional methods for several atomic and molecular properties. *Journal of Chemical Theory and Computation* **2007,** 3, 407-433.

[13] Jacquemin, D.; Wathelet, V.; Perpete, E. A.; Adamo, C., Extensive TD-DFT benchmark: Singlet-excited states of organic molecules. *Journal of Chemical Theory and Computation* **2009,** 5, 2420-2435.

[14] Taylor, D. J.; Paterson, M. J., Calculations of the low-lying excited states of the TiO_2 molecule. *Journal of Chemical Physics* **2010,** 133.

[15] Bally, T.; Borden, W. T., Calculations on open-shell molecules: A beginner's guide. In *Reviews in computational chemistry*, John Wiley & Sons, Inc.: 2007; pp 1-97.

[16] Sherrill, C. D.; Lee, M. S.; Head-Gordon, M., On the performance of density functional theory for symmetry-breaking problems. *Chemical Physics Letters* **1999,** 302, 425-430.

[17] Cohen, R. D.; Sherrill, C. D., The performance of density functional theory for equilibrium molecular properties of symmetry breaking molecules. *Journal of Chemical Physics* **2001,** 114, 8257-8269.

[18] Li, S. G.; Dixon, D. A., Molecular structures and energetics of the $(TiO_2)_n$ (n=1-4) clusters and their anions. *Journal of Physical Chemistry A* **2008,** 112, 6646-6666.

[19] M. J. Frisch, G. W. T., H. B. Schlegel, G. E. Scuseria, ; M. A. Robb, J. R. C., G. Scalmani, V. Barone, B. Mennucci, ; G. A. Petersson, H. N., M. Caricato, X. Li, H. P. Hratchian, ; A. F. Izmaylov, J. B., G. Zheng, J. L. Sonnenberg, M. Hada, ; M. Ehara, K. T., R. Fukuda, J. Hasegawa, M. Ishida, T. Nakajima, ; Y. Honda, O. K., H. Nakai, T. Vreven, J. A. Montgomery, Jr., ; J. E. Peralta, F. O., M. Bearpark, J. J. Heyd, E. Brothers, ; K. N. Kudin, V. N. S., R. Kobayashi, J. Normand, ; K. Raghavachari, A. R., J. C. Burant, S. S. Iyengar, J. Tomasi, ; M. Cossi, N. R., J. M. Millam, M. Klene, J. E. Knox, J. B. Cross, ; V. Bakken, C. A., J. Jaramillo, R. Gomperts, R. E. Stratmann, ; O. Yazyev, A. J. A., R. Cammi, C. Pomelli, J. W. Ochterski, ; R. L. Martin, K. M., V. G. Zakrzewski, G. A. Voth, ; P. Salvador, J. J. D., S. Dapprich, A. D. Daniels, ; O. Farkas, J. B. F., J. V. Ortiz, J. Cioslowski, ; Fox, D. J. *Gaussian 09, revision a.02*, Gaussian, Inc., Wallingford CT: 2009.

[20] Frisch, M. J.; Trucks, G. W.; Schlegel, H. B.; Scuseria, G. E.; Robb, M. A.; Cheeseman, J. R.; J. A. Montgomery, J.; Vreven, T.; Kudin, K. N.; Burant, J. C.; Millam, J. M.; Iyengar, S. S.; Tomasi, J.; Barone, V.; Mennucci, B.; Cossi, M.; Scalmani, G.; Rega, N.; Petersson, G. A.; Nakatsuji, H.; Hada, M.; Ehara, M.; Toyota, K.; Fukuda, R.; Hasegawa, J.; Ishida, M.; Nakajima, T.; Honda, Y.; Kitao, O.; Nakai, H.; Klene, M.; Li, X.; Knox, J. E.; Hratchian, H. P.; Cross, J. B.; Bakken, V.; Adamo, C.; Jaramillo, J.; Gomperts, R.; Stratmann, R. E.; Yazyev, O.; Austin, A. J.; Cammi, R.; Pomelli, C.; Ochterski, J. W.; Ayala, P. Y.; Morokuma, K.; Voth, G. A.; Salvador, P.; Dannenberg, J. J.; Zakrzewski, V. G.; Dapprich, S.; Daniels, A. D.; Strain, M. C.; Farkas, O.; Malick, D. K.; Rabuck, A. D.; Raghavachari, K.; Foresman, J. B.; Ortiz, J. V.; Cui, Q.; Baboul, A. G.; Clifford, S.; Cioslowski, J.; Stefanov, B. B.; Liu, G.; Liashenko, A.; Piskorz, P.; Komaromi, I.; Martin, R. L.; Fox, D. J.; Keith, T.; Al-Laham, M. A.; Peng, C. Y.; Nanayakkara, A.; Challacombe, M.; Gill, P. M. W.; Johnson, B.; Chen, W.; Wong, M. W.; Gonzalez, C.; Pople, J. A. *Gaussian 03*, Revision D.01; Gaussian Inc.: Wallingford CT, 2004.

[21] Dunning, T. H., Gaussian-basis sets for use in correlated molecular calculations .1. The atoms boron through neon and hydrogen. *Journal of Chemical Physics* **1989,** 90, 1007-1023.

[22] Balabanov, N. B.; Peterson, K. A., Systematically convergent basis sets for transition metals. I. All-electron correlation consistent basis sets for the 3d elements Sc-Zn. *Journal of Chemical Physics* **2005,** 123.

[23] Qu, Z. W.; Kroes, G. J., Theoretical study of the electronic structure and stability of titanium dioxide clusters $(TiO_2)_n$ with n=1-9. *Journal of Physical Chemistry B* **2006,** 110, 8998-9007.

[24] Zhao, Y.; Truhlar, D. G., The M06 suite of density functionals for main group thermochemistry, thermochemical kinetics, noncovalent interactions, excited states, and transition elements: Two new functionals and systematic testing of four M06-class functionals and 12 other functionals. *Theor Chem Acc* **2008,** 120, 215-241.

Chapter 5: Application of Monte Carlo Configuration Interaction Method to Challenging Systems.

As described in chapter 2, in theory FCI provides the exact solution to the schrödinger equation with a given basis ansatz. However, such a solution proves intractable but for the smallest of systems due to the dramatic increase in the number of configurations. This is overcome by truncating the FCI method in some way. One of the main problems with such truncated methods, based on the FCI method, is how to select the configurations to use in the calculation. Truncation of the wave function is required in order to reduce the size of the calculation to the point where it can be solved, in an appropriate time frame, with the available computer resources and predetermining which configurations will contribute significantly to the solution has proven so far impossible. One important feature of the FCI wave function is that it is very sparse, only a small percentage of configurations involved contribute significantly to the solution, with many coefficients that are effectively zero. A truncated CI method designed to take advantage of this sparseness called Monte Carlo Configuration Interaction (MCCI) was proposed in the 1990s[1, 2]. Whereby a reference wave function made up of a single (or number of) starting configuration(s) is expanded using new configurations generated randomly using a Monte-Carlo method. The method generates these new configurations such that they couple with the existing configurations of the reference wave function. New configurations whose coefficients contribute significantly to the resulting solution are retained, while those that do not are discarded. In this way a compact wave function made up only of those significant configurations is created, much smaller than the FCI wave function, which is able to recover a large proportion of the energy of the FCI wave function.

A MCCI computer program has been developed and is documented in [3]. It is written in Fortran and when used in conjunction with a suitable quantum chemistry electronic structure program (such as the Columbus or MOLPRO programs), which supplies the one and two electron molecular integrals, can apply the MCCI method to molecular systems.

A number of studies of the MCCI method have been carried out using this program. In refs. [4, 5] the best level of basis set to use in MCCI calculations is investigated and MCCI is compared to FCI in its ability to accurately describe molecular dissociation. The results of this investigation show that MCCI can be consistent in its treatment of the correlation effects of different systems during their dissociation. While in [6] the energies of a number of molecules (Ne, CH_2, C_2, N_2 and H_2O) are found using MCCI and compared to those found using FCI. The singlet and triplet electronic excitation energies calculated using MCCI were found to within a few meV of the FCI results. This was achieved using far fewer configurations and lesser computer processing time. Thus the MCCI method takes advantage of the extreme scarcity of the CI Hamiltonian matrix.

More recently the MCCI method has been extended to use natural orbitals and integrated with the second-order perturbation scheme[7]. State averaging was added to MCCI (SA-MCCI) and applied to electronically excited states[8]. Further MCCI has been applied to calculations of potential energy surfaces[9]; multipole moments, ionization energies, and electron affinities[10]; transition metal dimers[11]; hyperpolarizabilities[12]; characterising a configuration interaction excited state using natural transition geminals[13];

5.1 The MCCI Program

A MCCI wave function is created by first generating a wave function separately using a SCF method in a suitable quantum chemistry package. This reference wave function and the corresponding one- and two-electron integrals from the quantum chemistry package are then input into the MCCI program and used as a starting point to build the MCCI wave function. After this initialisation a loop begins, that forms the main body of the program. The basic procedures that make up this loop (branching, diagonalisation and pruning) are detailed in Figure 5-1.

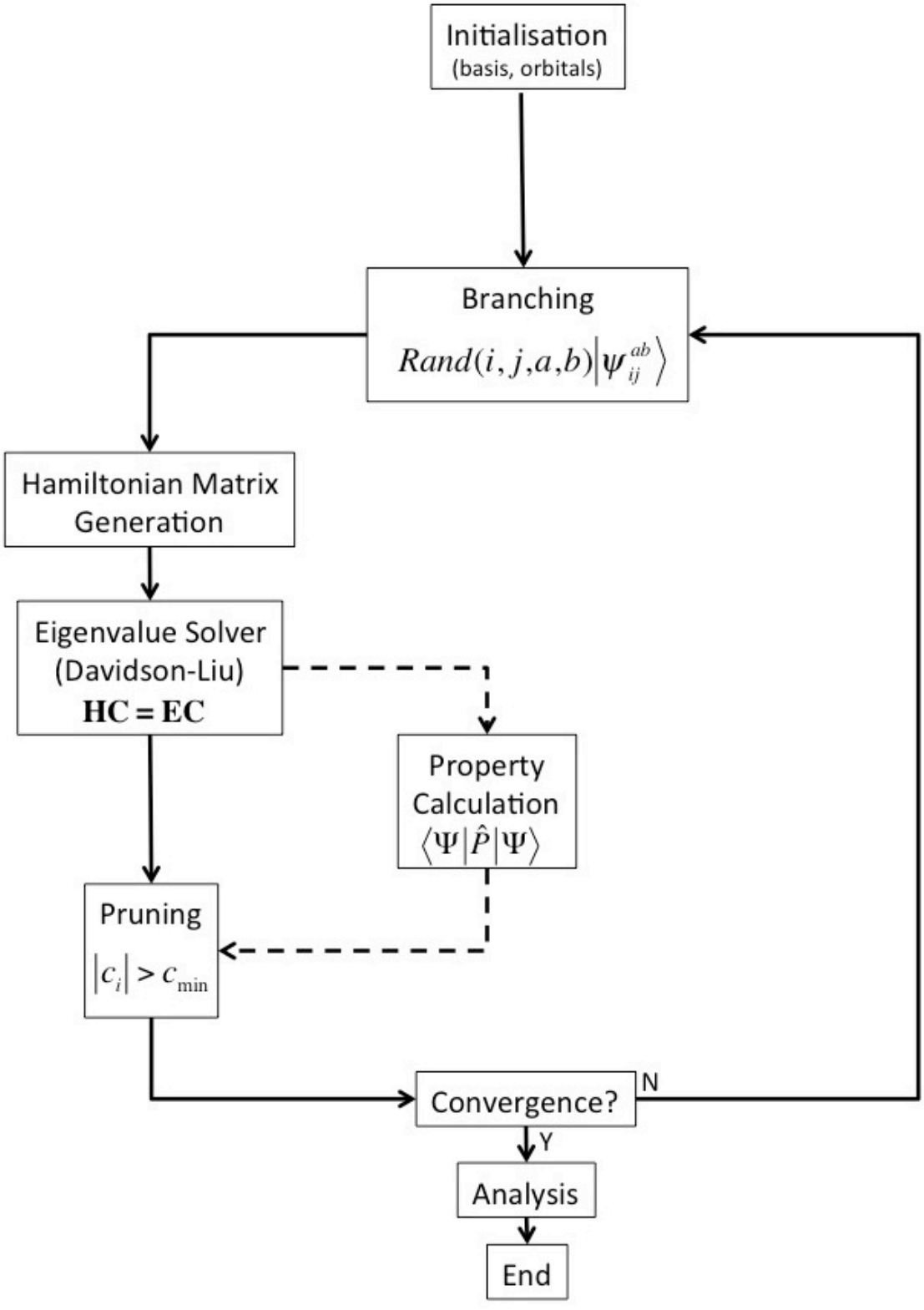

Figure 5-1: schematic of the MCCI program algorithm

The first step of this loop, called branching, involves the generation of new configurations. These new configurations are created using a random single or double excitation from a configuration chosen at random from the reference wave function. The newly generated configurations are added to the wave function, which is then

diagonalised in a configuration interaction calculation. An additional step that can be performed at this point is the calculation of a non-variational property of the system. Next, a process of pruning is entered, whereby new configurations that do not contribute significantly to the final wave function are removed. This can be with regard to the energy or of a non-variational value of interest (in chapter 6 where configurations are selected according to their contribution to the dipole moment). This is achieved by discarding those new configurations with a coefficient below a user defined cut-off value, c_{min}. Every k steps, for this work k=10, a full pruning step is preformed where all configurations are considered for pruning.

In Figure 5-2 the MCCI (c_{min} = 5 x 10^{-4}) energy against program iterations is plotted for the Neon atom, using the cc-pVDZ basis. Also shown are the energies calculated using FCI and a number of truncated CI methods of varying accuracy.

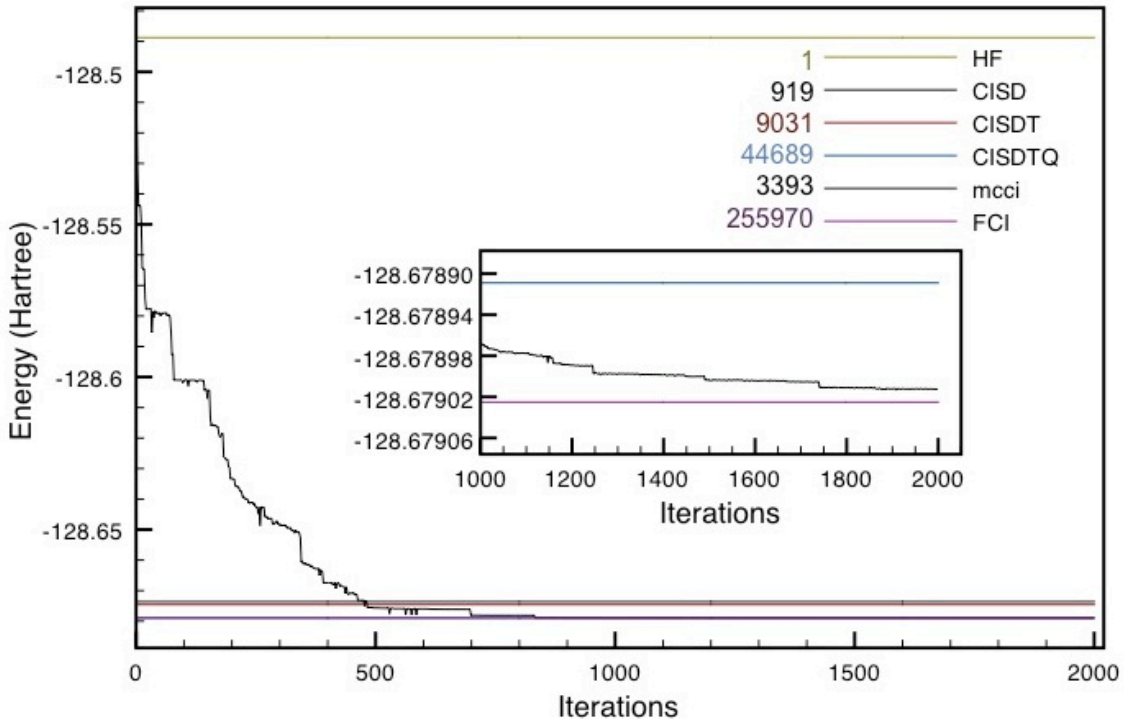

Figure 5-2: Convergence of truncated CI and MCCI with respect to FCI for Neon atom in the cc-pVDZ basis (c_{min} = 5 x 10^{-4}). Inset: Close up of the MCCI curve between 1000-2000 iterations. MCCI standard error over 50 MCCI runs is 5.8 x 10^{-8} au.

The MCCI energy reduces as the number of program iterations increases, as new configurations are added to the reference wave function. The MCCI value converges toward the FCI result. In this case the criteria for leaving the MCCI program loop was the number of iterations (2000 iterations). The energy decreases rapidly and then levels

out and cannot be seen to change within the scale of the plot, but a close-up plot of the MCCI curve shown in Figure 5-2 reveals that the energy does still continue to decrease. Eventually the MCCI calculation reaches a point where no new configurations are found. At this point, coefficients of the new configurations generated fall below the c_{min} and so are immediately pruned. The energy can be thought of as being converged to the value of c_{min}. The change in the number of configurations and energy of the wave function between iterations present two other criteria that can be used to test for convergence of the wave function.

By changing c_{min} the accuracy of the final MCCI wave function can be changed. The accuracy of the MCCI wave function generated is improved by decreasing the value of c_{min}, but this is at the expense of greater computer processing time. At a value of $c_{min} = 0$, all configurations generated would be included in the wave function and would represent a FCI wave function. Therefore, using this single value of c_{min} it is possible to make systematic improvements to the wave function. MCCI is a statistical method that will therefore find a variation in the result calculated from run to run. Accordingly, a standard deviation in the result can be calculated from repeated program runs of the same system. The standard deviation of the MCCI method has been calculated for a number of systems. For example, the MCCI calculation of the energy of the Ne atom (Figure 5-2) over 80 runs the standard deviation was found to be 5.8×10^{-8} au. On the scale of Figure 5-2 this standard deviation would be indistinguishable from the curve itself. For the systems for which the standard deviation has been calculated over multiple runs, the standard deviations have all been of a similar scale. Thus our use of the MCCI method is to obtain a converged approximation to the FCI wave function. For the results presented in this thesis it is believed that the MCCI is being run to convergence and therefore the result of a single run are quoted.

The program can be run in parallel by running the MCCI program loop on multiple processors, with each processor getting a copy of the configurations. After the completion of each loop the new sets of configurations generated by each processor are recombined and duplicate configurations are discarded. In the case of this work all calculations where run on either 8 or 12 processors.

In the following chapters investigations that expand on prior work into uses for the MCCI method are presented. Firstly, MCCI is applied to a PEC of a selection of small molecules and the accuracy of the results is discussed[9].

Then in chapter 6 the application of MCCI to the calculation of multipole moments is investigated. MCCI is applied to a number of small systems and the results are compared to experiment and FCI.

5.1.1 Advantages and Disadvantages of MCCI Method.

The advantages of the MCCI method over other truncated methods centre on the random way configurations that only contribute significantly are included in the wave function. This allows the method to treat larger systems than the FCI method without the explicit truncation of the expansion space. The random selection of configurations allows for the inclusion of multireference character of a system while keeping the number of configurations low. Through the variation of a single parameter, c_{min}, the result of the calculation can be systematically improved, recovering a large percentage of the correlation energy and approaching the FCI result. Moreover, the MCCI method is variational, requires a lower computational overhead than FCI and is well suited to parallel computing. The random nature of this generation of new configurations means that little foreknowledge of the system is required and the amount of user guidance is minimal.

Although the MCCI method is able to deal with larger systems than the FCI method and recover much of the correlation energy, it still has limits. The calculation cost still increases with system size though at a much slower rate than FCI. Although the diagonalisation steps for MCCI are much smaller, and therefore computationally less intensive than that of a FCI calculation, it must be repeated many times within a single MCCI calculation. Like all truncated CI methods, the MCCI method is not expected to be size consistent nor size extensive. The method assumes that all configurations can be sampled, given enough time from a single reference configuration. A problem encountered during this work was one of when to end calculations, it is not always clear

if a run is complete or if more time is required to reach remote, but important, configurations. Though it is believed that all runs presented here were fully converged.

5.2 Monte Carlo Configuration Interaction Applied to Challenging Potential Energy Curves

As described in chapter 2, PES of even a simple molecule can be quite complex. With many different interconnected features that make up the surface, which can be used to describe the behaviour of the molecule when excited both electronically and/or kinetically. An accurate representation of the PES of a molecular system can allow for a greater understanding of reactions and behaviours associated with it. Much of the subtleties of a given molecules' PES aren't described sufficiently if the correlation energy is neglected. So it is important to recover a sufficient amount of the electron correlation in order to produce an accurate PES.

In this work the 2D potential energy curves (PEC) of a number of different systems are considered, in each case a restricted Hartree-Fock wave function is used as the reference wave function. The PEC was defined by a selected number of geometries along the curve, with a new set of Hartree-Fock orbitals generated for each new geometry. Either the Columbus or MOLPRO programs were used to generate these orbitals.

As previously stated it is the accuracy of the PES that is important; the shape and position of the features that make up the surface. So in the case of a PEC, an approximate CI method would do a good job of describing the curve if it was the same shape as the FCI curve but transposed by a constant energy. A useful way of evaluating the accuracy of such potential curves called the non-parallelity error (NPE) is described in [14, 15]. Defined as:

$$NPE = \max_{R} \left| E_R^{FCI} - E_R^{approx} \right| - \min_{R} \left| E_R^{FCI} - E_R^{approx} \right| \tag{5.1}$$

Where R is over all of the points calculated in the curve and the E^{approx} are the energy calculated by the approximate method at point R. Essentially, the error is calculated as the difference between the absolute maximum and the minimum deviations from the

FCI values over the coordinates considered. Where FCI results are available the NPE is used to define how closely the E_{approx} follows the FCI curve.

5.2.1 Hydrogen Dissociation

Some of the simplest dissociations, those of the dissociation of hydrogen are investigated here as a first test of MCCI methods ability to describe ground state PEC. The three such cases that MCCI is applied to here are HF, BH, and CH_4. It is expected that these systems will have some multireference character and their PEC have been well defined in past investigations using FCI, CC and multireference methods by Sherill et al[15-17].

5.2.1.1 HF

The case of hydrogen fluoride (HF) is considered first. In [15] the FCI results used 6-31G** and a single frozen core orbital, therefore in order to be consistent the same conditions where used for all MCCI calculations. The PEC generated using the MCCI method, using two different c_{min} values ($5x10^{-3}$ & $5x10^{-4}$), are presented along with the FCI potential curve in Figure 5-3.

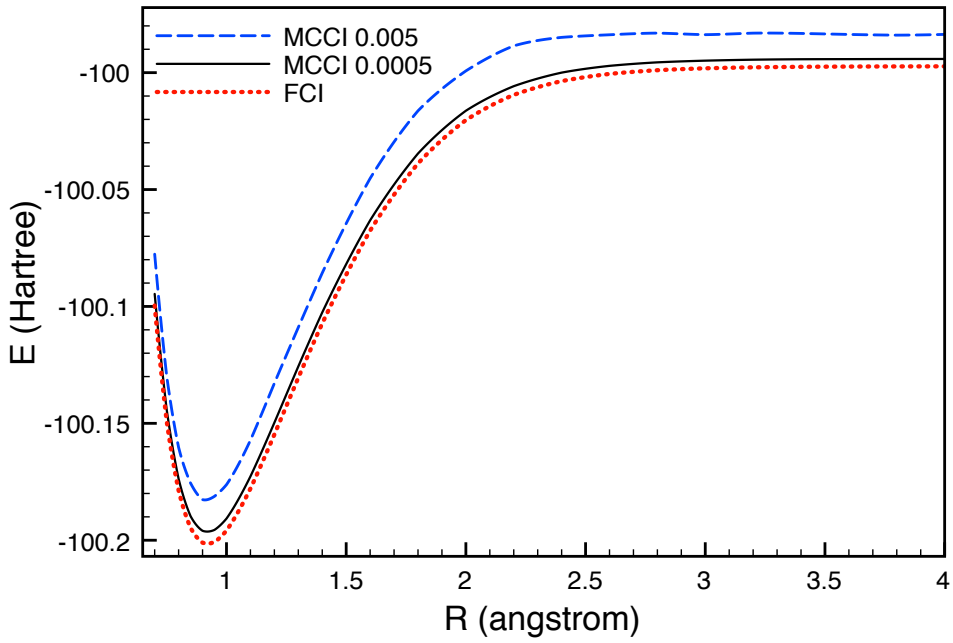

Figure 5-3: Energy (Hartree) against bond length (angstrom) for the HF molecule using MCCI and FCI methods. Both using the 6-31G** basis set and a single frozen core orbital.

It can be seen visually that the MCCI curves are reasonably consistent in shape in comparison to the FCI curve; they follow the shape of the FCI curve quite closely. Apart from at low R where the curves converge together slightly, the curves appear similar but just shifted by a constant energy. The NPE for these curves are found to be 5.7 kcal/mol for the larger c_{min} (0.005) and 1.3 for the smaller (c_{min}=0.0005). These NPE values compare favourably with those of single reference methods published in [15], where for CCSD NPE was found to be 13.0 kcal/mol and for CCSD(T) was 26.8 kcal/mol, significantly larger than both MCCI results. Also with the multireference methods of Ref. [16] which found an NPE of 17.69 kcal/mol for CAS(8,5), and NPE=4.83 kcal/mol using CAS(8,8). These results were further improved using CASPT2 resulting in an NPE = 2.77 kcal/mol (CASPT2(8,5)) and 0.5 kcal/mol (CASPT2(8,8)). NPEs of Second order CI (SOCI) calculations were also reported, SOCI(8,5) and SOCI(8,8) where 3.2 and 0.04 kcal/mol, respectively. Another multireference study[17] of HF used a minimal CAS(2,2) calculation which gave a PEC with a NPE = 18.66 kcal/mol, application of CASPT2 in this case resulted in a CASPT2(2,2) curve with a NPE = 0.47 kcal/mol.

In comparison to the FCI calculation the MCCI method required significantly fewer configurations. While for FCI 3,756,816 SD[15] were required for each R, the MCCI method averaged 173.2 CSF's for C_{min}=0.005 and 1,337 for c_{min}=0.0005. These represent a significant reduction in number of configurations of 0.0046% and 0.036% respectively, while still managing to reproduce the shape of the curve to within an NPE accuracy of a few kcal/mol.

In Figure 5-4 and Figure 5-5 the error in the MCCI result compared to the FCI is shown, over two different MCCI program runs, for each of the c_{min} cut-offs used.

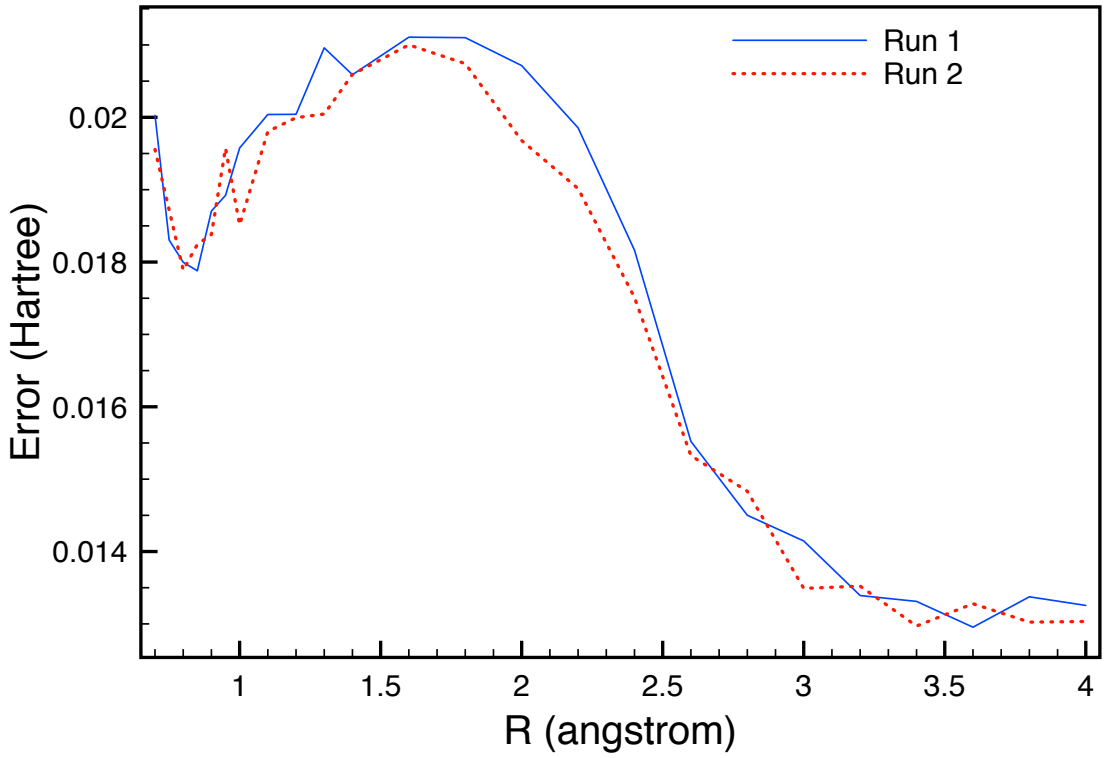

Figure 5-4: Error (Hartree) in MCCI result (c_{min}=5 x 10^{-3}) in comparison to FCI against bond length R (angstrom) for the HF molecule. The results for two separate MCCI runs are shown for comparison. All calculations using the 6-31G** basis set and a single frozen core orbital.

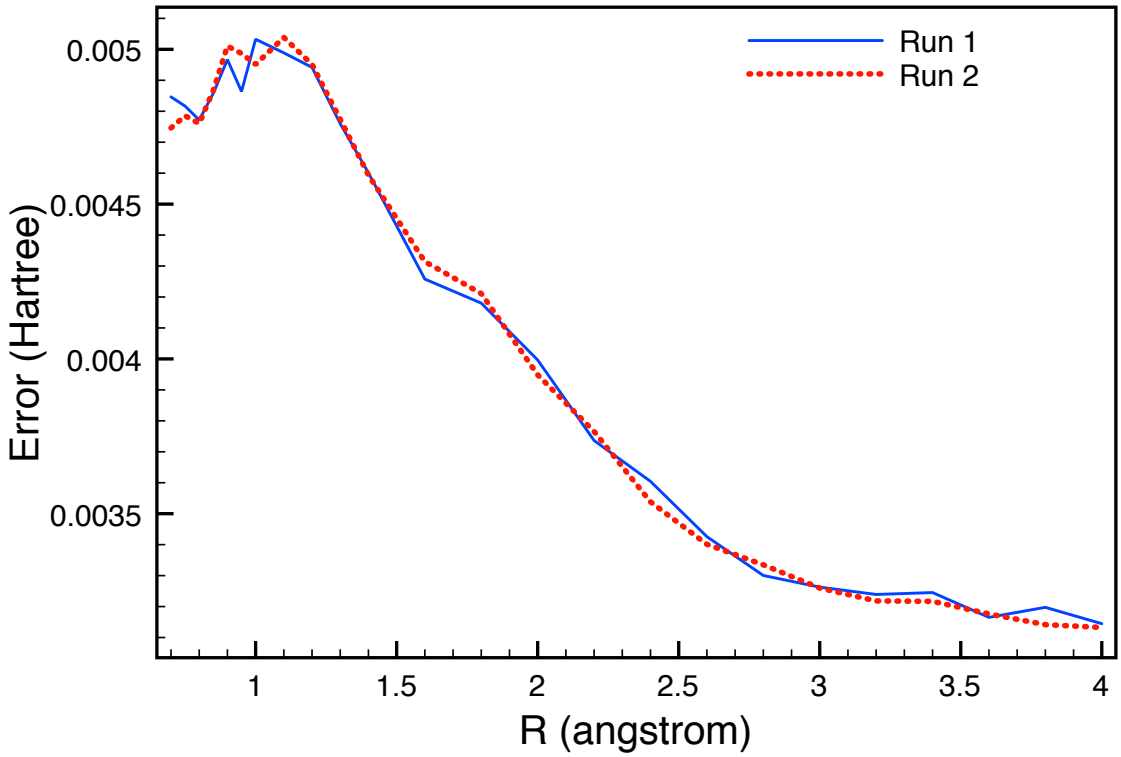

Figure 5-5: Error (Hartree) in MCCI result (c_{min}=5 x 10^{-4}) in comparison to FCI against bond length R (angstrom) for the HF molecule. The results for two separate MCCI runs are shown for comparison. All calculations using the 6-31G** basis set and a single frozen core orbital.

The MCCI method is more accurate at longer bond lengths in both cases, with larger errors at shorter bond lengths. Rerunning the calculation using a different seed (for the random number generator) doesn't seem to greatly affect the error. More broadly variations in the error for each run at R can be seen, which demonstrates the random nature of the new configurations generated. Only if given enough time to sample the configuration space, over each run, would the results be expected to be exactly the same. This is demonstrated in Figure 5-6 where three separate MCCI runs are shown, which are otherwise equal and differ only in the seed used in the random number generator. Such a difference is typical of the calculation and a similar plot could be made for any value of R.

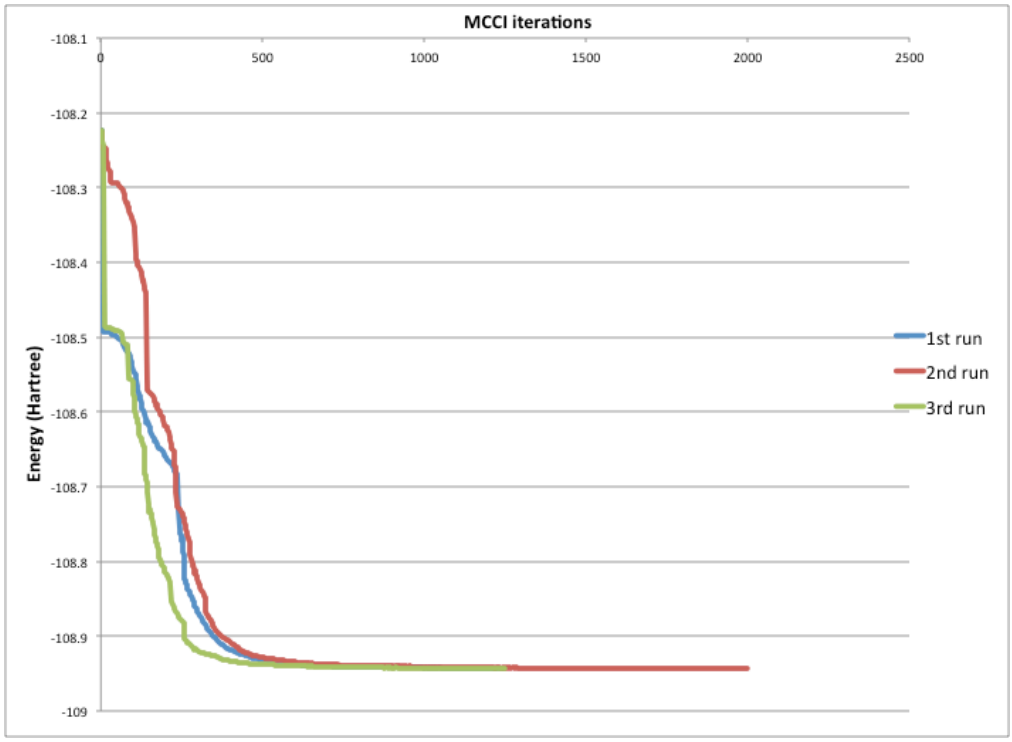

Figure 5-6: Energy (Hartree) against program iterations for the runs using different random number seeds.

5.2.1.2 BH

Energy (Hartree) from MCCI against bond length R (angstrom) for BH, using the aug-cc-pVQZ with one frozen orbital, is displayed in Figure 5-7. FCI results from Ref. [15] are included also for comparison. At the $c_{min} = 5 \times 10^{-3}$ level the MCCI PEC is in reasonably good agreement with the FCI curve, with the minimum in approximately the correct place and in general the PEC is qualitatively correct. The exceptions being that

a small shoulder is present on the potential around R = 3Å and that the energy limiting value is reached too early.

When the c_{min} is reduced to 5 x 10^{-4} the PEC is much improved, being almost exactly the same as the FCI curve just shifted by a small energy. The problems with the PEC at c_{min} = 5 x 10^{-3} are removed by reducing the c_{min}. The difference in the quality of the curves at the two c_{min} is nicely demonstrated using the NPE values. The NPE for the MCCI curve is decreased from 22.8 kcal/mol to 2.6 kcal/mol when the c_{min} value is reduced. While, the NPE for CCSD was 8.1 kcal/mol and for CCSD(T) it was 23.3 kcal/mol[15]. For c_{min} = 5 x 10^{-4} required 4220 CSFs on average while c_{min} = 5 x 10^{-3} used on average 330. These represent a very small percentage of the 1.5 x 10^{7} SDs that would be required for a FCI calculation.

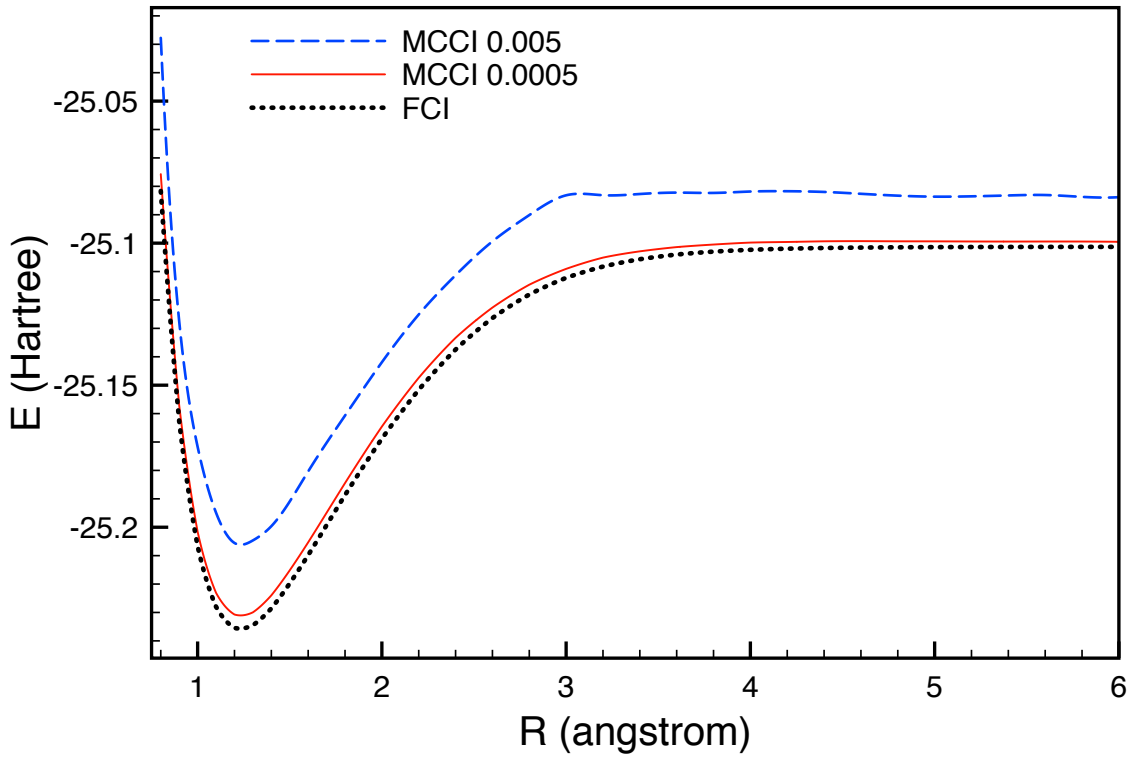

Figure 5-7: Energy (Hartree) from MCCI and FCI results[15] against bond length R (angstrom) for BH. Using the aug-cc-pVQZ with one frozen orbital. Adapted from Ref. [18].

In Ref. [16] BH PECs generated using multireference methods were compared to FCI. These PEC were over a smaller range of R and used the cc-pVQZ basis set, rather than the aug-cc-pVQZ basis set, due to convergence problems. CAS(4, 4) had an NPE=12.68 kcal/mol, which was extended in CASPT2 giving NPE=3.16 kcal/mol, and CAS(4,5) had an NPE of 9.38 kcal/mol. SOCI(4,4) gave an NPE = 0.29 kcal/mol. The

MCCI NPE compare well with these multireference results, with only the SOCI(4,4) NPE being better than the MCCI. Though it should be noted that this isn't a direct comparison, due to the difference in basis sets.

In Figure 5-8 the energy error (Hartree) in MCCI (c_{min}=5 x 10^{-4}) compared to the FCI result against bond length R (angstrom) for BH is shown. As the bond length R is increased the error in the MCCI energy with respect to the FCI energy decreases. At R = 6 Å the difference between the MCCI energy and the sum of the MCCI energies of the fragments is measured at 6.6 kcal/mol at c_{min} = 5 x 10^{-3} and 0.83 kcal/mol at c_{min} = 5 x 10^{-4}.

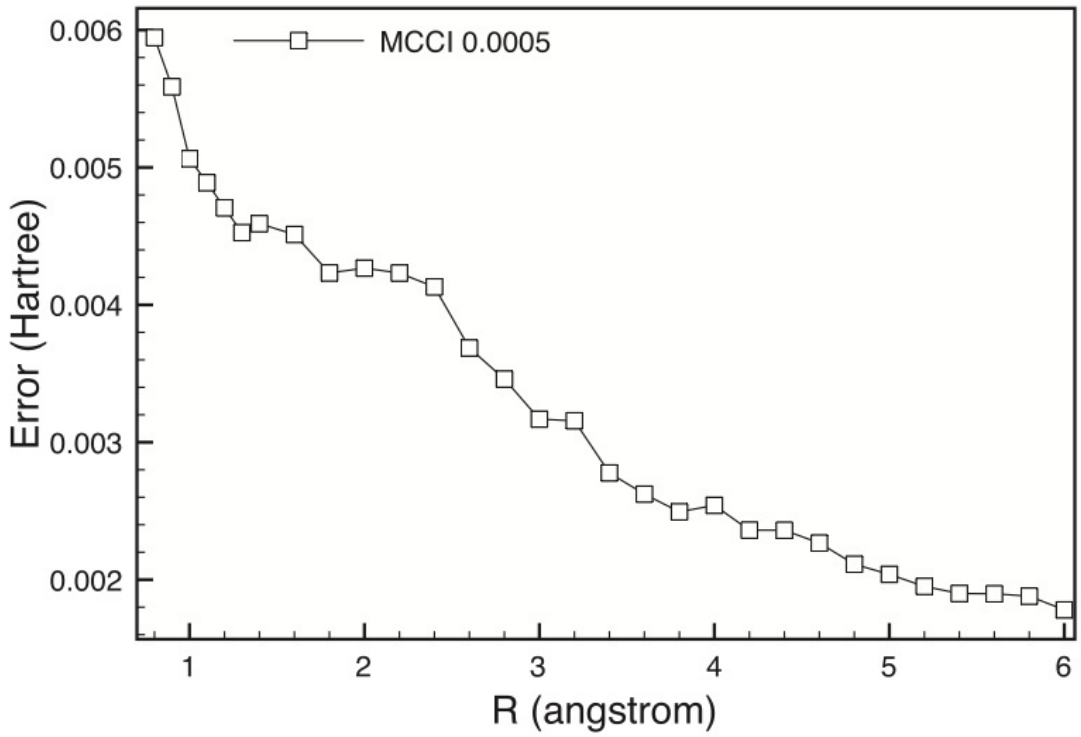

Figure 5-8: Energy error (Hartree) in MCCI (c_{min}=5 x 10^{-4}) compared to the FCI result against bond length R (angstrom) for BH. Using the aug-cc-pVQZ basis set with one frozen core orbital. NPE = 2.6 kcal/mol.

5.2.1.3 Methane, CH_4

Preliminary MCCI results for the PEC of Methane (CH_4) were first published in Ref. [18]. As in Ref. [15] the hydrogen dissociation is described by the stretching of a single CH bond from a tetrahedral geometry with bond lengths of 1.086 Å for the three unvaried CH bonds. Figure 5-9 shows Energy (Hartree) from MCCI against bond length R (angstrom) for CH_4, using the 6-31G* basis set with one frozen core orbital.

FCI results from Ref. [15] are included for comparison. At c_{min} = 5 x 10^{-3} the curve appears to match the FCI quite well with the minimum in approximately the right place, though at longer bond lengths the energy is slightly too high. In common with the previous cases at the reduced c_{min} = 5 x 10^{-4} the PEC is much improved, matching the FCI very closely. This is quantified by the NPE results of 10.3 kcal/mol for 5 x 10^{-3} and 0.6 kcal/mol for 5 x 10^{-4}. This compares favourably to the CCSD NPE of 10.3 kcal/mol[15].

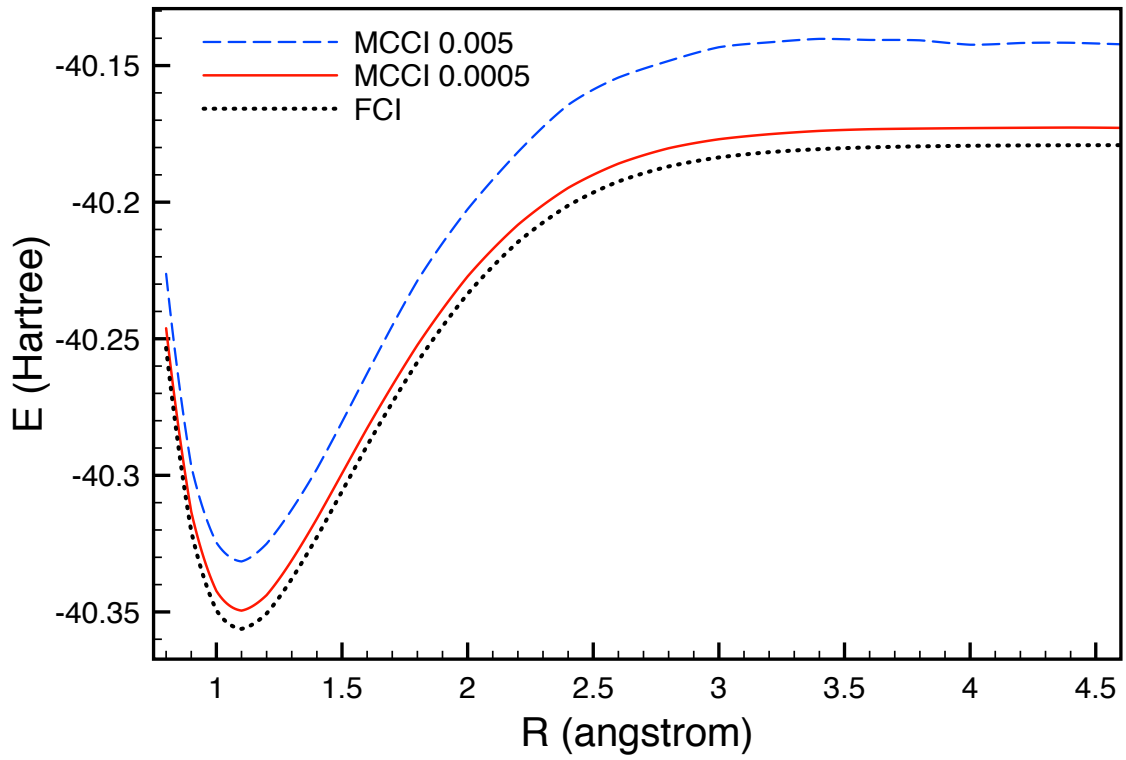

Figure 5-9: Energy (Hartree) from MCCI and FCI results[15] against bond length R (angstrom) for CH_4. Using the 6-31G* basis set with one frozen core orbital. Adapted from Ref. [18].

This system is also studied using multireference methods[16] where CAS(8,8) gave an NPE = 6.34 kcal/mol and CASPT2(8,8) gave 1.56 kcal/mol. In this study only SOCI(8,8) had a better NPE of 0.3 kcal/mol. While in Ref. [17] the minimal active space CAS(2,2) gave an NPE = 9.25 kcal/mol, CASPT2(2,2) gave 1.22 kcal/mol, and SOCI(2,2) gave an NPE = 0.6 kcal/mol. On average the number of CSFs used in the MCCI calculations were 417 (5 x 10^{-3}) and 4272 (5 x 10^{-4}). While the FCI space is around 26.7 x 10^{6} SDs[15].

In Figure 5-10 the error in the energy for MCCI (c_{min}=5 x 10^{-4}) in comparison to FCI are all very small in general. The greater error occurs at shorter bond length, while the

smallest error occurs at bond lengths slightly longer than the equilibrium. At R = 4.6 Å the difference in the MCCI energy in comparison to the sum of the MCCI energies of the fragments is calculated at 15 kcal/mol with the larger c_{min} and 0.79 with the smaller c_{min}.

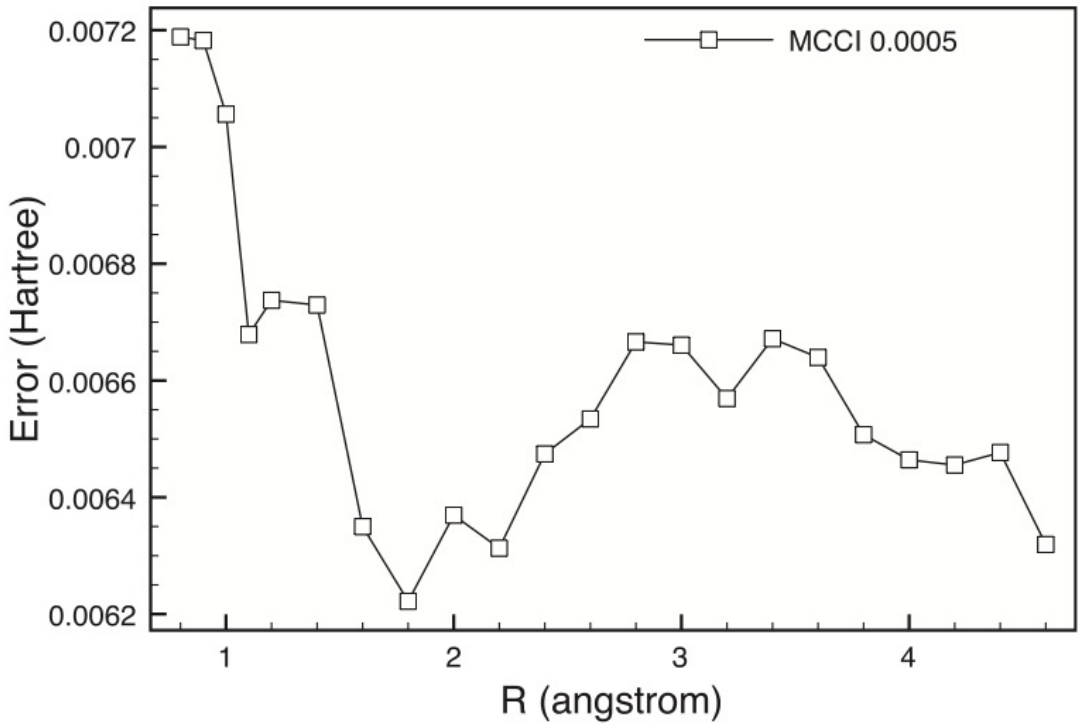

Figure 5-10: Energy error (Hartree) in MCCI (c_{min}=5 x 10^{-4}) compared to the FCI result against bond length R (angstrom) for CH_4. Using the 6-31G* Basis set with one frozen core orbital. NPE = 0.6 kcal/mol.

Method	*HF*	*BH*	*CH_4*
MCCI (5 x 10^{-3}) CSFs	172.3	333.1	417.0
MCCI (5 x 10^{-4}) CSFs	1337.0	4219.6	4272.0
FCI SDs	3,756,816	15,132,412	26, 755,625
MCCI (5 x 10^{-3}) fraction	0.0046 %	0.0022 %	0.0016 %
MCCI (5 x 10^{-4}) fraction	0.036 %	0.028 %	0.016 %

Table 5-1: MCCI mean CSFs compared to FCI symmetry adapted SDs for three cases of hydrogen dissociation (HF, BH, and CH_4).

It has been shown that for the systems of hydrogen dissociation, which been have considered, that using a c_{min} of 5 x 10^{-4} the shape of the FCI PEC is reproduced to high accuracy. In Table 5-1 it is clear that this is achieved using only a tiny fraction of the FCI space. The NPE of the MCCI (5 x 10^{-4}) curves was only bettered by higher cost multireference CASPT2 and SOCI calculations, using large active spaces or smaller active spaces constructed with greater user input. The number of CSFs (or SDs) used

for these multireference calculations was not reported and so comparison could not be made.

5.2.2 Carbon Dimer, C_2

The next system considered is the dissociation of the carbon dimer C_2. The system is known to be multireference with low-lying states, making it a stern test for MCCI. FCI results of the dimer for the three lowest-lying states have been published[19]. These are presented along side the MCCI (c_{min}==5 x 10^{-4}) results in Figure 5-11. The 6-31G* basis set with two frozen core orbitals was used in these calculations. Preliminary MCCI results for C_2 were first published in Ref. [18].

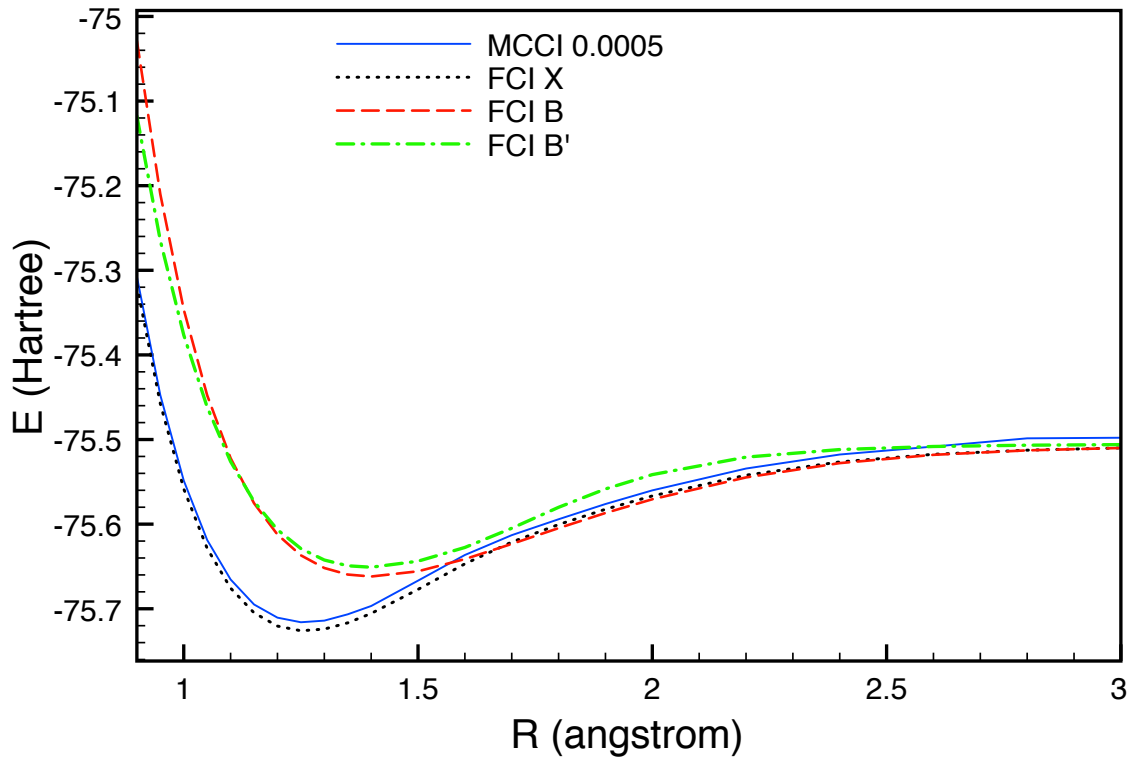

Figure 5-11: Energy (Hartree) from MCCI (c_{min}=5 x 10^{-4}) and FCI results[19] against bond length R (angstrom) for C_2. Using the 6-31G* basis set with 2 frozen core orbitals. Here X and B' are $^1\Sigma^+_g$ and B is $^1\Delta_g$. Adapted from Ref. [18].

The FCI curves of the excited states are very close together, making judging the accuracy of the MCCI curve by eye difficult. The MCCI PEC does seem to follow the FCI X (ground state) curve quite well, apart from at long bond length (R=~3 Å) where the curve is closer in energy to the FCI B' excited state curve. Suggesting that at this R

the MCCI calculation has converged to this low-lying excited state rather than the ground state. For the FCI curves between 1.7 and 2.5 Å the lowest energy state is the B curve rather than the X curve. Therefore it is possible that the MCCI method may have converged to the B state, as the two states have the same symmetry in the abelian point group (D_{2h}) used for the MCCI calculation. The three excited states appear to be trending towards a degenerate state as the system dissociates.

The FCI calculations in Ref. [19] required 52,407,353 symmetry adapted SDs, while on average the MCCI (c_{min}=5 x 10^{-4}) only used ~6900 CSFs. The NPE of the MCCI curve was in this case 4.9 kcal/mol. This is a much better performance than CCSD (NPE = 24.3 kcal/mol) and CCSD(T) (NPE = 61.3 kcal/mol), which highlights CCs instability at large R[19]. CISDTQ gave a curve with NPE=16.6 kcal/mol and, without symmetry, would require about 3 x 10^6 SDs for the calculation. This highlights the usefulness of the MCCI method that gives a curve with a better NPE using far fewer configurations, even after allowing for a reduction in the size of the CISDTQ space if symmetry and CSFs are used.

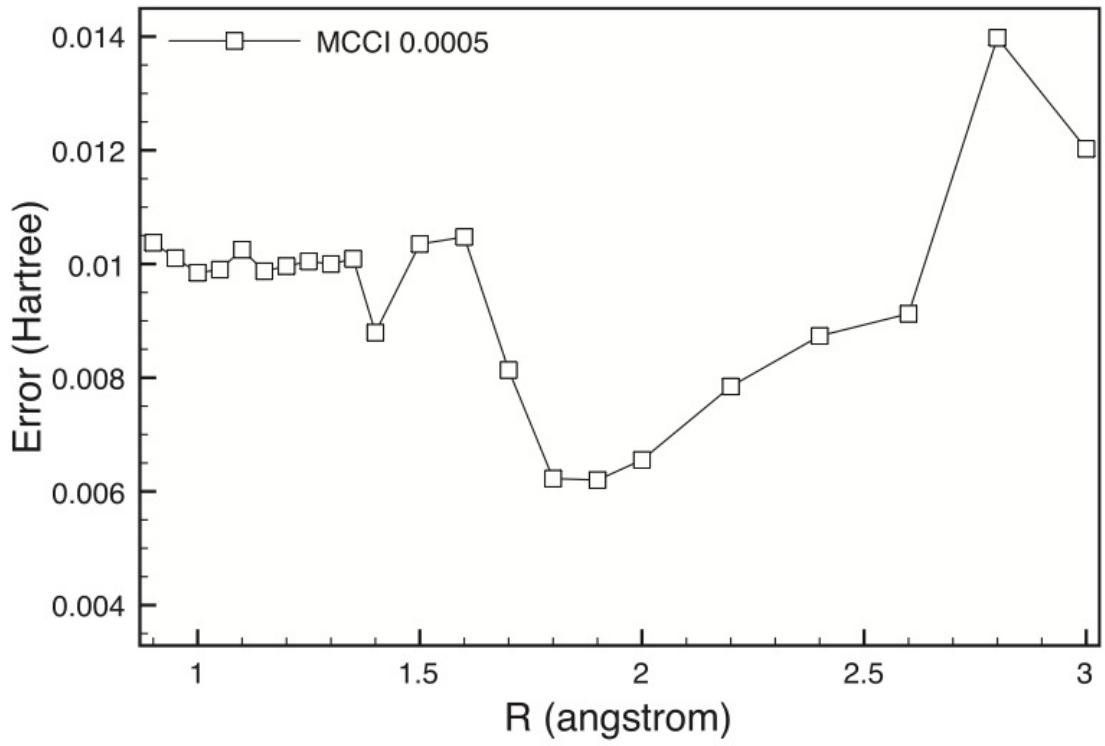

Figure 5-12: Energy error (Hartree) in MCCI (c_{min}=5 x 10^{-4}) compared to the FCI result against bond length R (angstrom) for C_2. Using the 6-31G* Basis set with 2 frozen core orbitals. NPE = 4.9 kcal/mol.

In Figure 5-12 the energy error (Hartree) in MCCI (c_{min}=5 x 10^{-4}) compared to the FCI result against bond length R (angstrom) is plotted for C_2. The NPE for the curve was 4.9

kcal/mol, slightly better than the mean single-point error (MSPE) of 6.0 kcal/mol. If the points around 3 Å, where it is believed that the MCCI may have converged to a low-lying excited state, are excluded the MSPE reduces to 5.7 kcal/mol and the NPE drops to 2.7 kcal/mol. Comparing the MCCI energy at 3 Å to the sum of the MCCI energies of the fragments a difference of 3.2 kcal/mol is found.

5.2.2.1 Analysis of the C_2 MCCI Wave function

The results of the MCCI PEC of C_2 can possibly be explained by analysis of the C_2 MCCI wave function at different points along the curve. The ten largest coefficients of C_2 at the equilibrium bond length R = 1.25 Å for the MCCI wave function are presented in Table 5-2, where the number of substitutions with respect to the Hartree-Fock reference are listed by spin for each of the configurations. Here at the equilibrium geometry the Hartree-Fock reference configuration is the dominant configuration.

Coefficient	*α substitutions*	*β substitutions*
-0.830	0	0
0.331	1	1
-0.184	1	1
-0.180	1	1
-0.179	1	1
-0.160	0	2
0.158	1	1
0.158	1	1
-0.142	0	1
0.106	2	2

Table 5-2: Ten largest coefficients of C_2 (R=1.25 Å) MCCI wave function with the number of substitutions with respect to the Hartree-Fock reference listed by spin.

At R=2 Å the two largest coefficients are -0.636 and 0.557. The dominant configuration is now one with a double substitution from the Hartree-Fock reference. This could indicate that the lowest lying B state has been converged to here, rather than the equilibrium ground state (X) curve. Or alternatively it could just be an aspect of the multi-configurational nature of the curve. By R=3 Å a third configuration, different from the dominant configurations earlier in the curve, becomes dominant. This may suggest that at large R a different potential curve has been converged upon.

5.2.3 F_2

In Figure 5-13 the PEC calculated using MCCI (c_{min}=5 x 10^{-4}), Hartree-Fock, and full valence CI for the F_2 molecule is plotted. Despite no frozen orbitals being used in the MCCI calculations the resulting curve follows that of the full valence CI results of Ref. [20]. The Hartree-Fock curve increases in energy too quickly at longer R, resulting in an overestimate of the well depth and an improper description of the dissociation.

With c_{min}=5 x 10^{-4} MCCI required on average 3577 CSFs for the points considered along the curve. This is approximately 8.3 x 10^{-7} % of the FCI space (4.3 x 10^{11} SDs) that would be required for a single FCI calculation with 2 frozen core orbitals. The NPE for MCCI was found to be 6.2 kcal/mol in this case.

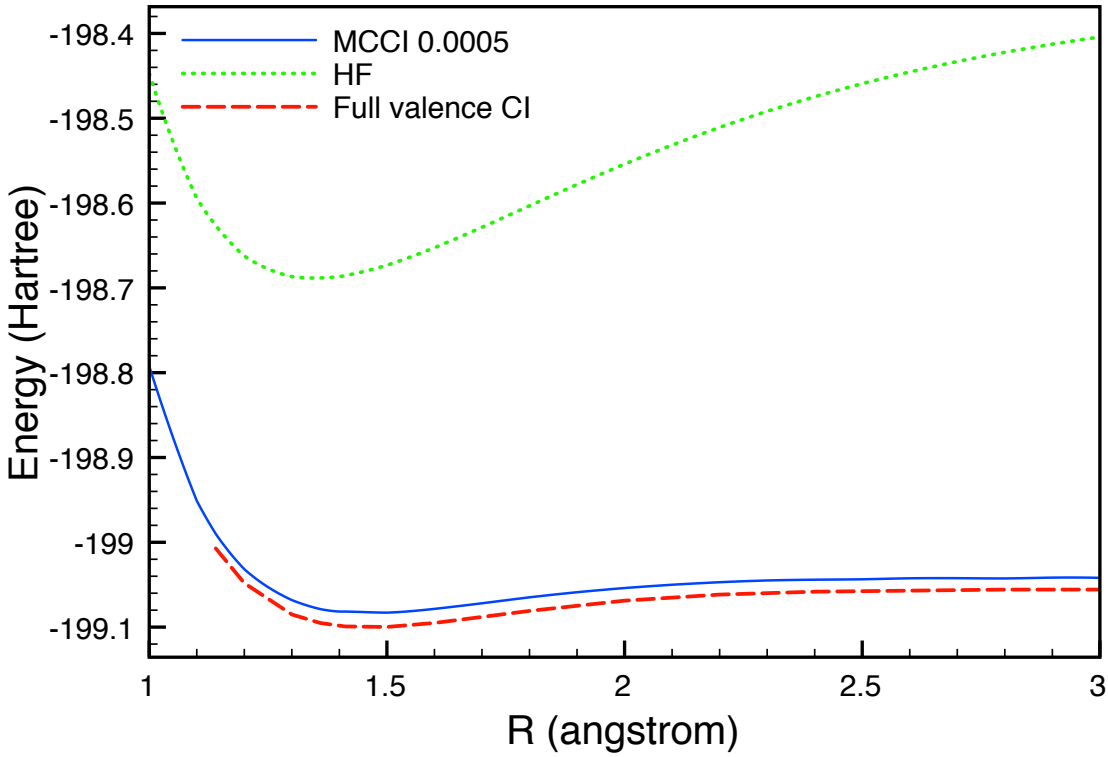

Figure 5-13: Energy (Hartree) from MCCI (c_{min}=5 x 10^{-4}), Hartree-Fock, and full valence CI[20] against bond length R (angstrom) for F_2, using the cc-pVDZ basis set.

Figure 5-14 shows the energy error (Hartree) in MCCI (c_{min}=5 x 10^{-4}) compared to the full valence CI result[20] against bond length R (angstrom) for F_2. Here the error tends to decrease as the bond length increases. A difference of 7.6 kcal/mol is found between the energy of two separate F atoms and the energy of the system at 3 Å.

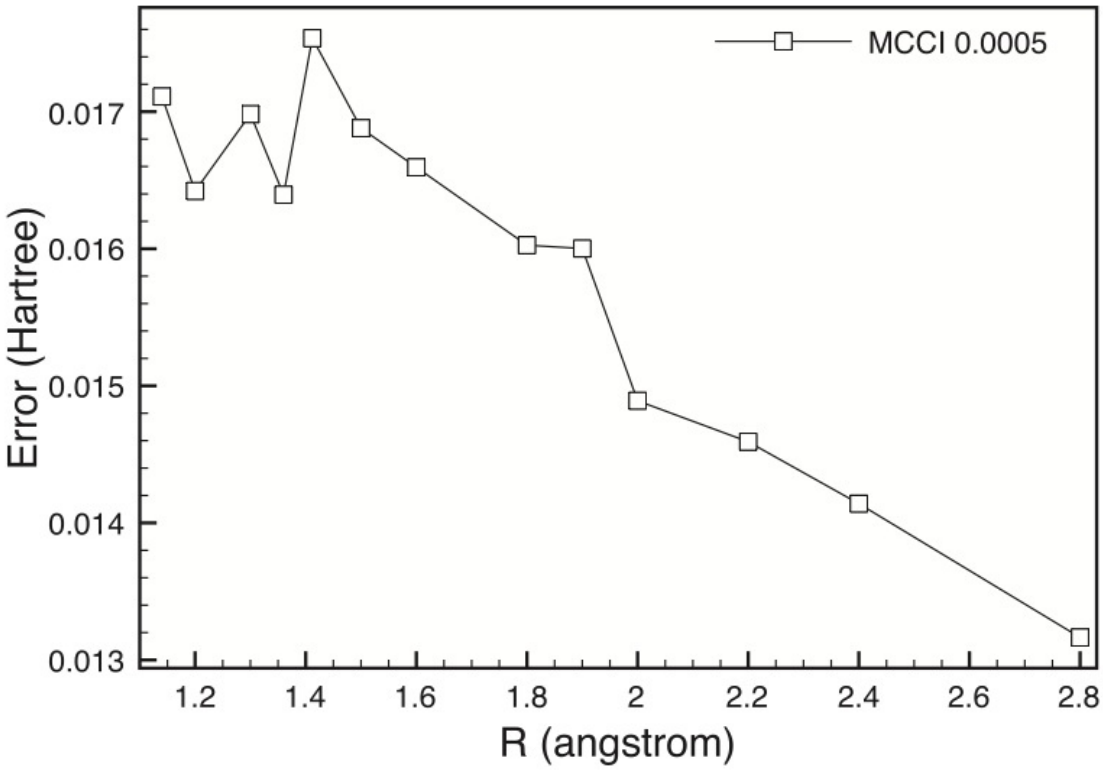

Figure 5-14: Energy error (Hartree) in MCCI (c_{min}=5 x 10^{-4}) compared to the full valence CI result[20] against bond length R (angstrom) for F_2, using the cc-pVDZ Basis. NPE = 6.2 kcal/mol.

5.2.4 N_2

The bond breaking of the nitrogen molecule (N_2) is now considered. This should be a good test of the MCCI method, as it exhibits multireference character especially at longer bond length. In fact some single reference based methods fail to describe the dissociation[21]. The PEC of the N_2 bond breaking calculated by MCCI (c_{min}=10^{-3}) using the cc-pVDZ basis with 2 frozen core orbitals is presented in Figure 5-15. In order to reproduce the FCI N_2 bond breaking PEC shown, the FCI results from a number of sources[22-24] were collated.

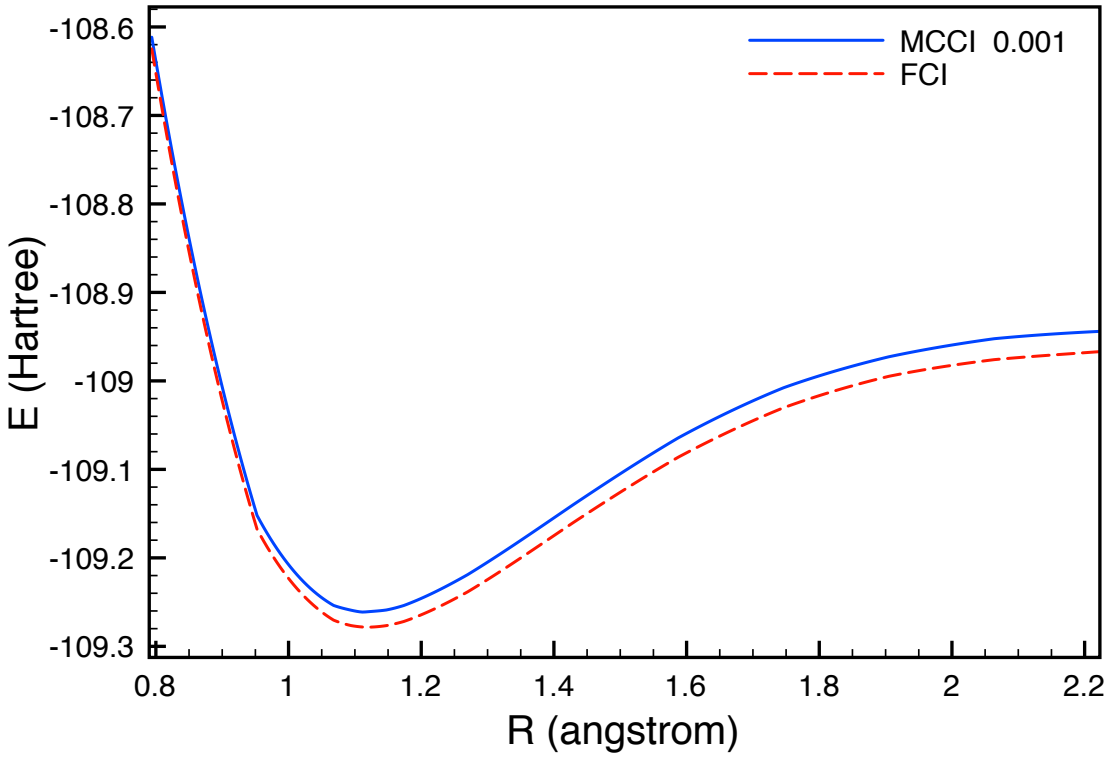

Figure 5-15: MCCI ($c_{min}=10^{-3}$) and FCI energy[22-24] (Hartree) against bond length R (angstrom) for the N_2 Molecule, using the cc-pVDZ basis set with two frozen orbitals.

By inspection it is clear that the general shape of the MCCI curve is correct, though the energy difference isn't consistent at short R, where it converges toward the FCI curve. The NPE in this case is calculated to be 6.6 kcal/mol. The number of CSFs required by the MCCI program ranged from about 1000 at the shortest R to about 5000 at the longest, where the multireference character is expected to be greater. The amount of computing time required for the calculations increases as the number of configurations increases; at the shortest R 200 iterations required 3 minutes while at the longest 200 iteration took 1.3 hours. The average number of CSFs over all the R considered was 2854, significantly less than the $4.3\text{x}10^9$ SDs required for a FCI calculation, if spatial symmetry is ignored.

Ref. [24] considers 6 of the FCI points presented in Figure 5-15, for those points the NPE results for a number of methods were presented. The NPE of CCSD and CCSD(T) were found to be 108.386 kcal/mol and 36.241 kcal/mol respectively. Also, using a CAS(6,6) reference wave function, the NPE of MRCI was found to be 0.291 kcal/mol and that of MRCC was found to be 0.459 kcal/mol. While the NPE value for MCCI at $c_{min}=10^{-3}$ is 3.370 kcal/mol for these points. This falls between the values calculated for the single reference (CCSD and CCSD(T)) and multireference (MRCI and MRCC)

methods, unfortunately the number of CSFs used is not stated in Ref. [24] so a comparison of the different calculation size cannot be made.

Using the 13 FCI points from Ref. [22], Ref. [17] presents the NPE of a set of CASSCF calculations of different sizes. CAS(10,10) gave an NPE of 22.93 kcal/mol, CAS(10,8) had an NPE of 15.03 kcal/mol, while the smallest active space CAS(6,6) found an NPE of 14.59 kcal/mol. Further refining these results using CASPT2 the NPEs were calculated as; CASPT2(6,6) had a NPE of 5.2 kcal/mol and CASPT2(10,10) had a NPE of 1.88 kcal/mol. These results compare well with the previously stated NPE for MCCI of 6.6 kcal/mol. However if only the 13 points from Ref. [22] are considered for the NPE of the MCCI curve, it is improved to 5.9 kcal/mol. Clearly, at this c_{min}, MCCI is able to replicate the results of CASPT2 calculations quite closely. But, while the CASPT2 calculations require a great deal of user-defined guidance as to the make-up of the active space, the MCCI requires a minimum of input.

Figure 5-16 shows the Error in MCCI ($c_{min}=10^{-3}$) results in comparison to the FCI calculation against bond length, R. In contrast to the results for HF the lowest error is at shorter R and increases as R increases.

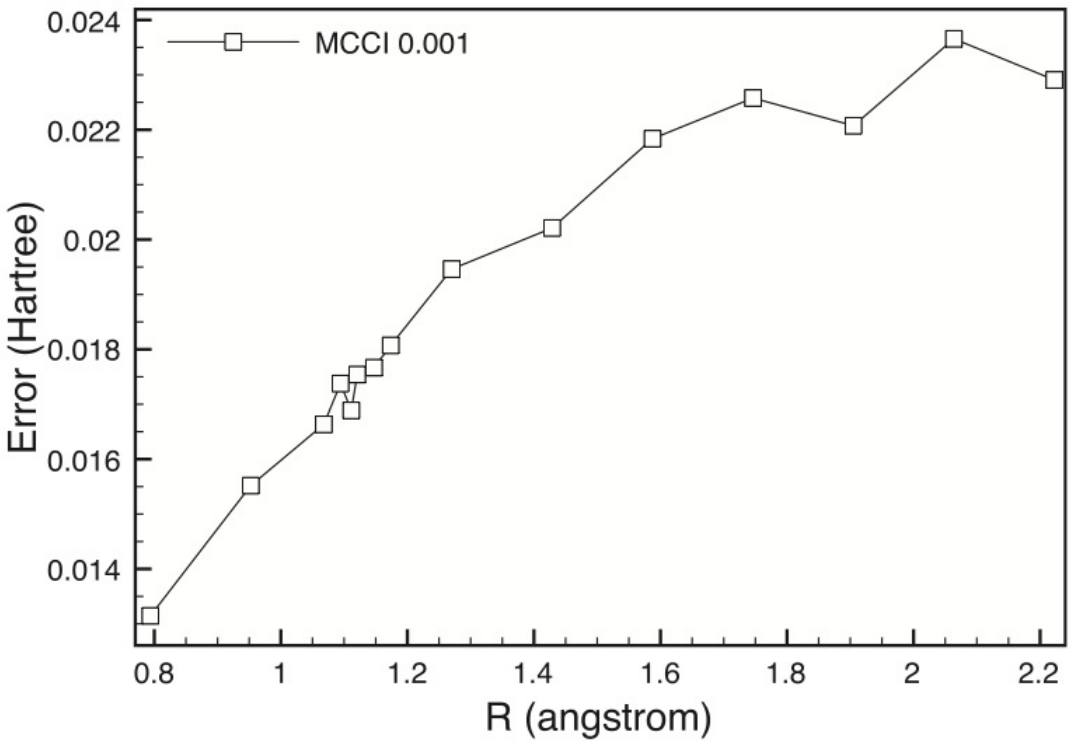

Figure 5-16: Error in MCCI ($c_{min}=10^{-3}$) result in comparison to the FCI calculation against bond length R (angstrom) in N_2, using the cc-pVDZ basis set with two frozen orbitals.

The N_2 PEC was also calculated using the cc-pVTZ basis set. MCCI energies (Hartree) against bond length R (angstrom) for the N_2 Molecule, using the cc-pVTZ basis set with two different c_{min} (10^{-3} and 5 x 10^{-4}) are displayed in Figure 5-17. Inset in Figure 5-17 is a plot of the energy difference between the MCCI results at the two c_{min}.

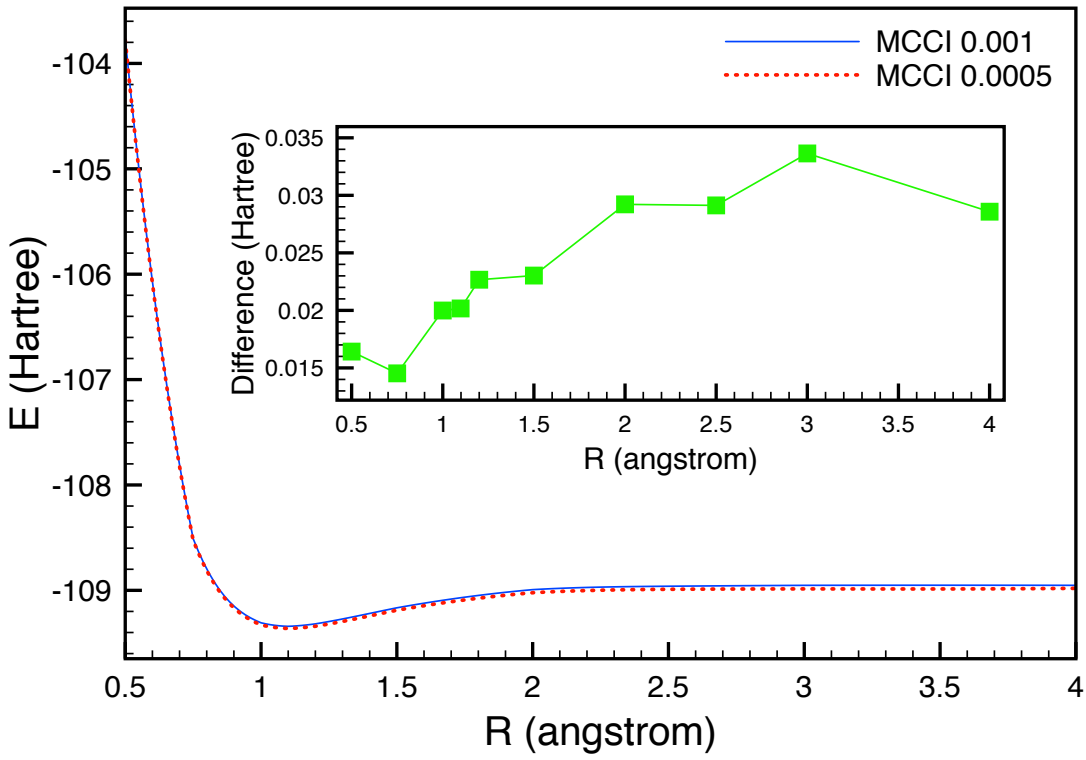

Figure 5-17: MCCI energy (Hartree) against bond length R (angstrom) for the N_2 Molecule, using the cc-pVTZ basis set with two different c_{min} (10^{-3} and 5 x 10^{-4}). Inset: the energy difference between the MCCI results at the two c_{min}.

The mean number for CFSs required for the $c_{min}=10^{-3}$ and the $c_{min}=5$ x 10^{-4} curves were around 4600 and 10600, respectively. Without symmetry considerations a FCI calculation would require 10^{17} SDs and this large size means a comparative FCI calculation in the same basis set is impossible. However an approximate comparison with the FCI results using the ANO[4s3p1d] with two frozen cores of Ref. [25] is attemped here. Using the equilibrium geometry point used in the MCCI calculations of 1.098 Å and the maximum bond length considered of 4 Å the dissociation energy is calculated to be 0.381 Hartree at 5 x 10^{-4} c_{min}. In Ref. [25] the points at 2.1 Bohr and 40 Bohr were used to calculate a FCI dissociation energy of 0.321 Hartree, which compares reasonably well to this MCCI value. Comparing the MCCI energy at 4 Å

with the MCCI energies of the nitrogen fragments a difference of 56.8 kcal/mol is found with $c_{min}=10^{-3}$ and 41.8 kcal/mol with $c_{min}=5 \times 10^{-4}$.

In an attempt to make a fairer comparison to the FCI result of Ref. [25] the MCCI ($5x10^{-4}$) calculation was repeated using the same geometry points as Ref. [25] (2.1 and 40 Bohr) and the cc-pVTZ basis set with the f orbitals removed. At R=2.1 Bohr an energy of -109.296 Hartree was found using 12,664 CSFs. However, at R=40 Bohr the MCCI result was far too high in energy, -93.66 Hartree using 5,029 CSFs. This is attributed to the restricted Hartree-Fock reference wave function being qualitatively incorrect at this bond length. The number of configurations required to compensate for using this poor reference seems to be too large for the c_{min} used. Using instead the previous point at 4 Å (7.56 Bohr) with this new basis set an energy value of -108.959 Hartree was calculated using 19,156 CFSs. In this case the MCCI result is only about 10 kcal/mol from the FCI dissociation energy of Ref. [25].

5.2.5 BeH_2

BeH_2 is a classic test system for methods due to its highly multireference behaviour at a small system size. The case of BeH_2 is far tougher for computational methods than any of the examples considered earlier in the chapter. The model reaction for the formation of BeH_2 was investigated using MCCI ($c_{min}=10^{-3}$) with cc-pVDZ basis set. Comparing those results to those of the Hartree-Fock and FCI methods calculated using MOLPRO[26], a plot of these results against the reaction coordinate x (Bohr) is shown in Figure 5-18.

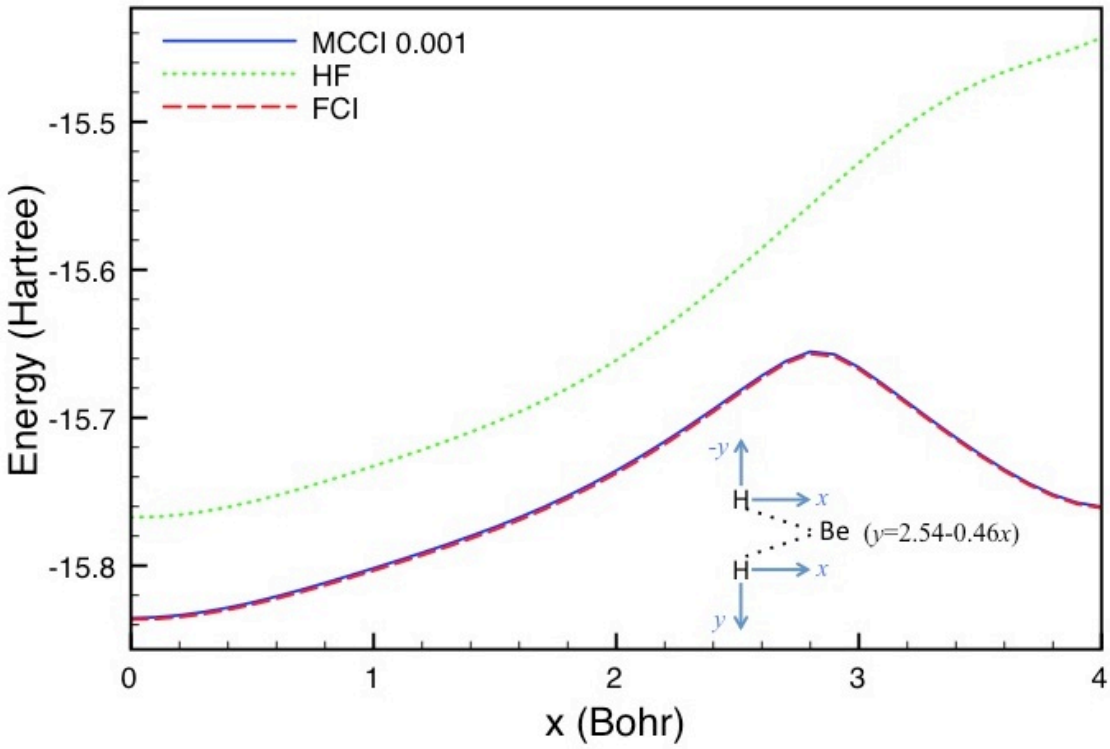

Figure 5-18: Energy (Hartree) from MCCI ($c_{min}=10^{-3}$), Hartree-Fock, and FCI against reaction coordinate x (Bohr) for BeH_2, using the cc-pVDZ basis set. Inset: the reaction coordinates.

It is clear that Hartree-Fock completely fails to describe the curve and predicts in fact that BeH_2 is not stable. The MCCI results recover the FCI curve extremely well not just in the shape but also in the energy values. In sharp contrast the Hartree-Fock results produce a complete different behaviour to the curve. The MCCI NPE of 0.653 kcal/mol confirms the high accuracy of the MCCI results. Which is impressive given the mean number of CSFs used in the MCCI curve is only 628, compared to 4×10^6 SDs required when neglecting symmetry in a FCI calculation. In Figure 5-19 the error in the MCCI ($c_{min}=5 \times 10^{-3}$) Energy (Hartree) compared to the FCI result against reaction coordinate x (Bohr) for BeH_2 is plotted.

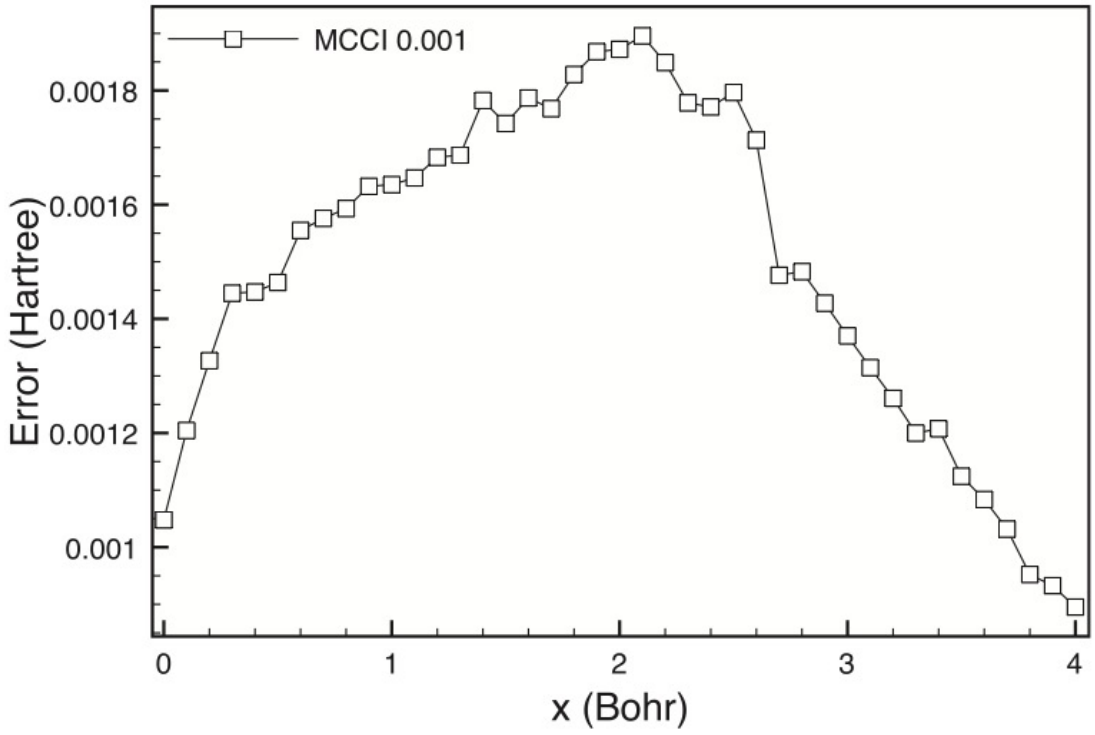

Figure 5-19: Energy error (Hartree) in MCCI (c_{min}=5 x 10^{-3}) compared to the FCI result against reaction coordinate x (Bohr) for BeH_2, using the cc-pVDZ Basis. NPE = 0.63 kcal/mol.

The error is at its lowest at the longest x considered (4 Bohr), the error increases as the reaction coordinate is decreased until around 2 Bohr. Lower than about 2 Bohr the error decreases again.

5.2.6 Ammonia Inversion

Here MCCI is used to reproduce the PEC of ammonia inversion, as its triagonal pyramid structure inverts through a planar structure. The cc-pVDZ basis set with a single frozen core orbital was used. The geometry used in the MCCI calculations has a NH bond length of 1.025 Å with each hydrogen at an angle of 120° to each other. The angle θ shown in the graphs is the angle the NH bond makes with a line passing through the nitrogen, perpendicular to the hydrogen plane. In Figure 5-20 the Energy in Hartree from MCCI (c_{min}=10^{-3}), Hartree-Fock, and FCI calculation is plotted against angle θ (degrees) for NH_2. Where the Hartree-Fock and FCI calculations were performed in MOLPRO[26]. The values were found for half of the plot and then mirrored about θ=90°.

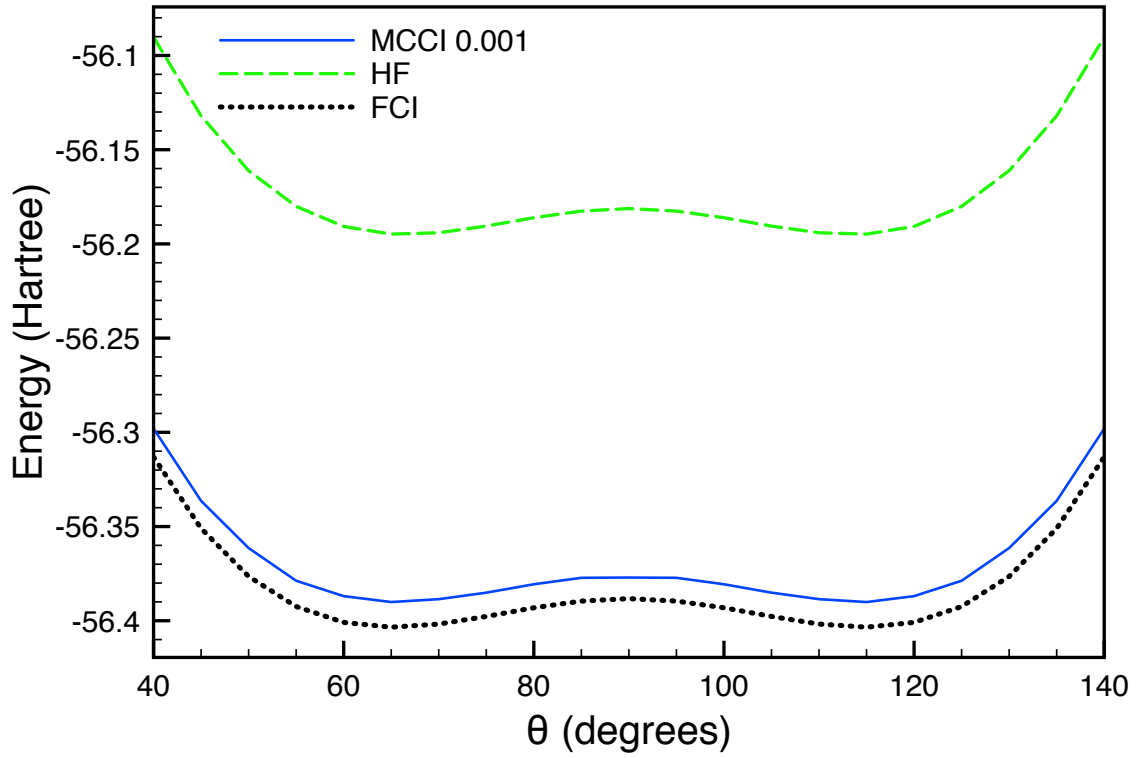

Figure 5-20: Energy (Hartree) from MCCI ($c_{min}=10^{-3}$), Hartree-Fock, and FCI against angle θ (degrees) for NH_3. Using the cc-pVDZ basis set and one frozen core orbital.

It can be seen that both MCCI ($c_{min}=10^{-3}$) and Hartree-Fock generally do a good job of recovering the shape of the FCI PEC. Though the MCCI curve does seem a bit flat about θ=90°. The NPE for Hartree-Fock is 9.9 kcal/mol, while for MCCI ($c_{min}=10^{-3}$) it is 2.4 kcal/mol. Over the length of the curve for the points calculated the number of CSFs used by MCCI ranged from 1226 to 1824, with a mean value of 1629. While the FCI calculation, neglecting symmetry, uses about 4×10^8 SDs.

The error in the energy (Hartree) calculated in MCCI ($c_{min}=10^{-3}$) compared to the FCI result against angle θ (degrees) for NH_3 is shown in Figure 5-21. The error is lowest at the transition state and increases as the angle moves away.

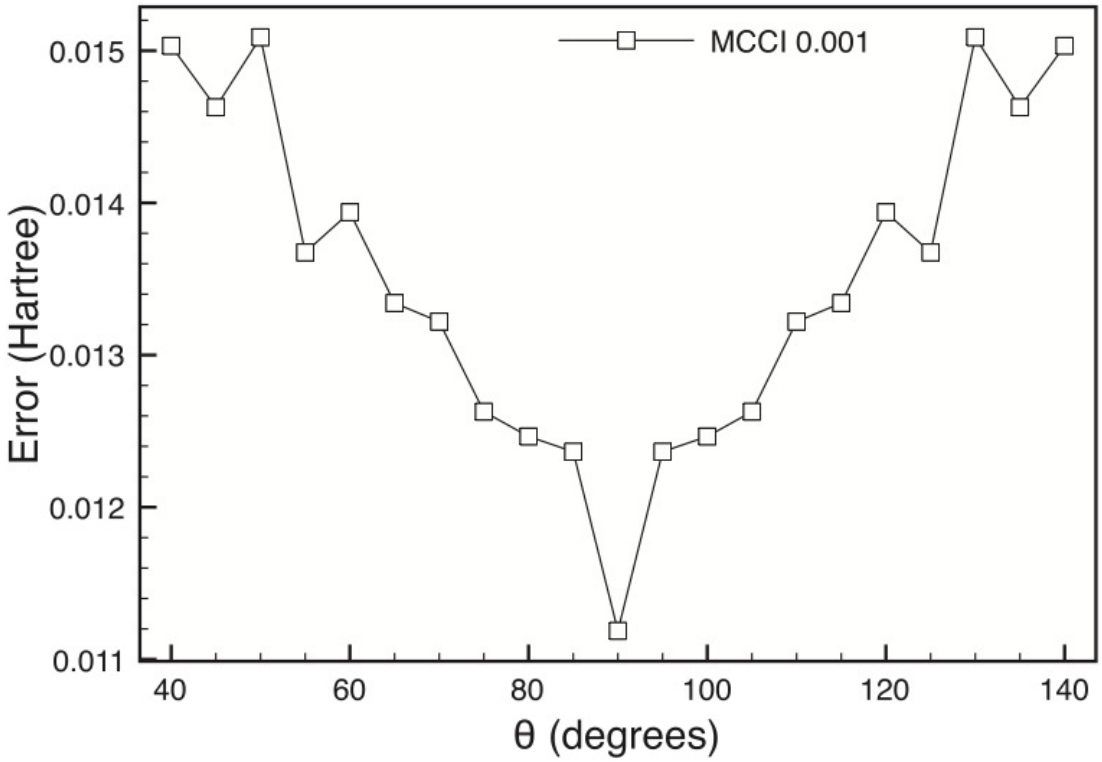

Figure 5-21: Energy error (Hartree) in MCCI ($c_{min}=10^{-3}$) compared to the FCI result against angle θ (degrees) for NH_3. Using the cc-pVDZ basis set and one frozen core orbital. NPE = 2.4 kcal/mol.

5.2.7 Hydrogen Lattice

Now a strongly correlated one-dimensional lattice made up of a linear chain of hydrogen atoms is considered. The ratio of static to dynamic correlation energy changes as the distance between the hydrogen atoms in the chain is altered. Progressing from largely dynamic to largely static as the distance between hydrogen is increased. These systems therefore pose an interesting challenge for MCCI. It is expected that modelling techniques for strongly correlated one-dimensional lattices, such as density matrix renormalisation group (DMRG)[27], should be more suitable for such a system than MCCI. A linear chain of 50 Hydrogen atoms was investigated using DMRG with the STO-6G basis set[28].

Firstly, a shorter chain of 12 hydrogen atoms for which FCI results can be calculated is considered. FCI results were calculated using MOLPRO with the STO-6G basis set. At Hydrogen separation R=1.0 Bohr only two coefficients have a value greater than 0.05 compared to 19 at R=4.2 Bohr, where the largest is only 0.22.

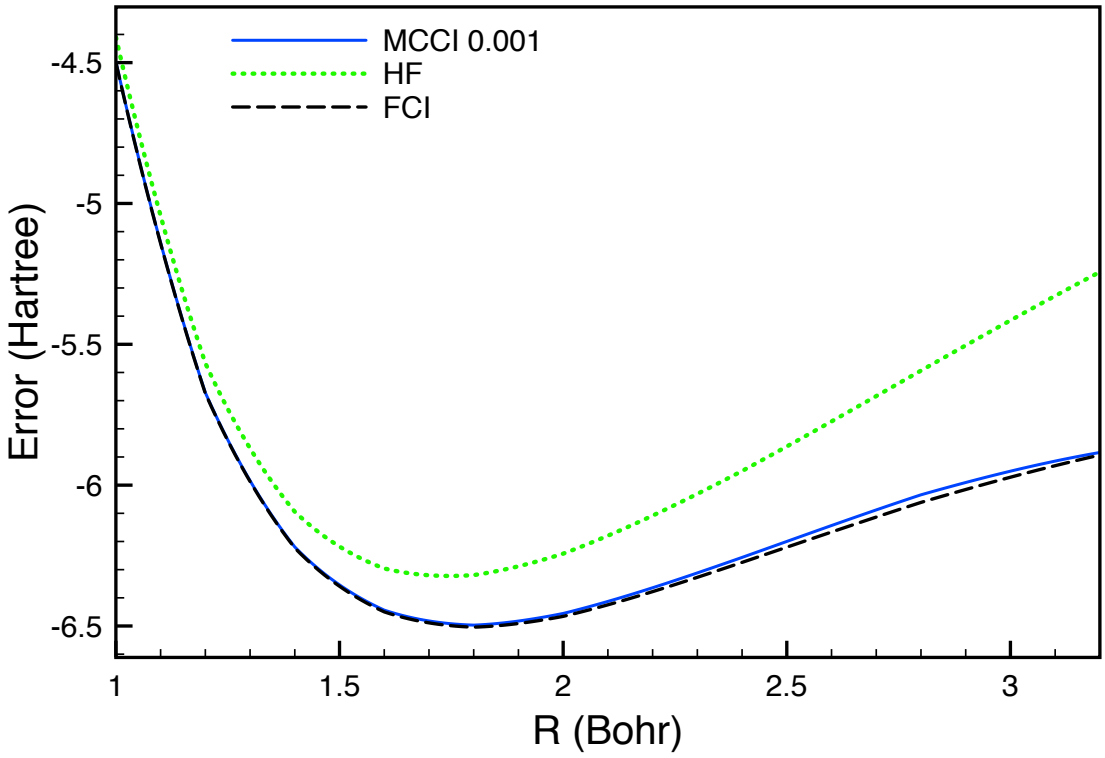

Figure 5-22: Energy (Hartree) from MCCI ($c_{min}=10^{-3}$), Hartree-Fock, and FCI against separation between atoms R (Bohr) for a chain of 12 hydrogen atoms. Using the STO-6G basis set.

In Figure 5-22 Energy (Hartree) from MCCI ($c_{min}=10^{-3}$), Hartree-Fock, and FCI against separation between atoms R (Bohr) for a chain of 12 hydrogen atoms is plotted. The Hartree-Fock energy increases far too quickly as the separation between hydrogen atoms increases, while the MCCI ($c_{min}=10^{-3}$) is a fairly good fit to the FCI curve. It must be noted here a numerical issue encountered with the MCCI results. For R > 3.2 Bohr the MCCI results are lower in energy than the FCI. This was found to be an issue with the very poor quality of the MOs used, as when the calculation was repeated using orthogonal atomic orbitals this issue was resolved. This suggests that the use of poor quality MOs in challenging systems should be done with caution as similar numerical issues may be encountered. The FCI calculation required 853,776 SDs, while the number of CSFs required for MCCI ranged from 342 at R= 1 Bohr to 6477 at R=2.8 Bohr. With an average 2701 CSFs required over all MCCI points.

In Figure 5-23 the energy error (Hartree) for MCCI ($c_{min}=10^{-3}$) compared to the FCI result against separation between atoms R (Bohr) for a chain of 12 hydrogen atoms is plotted. The error in the MCCI result increases in value as R is increased from 1 Bohr to 2.8 Bohr. The NPE for the MCCI curve was 15.8 kcal/mol.

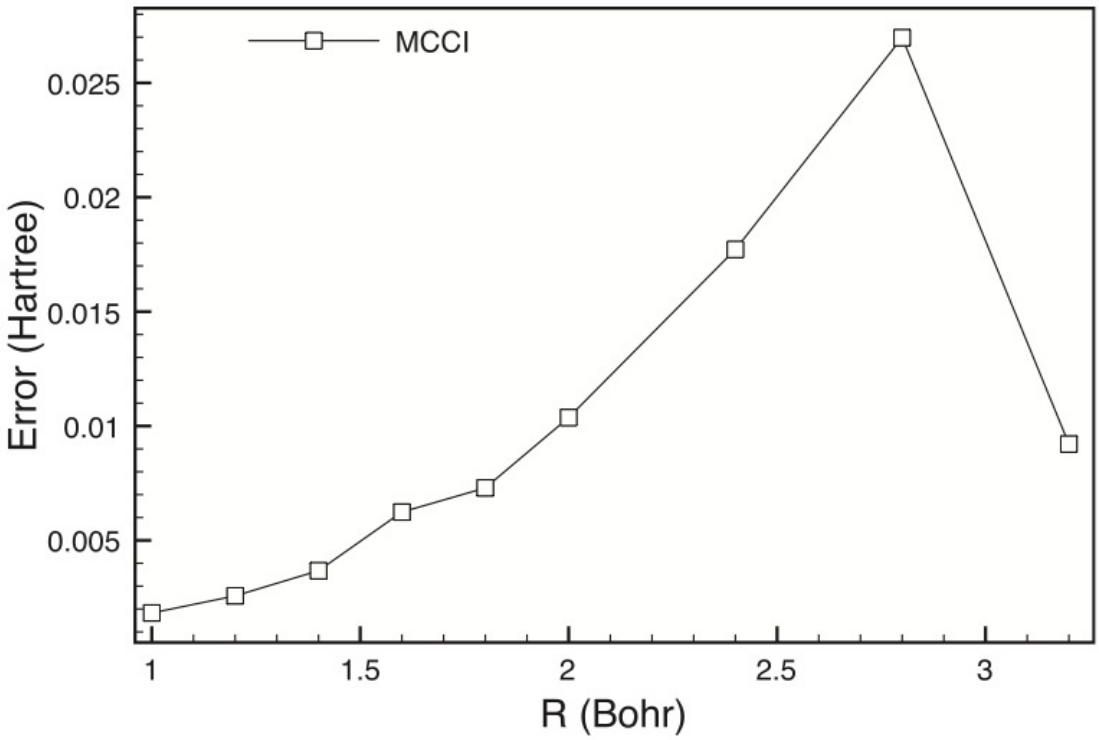

Figure 5-23: Energy error (Hartree) in MCCI ($c_{min}=10^{-3}$) compared to the FCI result against distance between atoms R (Bohr) for a chain of 12 hydrogen atoms. Using the STO-6G basis set. NPE = 15.8 kcal/mol.

It can be seen in Figure 5-24, that when considering a linear chain of 50 hydrogen atoms, MCCI ($c_{min}=5 \times 10^{-4}$) does not perform very well, giving a curve that is closer in shape to the Hartree-Fock curve than that of DMRG results of Ref. [28]. Though it is clear that the Hartree-Fock result has been improved upon. It is suggested that this is due to the methods small sampling of the extremely large configuration space (10^{28}). Only about 10^{-21} % of the configuration space is included in the ~80,000 CSFs of the MCCI calculation. This appears to be much too small a sample to accurately reproduce the required shape of the PEC.

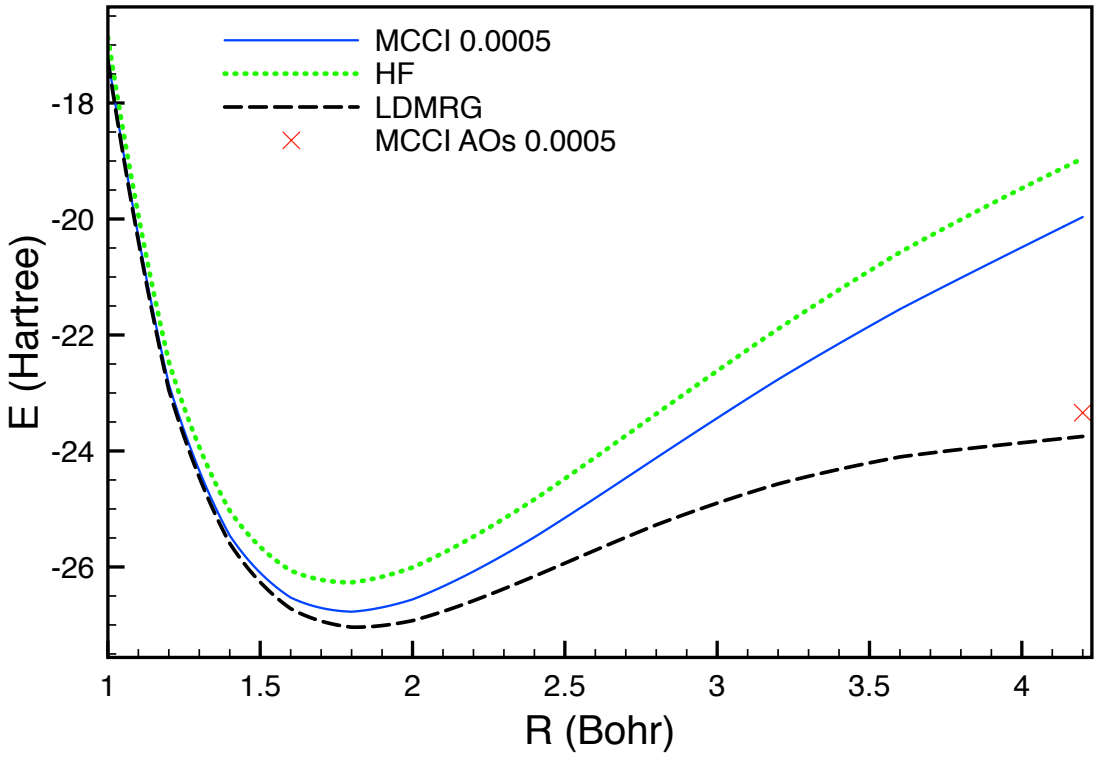

Figure 5-24: Energy (Hartree) from MCCI (c_{min}=5 x 10^{-4}), Hartree-Fock, and LDMRG(500) see Ref. [28] and MCCI (c_{min}=5 x 10^{-4}) using orthogonal atomic orbitals (AOs) against distance between atoms R (Bohr) for a chain of 50 hydrogen atoms. Using the STO-6G basis set.

At Large R the individual hydrogen in the chain could be far enough apart to be considered essentially dissociated. The system would be expected to be closer to a collection of non-interacting hydrogen atoms rather than an interacting chain. Therefore atomic orbital (AO) may be a better basis set than Hartree-Fock MOs at larger R. Starting with the left most atomic orbital, orthogonal atomic orbitals were constructed using the Gram-Schmidt procedure. By using CSFs, a single electron can be in each atomic orbital while still maintaining the correct spin of S=0. Applying this AO to a hydrogen chain separation distance R=4.2 Bohr produces the single point marked on Figure 5-24. The point is 0.4 Hartree above the DMRG curve. But the MCCI method seems unable to improve on the value of this single CSF as no other configurations are then found.

5.2.8 Ethylene Torsional Angle

Now considered is the case of torsional twisting of the C=C double bond of ethylene (C_2H_4). As no FCI results are available, the NPE cannot be found. Instead the

transition barrier height is compared to the results published in Ref. [29]. In Ref. [29] the barrier height of the C=C torsion was calculated using HF, CASSCF(12,12) and CASPT2, giving results of 111.8, 68.2 and 65.5 kcal/mol respectively. For the MCCI calculations, the ethylene geometry used was $R_{C=C}$ = 1.325 Å, R_{C-H} = 1.090 Å, and <HCC = 120.252°. These dimensions remain fixed for all calculations, the only change being the varying of the torsion angle. However, it should be noted that it is unclear from Ref. [29] whether exactly the same geometry was used and also if they allowed the molecular geometry to be relaxed at each torsion angle.

The MCCI results were computed using $c_{min}=10^{-3}$ and in keeping with the results of Ref.[29] the cc-pVDZ basis was used. The potential curve of the C=C bond torsion against energy is presented in Figure 5-25, these results were mirrored about the line x = 90.

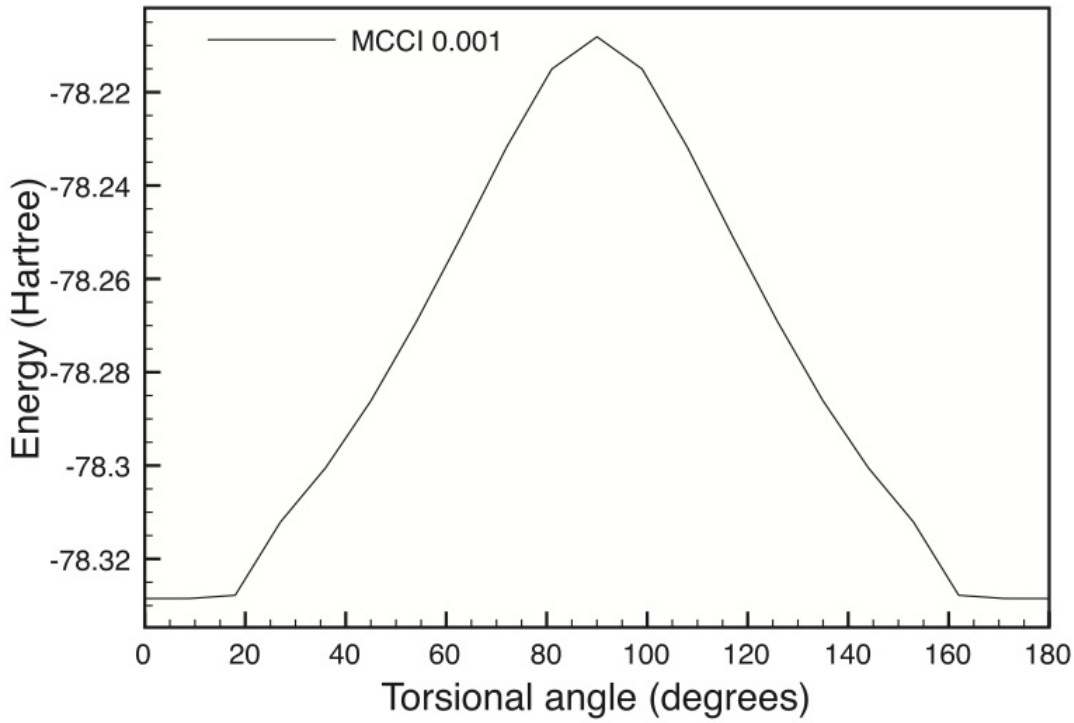

Figure 5-25: Energy against C=C bond torsional angle (degrees) of Ethylene with the cc-pVDZ basis and $c_{min}=10^{-3}$

The barrier height for this transition to be 75.52 kcal/mol when calculated from these MCCI results, which compares quite well with the results of Ref. [29]. Though, this may not be comparing like for like comparison. The number of CSFs used in the MCCI calculations increased from 5900 to 11200 as the torsion moved from 0 to 90 degrees, with an average of 8250 CSFs. This is a significant reduction in comparison to a FCI

calculation where approximately 10^{17} SD would be required, if any possible spatial symmetries are ignored.

5.2.9 Cr_2

The final PEC considered is that of the bond breaking of Cr_2. Cr_2 proves a very challenging test for theoretical calculation, as the wave function is very complex. The Cr atom has a high spin ^7S ground state with 6 unpaired electrons $(3d)^5(4s)$, which allows that 2 Cr atoms can in principle form 6 bonds. It is highly multi-configurational, the dominant configuration only contributes to 47% of the total[30]. Experimental investigation of the Cr_2 molecule identifies a minimum at 1.68 Å and further a flat shelf region around 2.5 Å[31]. The inner minimum corresponds to a 3d-3d dominated bond and the shelf corresponds to 4s-4s bonding. The binding energy (D_e) of Cr_2 has been experimentally measured as 1.53 ± 0.06 eV[32].

A FCI investigation of Cr_2 would be currently impossible due to the size of the system and consequently no FCI results exist for it. Basic single reference methods (such as MP2) completely fail to describe the chemical bond in the case of the Cr_2 molecule, predicting that the molecule does not exist. Using restricted CCSD(T) a single shallow minimum (D_e=0.38 eV) is predicted at 1.6 Å. While using unrestricted CCSD(T) the binding energy is improved to 0.89 eV, but at the expense of the minima location that moves to 2.54 Å[33]. With a CAS(12,12) treatment, that can recover the static correlation, only a weak and shallow minimum at about 3 Å is observed, with no shelf region reproduced[34].

Using multireference or second order methods are required in order to obtain a correct description of the Cr_2 chemical bond. Using the CASSCF wave function as a reference, these methods can recover the missing dynamic correlation and correctly reproduce the shape of the Cr_2 PEC. Clearly, a large percentage of the correlation energy must be recovered in order to approach a correct description of the molecule. MRCI gives a minima at 1.72 Å with a D_e=1.09 eV[35], MRCC gives a minima at 1.71 Å with D_e=1.22 eV[36], and CASPT2 finds a minima at 1.70 Å with D_e=0.97 eV[34].

5.2.9.1 Investigating the Cr_2 Dissociation PEC with MCCI

The PEC of Cr_2 dissociation was calculated using the MCCI method using the cc-pVDZ basis and c_{min} of 10^{-3}. The results of these calculations are presented in Figure 5-26.

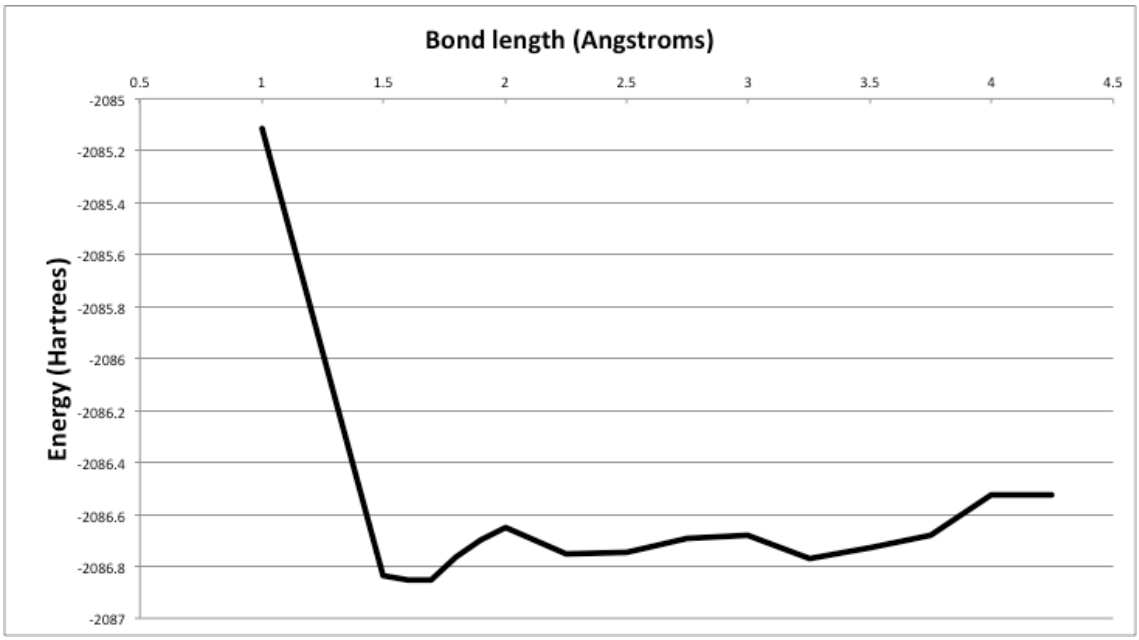

Figure 5-26: MCCI energy (Hartrees) against bond length (Angstrom) for Cr_2 with the cc-pVDZ basis and c_{min}=0.001

Due to the lack of FCI results for Cr_2, it is not possible to find the NPE of the MCCI curve. Inspecting Figure 5-26 it can be seen that MCCI has successfully predicted the minima at around 1.6 Å, though due to the number of points used it is impossible to refine the position of the minima further. Taking the 1.6 Å as the minima and the final point at 4.25 Å as being dissociation, the well depth is calculated as being D_e=8.94 eV. While the minimum appears to be in approximately the right position, the well depth is over estimated and is too deep. The 2.5 Å shelf is present, but is poorly resolved. It would appear that at this c_{min} (10^{-3}) the MCCI method is unable to correctly describe the PEC at longer bond lengths. The result should be improved by reducing the value of c_{min}.

Subsequent to this work, additional work by our group has improved upon the Cr_2 results presented here. Successfully reproducing the correct curve shape for Cr_2 using MCCI[11].

5.3 Conclusions

MCCI has been shown here to be capable of describing potential curves of small systems to a good accuracy. Though MCCI cannot be considered size consistent nor size extensive, when a low enough c_{min} is used MCCI is sufficiently size consistent to correctly describe the PEC of systems. The size consistency can be quantified by comparing the difference in the molecules MCCI energy at the longest bond length and the sum of the MCCI energies of the system's fragments. Most systems considered found a difference of less than 10 kcal/mol, with exception of N_2 that had a difference of 41.8 kcal/mol with the cc-pVTZ basis set. The cases of hydrogen dissociation had differences of less than 1 kcal/mol.

In Table 5-3 the mean CSFs to FCI SDs (neglecting symmetry) ratio, mean CSFs to FCI CSFs (neglecting symmetry), NPE (kcal/mol), and mean single point error (MSPE) in kcal/mol for the systems investigated are shown.

System	*% FCI SD space*	*% FCI CSF space*	*NPE*	*MSPE*
HF	0.014 %	0.056 %	1.3	2.6
BH	0.007 %	0.021 %	2.6	2.1
CH_4	0.012 %	0.049 %	0.6	4.1
C_2	0.003 %	0.013%	4.9	6.0
F_2	8.3×10^{-7} %	4.9×10^{-6} %	6.2	9.0
N_2	6.6×10^{-5} %	3.2×10^{-4} %	6.6	11.9
H_{12}	0.32 %	1.2 %	15.8	6.0
BeH_2	0.016 %	0.052 %	0.63	0.94
NH_3	4×10^{-4} %	1.7×10^{-3} %	2.4	8.4

Table 5-3: Mean CSFs to FCI SDs (neglecting symmetry) ratio, mean CSFs to FCI CSFs (neglecting symmetry), NPE (kcal/mol), and mean single point error (MSPE) in kcal/mol for the systems investigated where FCI results exist. All MCCI results are for the smallest c_{min} used.

NPE values often to around a few kcal/mol can be achieved using MCCI to generate a wave function that utilises a tiny percentage of the FCI space. With the exception of BH and H_{12}, the NPE of the MCCI curve is better than the MSPE of the constituent points. In general, at least for the systems considered, as the size of the FCI space increased the fraction of the FCI space used by the MCCI calculation decreased.

Three of the systems considered did not have FCI results for comparison. For the case of ethylene the calculated barrier of the PEC of the isomerisation was found to compare well with other computational results. For Cr_2, which is a very challenging case, while the minimum at around 1.6 Å was found, the shelf at 2.5 Å was poorly resolved and the well depth of the minimum was over estimated. This was shown to be a problem with the level of c_{min} used, and subsequent investigation resolved this problem[11]. The case of a large chain of 50 hydrogen atoms was to be too challenging for MCCI. Though the equilibrium geometry was in approximately the correct place, at long bond lengths the MCCI result was not a big improvement on the Hartree-Fock curve. A single CSF of orthogonal atomic orbitals provided an energy value closer to the DMFG curve here. It is suggested that this is due to the methods small sampling of the extremely large configuration space (10^{28}). It is possible that the MCCI result could be improved by the use of approximate natural orbitals and by letting the program run for more iterations, thereby giving the algorithm time to explore more of the FCI space.

Two potential limitations of the MCCI method when applied to potential energy surfaces have been noted. Firstly, if a sufficiently low c_{min} is not used the potential energy curve may not be smooth and features may not be properly resolved. This is due to the nature of the algorithm. Secondly, when a large sampling of the FCI is required, where the system is strongly correlated and/or the reference wave function is not qualitatively correct.

5.4 References

[1] Greer, J. C., Estimating full configuration-interaction limits from a monte-carlo selection of the expansion space. *Journal of Chemical Physics* **1995,** 103, 1821-1828.

[2] Greer, J. C., Monte carlo configuration interaction. *Journal of Computational Physics* **1998,** 146, 181-202.

[3] Tong, L. Y.; Nolan, M.; Cheng, T. W.; Greer, J. C., A monte carlo configuration generation computer program for the calculation of electronic states of atoms, molecules, and quantum dots. *Computer Physics Communications* **2000,** 131, 142-163.

[4] Greer, J. C., Consistent treatment of correlation-effects in molecular dissociation studies using randomly chosen configurations. *Journal of Chemical Physics* **1995,** 103, 7996-8003.

[5] Larsson, J. A.; Tong, L.; Cheng, T.; Nolan, M.; Greer, J. C., A basis set study for the calculation of electronic excitations using monte carlo configuration interaction. *Journal of Chemical Physics* **2001,** 114, 15-22.

[6] Győrffy, W.; Bartlett, R. J.; Greer, J. C., Monte carlo configuration interaction predictions for the electronic spectra of Ne, CH_2, C_2, N_2, and H_2O compared to full configuration interaction calculations. *Journal of Chemical Physics* **2008,** 129, 064103.

[7] Coe, J. P.; Paterson, M. J., Development of monte carlo configuration interaction: Natural orbitals and second-order perturbation theory. *The Journal of Chemical Physics* **2012,** 137, 20, 10 p.204108.

[8] Coe, J. P.; Paterson, M. J., State-averaged monte carlo configuration interaction applied to electronically excited states. *The Journal of Chemical Physics* **2013,** 139, 15, 11 p.154103.

[9] Coe, J. P.; Taylor, D. J.; Paterson, M. J., Calculations of potential energy surfaces using monte carlo configuration interaction. *The Journal of Chemical Physics* **2012,** 137, 12, 19 p.194111.

[10] Coe, J. P.; Taylor, D. J.; Paterson, M. J., Monte carlo configuration interaction applied to multipole moments, ionization energies, and electron affinities. *Journal of Computational Chemistry* **2013,** 34, 1083-1093.

[11] Coe, J. P.; Murphy, P.; Paterson, M. J., Applying monte carlo configuration interaction to transition metal dimers: Exploring the balance between static and dynamic correlation. *Chem. Phys. Lett.* **2014,** 604, 46-52.

[12] Coe, J. P.; Paterson, M. J., Approaching exact hyperpolarizabilities via sum-over-states monte carlo configuration interaction. *The Journal of Chemical Physics* **2014,** 141, 12, p. 124118.

[13] Coe, J. P.; Paterson, M. J., Characterising a configuration interaction excited state using natural transition geminals. *Molecular Physics* **2013,** 112, 733-739.

[14] Li, X.; Paldus, J., Comparison of the open-shell state-universal and state-selective coupled-cluster theories: H4 and H8 models. *The Journal of Chemical Physics* **1995,** 103, 1024-1034.

[15] Dutta, A.; Sherrill, C. D., Full configuration interaction potential energy curves for breaking bonds to hydrogen: An assessment of single-reference correlation methods. *The Journal of Chemical Physics* **2003,** 118, 1610-1619.

[16] Abrams, M. L.; Sherrill, C. D., An assessment of the accuracy of multireference configuration interaction (MRCI) and complete-active-space second-order perturbation theory (CASPT2) for breaking bonds to hydrogen. *The Journal of Physical Chemistry A* **2003,** 107, 5611-5616.

[17] Sears, J. S.; Sherrill , C. D., On the choice of reference in multi-reference electronic structure theory: Minimal references for bond breaking. *Molecular Physics* **2005,** 103, 803-814.

[18] Coe, J. P.; paterson, M. J., Novel truncated and stochastic approaches to configuration interaction. In *Recent research developments in chemical physics.*, Pandalai, S. G., Ed. Transworld Research Network: Kerala, India, 2012; Vol. 6, pp 41-65.

[19] Abrams, M. L.; Sherrill, C. D., Full configuration interaction potential energy curves for the X $^1\Sigma_g^+$,B $^1\Delta_g$, and B' $^1\Sigma$g+ states of C_2: A challenge for approximate methods. *The Journal of Chemical Physics* **2004,** 121, 9211-9219.

[20] Bytautas, L.; Nagata, T.; Gordon, M. S.; Ruedenberg, K., Accurate ab initio potential energy curve of F_2. I. Nonrelativistic full valence configuration interaction energies using the correlation energy extrapolation by intrinsic scaling method. *The Journal of Chemical Physics* **2007,** 127, pg 164317.

[21] Lyakh, D. I.; Ivanov, V. V.; Adamowicz, L., State-specific multireference complete-active-space coupled-cluster approach versus other quantum chemical methods: Dissociation of the N_2 molecule. *Molecular Physics* **2007,** 105, 1335-1357.

[22] Larsen, H.; Olsen, J.; Jørgensen, P.; Christiansen, O., Full configuration interaction benchmarking of coupled-cluster models for the lowest singlet energy surfaces of N_2. *The Journal of Chemical Physics* **2000,** 113, 6677-6686.

[23] Gwaltney, S. R.; Byrd, E. F. C.; Voorhis, T. V.; Head-Gordon, M., A perturbative correction to the quadratic coupled-cluster doubles method for higher excitations. *Chem. Phys. Lett.* **2002,** 353, 359-367.

[24] Chan, G. K.-L.; Kallay, M.; Gauss, J., State-of-the-art density matrix renormalization group and coupled cluster theory studies of the nitrogen binding curve. *The Journal of Chemical Physics* **2004,** 121, 6110-6116.

[25] Rossi, E.; Bendazzoli, G. L.; Evangelisti, S.; Maynau, D., A full-configuration benchmark for the N2 molecule. *Chem. Phys. Lett.* **1999,** 310, 530-536.

[26] H.-J. Werner, P. J. K., G. Knizia, F. R. Manby, M. Schütz, P. Celani, T. Korona, R. Lindh, A. Mitrushenkov, G. Rauhut, K. R. Shamasundar, T. B. Adler, R. D. Amos, A. Bernhardsson, A. Berning, D. L. Cooper, M. J. O. Deegan, A. J. Dobbyn, F. Eckert, E. Goll, C. Hampel, A. Hesselmann, G. Hetzer, T. Hrenar, G. Jansen, C. Köppl, Y. Liu, A. W. Lloyd, R. A. Mata, A. J. May, S. J. McNicholas, W. Meyer, M. E. Mura, A. Nicklass, D. P. O'Neill, P. Palmieri, K. Pflüger, R. Pitzer, M. Reiher, T. Shiozaki, H. Stoll, A. J. Stone, R. Tarroni, T. Thorsteinsson, M. Wang, and A. Wolf, *Molpro, version 2010.1, a package of ab initio programs,* , see http://www.molpro.net.

[27] White, S. R.; Martin, R. L., Ab initio quantum chemistry using the density matrix renormalization group. *The Journal of Chemical Physics* **1999,** 110, 4127-4130.

[28] Hachmann, J.; Cardoen, W.; Chan, G. K.-L., Multireference correlation in long molecules with the quadratic scaling density matrix renormalization group. *The Journal of Chemical Physics* **2006,** 125, (14), 144101.

[29] Piris, M.; Lopez, X.; Ruipérez, F.; Matxain, J. M.; Ugalde, J. M., A natural orbital functional for multiconfigurational states. *The Journal of Chemical Physics* **2011,** 134, 164102.

[30] Ruipérez, F.; Aquilante, F.; Ugalde, J. M.; Infante, I., Complete vs restricted active space perturbation theory calculation of the Cr_2 potential energy surface. *Journal of Chemical Theory and Computation* **2011,** 7, 1640-1646.

[31] Casey, S. M.; Leopold, D. G., Negative ion photoelectron spectroscopy of chromium dimer. *The Journal of Physical Chemistry* **1993,** 97, 816-830.

[32] Simard, B.; Lebeault-Dorget, M.-A.; Marijnissen, A.; ter Meulen, J. J., Photoionization spectroscopy of dichromium and dimolybdenum: Ionization potentials and bond energies. *The Journal of Chemical Physics* **1998,** 108, 9668-9674.

[33] Bauschlicher Jr, C. W.; Partridge, H., Cr_2 revisited. *Chem. Phys. Lett.* **1994,** 231, 277-282.

[34] Andersson, K.; Roos, B. O.; Malmqvist, P. Ö.; Widmark, P. O., The Cr_2 potential energy curve studied with multiconfigurational second-order perturbation theory. *Chem. Phys. Lett.* **1994,** 230, 391-397.

[35] Dachsel, H.; Harrison, R. J.; Dixon, D. A., Multireference configuration interaction calculations on Cr_2: Passing the one billion limit in MRCI/MRACPF calculations. *The Journal of Physical Chemistry A* **1998,** 103, 152-155.

[36] Müller, T., Large-scale parallel uncontracted multireference-averaged quadratic coupled cluster: The ground state of the chromium dimer revisited, *The Journal of Physical Chemistry A* **2009,** 113, 12729-12740.

Chapter 6: Application of Monte Carlo Configuration Interaction Method to Multipole Moments.

As stated in chapter 5, in the version of the MCCI program used here a configuration's contribution to a required property can be used to judge its inclusion to the wave function, rather than just the configuration's energy contribution. Therefore it is expected that all properties of the exact wave function should be approximated with sufficient accuracy by the calculation. In this chapter investigations of the application of MCCI to the calculation of multipole moments[1] are presented. In Ref. [1], in addition to multipole moments, ionization energies and electron affinities were also considered. While MCCI is shown to be a useful alternative for the calculation of atomic ionisation energies, electron affinities proved far more challenging. Dipole moments and excited state energies of TiO_2 calculated using MCCI appear at the end of the chapter, which ties in to the TiO_2 results presented in chapter 3.

Hartree-Fock molecular orbitals are used to generate the reference wave function where unless otherwise stated all electrons are correlated. The Molecular orbital integrals were generated using the Columbus program[2]. In addition to MCCI, the PSI3 program[3] was used for the FCI and multipole moment calculations, and spin-unrestricted CCSD (UCCSD) dipole moments were calculated in MOLPRO[4].

6.1 Dipole Moments

The dipole moment of a linear molecule oriented along the z-axis can be calculated as:

$$\mu = -\langle \Psi | \mathbf{z} | \Psi \rangle + \sum_i z_i Q_i \tag{6.1}$$

Where the dipole moment is calculated in atomic units and here Q_i is the nuclear charge of an atom i. In this section MCCI is used to calculate the dipole moments of the ground and excited states of carbon monoxide and for the ground state of NO. These

results are then compared to experimental and FCI results in order to assess the quality of the MCCI results.

6.1.1 Carbon Monoxide (CO)

Firstly, the ground state dipole moment of CO is considered. Experiment has previously defined the CO bond length (2.1316 Bohr) and dipole (0.122 Debye)[5]. Here the positive value dipole signifies a polarity of C^-O^+. Though it would appear to be a rather simple system the calculation of the dipole moment does still have some difficulties. The HF method incorrectly describes the dipole moment, giving the wrong sign for the dipole, effectively getting the direction of the dipole backwards. The quality of a dipole moment result has been associated to the amount of correlation accounted for by a given method[6].

In Figure 6-1 the MCCI (c_{min}=5 x10^{-3}) results of CO dipole moment (e Bohr) against program iteration are shown. PSI3 was used to find the FCI energy (-113.05583 Hartree) and dipole moment (0.23D), and these results are shown in Figure 6-1 for comparison. All calculations were performed using the cc-pVDZ basis set with two frozen core orbitals.

The MCCI result starts from a value close to the incorrect HF method value, but quickly changes sign as new configurations are generated and more of the correlation is recovered. The MCCI dipole moment eventually converges to about half of the FCI dipole value, the non-variational nature of the dipole can be seen at points in the calculation where the MCCI dipole value exceeds that of FCI. This MCCI calculation only used 833 CSFs, a tiny fraction of the 10^9 SD required for FCI calculation (if spatial symmetry considerations are ignored).

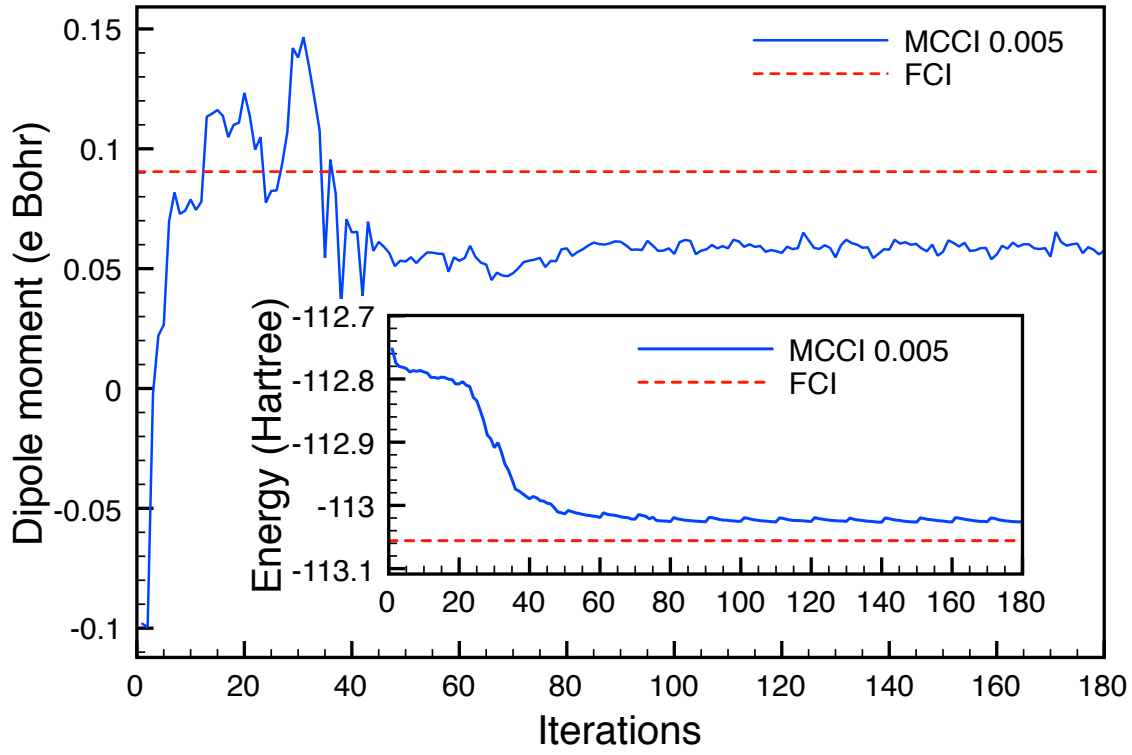

Figure 6-1: MCCI (c_{min}=5 x 10^{-3}) results of CO dipole moment (e Bohr) against program iteration, presented with FCI result. Calculations using the cc-pVDZ basis set with two frozen core orbitals. Adapted from Ref. [7]. Inset: Energy (Hartree) against program iteration number.

The convergence of the MCCI energy toward the FCI energy is also shown inset in Figure 6-1. At this value of c_{min} (5 x 10^{-3}) only 88% of the FCI energy is recovered. Clearly there is room to improve upon these results and recover more of the correlation energy.

The MCCI calculation was restarted from the converged c_{min}=5 x 10^{-3} wave function, this time with lower c_{min} value of 5 x 10^{-4}. This was repeated at 3 x 10^{-4} with the c_{min}=5 x 10^{-4} wave function as a reference. The MCCI energy against program iteration number is shown in Figure 6-2 for both these new c_{min} and again the FCI result is shown for comparison. The lowest c_{min} (3 x 10^{-4}) 98% of the correlation energy is now recovered, while using only approximately 4 x 10^4 CSFs. A characteristic saw tooth pattern is evident in these curves at convergence; this pattern is due to the full pruning steps that occur at regular intervals (10 iterations). Additional configurations generated in the interim steps reduce the energy, but are not checked for deletion as part of the entire wave function until this full pruning step.

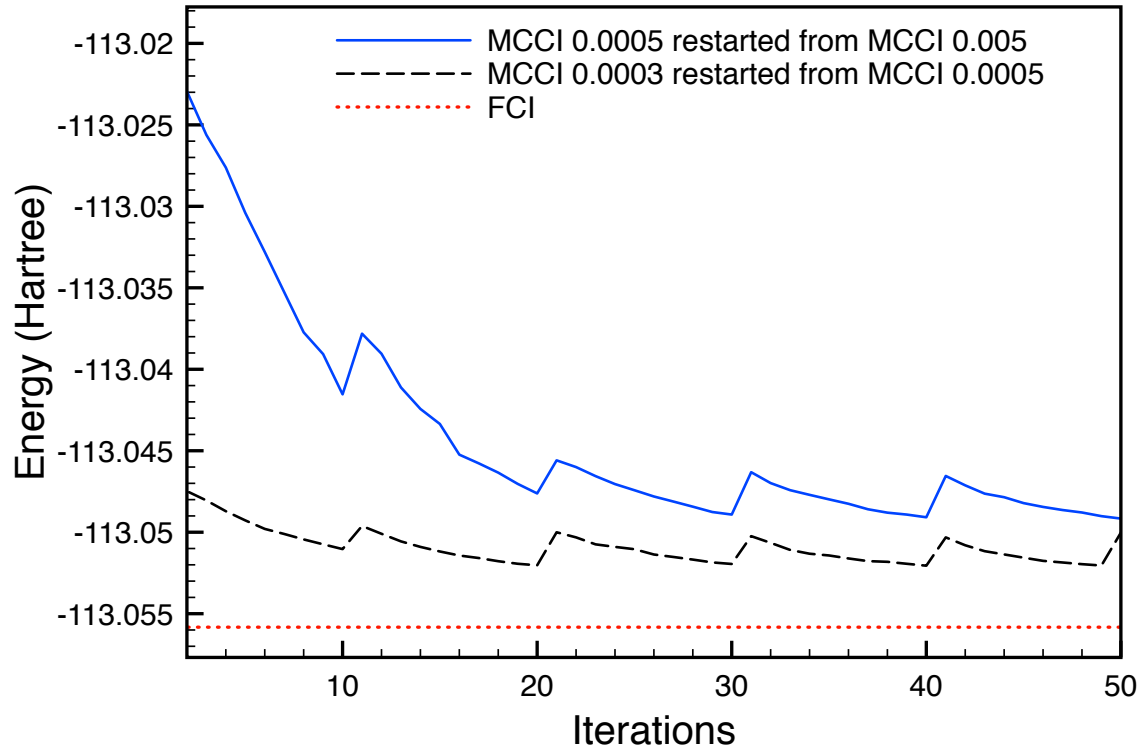

Figure 6-2: MCCI (c_{min}= 5x10^{-3} & 5x10^{-4}) and FCI energy against program iteration number for CO, using the cc-pVDZ basis set with 2 frozen core orbitals.

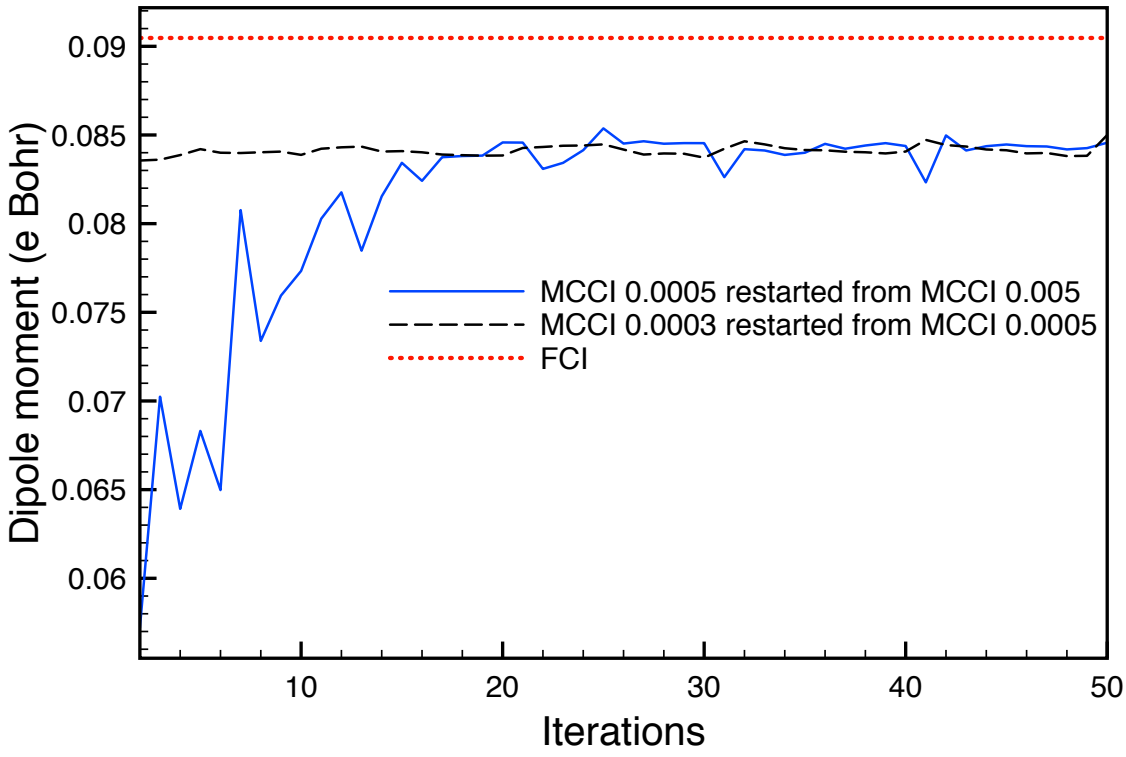

Figure 6-3: CO MCCI results of dipole moment (e Bohr) against program iteration number, using the cc-pVDZ basis set with 2 frozen core orbitals. Adapted from Ref. [7].

In Figure 6-3 dipole moments of CO can be seen for both the MCCI 0.0005 and the MCCI 0.0003 runs. It would appear that the dipole moment result is improved as the c_{min} cut-off value is reduced. Though there is not a big difference in the two final results, this can be put down to the small difference in the c_{min} values used.

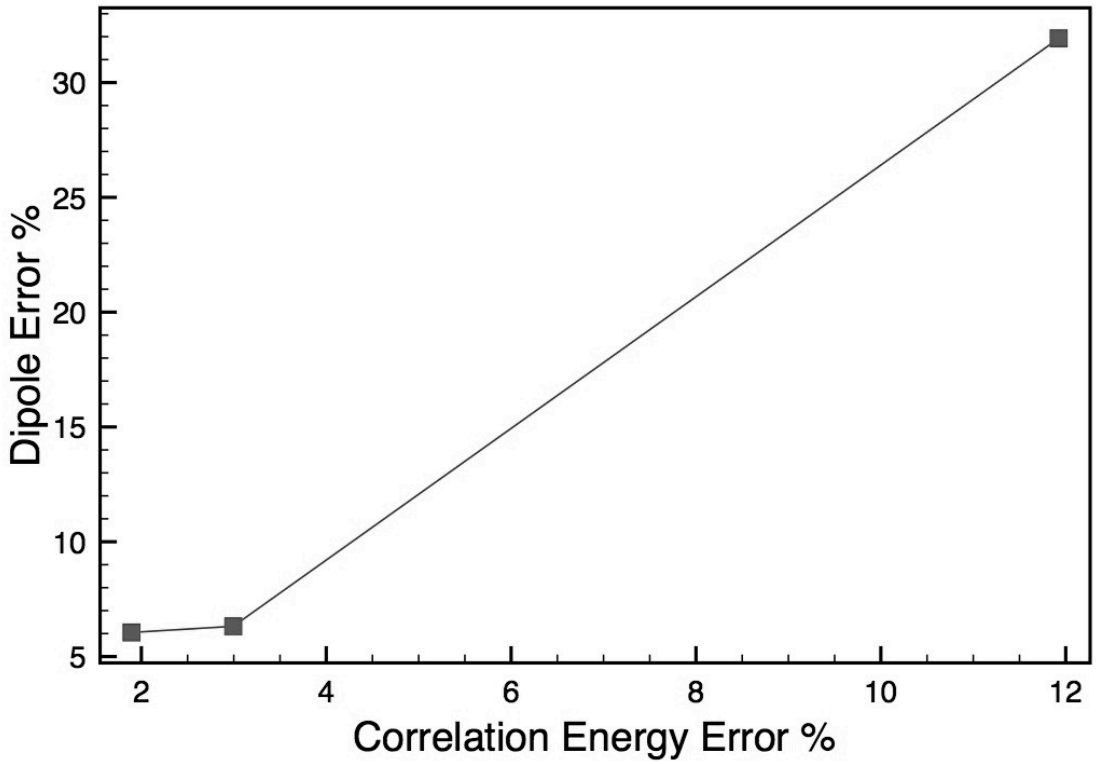

Figure 6-4: Dipole percentage error against correlation energy percentage error for CO, using the cc-pVDZ basis set and 2 frozen orbitals. Percentage errors for MCCI are in comparison to FCI result. Here, three values of c_{min} ($5x10^{-3}$, $5x10^{-4}$, and $3x10^{-4}$) are presented where decreasing correlation energy percentage error corresponds to decreasing c_{min}.

The percentage errors in the MCCI results in comparison to the FCI results are displayed in Figure 6-4. With decreasing correlation energy percentage error corresponding to decreasing the c_{min} ($5x10^{-3}$, $5x10^{-4}$, and $3x10^{-4}$), the dipole percentage error is plotted against the correlation energy percentage error. The dipole error does indeed appear to decrease with the decreasing correlation energy error.

Going back to the FCI dipole, there is a disparity with the experimental result. Though the absolute error is relatively small (~ 0.1 D), as a percentage error it is quite large. This is put down to the inability of the cc-pVDZ basis set to properly describe the wave function at distance from the atoms accurately. Proper treatment of the wave function further away from the atom is important to the accuracy of the multipole moments calculated. Adding diffuse functions to the basis set, in the form of the aug-cc-pVDZ

basis set should improve the MCCI results. The prior MCCI calculations were repeated using the aug-cc-pVDZ basis set with no frozen orbitals; unfortunately such calculations are far beyond FCI at this basis, therefore MCCI results are compared to experiment.

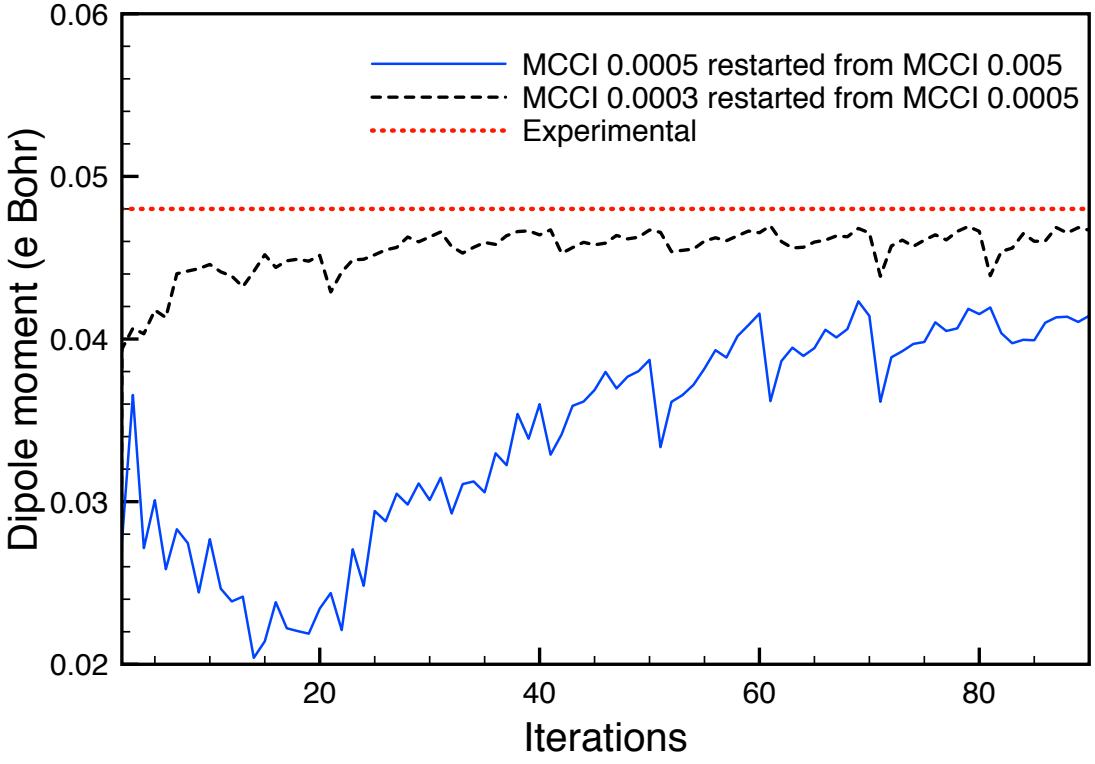

Figure 6-5: CO MCCI results for the dipole moment (e Bohr) against program iteration number, using the aug-cc-pVDZ basis set. Adapted from Ref. [7].

Figure 6-5 depicts the CO MCCI results for the dipole moment (e Bohr) against program iteration number, using the aug-cc-pVDZ basis set. At c_{min}=3 x 10^{-4} a dipole of 0.11 D was calculated with 55,913 CSFs used, in much better agreement with the experimental result. This is just a fraction of the SDs (10^{15} if no symmetry is used) that would be required for the FCI calculation.

More conventional methods such as CCSD can calculate the dipole moment of this ground state at equilibrium geometry more efficiently. A CCSD calculation using the cc-pVDZ basis set gives a dipole of 0.0996 Debye without a lot of computing time. However, in the next example a case is considered where CCSD is expected to perform poorly.

6.1.1.1 CO Stretched Bond Length

CO at a stretched bond length of 4 Bohr is now considered. Its dipole moment (e Bohr) against program iteration number for MCCI is presented, alongside results of the FCI and CCSD methods, in Figure 6-6. The FCI was calculated in PSI3 and CCSD in MOLPRO[4]. While the CCSD result is clearly poor, the MCCI dipole quickly converges to the FCI result and at the scale of the graph the two results appear almost indistinguishable.

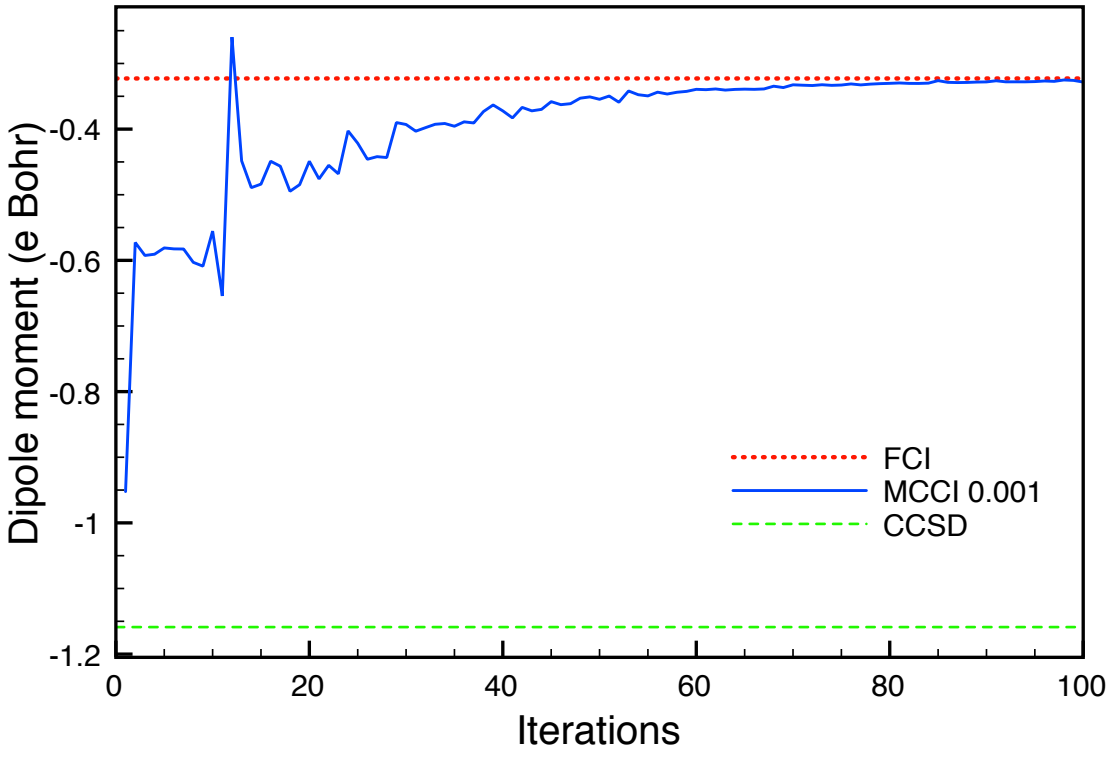

Figure 6-6: CO dipole moment (e Bohr) against program iteration number for MCCI, FCI, and CCSD methods. Using the cc-pVDZ basis set with two frozen core orbitals, CO stretched geometry of bond length R=4 Bohr.

By considering the FCI wave function it can be seen that the system is strongly multireference, as the nine largest coefficients have values between 0.24 and 0.30. This explains why in this case CCSD performs poorly, as methods based on a single reference would be expected to struggle. The MCCI method, which has no inherent problems with multireference systems, performs well. The final MCCI wave function was comprised of only 12,669 CSFs, a fraction of the 10^9 SDs required for FCI.

6.1.1.2 CO Triplet State

Using the experimental bond length of 2.278 Bohr cited in Ref. [8], the first triplet state of CO ($^3\Pi$) is now considered. The dipole moment of the first triplet state has been measured experimentally as -1.3740 Debye[9]. The MCCI ($c_{min}=10^{-3}$) result using cc-pVDZ basis set with 2 frozen core orbitals is presented against program iteration number in Figure 6-7. The MCCI dipole calculated is fairly close to the FCI result, but required only 5447 CSFs verses the 8.6 x 10^8 SDs for FCI.

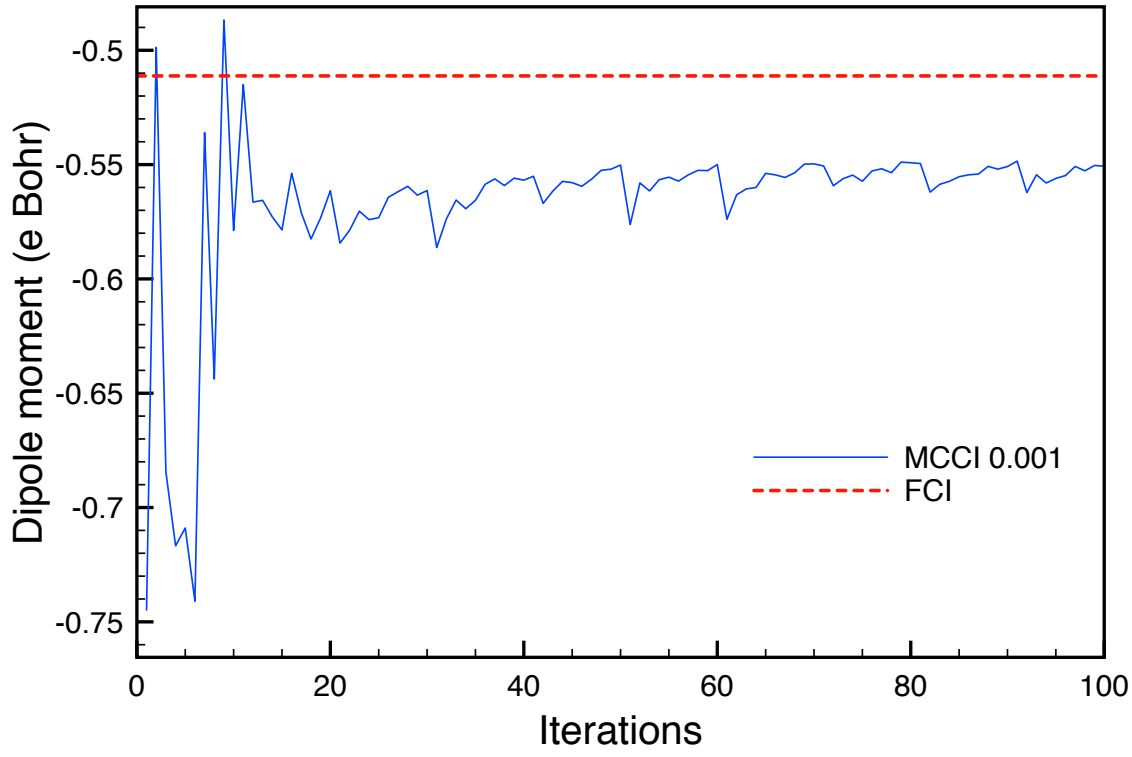

Figure 6-7: CO (at 2.278 Bohr) dipole moment (e Bohr) against program iteration number for the triplet state using MCCI ($c_{min}=10^{-3}$). Presented with the FCI result, both using the cc-pVDZ basis set with 2 frozen core orbitals.

Using the aug-cc-pVDZ basis set with no frozen orbitals MCCI, with a $c_{min}=10^{-3}$ requiring 7047 CSFs, gives a dipole of -1.584 Debye. This is in reasonable agreement with the experiment result. This result is further improved by lowering the c_{min}, to 10^{-4}, where 14,771 CSFs find a dipole of -1.49 Debye. Using this basis set and no consideration to symmetry, a FCI calculation would require in the region of 10^{15} SDs to perform these calculations.

6.1.1.3 CO Singlet Excited State

This section considers the first excited state $^1\Pi$ (of B_1 or B_2 symmetry within C_{2v}) of CO, using the experimental bond length of 2.334 Bohr cited in Ref. [10]. In Figure 6-8 the MCCI and FCI results using the cc-pVDZ basis set with 2 frozen core orbitals are plotted.

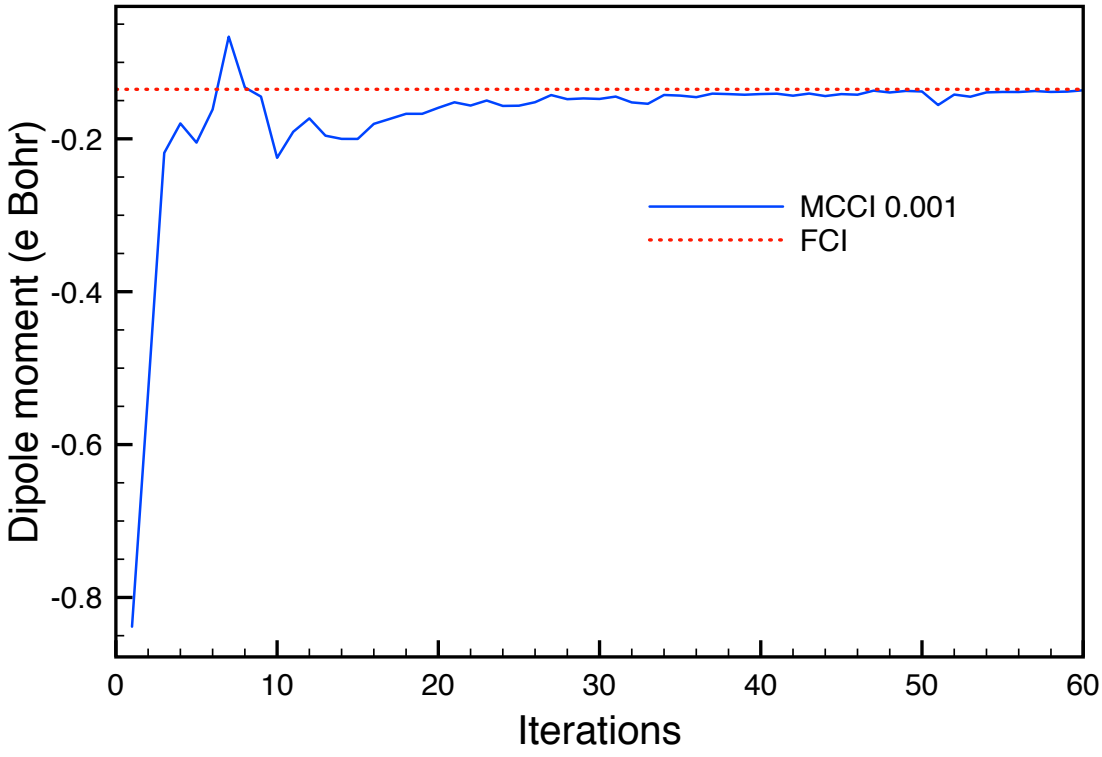

Figure 6-8: MCCI ($c_{min}=10^{-3}$) and FCI result for the dipole moment (e Bohr) for the first excited state of CO ($^1\Pi$ state with B_1 symmetry within C_{2v}) against program iteration number, using the cc-pVDZ basis set with 2 frozen core orbitals. Experimental bond length of 2.334 Bohr was used.

The MCCI method using a $c_{min}=10^{-3}$ quickly converges to a value close to the FCI result, using far fewer configurations (10,375 CSFs verses ~ 10^9 SDs in the symmetry adapted FCI space).

When the MCCI calculations were repeated using the aug-cc-pVDZ basis set at the ground state geometry using no frozen core orbitals, the dipole moment is calculated as -0.548 Debye. This required 16,487 CSFs. This compares well to the experimental result of -0.335 ± 0.013 Debye from Ref. [11], the sign having been originally determined theoretically in Ref. [10]. This MCCI result is improved upon by lowering c_{min} to 5 x 10^{-4}, giving -0.418 Debye using 45,274 CSFs.

Another excited state of CO considered in Refs. [10] and [11] is the first excited state of A_1 symmetry with C_{2v} ($^1\Sigma^+$). The dipole moment for this excited state was calculated using MCCI and FCI, with the cc-pVDZ basis set and the experimental bond length of 2.116 Bohr cited in Ref. [10]. The results are presented in Figure 6-9.

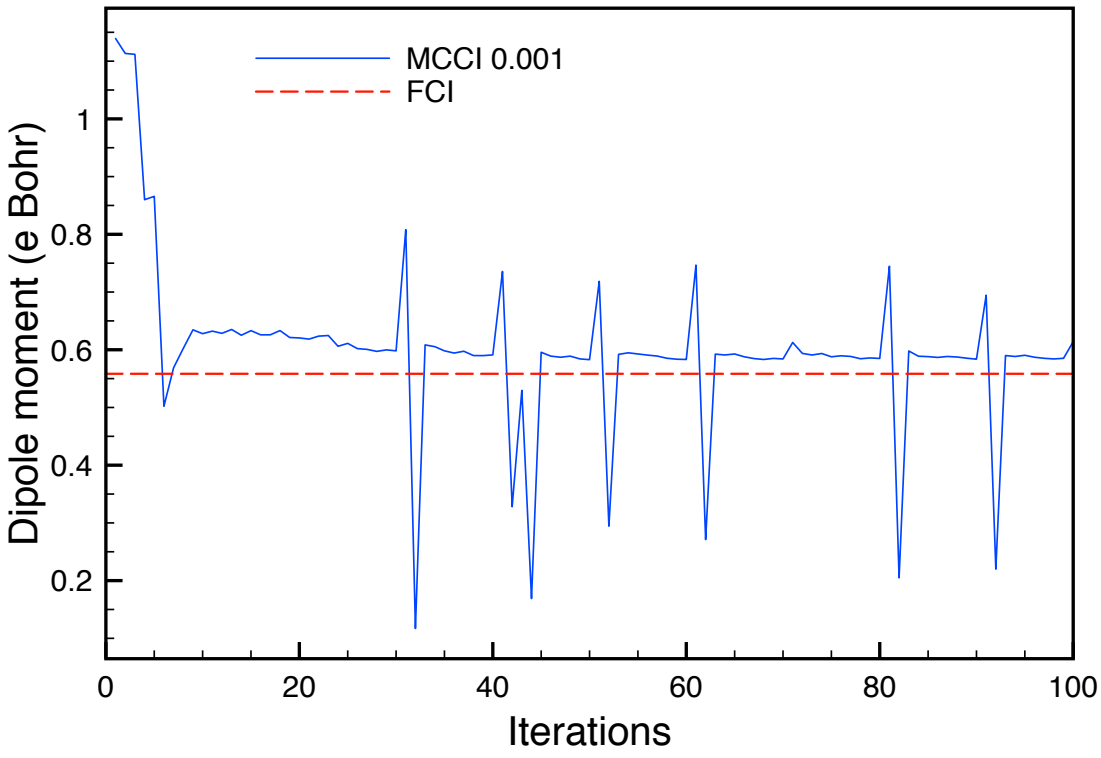

Figure 6-9: MCCI ($c_{min}=10^{-3}$) dipole moment (e Bohr) for the first ($^1\Sigma^+$) excited state of CO (at 2.116 Bohr A_1 symmetry within C_{2v}) against program iteration number, using the cc-pVDZ basis set with 2 frozen core orbitals. Presented with the FCI result.

At $c_{min}=10^{-3}$ the MCCI dipole moment quickly converges to a value slightly higher than the FCI result. At later iterations, this convergence does not seem stable with sharp oscillations away from the converged value. The energy occasionally rises sharply after a full pruning step. Concurrently, at these points, the dipole moment is seen to sharply increase and then decrease, before eventually returning to a converged value. It appears that during the full pruning step configurations important to the system are sometimes removed, resulting in the oscillations of the dipole value. This sensitivity may be as a result of the c_{min} size used. 8988 CSFs were used in this MCCI calculation compared to the symmetry adapted FCI which required approximately 10^9 SDs.

The experimental dipole was found to be 1.95 ± 0.03 Debye[11]. The sign was not determined in this experiment, but was determined theoretically in Ref. [10] where a dipole of approximately -2.79 Debye was found using MCSCF and CIS with about 27,000 CSFs. They also calculated the dipole of the ground state to be 0.32 Debye; they found a change in the direction of the dipole between the ground and excited state.

Using MCCI with a $c_{min}=10^{-3}$ and the aug-cc-pVDZ basis set a dipole of 1.762 Debye was calculated, which required 22,198 CSFs. Using a lower c_{min} (5×10^{-4}) the dipole was found to be 1.69 Debye, this time requiring 71,857 CSFs. For this result the final value was discounted due to an oscillation, so the iteration prior to this where a full pruning has occurred was used. There were few oscillations using this basis set and the number of oscillations was reduced further as a lower c_{min} is used. The sign of the dipole moments calculated for the excited state differs from that of the computation study in Ref. [10]. A change in direction of the dipole between the ground and excited states was not found when using MCCI. Also, EOM-CCSD calculations performed in MOLPRO[4] agree with both the sign and magnitude of the MCCI results, giving a dipole of 1.60 Debye with the cc-pVDZ basis and 1.72 Debye with the aug-cc-pVDZ basis (both using 2 frozen core orbitals).

6.1.2 NO

The doublet grounds state of NO has been investigated experimentally; its dipole moment is found to be 0.157 Debye[12], and the sign of the dipole confirmed positive[13], corresponding to N^-O^+. In this work the experimental bond length of 1.1508 Å cited in Ref. [14] was used.

In Figure 6-10 the MCCI ($c_{min}=10^{-3}$) dipole moment (e Bohr) for NO, using the 6-31G basis set, is plotted against program iteration number. Also shown are the FCI result calculated in PSI3, and the spin-unrestricted CCSD (UCCSD) result calculated using MOLPRO[4]. Starting from close to the incorrect HF dipole, which has the wrong sign, the MCCI result converges over the run to a dipole that lies between the FCI and UCCSD results. The MCCI dipole is calculated as 0.0122 D, while the FCI and

UCCSD results are 0.0201 D and 0.0041 D respectively. The FCI space with symmetry considered requires about 3 x 10^8 SDs, compared to the 3274 CSFs for the MCCI.

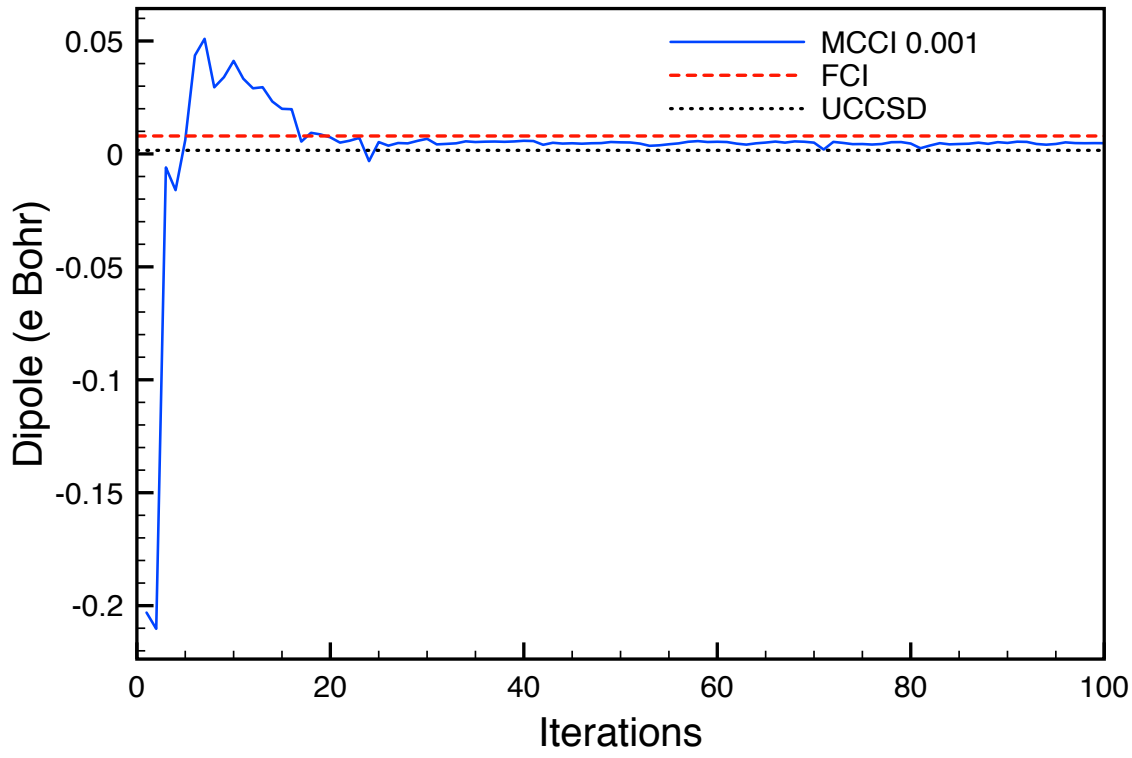

Figure 6-10: MCCI ($c_{min}=10^{-3}$) dipole moment (e Bohr) against program iteration number for NO, using the 6-31G basis set. Presented with the FCI and UCCSD results.

Using the larger aug-cc-pVDZ basis, in Figure 6-11 the MCCI with a $c_{min}=5 \times 10^{-3}$ gives a result that appears close in value to the experimental result, with the UCCSD value slightly lower. However, when MCCI calculations accuracy is improved by reducing the c_{min}, in attempt to improve the result, the result actually gets worse. At $c_{min}=5 \times 10^{-4}$ the MCCI result is now further from the experimental result than the UCCSD value. Though the dipole of 0.12 Debye, calculated at this lower c_{min}, still agrees reasonably well with the experimental result. 17,188 CSFs are used for this MCCI calculation compared to about 10^{16} SDs for the FCI space, without symmetry considerations.

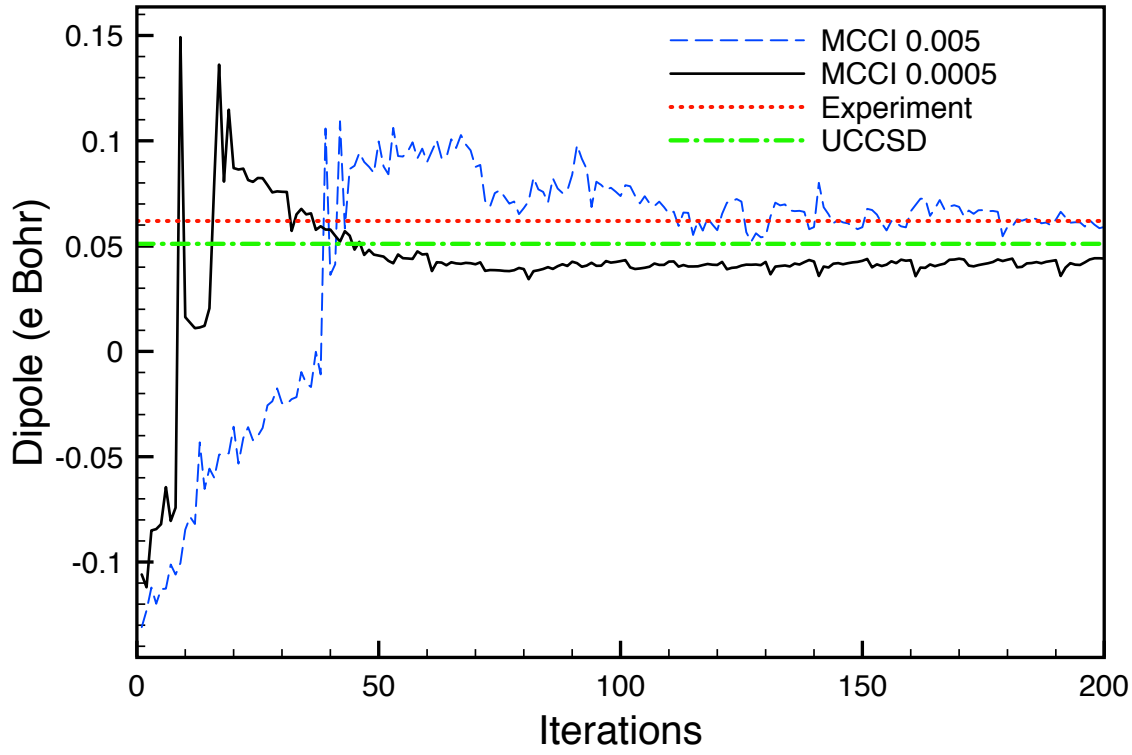

Figure 6-11: MCCI (cmin= $5x10^{-3}$ & $5x10^{-4}$) dipole moment (e Bohr) against program iteration number for NO, using the aug-cc-pVDZ basis set. Presented with the UCCSD and experimental results.

6.2 Quadrupole Moments

In the sections that follow the quadrupole moments (Q_{ZZ}) of N_2 and BH are investigated. The MCCI method is used in conjunction with the equation for the traceless quadrupole moment defined by Buckingham[15] and the results are compared to those of CC, FCI and experiment.

6.2.1 Nitrogen Molecule (N_2)

In this work the experimental bond length of 2.07432 Bohr for N_2 cited in Ref. [16] was used. The traceless quadrupole has been measured experimentally[17] to be (-4.65 ± 0.08)$x10^{-40}$ cm^2, which was revised in a later theoretical work[16] to (-5.01 ± 0.08)$x10^{-40}$ cm^2. The difference in the values being due to an improvement in a correction term used. Both these values are presented in Figure 6-13 as the upper and lower experimental bounds for the N_2 traceless quadrupole moment.

The traceless quadrupole moment Q_{zz} (e Bohr^2) against program iteration number for N_2, using MCCI ($c_{min}=10^{-3}$) and the cc-pVDZ basis set with 2 frozen core orbitals is presented in Figure 6-12. Included in the figure is the FCI result calculated, with the same basis and frozen orbitals, using the PSI program. The MCCI method seems to produce results that agree reasonably well with the FCI, especially given the relatively large c_{min} used. When symmetry is considered the FCI calculation uses 5.4 x 10^8 configurations, far more than the 5761 CFSs involved in the MCCI.

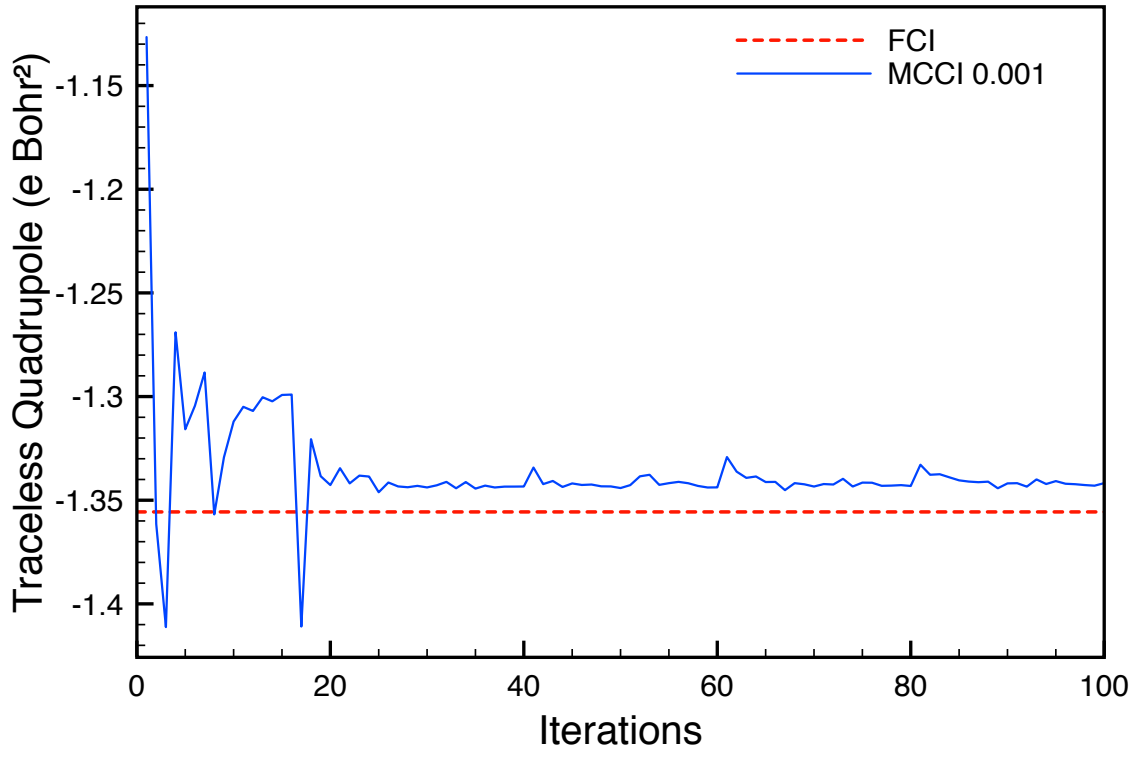

Figure 6-12: The traceless quadrupole moment Q_{zz} (e Bohr^2) against program iteration number for N_2, using MCCI ($c_{min}=10^{-3}$) and the cc-pVDZ basis set with 2 frozen core orbitals. Presented with the FCI result.

With the larger aug-cc-pVDZ basis and a c_{min} of 5 x 10^{-3}, the MCCI result falls between the experimental bounds (see Figure 6-13). This result of -1.105 e Bohr^2 compares well with the CCSD(T) result calculated in Ref. [16] of Q_{ZZ}=-1.1116 e Bohr^2 when only valence electron were correlated (aug-cc-pVDZ) and Q_{ZZ}=-1.1159 e Bohr^2 when using the larger aug-cc-pCVQZ with all electron correlated. If spatial symmetries were ignored FCI would require 10^{15} SDs, whereas MCCI used 22,000 CSFs.

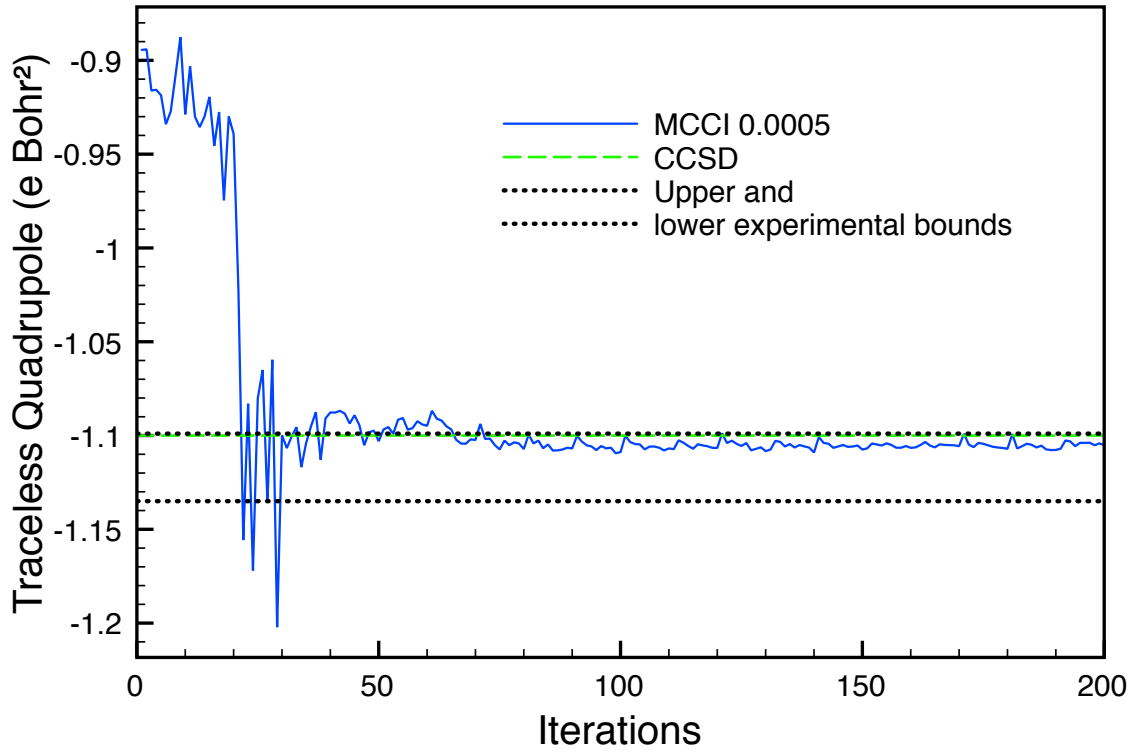

Figure 6-13: The traceless quadrupole moment Q_{zz} (e Bohr^2) against program iteration number for N_2, using MCCI (c_{min}=5x10^{-4}) and the aug-cc-pVDZ basis set. Presented with the CCSD, and the upper and lower bounds of the experimental results. Adapted from Ref. [7].

6.2.2 BH

Here MCCI is used to calculate the quadrupole moment of BH. In order to make direct comparison to the FCI and CC quadrupole moments calculated in Ref. [18], the experimental bond length of 2.3289 Å and aug-cc-pVDZ basis, as used in that work, was used here. When calculating the centre of mass, the mass of the most common Boron isotope was used (^{11}B).

In Figure 6-14 the MCCI results are presented with the FCI, CCSD, and CCSD(T) results of Ref. [18]. In this case the MCCI method out performs CCSD and is of comparable accuracy to the CCSD(T) and FCI methods. Though the MCCI method achieved this accuracy using far fewer configurations than FCI (4276 CFSs vs. 5 x 10^7 SDs without symmetry considerations).

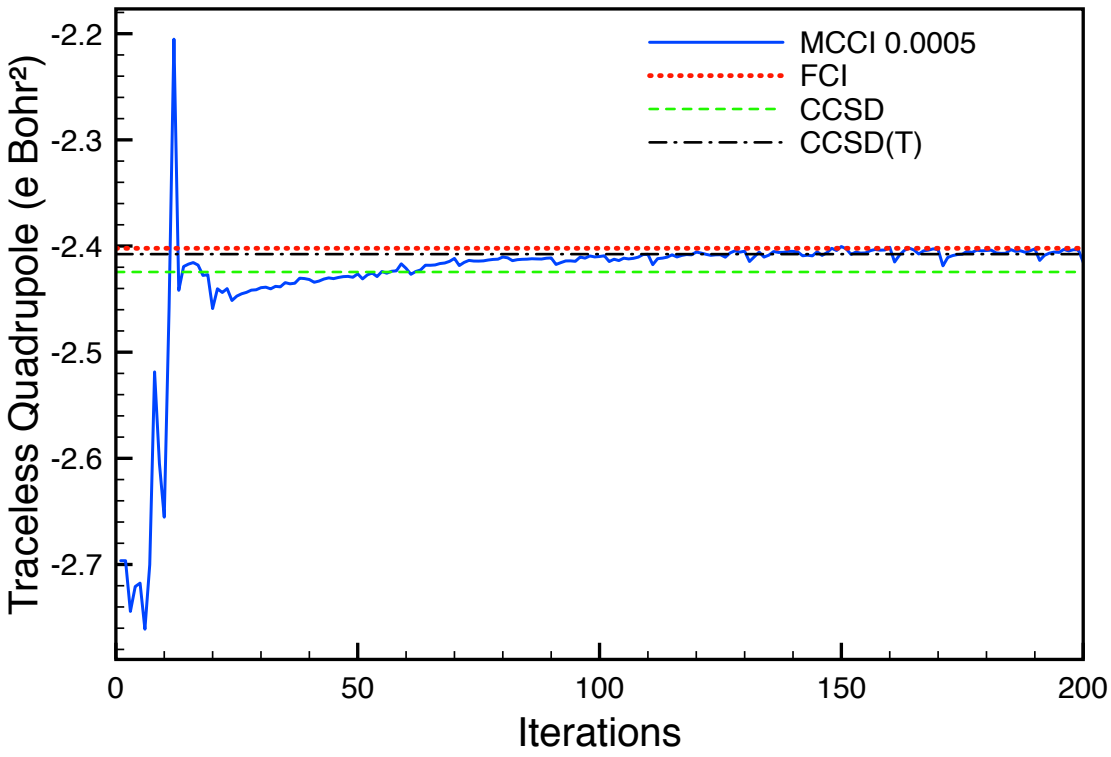

Figure 6-14: The traceless quadrupole moment Q_{zz} (e Bohr^2) against program iteration number for BH, using MCCI (c_{min}=5x10^{-4}) and the aug-cc-pCVDZ basis set. Presented here with the FCI and coupled cluster results from Ref. [18].

6.3 Octopole Moments

This section considers the octopole moment (Ω_{XXZ}) for the single case of methane (CH_4). The traceless octopole moment of Buckingham[15] is used to calculate the octopole along with MCCI and again compare the results with FCI results calculated using PSI3[3] and CC results produced using Dalton[19].

6.3.1 Methane (CH_4)

The geometry of methane used in the calculations is of a tetrahedral symmetry and a CH bond length of 2.052 Bohr from experiment[20]. All calculations used the cc-pVDZ basis set with a single frozen core orbital.

The MCCI result of the Ω_{XXZ} of methane is presented in Figure 6-15. For comparison the CISD and FCI results calculated using PSI3, and the CCSD result from Dalton, are also represented. The MCCI (at $c_{min}=10^{-3}$) octopole converges relatively quickly to a value better than the CISD result. Unsurprisingly CCSD performs better at this equilibrium geometry, giving a result closer to the FCI result. The FCI wave function consisted of about 4 x 10^8 SD, while MCCI only required 3330 CSFs.

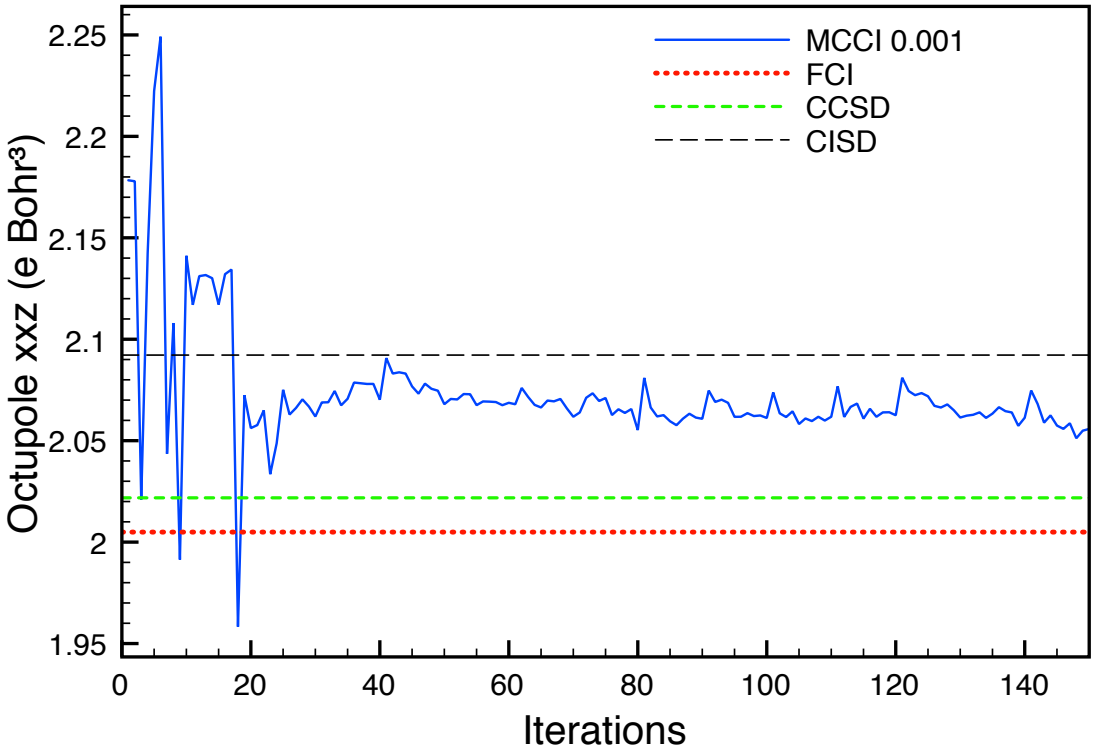

Figure 6-15: MCCI ($c_{min}=10^{-3}$) for Ωxxz (e Bohr^3) of methane against program iteration number, using the cc-pVDZ basis set with 1 frozen core orbital. Presented with the CISD, CCSD, and FCI results.

6.3.1.1 CH_4 Stretched Bond Length

A methane geometry with a stretched CH bond length is now considered, moving the molecule away from the equilibrium geometry. Using a bond length of 5 Bohr where the system is much more likely to be multireference, the calculations of 6.3.1 were repeated and the results presented in Figure 6-16.

Comparing Figure 6-15 to Figure 6-16, it is clear that at this stretched geometry that CISD and CCSD perform a lot more poorly. Giving a result for the octopole moment of over six times the FCI value. MCCI is more consistent, even at a relatively large c_{min} (10^{-3}), giving a result far closer to the FCI. The MCCI result is still relatively far from

the FCI; it is about 1.6 times smaller, but lowering of the c_{min} value gives scope to improve upon the result.

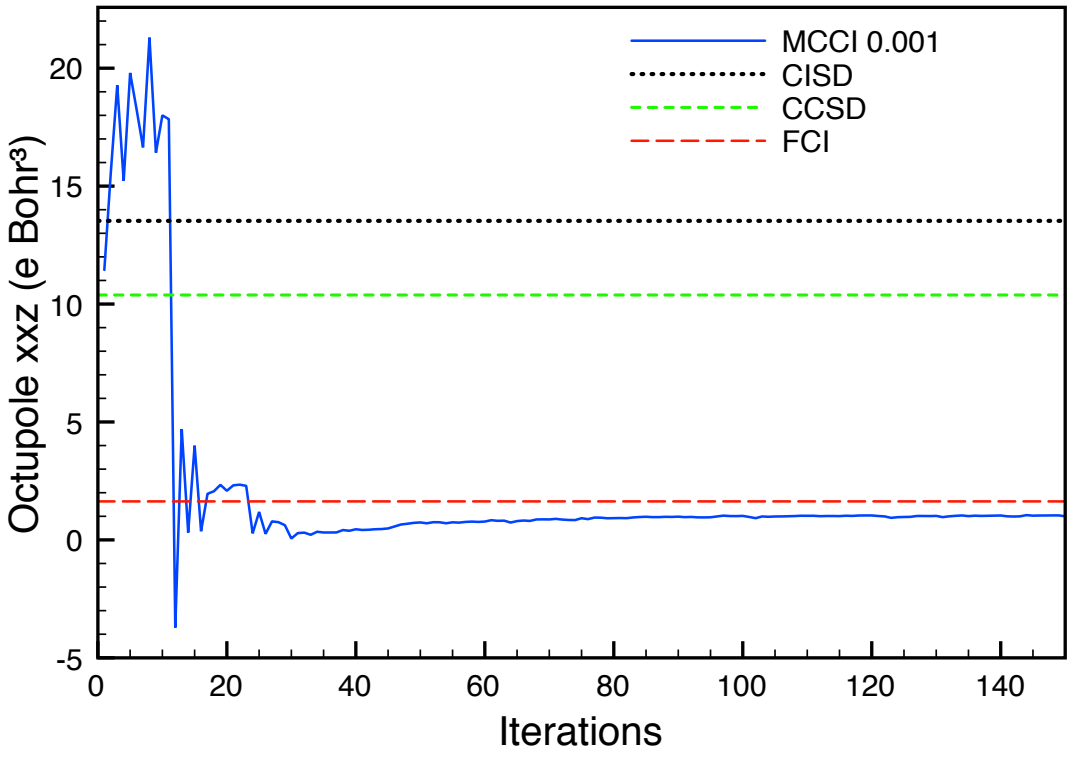

Figure 6-16: MCCI ($c_{min}=10^{-3}$) for Ωxxz (e Bohr^3) of methane (at stretched bond length R=5 Bohr) against program iteration number, using the cc-pVDZ basis set with 1 frozen core orbital. Presented with the CISD, CCSD, and FCI results.

6.4 Applying MCCI to the Ground and Excited States of the TiO_2 Monomer: Energies and Dipole Moments.

Returning to the TiO_2 monomer, which was considered in some depth in Chapter 3, the MCCI method is applied here to the same system. In chapter 3 calculations of the lowest excited states of the TiO_2 molecule were presented. It was shown that TiO_2 is a surprisingly strenuous test for correlated excited state methods. Lower cost wave function based methods completely fail to describe the lowest $^1B_2$ and $^1A_2$ states of the molecule[21].

Though TiO_2 is a small system, it is currently too large to be considered for FCI calculation. In a large FCI space the limiting step of the MCCI calculation is the diagonalisation using the Davidson algorithm. The MCCI wave function is thus currently restricted to a maximum of around 10^5 CSFs[1]. In order to make direct

comparison to the results of Chapter 3 the cc-pVTZ or ANO basis sets would be required, however MCCI calculations using that basis set and a suitably small c_{min} very quickly reached this limit. TiO_2 pushes the limits of the size of system that can be studied using the current version of the MCCI program. Therefore, in order to keep below the limit the cc-pVDZ basis set and 2 frozen core orbitals had to be used in these calculations. Even at this level of basis, at points in the calculation more than 80,000 CSFs would be included in the wave function. This restriction in the size of basis set makes direct comparison of the results of chapter 3 difficult.

The geometries used were those described earlier in chapter 3. The calculation of the dipole moment differed from those earlier in this chapter, in that the dipole was found using a single step of the version of the MCCI program modified to calculate the dipole moment. A wave function from a MCCI calculation that converged the energy in the original MCCI program was used as a starting point for the dipole calculation. It was assumed that at the point the MCCI energy had converged that the dipole had also converged. The quantities for the TiO_2 molecule that were calculated using MCCI with a $c_{min}=10^{-3}$ using the cc-pVDZ basis set and 2 frozen core orbitals are shown in Table 6-1.

Quantity	*MCCI ($c_{min}=10^{-3}$) Result*
Vertical excitation energy ($1\ ^1B_2 \leftarrow 1\ ^1A_1$)	1.789 eV
Adiabatic excitation energy ($1\ ^1B_2 \leftarrow 1\ ^1A_1$)	1.682 eV
Vertical excitation energy ($1\ ^1A_2 \leftarrow 1\ ^1A_1$)	3.992 eV
$1\ ^1A_1$ μ	7.80 D
$1\ ^1B_2$ μ	5.98 D

Table 6-1: MCCI ($c_{min}=10^{-3}$) results for the TiO_2 monomer, using the cc-pVDZ basis set and 2 frozen core orbitals.

The MCCI wave functions in these calculations required about 40,000 CSFs. Unlike the lower cost wave function methods discussed in chapter 3, MCCI ($c_{min}=10^{-3}$) appears to be able to correctly describe the lowest $1\ ^1B_2$ and $1\ ^1A_2$ states of the molecule. The vertical excitation energies from the $1\ ^1A_1$ ground state to the $1\ ^1B_2$ and $1\ ^1A_2$ compare favourably to the results calculated by CCSD using the ANO basis sets, which calculated 2.386 eV and 3.045 eV respectively. The adiabatic excitation energy from the $1\ ^1A_1$ ground state to the $1\ ^1B_2$ first excited state gives a value of 1.682 eV with MCCI at this level. This too compares well with the higher cost CC results. The MCCI method ($c_{min}=10^{-3}$) and the cc-pVDZ basis set (with 2 frozen core orbitals) calculated

the Dipole moments for the ground ($1\ ^1A_1$) and first excited state ($1\ ^1B_2$) as 7.80 D and 5.98 D, respectively. These results are reasonably close to the MRCI results of Ref. [22], of 6.73 D and 5.07 D.

These TiO_2 MCCI calculations are a preliminary test of the methods capabilities and, though the calculations use a smaller basis set, they compare well with the results of high-level multireference and CC methods. The MCCI method provides two avenues to further improve the results; decreasing the c_{min} and increasing the basis set size.

6.5 Conclusions

A summary of the multipole moment results of the MCCI and FCI methods from Ref. [1] is presented Table 6-2. In each case the MCCI result with the smallest c_{min} is presented. Over the range of molecules and geometries considered the MCCI method performs well in comparison to FCI. With a small fraction of the FCI SD space, MCCI can produce the multipoles very close in value to the FCI result.

Property	*MCCI*	*FCI*	*% FCI space*	*E_{corr} error (%)*	*Property error (%)*
CO μ	0.0850	0.0905	3.63×10^{-3}	1.89	6.05
CO R=4 μ	-0.328	-0.323	1.17×10^{-3}	3.79	1.70
CO $^3\Pi$ μ	-0.551	-0.511	6.33×10^{-4}	4.31	7.73
CO $^1\Pi$ μ	-0.138	-0.135	9.59×10^{-4}	-	2.22
CO excited $^1\Sigma^+$ μ	0.614	0.558	8.31×10^{-4}	-	9.97
NO μ	0.00475	0.00794	9.55×10^{-4}	1.35	40.2
N_2 QZZ	-1.342	-1.356	1.07×10^{-3}	1.06	1.02
CH_4 Ω_{XXZ}	2.056	2.0049	7.95×10^{-4}	4.98	2.54
CH_4 R=5 Ω_{XXZ}	1.000	1.631	3.24×10^{-3}	1.25	38.7

Table 6-2: MCCI and FCI multipoles in atomic units. The cc-pVDZ basis set is used for all calculations with the exception of NO μ where the 6-31G basis was used. 2 frozen orbitals were used for all cases, apart from CH_4 Ω_{XXZ} that used one frozen orbital and NO μ for which no frozen orbitals were used. Experimental geometries described earlier in the chapter were used unless specified. The percentage errors in the MCCI results are in comparison to the FCI result. For the percentage of FCI space used in the MCCI calculation, the number of CSFs used in MCCI is compared to the number of SDs of the symmetry adapted FCI calculation.

The largest percentage errors occur in the cases of NO μ and CH_4 R=5 Ω_{XXZ} (40.2 and 38.7 % respectively). In the case of the NO μ this can be put down to the dipole being very small, the absolute error is only 0.00391. While the disparity in the CH_4 R=5 Ω_{XXZ} results may be due to the strong multireference nature of the system. With the exception of these two cases, generally the percentage error in the multipole is of similar scale to that of the correlation energy.

Even though the TiO_2 molecule pushes the limits of what the current MCCI program can handle, MCCI results for the system seem to give satisfactory results. MCCI manages to avoid the problems encountered by lower cost wave function methods, such as CC2 and CIS(D), while producing results that appear comparable to the higher cost methods considered in chapter 3.

6.6 References

[1] Coe, J. P.; Taylor, D. J.; Paterson, M. J., Monte carlo configuration interaction applied to multipole moments, ionization energies, and electron affinities. *Journal of Computational Chemistry* **2013,** 34, 1083-1093.

[2] Lischka, H.; Shepard, R.; I. Shavitt; R. M. Pitzer; M. Dallos; Th. Müller; P. G. Szalay; F. B. Brown; R. Ahlrichs; H. J. Böhm; A. Chang; D. C. Comeau; R. Gdanitz; H. Dachsel; C. Ehrhardt; M. Ernzerhof; P. Höchtl; S. Irle; G. Kedziora; T. Kovar; V. Parasuk; M. J. M. Pepper; P. Scharf; H. Schiffer; M. Schindler; M. Schüler; M. Seth; E. A. Stahlberg; J.-G. Zhao; S. Yabushita; Z. Zhang; M. Barbatti; S. Matsika; M. Schuurmann; D. R. Yarkony; S. R. Brozell; E. V. Beck; and J.-P. Blaudeau; M. Ruckenbauer; B. Sellner; F. Plasser; and J. J. Szymczak *Columbus, an ab initio electronic structure program*, release 5.9.2 (2012).

[3] Crawford, T. D.; Sherrill, C. D.; Valeev, E. F.; Fermann, J. T.; King, R. A.; Leininger, M. L.; Brown, S. T.; Janssen, C. L.; Seidl, E. T.; Kenny, J. P.; Allen, W. D., PSI3: An open-source ab initio electronic structure package. *Journal of Computational Chemistry* **2007,** 28, 1610-1616.

[4] H.-J. Werner, P. J. K., G. Knizia, F. R. Manby, M. Schütz, P. Celani, T. Korona, R. Lindh, A. Mitrushenkov, G. Rauhut, K. R. Shamasundar, T. B. Adler, R. D. Amos, A. Bernhardsson, A. Berning, D. L. Cooper, M. J. O. Deegan, A. J. Dobbyn, F. Eckert, E. Goll, C. Hampel, A. Hesselmann, G. Hetzer, T. Hrenar, G. Jansen, C. Köppl, Y. Liu, A. W. Lloyd, R. A. Mata, A. J. May, S. J. McNicholas, W. Meyer, M. E. Mura, A. Nicklass, D. P. O'Neill, P. Palmieri, K. Pflüger, R. Pitzer, M. Reiher, T. Shiozaki, H. Stoll, A. J. Stone, R. Tarroni, T. Thorsteinsson, M. Wang, and A. Wolf, *Molpro, version 2010.1, a package of ab initio programs,* , see http://www.molpro.net.

[5] Muenter, J. S., Electric dipole moment of carbon monoxide. *Journal of Molecular Spectroscopy* **1975,** 55, 490-491.

[6] Scuseria, G. E.; Miller, M. D.; Jensen, F.; Geertsen, J., The dipole moment of carbon monoxide. *The Journal of Chemical Physics* **1991,** 94, 6660-6663.

[7] Coe, J. P.; paterson, M. J., Novel truncated and stochastic approaches to configuration interaction. In *Recent research developments in chemical physics.*, Pandalai, S. G., Ed. Transworld Research Network: Kerala, India, 2012; Vol. 6, pp 41-65.

[8] Peterson, K. A.; Woods, R. C., Theoretical dipole moment functions involving the a $^3\Pi$ and a′ $^3\Sigma^+$ states of carbon monoxide. *The Journal of Chemical Physics* **1990,** 93, 5029-5036.

[9] Wicke, B. G.; Field, R. W.; Klemperer, W., Fine structure, dipole moment, and perturbation analysis of a $^3\Pi$ CO. *The Journal of Chemical Physics* **1972,** 56, 5758-5770.

[10] Cooper, D. L.; Kirby, K., Theoretical study of low-lying $^1\Sigma^+$ and $^1\Pi$ states of CO. I. Potential energy curves and dipole moments. *The Journal of Chemical Physics* **1987,** 87, 424-432.

[11] Drabbels, M.; Meerts, W. L.; ter Meulen, J. J., Determination of electric dipole moments and transition probabilities of low-lying singlet states of CO. *The Journal of Chemical Physics* **1993,** 99, 2352-2358.

[12] Hoy, A. R.; Johns, J. W. C.; McKellar, A. R. W., Stark spectroscopy with the CO laser: Dipole moments, hyperfine structure, and level crossing effects in the fundamental band of NO. *Canadian Journal of Physics* **1975,** 53, 2029-2039.

[13] Gijsbertsen, A.; Siu, W.; Kling, M. F.; Johnsson, P.; Jansen, P.; Stolte, S.; Vrakking, M. J. J., Direct determination of the sign of the NO dipole moment. *Physical Review Letters* **2007,** 99, 213003.

[14] Sayós, R.; Valero, R.; Anglada, J. M.; González, M., Theoretical investigation of the eight low-lying electronic states of the cis- and trans-nitric oxide dimers and its isomerization using multiconfigurational second-order perturbation theory (CASPT2). *The Journal of Chemical Physics* **2000,** 112, 6608-6624.

[15] Buckingham, A. D., Molecular quadrupole moments. *Quarterly Reviews, Chemical Society* **1959,** 13, 183-214.

[16] Halkier, A.; Coriani, S.; Jørgensen, P., The molecular electric quadrupole moment of N_2. *Chem. Phys. Lett.* **1998,** 294, 292-296.

[17] Graham, C.; Imrie, D. A.; Raab, R. E., Measurement of the electric quadrupole moments of CO_2, CO, N_2, Cl_2 and BF_3. *Molecular Physics* **1998,** 93, 49-56.

[18] Halkier, A.; Larsen, H.; Olsen, J.; Jørgensen, P.; Gauss, J. r., Full configuration interaction benchmark calculations of first-order one-electron properties of BH and HF. *The Journal of Chemical Physics* **1999,** 110, 734-740.

[19] Aidas, K.; Angeli, C.; Bak, K. L.; Bakken, V.; Bast, R.; Boman, L.; Christiansen, O.; Cimiraglia, R.; Coriani, S.; Dahle, P.; Dalskov, E. K.; Ekström, U.; Enevoldsen, T.; Eriksen, J. J.; Ettenhuber, P.; Fernández, B.; Ferrighi, L.; Fliegl, H.; Frediani, L.; Hald, K.; Halkier, A.; Hättig, C.; Heiberg, H.; Helgaker, T.; Hennum, A. C.; Hettema, H.; Hjertenæs, E.; Høst, S.; Høyvik, I.-M.; Iozzi, M. F.; Jansík, B.; Jensen, H. J. A.; Jonsson, D.; Jørgensen, P.; Kauczor, J.; Kirpekar, S.; Kjærgaard, T.; Klopper, W.; Knecht, S.; Kobayashi, R.; Koch, H.; Kongsted, J.; Krapp, A.; Kristensen, K.; Ligabue, A.; Lutnæs, O. B.; Melo, J. I.; Mikkelsen, K. V.; Myhre, R. H.; Neiss, C.; Nielsen, C. B.; Norman, P.; Olsen, J.; Olsen, J. M. H.; Osted, A.; Packer, M. J.; Pawlowski, F.; Pedersen, T. B.; Provasi, P. F.; Reine, S.; Rinkevicius, Z.; Ruden, T. A.; Ruud, K.; Rybkin, V. V.; Sałek, P.; Samson, C. C. M.; de Merás, A. S.; Saue, T.; Sauer, S. P. A.; Schimmelpfennig, B.; Sneskov, K.; Steindal, A. H.; Sylvester-Hvid, K. O.; Taylor, P. R.; Teale, A. M.; Tellgren, E. I.; Tew, D. P.; Thorvaldsen, A. J.; Thøgersen, L.; Vahtras, O.; Watson, M. A.; Wilson, D. J. D.; Ziolkowski, M.; Ågren, H., The Dalton quantum chemistry program system. *Wiley Interdisciplinary Reviews: Computational Molecular Science* **2014,** 4, 269-284.

[20] Gray, D. L.; Robiette, A. G., The anharmonic force field and equilibrium structure of methane. *Molecular Physics* **1979,** 37, 1901-1920.

[21] Taylor, D. J.; Paterson, M. J., Calculations of the low-lying excited states of the TiO_2 molcule. *Journal of Chemical Physics* **2010,** 133.

[22] Grein, F., Density functional theory and multireference configuration interaction studies on low-lying excited states of TiO_2. *Journal of Chemical Physics* **2007,** 126, 034313.

Chapter 7: Conclusions and Future Work

This thesis presented computational investigations of challenging systems using a variety of correlated electronic structure methods. Applying approximate methods to such challenging systems can be problematic, a compromise must be made between the accuracy of the model (or method) used opposed to the time and computer resource devoted to the problem. Care must be taken to ensure the accuracy of any method used or else incorrect conclusions may well be drawn from a poor result. Low-level methods can even fail to properly describe seemingly simple small molecules, if the system is sufficiently challenging. The thesis began with an in depth investigation of the challenging $(TiO_2)_n$ (n=1-4) clusters system, which demonstrated several challenges for established correlated electronic structure methods. Then the novel Monte Carlo Configuration Interaction method (MCCI) was described and it was shown how this method performs in relation to the FCI method for calculations of the potential energy surfaces and multipole moments of several small challenging systems.

In Chapter 3 we presented an investigation of the low-lying excited states of the Titanium dioxide clusters with the form $(TiO_2)_n$ (n=1-4). In our more in depth analysis of the TiO_2 monomer, it was shown that high-level methods are required to properly describe this simple molecule. Strong but differing electron correlation effects present in the ground and valence excited electronic states in such systems may be the source of these problems. The effects were not so strong as to invalidate single-reference approaches completely, CCSD works very well and DFT can also do so. However the approximate second-order approaches, such as CC2, were shown to breakdown when applied to this system. The CC2 method is a very popular method, which having generally performed well in benchmarks is believed to be a robust excited state method for organic chromophores[1, 2]. A priori it was expected to work qualitatively well for more strongly correlated systems containing transition metals, if the single reference picture was valid, but we showed in this chapter that this is not the case. The results of the n=2-4 clusters exhibited further problems, there appeared to be no consistency in the ordering of states between results (though, this may be due to the differences in the basis sets used). On the basis of the results of this chapter we advise that caution should

be exercised when applying lower cost excited state response methods to some transition metal oxide systems.

Chapter 4 presented a study of the pseudo-Jahn-Teller effects in the Titanium dioxide clusters. Structures of the neutral closed-shell, radical cationic and radical anionic clusters at each size were described and rationalised in terms of the pseudo-Jahn-Teller effect. This effect, i.e. the vibronic coupling between potential energy surfaces, causes the shape of the ground state potential energy surface to be altered and resulting minimum structures are of lower symmetry than would be expected. A test for the pseudo-Jahn-Teller effect, proposed by Bearpark et al[3], that uses analytical hessians in the CASSCF method was applied. This showed that the pseudo-Jahn-Teller is manifest in certain neutral, cation, and anion clusters of TiO_2. We found that positive and negative radical clusters often undergo different vibronic interactions and consequently adopt differing geometries. It was also shown that while in general DFT performs quite well in describing these geometries, DFT functionals could demonstrate artificial symmetry breaking for some of these radical clusters. This occurs in a non-systematic way, adding a further difficulty when using such functional methods.

We begin Chapter 5 with a description of the novel Monte Carlo Configuration Interaction of J.C. Greer et al[4-7]. This truncated CI method is designed to take advantage of the sparseness of the FCI wave function. A compact wave function, much smaller than the FCI wave function, made up only of significant configurations is generated using the Monte Carlo method. This compact wave function is however still able to recover a large proportion of the energy of the FCI wave function. We then applied the MCCI method to the potential energy surfaces of a number of small challenging systems. Using the non-parallelity error (NPE) we showed that MCCI is capable of describing potential curves of these small systems to a good accuracy. Even though the method is not exactly size consistent, when a low enough c_{min} was used MCCI was shown to be sufficiently size consistent to reproduce the FCI curve shape. The MCCI method was pushed to its limits in the case of a large hydrogen chain of 50 atoms. Though the equilibrium geometry was in approximately the correct place, at long bond lengths the MCCI result was not a big improvement on the Hartree-Fock curve. We suggested that this is due to the small sampling of the extremely large configuration space of this system.

In Chapter 6 we presented an investigation of the multipole moments of a number of challenging systems using MCCI. We showed that over the range of molecules and geometries considered the MCCI method performs well in comparison to FCI. The MCCI method was able to reproduce results close to the FCI results, but at a far lower computational cost. With the exception of the NO μ and CH_4 R=5 Ω_{XXZ}, all of the % errors in the property calculated were less than 10%. In the case of the NO μ we attributed the large % error to the dipole being very small, the absolute error is in fact very small. The disparity in the CH_4 (R=5) Ω_{XXZ} results may have been due to the strong multireference nature of the system. Finally, we returned to the case of TiO_2, applying the MCCI method to the TiO_2 monomer. This pushed the limits of what the current MCCI program can handle. We found that MCCI produced results that appear comparable to the higher cost methods considered in chapter 3 and manages to avoid the problems encountered by lower cost wave function methods, such as CC2 and CIS(D).

Future work, from the work of this thesis, is on-going. Studies that increase our knowledge and understanding of TiO_2 clusters have been performed[8-10], and some of our work presented here has been extended to other transition metal oxide systems[11]. The MCCI method has been developed further increasing its functionality and the applicability of the method for different properties has been tested using a wider range of systems[12-16].

7.1 References

[1] Schreiber, M.; Silva-Junior, M. R.; Sauer, S. P. A.; Thiel, W., Benchmarks for electronically excited states: CASSPT2, CC2, CCSD, and CC3. *The Journal of Chemical Physics* **2008,** 128, 134110.

[2] Sauer, S. P. A.; Schreiber, M.; Silva-Junior, M. R.; Thiel, W., Benchmarks for electronically excited states: A comparison of noniterative and iterative triples corrections in linear response coupled cluster methods: CCSDR(3) versus CC3. *Journal of Chemical Theory and Computation* **2009,** 5, 555-564.

[3] Bearpark, M. J.; Blancafort, L.; Robb, M. A., The pseudo-jahn-teller effect: A CASSCF diagnostic. *Molecular Physics* **2002,** 100, 1735-1739.

[4] Greer, J. C., Estimating full configuration-interaction limits from a monte-carlo selection of the expansion space. *Journal of Chemical Physics* **1995,** 103, 1821-1828.

[5] Greer, J. C., Consistent treatment of correlation-effects in molecular dissociation studies using randomly chosen configurations. *Journal of Chemical Physics* **1995,** 103, 7996-8003.

[6] Greer, J. C., Monte carlo configuration interaction. *Journal of Computational Physics* **1998,** 146, 181-202.

[7] Győrffy, W.; Bartlett, R. J.; Greer, J. C., Monte carlo configuration interaction predictions for the electronic spectra of Ne, CH_2, C_2, N_2, and H_2O compared to full configuration interaction calculations. *Journal of Chemical Physics* **2008,** 129, 064103.

[8] Berardo, E.; Hu, H.-S.; Kowalski, K.; Zwijnenburg, M. A., Coupled cluster calculations on TiO_2 nanoclusters. *The Journal of Chemical Physics* **2013,** 139, 064313.

[9] Berardo, E.; Hu, H.-S.; Shevlin, S. A.; Woodley, S. M.; Kowalski, K.; Zwijnenburg, M. A., Modeling excited states in TiO_2 nanoparticles: On the accuracy of a TDDFT based description. *Journal of Chemical Theory and Computation* **2014,** 10, 1189-1199.

[10] Berardo, E.; Hu, H.-S.; van Dam, H. J. J.; Shevlin, S. A.; Woodley, S. M.; Kowalski, K.; Zwijnenburg, M. A., Describing excited state relaxation and localization in TiO_2 nanoparticles using TD-DFT. *Journal of Chemical Theory and Computation* **2014,** 10, 5538-5548.

[11] Almeida, N. M. S.; McKinlay, R. G.; Paterson, M. J., Excited electronic states of MnO_4^-: Challenges for wavefunction and density functional response theories. *Chemical Physics* **2015,** 446, 86-91.

[12] Coe, J. P.; Paterson, M. J., Development of monte carlo configuration interaction: Natural orbitals and second-order perturbation theory. *The Journal of Chemical Physics* **2012,** 137, 20, 10 p.204108

[13] Coe, J. P.; Paterson, M. J., State-averaged monte carlo configuration interaction applied to electronically excited states. *The Journal of Chemical Physics* **2013,** 139, 15, 11 p.154103.

[14] Coe, J. P.; Paterson, M. J., Characterising a configuration interaction excited state using natural transition geminals. *Molecular Physics* **2013,** 112, 733-739.

[15] Coe, J. P.; Murphy, P.; Paterson, M. J., Applying monte carlo configuration interaction to transition metal dimers: Exploring the balance between static and dynamic correlation. *Chem. Phys. Lett.* **2014,** 604, 46-52.

[16] Coe, J. P.; Paterson, M. J., Approaching exact hyperpolarizabilities via sum-over-states monte carlo configuration interaction. *The Journal of Chemical Physics* **2014,** 141, 12, p. 124118